

**Bridging *in vitro* and *in vivo* testing:
the utilisation of a novel *in vitro*
three-dimensional model of human
bone marrow for toxicity and
genotoxicity testing.**

Alexander Robert Vernon

A thesis submitted in partial fulfilment of the requirements of the University of the West of England, Bristol for the degree of Doctor of Philosophy

This research programme was carried out in collaboration with AstraZeneca and funded by Medical Research Councils ITTP initiative

Faculty of Health and Applied Sciences, University of the West of England, Bristol

June 2021

Author's declaration

This thesis is submitted in fulfilment of the requirements of the Ph.D. Project, and except where duly acknowledged or referenced, it is entirely my own work. Experiments conducted within both the University of the West of England, Bristol and AstraZeneca were conducted entirely by myself. It has not been submitted, either in whole or part, for any other award at the University of the West of England or elsewhere.

Signed:

Date:.....

Copyright disclaimer

This copy of the thesis has been supplied on the understanding that it is copyright material, quotation from the thesis may not be published without permission and proper acknowledgement.

Abstract

Genotoxicity testing is required for all new compounds utilising 2D assays, such as the *in vitro* micronucleus (MN) assay, before moving to *in vivo* assays such as the rodent bone marrow MN assay. Two-dimensional cell culture has traditionally been used for *in vitro* research. However, the *in vivo* setting comprises a three-dimensional (3D) environment and within the bone marrow (BM), mesenchymal and haematopoietic stem cells interact together. It has been found that even though the *in vitro* MN assay is intended to be predictive of the *in vivo* BM, glucocorticoids were found to have an increased level of micronuclei *in vivo* than predicted within the *in vitro* MN assay, therefore these have been labelled pharmacological positives. As 3D cell culture has been shown to simulate the *in vivo* scenario more closely, the aim of the current study was to create a reproducible model of the BM, using cell lines, which simulates the level of genotoxicity and cytotoxicity seen with the *in vivo* setting, for eventual use of identifying the mechanism(s) by which this change in MN induction occurs.

Initially, an appropriate scaffold was identified for the primary culture of the fibroblast cell line HS-5. Once evaluated, a pre-culture of HS-5 cells on the scaffold established a microenvironment suitable for later seeding of the TK6 cell line. Together with medium changes and optimised seeding a model was developed which supported an exponential phase of growth suitable for executing the MN assay in three-dimensions. Utilising this novel 3D model, TK6 cells were then dosed with known genotoxic positive (mitomycin c, etoposide and paclitaxel), negative (caffeine) and pharmacological positive (dexamethasone and prednisolone) compounds for induction of micronuclei in comparison to *in vitro* and historical *in vivo* data.

The expression of 84 genes associated with metabolism was compared between 2D HS-5 vs 3D HS-5 ± TK6 to identify if this may play a role in the induction of MN. Those expressed in 3D HS-5 ± TK6 were more comparable to the *in vivo* BM than those HS-5 grown in 2D.

In conclusion, this 3D *in vitro* model simulates the induction of genotoxic and cytotoxic damage of compounds, seen within the *in vivo* BM, with more accuracy than the conventional 2D *in vitro* MN assay. This research provides a more *in vivo* relevant setting for further *in vitro* investigation of the mechanism behind compound toxicity allowing a safe drug discovery pathway.

Acknowledgments

This thesis could not have been accomplished without the love, support and encouragement of numerous people including my family, friends and colleagues. I would like to acknowledge all of those people who have made this journey unforgettable for me.

Firstly, I would like to acknowledge the unwavering support, guidance and knowledge base that is my director of studies, Dr Ruth Morse. I am grateful for her making time to discuss extensively my research, but also being an open ear for any problems I had outside of academia. I would also like to thank my additional supervisors Dr Rhiannon David, Professor Ann Doherty and Dr Roy Pemberton, without their knowledge and expertise in regulatory genetic toxicology and 3D modelling this thesis would not have been possible.

I am most grateful to the MRC and AstraZeneca for providing the funding for this research. My time at UWE and AstraZeneca was made enjoyable in large part by members of the genotoxic team, PhD student community and the ‘Morse innovation group’, who were an amazing source of advice and encouragement. In particular, I would like to express my appreciation for the assistance and technical advice provided by Mr David Corry at UWE and Dr Amy Wilson, Dr Anne Ashford and Dr Joanne Elloway of AstraZeneca. I would also like to thank a previous doctoral student Dr Simon Andrews for his support during this period. I am also grateful to Dr David Patton, for his assistance with scanning electron microscopy work. The ITTP summer school funded by the MRC was also a great pleasure to attend, helping me understand complex issues within the world of toxicology and may it continue to run. Therefore, to the creator and head of the ITTP scheme, Professor Andy Smith, I am truly grateful.

This PhD would not have been possible without the consistent support of my family. Foremost, an enormous thank you to my parents Mr Robert and Mrs Maxine Vernon for their love and unwavering support. I am grateful for everything they have given to support me in achieving any goal I set out to accomplish. I am deeply thankful to my grandparents Mr David Ryding MBE, Mr Malcom Vernon, Mrs Freda Vernon and my late nan, Mrs Jean Ryding who I feel has been by my side every step of this journey, for their everlasting love, care and encouragement I am truly grateful. I would also like to thank my father and mother-in-law Mr Neil and Mrs Angela Roberts, for their help and support throughout this journey.

Finally, but definitely not least, I express my deep gratitude to my wife Rebecca. I am so appreciative of all her love and patience over the last five years, always there to cheer me up, standing by my side through the good and bad times. I would not have been able to do this without you my love.

Table of contents

Author's declaration	i
Copyright disclaimer	ii
Abstract.....	iii
Acknowledgments	iv
Table of contents.....	vi
List of Figures.....	i
List of Tables	i
Abbreviations.....	i
Chapter One	1
1. Introduction	1
1.1. Bone marrow	1
1.1.1. The bone marrow microenvironment.....	3
1.2. Genetic toxicology.....	7
1.2.1. Types of genotoxic DNA damage.....	9
1.2.2. Regulatory testing of new compounds.....	11
1.2.2.1. <i>In vitro/ in vivo</i> micronucleus assay	15
1.2.2.2. The mechanism by which clastogenic and aneugenic compounds induce genotoxicity and their use in the <i>in vitro</i> and <i>in vivo</i> MN assay	16
1.2.2.3. Pharmacological positives	19
1.2.3. The protective role of the bone marrow microenvironment	20
1.3. The need for 3D modelling.....	21
1.3.1. 3D vs 2D cell culture	21
1.3.2. Common 3D culture methods used within supplementation systems	24
1.3.2.1. The use of scaffold free spheroids for 3D culture	26
1.3.2.2. The use of hydrogels and prefabricated hard scaffold for 3D culture	27
1.3.3. 3D culture supplementation systems	28
1.3.4. Current 3D models of the bone marrow for genetic toxicology testing.	30
1.4. The focus of this current study	32
1.5. Aim	33
1.6. Objectives	33
Chapter Two	35
2. General Methods.....	35
2.1. Materials.....	35
2.2. Tissue culture.....	35
2.2.1. Cell count and viability	36
2.2.2. Identifying TK6 exponential phase in 2D.....	36
2.2.3. Cryopreservation and thawing of cell lines	36
2.2.4. Trypsinisation of adherent cells.....	37
2.3. The finalised AlgiMatrix™ scaffold seeding protocol.....	37
2.3.1. Initial HS-5 seeding and long-term culture.....	37
2.3.2. Addition of TK6 cells	37
2.4. Flow cytometry.....	38
2.5. Microscopic examination	41
2.6. Screening of positive, negative and potential genotoxic compounds in 2D.....	41
2.6.1. Industrial <i>in vitro</i> micronucleus assay	41
2.6.2. Scoring of micronuclei.....	43
2.7. Statistical Analysis	45
Chapter Three	46

3.	Developing a 3D model of the bone marrow using commercial cell lines.....	46
3.1.	Introduction	46
3.2.	Materials and methods.....	49
3.2.1.	Biomerix™ (hard) scaffold seeding development.....	49
3.2.1.1.	Original seeding of HS-5 onto a Biomerix™ scaffold	49
3.2.1.2.	Optimisation of HS-5 initial seeding time and density.....	49
3.2.1.3.	Evaluation of trypsinisation efficiency	50
3.2.2.	AlgiMatrix™ (gel) model development	50
3.2.2.1.	Identification of AlgiMatrix™ internal structure	50
3.2.2.2.	AlgiMatrix™ optimisation of cellular seeding and retrieval.....	51
3.2.2.2.1.	The effect of 55mM EDTA and dissolving buffer on HS-5 cells	51
3.2.2.2.2.	Proliferation index of HS-5 with/ without an AlgiMatrix™ scaffold present.....	51
3.2.2.2.3.	Washing regimen for increased cellular viability.....	52
3.2.2.2.4.	Proliferation index of TK6 cells in co-culture with HS-5 cells.....	53
3.2.3.	3D printing of in-house Alginate scaffolds.....	54
3.2.3.1.	Modification of a 3D printer for use with bioink and design of an <i>in vivo</i> relevant bone marrow scaffold.....	54
3.2.3.2.	Experimentation of a non-commercial bespoke hydrogel scaffold	55
3.2.3.3.	The effect of calcium chloride on bioink and HS-5 cells	55
3.2.4.	Identification of a single cell type in a co-culture.....	55
3.2.4.1.	Identification of TK6 within a co-culture system.....	55
3.2.4.1.1.	Use of the nanocrystal technology Qtracker 655.....	56
3.2.4.1.2.	Flow cytometry of TK6 specific markers.....	56
3.2.4.1.3.	Immunofluorescent differentiation of TK6 from HS-5 cells.....	57
3.3.	Results	58
3.3.1.	Biomerix™ scaffold seeding development.....	58
3.3.1.1.	The seeding of HS-5 onto Biomerix™ using a previously published method	58
3.3.1.2.	Optimisation of initial seeding density	59
3.3.2.	AlgiMatrix™ model development.....	62
3.3.2.1.	Optimisation of initial solidifying and eventual dissolving of AlgiMatrix™ scaffolds.	63
3.3.2.2.	Effect of firming buffer on incorporated HS-5 cells and optimisation of long-term culture conditions.....	67
3.3.2.3.	Identifying the optimal seeding density of HS-5 cells within AlgiMatrix™ scaffolds.	70
3.3.2.4.	Identification of TK6 cells utilising florescent CD markers	74
3.3.2.4.1.	Identifying an initial concentration of TK6 and optimal long-term co-culture condition.	75
3.3.3.	3D printing of an in-house Alginate scaffold	82
3.3.3.1.	Optimisation of a bespoke hydrogel for 3D printing and culture	82
3.3.3.2.	Conversion of a polylactic acid 3D printer to extrude biological material.....	86
3.3.4.	Identification of a single cell type within a co-culture	89
3.3.4.1.	Identification of TK6 cells from HS-5.....	89
3.4.	Discussion.....	92
3.4.1.	3D Scaffold assessment	92
3.4.1.1.	The Biomerix™ hard scaffold already in use at UWE.....	92
3.4.1.2.	Establishing a new model for 3D co-culture	94
3.5.	Conclusion.....	105
Chapter Four	106
4.	Screening of positive, negative and potential genotoxic compounds in 2D and 3D systems.	106
4.1.	Introduction	106

4.2.	Methods	108
4.2.1.	Identification of the exponential phase of TK6 cells in 2D culture	108
4.2.2.	The regulatory <i>in vitro</i> 2D micronucleus assay	108
4.2.3.	Selection and concentration of known positive, negative and pharmacological positive compounds	108
4.2.4.	Genotoxicity and cytotoxicity of known positive, negative and pharmacological positive compounds within a 3D multicellular model.	111
4.3.	Results	114
4.3.1.	Identifying the exponential phase of TK6 at UWE	114
4.3.2.	An initial dose range of known genotoxic positive compounds conducted at AZ	115
4.3.3.	Comparison of micronucleus induction at AZ and UWE for alignment of scoring	117
4.3.4.	Extended dose range of known positive genotoxicants conducted at UWE, utilising an initial range from AZ	119
4.3.5.	Dose range of known negative and pharmacological positives conducted at UWE	123
4.3.6.	Genotoxic assessment of positive, negative and pharmacological positive compounds within a multicellular, <i>in vitro</i> , 3D model of the bone marrow	126
4.4.	Discussion	140
4.4.1.	Genotoxicity of known positive, negative and pharmacological positive compounds within the <i>in vitro</i> regulatory 2D micronucleus assay	141
4.4.2.	Genotoxicity of known positive, negative and pharmacological positive compounds within the multicellular 3D model	143
4.4.2.1.	The addition of known genotoxic compounds	146
4.4.2.2.	The addition of pharmacological positive compounds	149
4.4.2.3.	The addition of a negative genotoxic compound	152
4.5.	Conclusion	153
Chapter Five		154
5.	Assessment of the metabolic status of the 3D <i>in vitro</i> cell line model	154
5.1.	Introduction	154
5.2.	Materials and methods	156
5.2.1.	Spheroid formation	156
5.2.2.	RNA extraction	156
5.2.3.	Assessment of RNA quality and concentration	157
5.2.4.	Quantitative polymerase chain reaction of human drug metabolism components.	157
5.2.5.	Addition of cyclophosphamide to HS-5 cells for the assessment of pro-drug activation	160
5.2.6.	qPCR analysis	161
5.3.	Results	162
5.3.1.	Spheroid formation	162
5.3.2.	RNA concentration and quality of each experimental condition	164
5.3.3.	QPCR analysis	165
5.3.3.1.	Raw CT values	165
5.3.3.2.	Fold regulation comparison between each experimental condition	168
5.3.4.	Addition of cyclophosphamide to TK6 seeded within a trans-well insert with or without HS-5 seeded scaffolds.	173
5.4.	Discussion	175
5.4.1.	The expression of Phase I metabolic enzymes	176
5.4.2.	The expression of Phase II metabolic enzymes	178
5.4.3.	The expression of drug transporter, receptor and protein genes associated with metabolism	183
5.4.4.	Assessment of the cytotoxicity of cyclophosphamide on TK6 cells with/ without HS-5 or S9	185

5.5. Conclusion	187
Chapter Six	189
6. Final Discussion	189
6.1. General discussion and conclusion.....	189
6.2. Limitations of the study.....	195
6.3. Future work	196
References.....	198
Appendices	238
Research output	240
Publications	240
Oral/ poster presentation	240

List of Figures

Figure 1-1. Schematic representation of the progression of haematopoietic stem cells (HSC) into their differentiated myeloid and lymphoid progenitors.....	2
Figure 1-2. Schematic model of the bone marrow microenvironment.....	4
Figure 1-3. A schematic representation of the development of mesenchymal stem cells (MSC) through commitment, progression, differentiation and eventual maturation into their specific lineages and eventual tissues.....	5
Figure 1-4. The drug development process within industry and where toxicology including genetic toxicology is located within this.....	8
Figure 1-5. Differing types of DNA damage that can occur as a result of drug interaction.....	10
Figure 1-6. The <i>in vitro</i> and <i>in vivo</i> micronucleus assay.....	16
Figure 1-7. Mechanism by which clastogenic/ aneuploidy inducing compounds interrupt cellular mitosis inducing micronuclei and aneuploidy within daughter cells.....	17
Figure 2-1. Flow cytometry gating strategy.....	39
Figure 2-2. Photomicrographs of the characteristic morphologies identified when scoring MN.....	44
Figure 3-1. Growth of HS-5 cells seeded onto Biomerix™ scaffolds at a density of 5×10^5 cells/ scaffold using a previously established method.....	58
Figure 3-2. Initial adherence time of HS-5 cells seeded onto Biomerix™ scaffolds at a concentration of 5×10^5	60
Figure 3-3. Initial adherence time of HS-5 cells seeded onto Biomerix™ scaffolds at a concentration of 1×10^6	61
Figure 3-4. Growth of HS-5 cells seeded onto Biomerix™ scaffolds at a concentration of 1×10^6	62
Figure 3-5. Images depicting the physical structural difference seen with increasing firming buffer concentration of AlgiMatrix™ scaffolds.....	63
Figure 3-6. Scanning electron microscopy (SEM) images of AlgiMatrix™ scaffolds hardened with a 10, 25 or 50% firming buffer.....	65
Figure 3-7. The effect of 55mM EDTA (A) and commercial dissolving buffer (B) on the viability (line) and total cell number (bar) of HS-5 cells.....	66
Figure 3-8. The effect of 55mM EDTA (B) and commercial dissolving buffer (C) on an AlgiMatrix™ 50% scaffold.....	67
Figure 3-9. Cell number and viability of HS-5 cells seeded at a concentration of 2.5×10^5 onto AlgiMatrix™ scaffolds.....	69
Figure 3-10. The growth of HS-5 cells in a 25cm ² flask, 24 and 12 well plate at an initial seeding density of 6×10^3 cells/cm ²	72
Figure 3-11. The growth of HS-5 cells seeded at 2.5, 5, 7.5 and 10×10^5 cells onto an AlgiMatrix™ scaffold.....	73
Figure 3-12 Histogram plot of CD19 and CD20 expression in TK6 and HS-5 cell lines.....	75
Figure 3-13. Initial seeding density and long-term culture of TK6 (CD19+) cells, co-cultured with pre-cultured AlgiMatrix™ scaffold.....	77
Figure 3-14. Light microscopy images of the bottom of a 12 well plate containing a seeded AlgiMatrix™ scaffold.....	79
Figure 3-15. Viability of HS-5 cells seeded onto an AlgiMatrix™ scaffold with the addition of TK6.....	81
Figure 3-16. Viability of HS-5 cells after 10 minute exposure to 100, 500, 700 and 1000 mM CaCl ₂	83
Figure 3-17 Image of crosslinked hydrogels after a 30 minute period to 100 mM or 1 M CaCl ₂ in medium.....	84
Figure 3-18 Scanning electron microscope (SEM) images of the bespoke alginate hydrogel.....	85
Figure 3-19 Process of building and converting a 3D printer whilst also creating a bespoke scaffold from scratch.....	88
Figure 3-20 Fluorescent microscopy images of TK6 cells stained with Qtracker combined in differing ratios with unstained HS-5 cells.....	89
Figure 3-21 Fluorescent confocal microscopy images of TK6 and HS-5 cells stained with CD19, CD20 and DAPI in differing ratios.....	91

Figure 4-1. Planned protocol, utilising the proliferation of cells in 3D, for micronucleus assessment of known positive, negative and pharmacological positive genotoxicants..	112
Figure 4-2. Schematic representation of the plate layout of AlgiMatrix™ scaffolds for 3 biological repeats of compound dosing.	113
Figure 4-3. TK6 growth curve over 102 hour period.	114
Figure 4-4. Baseline relative PD (RPD) and MN induction following 24 hour treatment with mitomycin C, etoposide, paclitaxel and 4-nitroquinolone-N-oxide at AstraZeneca for initial dose discovery.....	116
Figure 4-5. Comparison of micronucleus scoring between AZ and UWE within TK6 cells dosed with mitomycin C (A), etoposide (B), paclitaxel (C) and 4-nitroquinolone-N-oxide (D).	118
Figure 4-6. Extended dose range finder at UWE, identifying the relative PD (RPD) and micronucleus induction, of TK6, following a 24 hour treatment with mitomycin C, etoposide, paclitaxel and 4-nitroquinolone-N-oxide.....	120
Figure 4-7. Dose range finder of pharmacological positive compounds at UWE, identifying the relative PD (RPD) and micronucleus induction, of TK6, following a 24 hour treatment with dexamethasone and prednisolone.	124
Figure 4-8. Dose range finder of a known negative compound at UWE, identifying the relative PD (RPD) and micronucleus induction, of TK6, following a 24 hour treatment with caffeine.	125
Figure 4-9. Baseline counts taken from the medium and well of TK6 and HS-5 seeded Algimatrix™ scaffolds, 24 hours before and on the day of compound dosing.....	128
Figure 4-10. Total cell number of cells harvested from the medium and Algimatrix™ scaffold after dosing with compound.	130
Figure 4-11. MN induction in cells within the medium and scaffold, harvested from a 3D model after dosing with compound.	137
Figure 5-1. Light microscopy images of the formation of spheroids over a 6-day period in the HepG2 cell lines.	163
Figure 5-2. RNA integrity of each sample by agarose gel analysis.....	165
Figure 5-3. Raw CT values for each experimental condition.	166
Figure 5-4. The comparisons of gene expression, through FR, of HS-5 experimental conditions following normalisation.	169
Figure 5-5. The change in gene expression of each HS-5 experimental condition compared to HepG2 spheroids indicated as FR.....	171
Figure 5-6. The cytotoxic effect of cyclophosphamide on TK6 with and without HS-5 cells and S9 fraction..	174

List of Tables

Table 1-1. The International Council for Harmonisation of Technical Requirements for Pharmaceuticals for Human Use (ICH), strategies for genotoxicity test batteries.....	12
Table 1-2. An overview of standard <i>in vitro</i> genotoxic assays conducted by pharmaceutical companies.....	13
Table 1-3. An overview of standard <i>in vivo</i> genotoxic assays conducted by pharmaceutical companies.....	14
Table 1-4 An overview of cellular characteristics seen in simple 2D and 3D cultures.....	22
Table 1-5. Overview of current matrices for 3D culture.	25
Table 2-1. Details of the antibodies used for flow cytometry and confocal microscopy.	40
Table 4-1. Concentration of known genotoxic compounds used in the 2D <i>in vitro</i> micronucleus assay in assessing the correct dose to induce a <50% RPD score in TK6 cells.....	109
Table 4-2. Concentration of pharmacological positive compounds used in the 2D <i>in vitro</i> micronucleus assay in assessing genotoxicity of TK6 cells in 2D.....	110
Table 4-3 Concentration of a negative genotoxic compound used in the 2D and 3D <i>in vitro</i> micronucleus (MN) assay in assessing genotoxicity of TK6 cells.	110
Table 4-4 Concentration of known genotoxic compounds used in the 3D <i>in vitro</i> micronucleus assay in assessing genotoxicity of TK6 cells within the model.....	111
Table 4-5. Concentration of pharmacological positive compounds used in the 3D <i>in vitro</i> micronucleus (MN) assay in assessing genotoxicity of TK6 cells within the model.	111
Table 4-6. The population doubling of cells within the medium of the 3D <i>in vitro</i> multicellular model when exposed to mitomycin C, etoposide, paclitaxel, dexamethasone, prednisolone and caffeine.....	134
Table 5-1. The list of genes within the RT ² profiler PCR array of human drug metabolism plate.	159
Table 5-2. The ng/ml and absorbance ratios for RNA extracted from HS-5 cultured in 2D, 3D, 3D with the addition of TK6 and HepG2 spheroids.....	164
Table 5-3. Biologically relevant changes in gene expression compared to HepG2 spheroids.....	172

Abbreviations

18s	18s ribosomal RNA
24s	24s ribosomal RNA
2D	Two dimensional
3D	Three dimensional
4NQO	4-Nitroquinoline 1-oxide
AO	Acridine orange
ATCC	American Type Culture Collection
BER	Base excision repair
CaCl ₂	Calcium chloride
CD	Cluster of differentiation
cDNA	Complementary DNA
cm ²	Centimetre squared
CO ₂	Carbon dioxide
CPM	Cyclophosphamide
Ct	Cycle threshold
CXCL	C-X-C motif chemokine
CYP	Cytochrome P450
DAPI	4',6-diamidino-2-phenylindole
dCt	(delta) Δ cycle threshold
ddCt	(delta-delta) $\Delta \Delta$ cycle threshold
DMEM	Dulbecco's Modified Eagle's Medium
DMSO	Dimethyl sulphoxide
DNA	Deoxyribonucleic acid
DSB	Double strand break
ECACC	European Collection of Authenticated Cell Cultures
ECM	Extracellular matrix
EDTA	Ethylenediaminetetraacetic acid
FACS	Fluorescence-activated cell sorting buffer
FBS	Foetal bovine serum
FITC	fluorescein isothiocyanate
FSC	Forward scatter
HGDC	Human genomic DNA contamination

HR	Homologous repair
HSC	Haematopoietic stem cell
ICH	International Council for Harmonisation of Technical Requirements for Pharmaceuticals for Human Use
IL	Interleukin
JAK	Janus kinase
MgCl ₂	Magnesium chloride
ml	Millilitres
MMC	Mitomycin C
MMR	Mismatch repair
MN	Micronucleus
MSC	Mesenchymal stem cell
NHEJ	Non-homologous end joining
nM	Nanomolar
nMol/L	Nanomole per litre
°C	Degree Celsius
OECD	Organisation for Economic Co-operation and Development
PBS	Phosphate buffered saline
PD	Population doubling
PE	Phycoerythrin
PerCP-cy 5.5	Peridinin-chlorophyll-protein Complex: CY5.5
PI	Propidium iodide
PPC	Positive PCR control
RNA	Ribonucleic acid
ROS	Reactive oxygen species
RPD	Relative population doubling
RPMI	Roswell Park Memorial Institute
RT-PCR/ qPCR	Real time/ quantitative polymerase chain reaction
RTC	Reverse transcription control
SCF	Stem cell factor
SD	Standard deviation
SEM	Scanning electron microscopy
SSB	Single strand break
SSC	Side scatter

STAT3	Signal transducer of transcription 3
TB	Trypan blue
U/ml	International units per millilitre
UV	Ultraviolet
µg	Microgram
µg/ml	Micrograms per millilitre
µl	Microlitre
µm	Micrometre
µM	Micromolar

Chapter One

1. Introduction

1.1. Bone marrow

Bone marrow (BM) is one of the largest human organs, accounting for 4-5% of total body weight (Torisawa, 2019). The BM is composed of cartilage, haematopoietic and fat containing marrow, connective tissues and a meshwork of thin-walled capillary veins upon a core of extracellular collagen matrix (ECM) (Andrews *et al.*, 2013). These components fill the space of the trabecular ‘spongy’ bone, a lattice of fine bone plates which is surrounded by a protective barrier of ‘compact’ cortical bone (Zhao *et al.*, 2011; Cordeiro-Spinetti *et al.*, 2015). It is an adaptive organ which changes in functionality due to increasing age but maintains the haematopoietic and immunological systems throughout its life (Karampinos *et al.*, 2017). At birth the bone consists predominantly of haematologically active red marrow, however this is replaced gradually by yellow marrow consisting mainly of adipocytes. The conversion of red to yellow occurs over a 25-year period, primarily in the appendicular skeleton, leaving only the axial and long bones haematologically active in adults (Malkiewicz & Dziedzic, 2012; Hardouin *et al.*, 2014). The red marrow gains its colouration from haematopoietic tissue islands which facilitates differentiation of haematopoietic stem cells (HSCs) (Seita & Weissman, 2010). These HSCs have the ability to self-renew and develop into mature blood cells of both the myeloid and lymphoid lineages (Figure 1-1) (Birbrair & Frenetic, 2016; Jagannathan & Zon, 2013). This differentiation called ‘haematopoiesis’ occurs in the space between the outer surface of the BM blood vessels and trabecular/ cortical bone, aided by the vascular or perivascular BM niche (Anaei & Catafal, 2018).

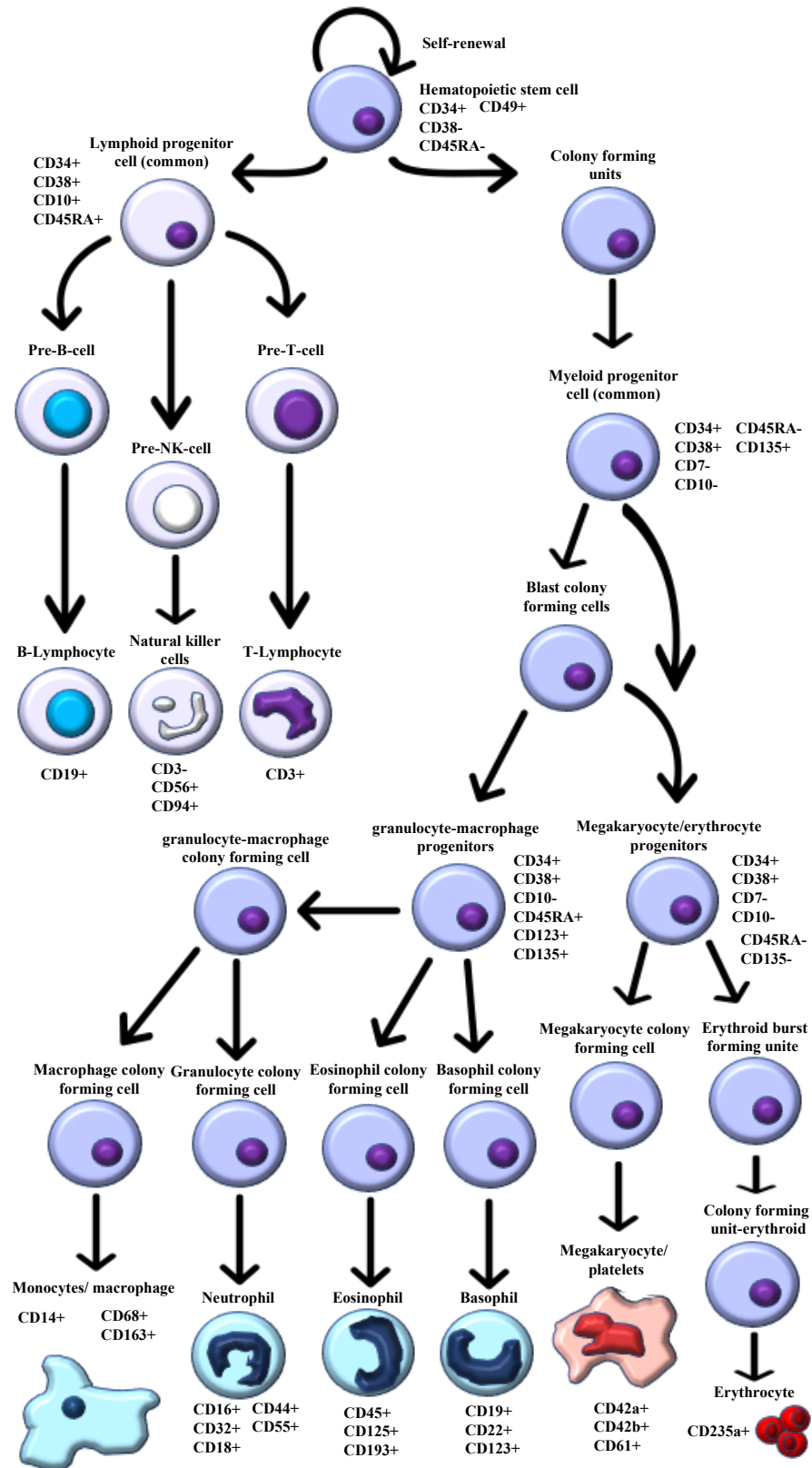


Figure 1-1. Schematic representation of the progression of haematopoietic stem cells (HSC) into their differentiated myeloid and lymphoid progenitors. The CD markers which are present (+) and absent (-), associated with key stages in maturation, are highlighted and are common to all subsets. This figure is drawn by the author based on information from Bakuraysah *et al.*, (2016); King *et al.*, (2011); Lee & Hong, (2019); Mart *et al.*, (2017); Firth & Yuan, (2012).

1.1.1. The bone marrow microenvironment

Differentiation and regulation of HSCs is thought to be regulated by the complex interplay of immature and terminally differentiated cellular components within an environment that only the BM microenvironment can provide such as, changes in oxygen tension, circadian rhythms and blood supply (Figure 1-2) (Tikhonova, 2019; Anaei & Catafal, 2018). The interaction between soluble factors, microRNAs, exosomes, extracellular matrix proteins and metabolism enzymes secreted from the array of cell types which populate the microenvironment ensure successful and intact haematopoiesis (Xu *et al.*, 2018; Kumar *et al.*, 2018; Duarte *et al.*, 2018). In this hierarchical, self-amplifying, self-renewing ecosystem dwell a small number of mesenchymal stem cells (MSCs); ~1 in 3.4×10^4 cells (Wexler *et al.*, 2003). These BM MSCs are multipotent, clonogenic, self-renewing stem cells which have the capacity to differentiate into osteogenic, chondrogenic and adipogenic derived cells, depending on expression of soluble factors which reside within the same perivascular niche as the HSCs (Figure 1-2) (Al-Nbaheen *et al.*, 2013; Wu *et al.*, 2018; Sasine *et al.*, 2016; Zhou *et al.*, 2014; Kowalski *et al.*, 2018). Residing upon the ECM lies a cellular population of MSC derived cells including endothelial, osteoblasts, adipocytes, fibroblasts, chondrocytes, macrophages and stromal cell lineages that make up the stroma of the BM (Figure 1-3) (Baryawno *et al.*, 2019).

The differentiated BM MSC lineages help support HSC self-renewal and multipotency by releasing chemokines, cytokines and metabolic enzymes into their surroundings creating a specialised haematopoietic perivascular niche (Abbuehl *et al.*, 2017). Reticular cells, which cover and synthesise the ECM of the BM, abundantly express the C-X-C motif chemokine 12 (CXCL12 also known as stromal cell-derived factor 1 (SDF1); Gomariz *et al.*, 2018). CXCL12 mediates the mobilisation, homing and retention of HSCs to the BM haematopoietic niche for differentiation into differing blood lineages (Yi *et al.*, 2019; Zhang *et al.*, 2016; Janssens *et al.*, 2018). This is achieved through the binding of CXCL12 to C-X-C chemokine receptor 4 (CXCR4) present on HSCs, stimulating the dissociation of guanosine triphosphate-loaded heterotrimeric G proteins (Suzuki *et al.*, 2014; Cuesta *et al.*, 2019).

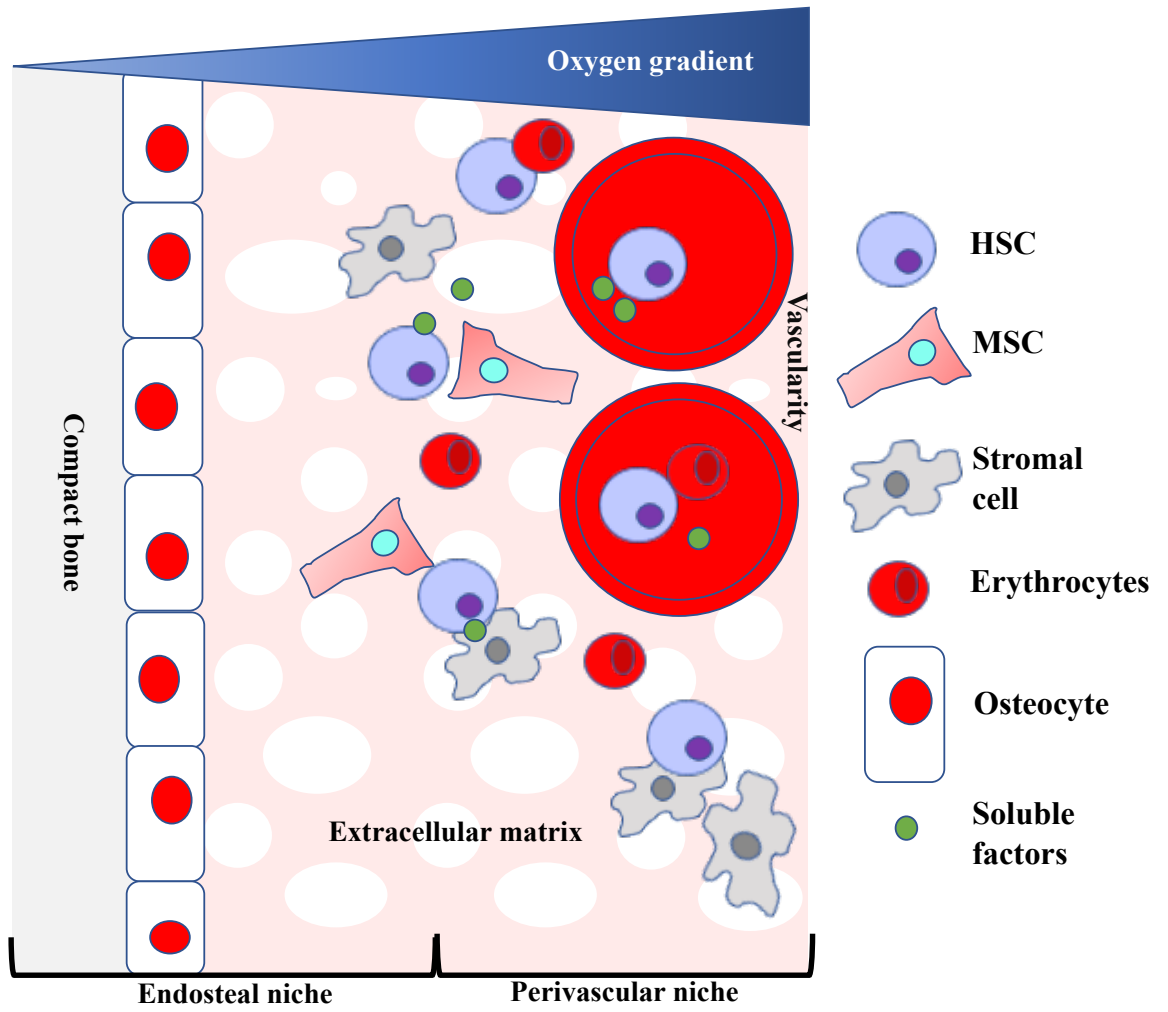


Figure 1-2. Schematic model of the bone marrow microenvironment. The schematic shows a selection of common cell types found within the bone marrow, which interact through soluble factors to regulate and repopulate the blood system and bone marrow microenvironment. The perivascular niche (high oxygen level which contains vascularity) and the endosteal niche (further from vascularity inducing hypoxic conditions) can also be seen. Adapted from Re'em & Cohn (2012)

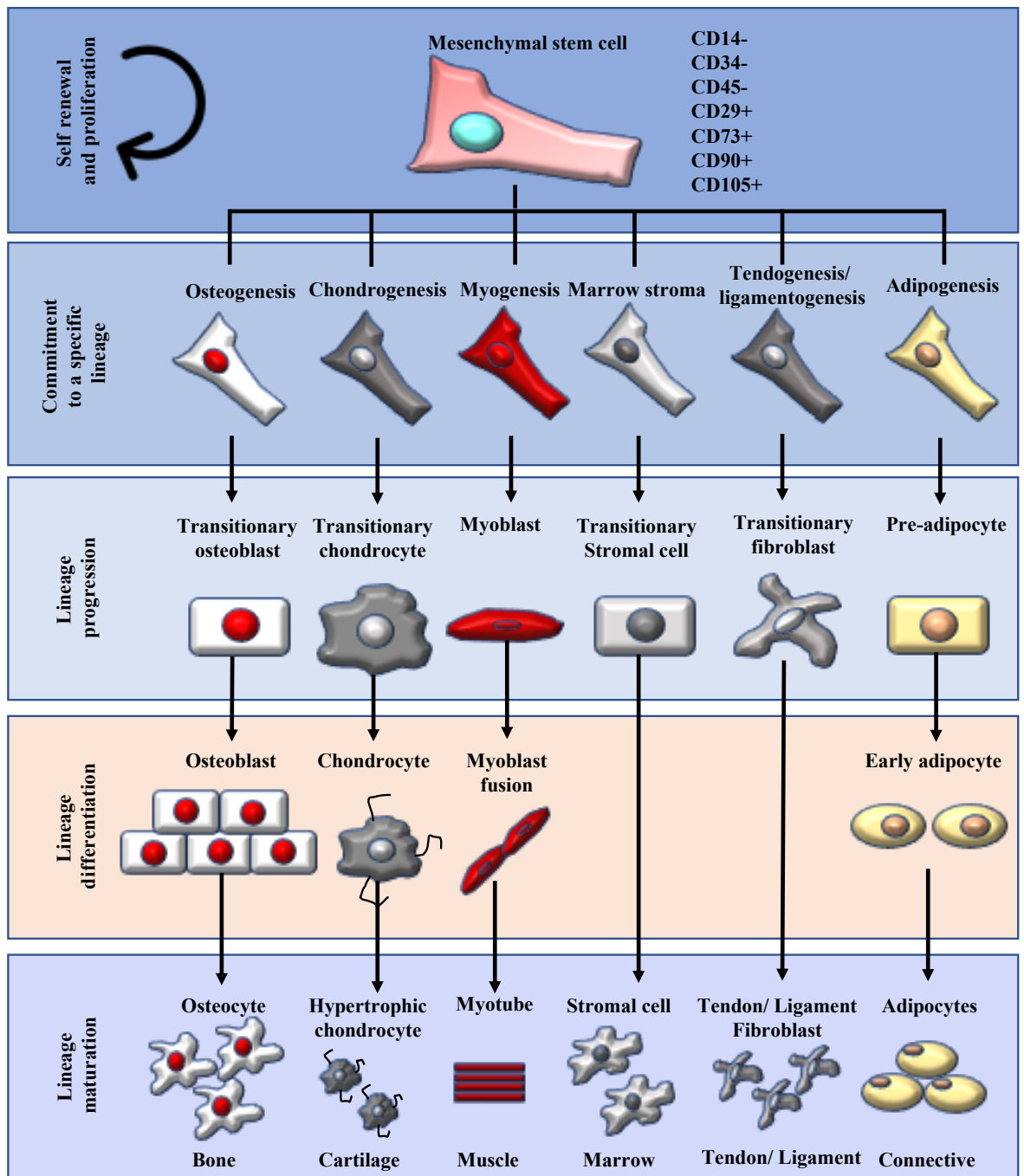


Figure 1-3. A schematic representation of the development of mesenchymal stem cells (MSC) through commitment, progression, differentiation and eventual maturation into their specific lineages and eventual tissues. The CD markers which are present (+) and absent (-), associated with primary uncommitted MSCs, have also been highlighted. This figure is drawn by the author based on information from Firth & Yuan, (2012); Kalinina *et al.*, (2011); Maleki *et al.*, (2014); Bateman *et al.*, (2017); Ullah *et al* (2015); Ren *et al* (2018).

Once HSCs have homed to the BM stroma, fibroblast and endothelial cells start to express the cytokine stem cell factor (SCF) (Li & MacDougald, 2019; Antony & Link, 2014; Addo *et al.*, 2019). SCF binds to the type III receptor tyrosine kinase (c-KIT) which is found on the membrane of many cell types including HSCs and MSCs in the BM stroma (Ho *et al.*, 2017; Czarna *et al.*, 2017). This binding promotes a signalling cascade which causes the proliferation of HSCs only, as c-KIT expression is lost after differentiation with around only 1% of peripheral blood cells expressing it (Babaei *et al.*, 2016). Once residing within the perivascular BM niche, HSCs differentiation can occur. The stromal cells release interleukin 7 (IL-7), which will lead HSCs down the lymphoid lineage. This cytokine is critical for the development of B and T lymphoid cells and is released in response to feedback loops (Rodrigues *et al.*, 2018; Yang *et al.*, 2018). To replenish the myeloid lineage, BM epithelial and fibroblasts release interleukin 3 (IL-3) and granulocyte-macrophage colony stimulating factor (GM-CSF) into the BM niche (Wittwer *et al.*, 2017; Beecher *et al.*, 2016; Ushach & Zlotnik, 2016).

It is this delicate interaction between the BM microenvironment and HSCs which provide the fundamental structural and functional support for healthy human life. Deletion, mutation or disruption of the genes which encode any of the cellular proteins and pathways above, can lead to varying disease states (Turner *et al.*, 2018). The loss or alteration of the *CXCL12* gene from expressing stromal cells, results in a decrease in long-term repopulation activity of HSC. This lack of repopulation of the blood and lymphatic system can lead to primary bone marrow failure (Greenbaum *et al.*, 2013; Risitano *et al.*, 2007). Likewise, a loss of function mutation to the *SCF* gene again causes HSC numbers to decrease and eventually deplete from the BM leading to complete primary bone marrow failure requiring an immediate bone marrow transplant (Ding *et al.*, 2012). The *c-KIT* gene codes for the c-KIT receptor for SCF, and is an example of a proto-oncogene. The receptor for SCF, *c-KIT* is an example of a proto-oncogene. The deregulation of *c-KIT* through gain/loss- of function mutation, due to chromosomal damage, is correlated with cancer (Babaei *et al.*, 2016; Wang *et al.*, 2018; Foster *et al.*, 2018). Similarly, loss of function mutation caused by single nucleotide substitutions in the *IL-7* gene, is associated with autoimmunity disorders (Lundstrom *et al.*, 2012). A gain-of function mutation of the *IL-3* gene causes an overexpression of the ligand seen in patients with haematological malignancies (Borriello *et al.*, 2019; Schreiber *et al.*, 2019).

The BM, as described above, is an active organ constantly replenishing cells of the blood and BM microenvironment through the release of soluble factors in order to maintain a healthy system. Therefore, is extremely sensitive to toxic insults (Robin & Durnad, 2010; Weng *et al.*, 2016). As described previously, induced DNA damage to any one of these cell lineages causes an alteration in the soluble factors released within the BM microenvironment which can have a devastating effect on the human. The vulnerability of this organ to toxic insults affecting the DNA, makes it an appropriate organ for assessing new drug compounds for their ability to induce alteration in the DNA. In order to predict the outcomes of a compound on cells of the BM pharmaceutical companies employ cell lines of the BM, expose these to concentrations of new compounds and assess the induced damage in a discipline of toxicology called genetic toxicology. If a compound does cause alterations in the DNA of the BM cell line, that compound is noted as being genotoxic.

1.2. Genetic toxicology

Toxicology encompasses many different disciplines including, but not limited to, cardiac, hepatic, respiratory, gastric and genetic. Testing for these different safety liabilities is conducted throughout the drug development process (Figure 1-4; target selection through to phase launch), in an effort to treat patients quickly, by early identification and elimination of drug candidates that will ultimately fail due to toxicity (Hornberg *et al.*, 2014). To identify potential compounds that have a detrimental effect on DNA (not as their intended effect), pharmaceutical industries have utilised genetic toxicology. Genetic toxicology is the study of the genetic alterations that may occur in somatic and/ or germ cells, including exposure to chemical compounds. A chemical compound could induce changes in DNA through indirect and/ or direct mechanisms in DNA replication (Hasselgren *et al.*, 2019).

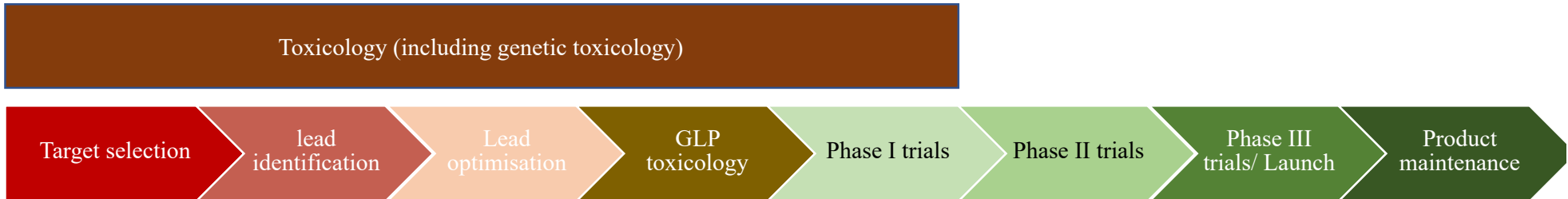


Figure 1-4. The drug development process within industry and where toxicology including genetic toxicology is located within this. GLP (good laboratory practice).

1.2.1. Types of genotoxic DNA damage.

The exposure of DNA to a genotoxic compound can result in DNA damage and/or mutational events, like those seen in Figure 1-5, where the corresponding repair pathway is unable to resolve the damage. Single strand breaks (SSB) within the DNA are the most frequent form of damage and are resolved via the base excision repair (BER) pathway which can also resolve small alkyl or oxidative lesions (Caldecott, 2008). A SSB occurs when one strand of the DNA duplex is separated, usually accompanied by the loss of a single nucleotide and damage at the 5'- and /or 3'- end of the site break (Eustermann *et al.*, 2015). The SSB, consisting of 3'-hydroxyl and 5'-deoxyribose phosphate ends, is identified by the corresponding damage-specific protein. These convert the 5'- and /or 3'- termini into 5'-phosphate and 3'-hydroxyl ends, allowing the inclusion of a short (single nucleotide replacement) or long-patch (2–10 new nucleotides are inserted) (Wallace, 2014).

The most dangerous genotoxic lesion occurs through the formation of double strand breaks (DSB). A DSB arises when both strands of the DNA duplex are cut, promoting potentially lethal chromosomal rearrangements (Wright *et al.*, 2018). The two repair mechanisms that can be implemented in the repair of DSB are homologous recombination (HR) and non-homologous end joining (NHEJ) with each differing in fidelity and template requirements. The HR pathway employs an undamaged homologous chromosome as a template, leading to an error free replication of the original sequence. In contrast, NHEJ cleaves the 5'- and 3'- termini and ligates them to each other regardless of homology leading to deletions and /or insertions (Piers *et al.*, 2017; Davis & Chen, 2013).

The formation of crosslinks, either intrastrand (between bases on the same strand) or interstrand (between bases on opposite DNA strands), can be extremely toxic to cells. The formation of a usually irreversible covalent interstrand crosslink prevent the separation of DNA, halting replication. However, intrastrand crosslinks residing only on one strand are less toxic as DNA polymerases can bypass this lesion on the unaltered strand (Deans & West, 2011). Similar to crosslinks, the formation of bulky adducts within the DNA halts replication, resulting in an increase in mutagenic and carcinogenic potential. An adduct is the result of an electrophilic chemical compound (e.g. polycyclic aromatic hydrocarbon) covalently bonded to the nucleophilic site in DNA (Ewa & Danuta, 2017). The repair of crosslinks and adducts utilises nucleotide excision repair. First the DNA lesion is identified, incisions made either side, the affected oligonucleotide removed, a new sequence is then

synthesised using an undamaged complementary strand and ligated into the original sequence allowing replication to continue (Spivak, 2015; Huang *et al.*, 2016). Finally, single nucleotides can be mutated, substituted, deleted or inserted, which can occur *de novo* as well as a consequence of a compound. In general, these alterations can be resolved via the mismatch repair pathway (MMR). The MMR pathway identifies mismatched nucleotides after the formation of a new DNA strand, HR or replication, cuts are made either side of the mismatch which is removed followed by ligation of a complementary nucleotide into the sequence (Marinus, 2012).

Hence, for a novel compound to be approved by regulatory bodies for use around the world, pharmaceutical companies must follow a strict regulatory drug development process to assess a compound's ability to produce these DNA lesions. If these lesions are not resolved adequately by their associated pathways, this may lead to unintended outcomes which could cause carcinogenicity. Therefore, pharmaceutical companies must identify any potential risk a compound may have before assessment within *in vivo* subjects is conducted.

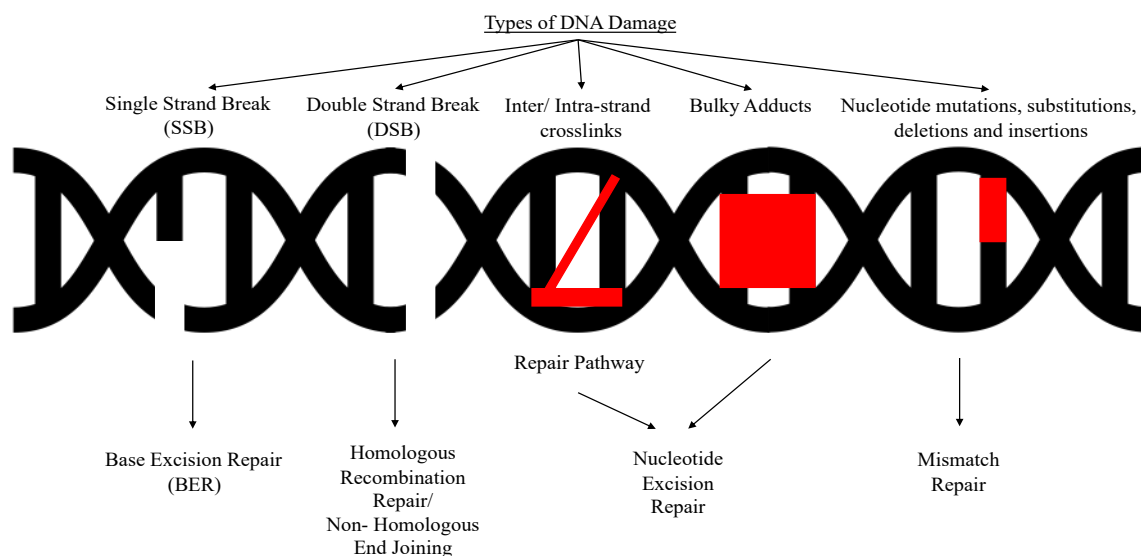


Figure 1-5. Differing types of DNA damage that can occur as a result of drug interaction. This figure has been adapted from O'Connor *et al.* (2015).

1.2.2. Regulatory testing of new compounds

Genetic toxicology is a key part of the safety assessment of new compounds in order to assess any carcinogenic risk they may possess. This testing is required for all compounds including oncology drugs, but due to their intended use are governed by a separate regulation put forward by the International Council for Harmonisation of Technical Requirements for Pharmaceuticals for Human Use (ICH) (ICH S9, 2009). Compounds recognised to have this inherent liability will not be allowed to progress into healthy volunteers or patients and are tested for evidence of genotoxicity throughout the whole development process from target selection to phase I clinical trials. To assess this risk within new compounds, governing bodies have put forward criteria in helping meet governmental regulatory requirements. The ICH has produced two options (Table 1-1) which incorporates individual *in vitro* (Table 1-2) and *in vivo* (Table 1-3) assays to produce a battery of tests (Nesslany, 2017). In order for each test within this strategy to meet governing regulations around the world, the Organisation for Economic Co-operation and Development (OECD) has created a set of guidelines. These guidelines are used by pharmaceutical companies to meet the requirements of the ICH. The pharmaceutical company AstraZeneca (AZ) has adopted option one (as it reduces unnecessary testing in animals) and routinely utilises the Ames assay, the *in vitro* micronucleus (MN) and *in vivo* MN assay.

Table 1-1. The International Council for Harmonisation of Technical Requirements for Pharmaceuticals for Human Use (ICH), strategies for genotoxicity test batteries (ICH, 2011)

	Test regime		
	i	ii	iii
Option 1	A gene mutation test in bacteria (Ames test).	A cytogenetic assay e.g. the <i>in vitro</i> micronucleus assay	An <i>in vivo</i> genotoxicity assay e.g. the <i>in vivo</i> micronucleus assay (rodent haematopoietic cells)
Option 2	A gene mutation test in bacteria (Ames test).	An <i>in vivo</i> assay in two differing tissue types e.g. micronuclei induction in rodent haematopoietic cells and an <i>in vivo</i> mammalian alkaline comet assay	

Table 1-2. An overview of standard *in vitro* genotoxic assays conducted by pharmaceutical companies (in accordance with regulatory guidelines) (Corvi & Madia, 2017).

<u>Assay</u>	<u>Cell Type</u>	<u>Brief overview</u>	<u>OECD Guideline</u>	<u>Aberration Detected</u>
Ames assay	<i>Salmonella typhimurium</i> and <i>Escherichia coli</i>	Reverse mutation of the artificially mutated -/- histidine gene.	OECD 471	Mutation
<i>In vitro</i> mammalian cell gene mutation tests using the thymidine kinase gene	TK6, L5178Y	A forward mutation in the thymidine kinase (<i>TK</i>) locus of \pm lymphoma cells.	OECD 490	Mutation
<i>In vitro</i> mammalian cell micronucleus assay	TK6, L5178Y, CHO, V79, CHL/IU	The induction of micronuclei separate from the main nucleus.	OECD 487	Chromosomal loss/ fragmentation producing a micronucleus
Comet assay	TK6, L5178Y, CHO, V79, CHL/IU	Single/ double strand breaks in DNA, quantified through amount of fragmented DNA electrophoresed from the point of origin under alkaline conditions.	There is no <i>in vitro</i> OECD guideline	DNA damage through strand breaks

CHO (Chinese hamster ovary), CHL/IU (Chinese hamster lung), TK6 (human lymphoblast), L5178Y (mouse lymphoblast) and V79 (Chinese hamster lung fibroblast)

Table 1-3. An overview of standard *in vivo* genotoxic assays conducted by pharmaceutical companies (in accordance with regulatory guidelines) (Corvi & Madia, 2017)

<u>Assay</u>	<u>Cell Type</u>	<u>Brief overview</u>	<u>OECD Guideline</u>	<u>Aberration detected</u>
Mammalian bone marrow chromosomal aberration test	Cells obtained from the bone marrow of healthy rodents (6-10 weeks old)	Asymmetrical structural chromosome aberrations within the bone marrow of rodents.	OECD 475	Changes in the structure of the chromosomes
<i>In vivo</i> mammalian alkaline comet assay	Cells obtained from the tissue of rodents	Single/ double strand breaks from fragmented DNA quantified through the amount of fragmented DNA electrophoresed from the point of origin under alkaline conditions.	OECD 489	DNA Damage through strand breaks
Mammalian erythrocyte micronucleus assay	Cells obtained from the bone marrow of healthy rodents (6-10 weeks old), specifically identifying maturing erythroblasts	The induction of micronuclei separate from the main nucleus.	OECD 474	Chromosomal loss/ fragmentation producing a micronucleus

1.2.2.1. *In vitro/ in vivo* micronucleus assay

The micronucleus (MN) assay is used to identify DNA damage in actively proliferating cells and is most commonly used in pharmaceutical studies. During normal mitosis two daughter cells are produced each with a full complement of chromosomes in their nucleus. If a compound has a genotoxic effect, the daughter cell may lose genetic material producing a secondary smaller 'micro' nucleus (Figure 1-6) (Rodrigues *et al.*, 2018). Depending on the mechanism of action of the compound the MN may contain fragments of, or whole chromosomes, which have separated from the main nuclei leading to possible carcinogenic/mutagenic events (Smart *et al.*, 2019). The *in vitro* MN assay utilises a single cell culture (either human or rodent) and is conducted within a 48 hour timescale (24 hour treatment & 24 hour recovery). If the compound is thought to be a pro-drug then the rat liver fraction (S9) is added at drug administration. In order to produce the S9 fraction, rats are treated with aroclor 1254 or phenobarbital to induce phase 1 drug metabolism enzymes such as the cytochrome P450 (CYP) family by the liver, from which the S9 fraction is taken. More specifically, aroclor 1254 or phenobarbital increases the expression of CYP1A and CYP2B isozymes but decreases the expression of CYP2C or CYP2D within the S9 fraction. However, as the S9 fraction is cytotoxic to cells, the testing regime is reduced to a 24-hour period (3hr treatment and 21-hour recovery) (Kishino *et al.*, 2019).

The *in vivo* MN assay conducted within the *in vivo* BM, utilises the development of proliferating erythrocytes in rodents to visualise this damage. Erythrocytes have no nucleus as it is extruded when the erythroblast matures. If a compound is genotoxic, when the nucleus is extruded, a MN can be clearly visible within the erythrocytes with no main nucleus (Figure 1-6 B). The visualisation of MN can give an indication of the level of genotoxicity the compound induces *in vivo* (Hayashi, 2016).

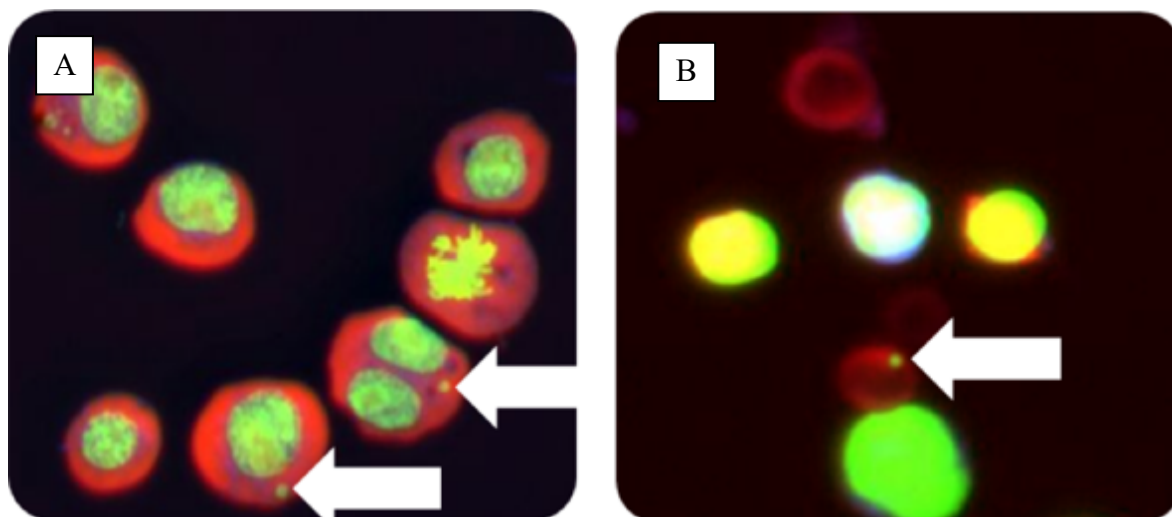


Figure 1-6. The *in vitro* and *in vivo* micronucleus assay. The *in vitro* assay (A) was performed in L5178Y cells with the white arrows identifying micronuclei. The *in vivo* assay (B) utilised cells from the bone marrow of rodents with the white arrow highlighting a micronucleus within an erythroblast (Images provided by AstraZeneca).

1.2.2.2. The mechanism by which clastogenic and aneugenic compounds induce genotoxicity and their use in the *in vitro* and *in vivo* MN assay

The MN assay, both *in vitro* and *in vivo*, are used to identify compounds which induce gross structural damage to DNA which could be the result of clastogenic or aneugenic events (Figure 1-7). A clastogenic compound affects the DNA directly by causing sections of the chromosome to be deleted, duplicated and rearranged through fragmentation (Chondrou *et al.*, 2018). A clastogenic compound will produce a MN with no centromere and daughter cells with a full complement of chromosomes but with shortened p/q arms (Hasselgren *et al.*, 2019). Conversely, an aneugenic compound doesn't affect DNA directly, instead it disrupts the cellular mechanisms around mitosis (specifically metaphase) such as disruption in spindle formation or inhibition of mitotic kinases resulting in chromosome lagging (Bernacki *et al.*, 2019). An aneugenic compound should produce a MN with a centromere, due to whole chromosome loss, and daughter cells with aneuploidy (Santovito *et al.*, 2018). As part of new compound assessment and validation, it is important to compare each new drug with a known well characterised genotoxic compound. Due to their genotoxic potential both clastogenic and aneugenic compounds are used as positive controls within the MN assay.

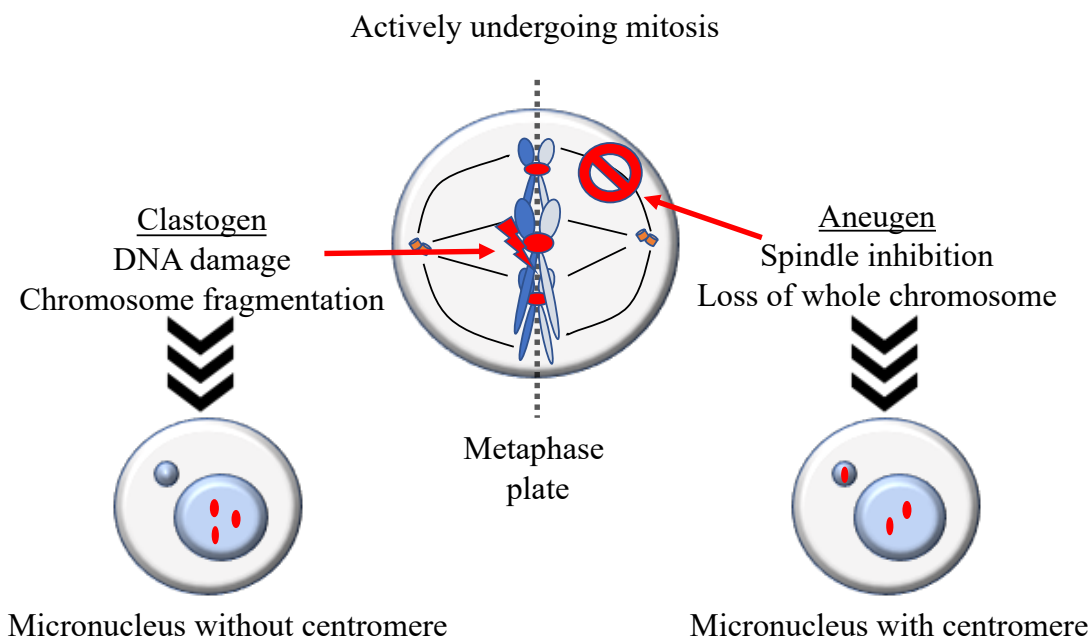


Figure 1-7. Mechanism by which clastogenic/ aneugenic compounds interrupt cellular mitosis inducing micronuclei and aneuploidy within daughter cells. This figure was drawn by the author with information provided from Kishino *et al.* (2019).

In order to measure the capability of a new compound to induce DNA damage using the MN assay, known clastogenic drugs including, but not limited to, mitomycin C (MMC), etoposide, 4-nitroquinoline 1-oxide (4NQO), cyclophosphamide (CPM) and benzo[a]pyrene (BaP) are used as a positive control routinely, with CPM and BaP requiring metabolic activation. A known aneugenic compound used in regulatory genetic toxicology is paclitaxel (Heard *et al.*, 2017). However, each compound above regardless of its clastogenic or aneugenic effect, has a different mechanism of action by which DNA damage is produced and MN created.

The antitumor antibiotic MMC, isolated from *Streptomyces caespitosus*, is used in the treatment of breast, stomach, colon, anal and bladder cancers (Amer *et al.*, 2018; Fang *et al.*, 2018). This antineoplastic compound exerts its therapeutic effect by inducing inter-strand crosslinks that alkylates double stranded DNA. The interstrand crosslinks produced between opposite deoxyguanosine residues at CpG sites, inhibit cell mitosis by blocking DNA synthesis leading to highly genotoxic DSBs (Ma *et al.*, 2013; Arranz-Marquez *et al.*, 2019; Lev *et al.*, 2017; Deans & West, 2011). Etoposide, a topoisomerase-II (TopoII) inhibitor derived from *Podophyllum peltatum*, is also used as an antineoplastic in lung, lymphoma, gastric, breast and testicular cancers (Qiu *et al.*, 2019). The TopoII enzyme uncoils DNA by

cutting both strands of the DNA helix simultaneously, causing DSB. The TopoII in the second step of the reaction re-ligates each strand of the DSB (Montecucco *et al.*, 2015). Etoposide exerts its therapeutic effect by binding to the TopoII cleavage complex attached the DSB. This binding stabilises the complex, inhibiting re-ligation and maintaining the DSB causing genotoxic and cytotoxic damage (Mehta *et al.*, 2018). The clastogen, 4NQO, is widely used in the study of DNA damage and repair to generate mutants for genetic screens (Downs *et al.*, 2014). It is a water-soluble quinoline derivative which forms stable bulky adducts on purines, primarily at the N2/ C8 positions of guanine and N6 position of adenine, leading to base pair substitution which in high numbers and left unrepaired, induces damage (Wang *et al.*, 2016; Brusehafer *et al.*, 2016).

Those compounds requiring metabolic activation include the pro-drug CPM, which is an alkylating agent used in the treatment of breast cancer, multiple myeloma and renal disease (Teles *et al.*, 2017). It is activated to its cytotoxic form, phosphoramidate mustard (PM), by the CYP450 enzymes CYP2B6, 2C19, 3A4 and 2C9 via oxidation of CPM (Kurauchi *et al.*, 2017). The resulting PM alkylates the N-7 position of guanine and forms phosphotriester monoadducts, N-7 monoadducts and N-7-guanine-N-7 guanine interstrand crosslinks. It is these crosslinks that block replication leading to DSB and cytotoxicity (Johnson *et al.*, 2012; Ganesan & Keating, 2015). The polycyclic aromatic hydrocarbon, BaP (formed through the process of incomplete combustion), also requires metabolic activation via the CYP450 enzymes (specifically CYP1A1, 1A2, 1B1 and to a lesser extent 2C9 and 3A4) to exert its clastogenic effect (Hardonnière *et al.*, 2016; Reizer *et al.*, 2019; Loss & Yu, 2018). The bioactivation of BaP requires CYP dependent epoxygenation to 7,8-dihydrodiol-9, 10-epoxide (BPDE). BPDE then reacts with DNA at the N2 position of guanine to producing an adduct at this location leading to a block in replication and DSB (Arlt *et al.*, 2008; Siddens *et al.*, 2012; Liamin *et al.*, 2017). The aneugenic compound paclitaxel, naturally produced in the bark and needles of *Taxus brevifolia*, is used in the treatment of ovarian, breast and lung cancers (Stage *et al.*, 2018; Zhu & Chen, 2019). It exerts its therapeutic effect by promoting and stabilising the assembly of microtubules during mitosis. This stabilisation of the α and β tubulin, that make up the spindle microtubules, reduces their attachment to the kinetochores of the chromatids. This in turn activates a signal cascade that delays mitotic progression leading the cell into arrest. If this cascade doesn't activate, uneven separation of chromosomes occurs leading to aneuploidy (Weaver, 2014). These compounds have been tested within both the *in vitro* and *in vivo* MN assay routinely with both tests coming back positive for genotoxicity. However, compounds can return a positive result for genotoxicity

in vivo but negative *in vitro* with no obvious clastogenic or aneugenic mechanism and thus are called pharmacological positives.

1.2.2.3. Pharmacological positives

Whilst this fundamental MN *in vitro* assay is meant to be predictive of the *in vivo* environment, AstraZeneca (AZ) noted that 16 out of 21 compounds in the last 10 years were positive in the *in vivo* MN assay but negative in the *in vitro* MN assay (Ponten *et al.*, 2013). Studies within the company found that known non-genotoxins such as glucocorticoid receptor (GR) agonists, gave a weak *in vivo* positive but were negative *in vitro*. Steroids of this nature, such as dexamethasone and prednisolone (used to reduce the formation, release and activation of inflammatory cytokines), have been on the market for a long period of time with no carcinogenic effect (WHO, 2019). Glucocorticoids (named for their effect on carbohydrate metabolism) are a class of corticosteroid (steroid hormones) that bind to glucocorticoid receptors and are generally used as anti-inflammatory agents (Kameyama *et al.*, 2018). They can be used to treat asthma, allergies, septic shock, arthritis, inflammatory bowel disease and multiple sclerosis (Ramamoorthy & Cidlowski, 2016). The glucocorticoid receptor-glucocorticoid complex up-regulates the production of inflammatory proteins via transactivation and inhibits the production of proinflammatory proteins via trans-repression (Paragliola *et al.*, 2017; Rhen & Cidlowski, 2005). Prednisolone is a short acting synthetic anti-inflammatory glucocorticoid which is four times more potent than cortisol. Dexamethasone, a long-acting synthetic anti-inflammatory glucocorticoid, however, has an affinity to its receptor seven times greater than prednisolone suppressing adrenocorticotrophic hormone levels (Ponticelli & Locatelli, 2018).

As these GR agonists are only synthetic versions of naturally occurring steroid hormones within the body, questions have been asked over the mechanism by which these compounds are giving an *in vivo* positive. One hypothesis is that the compound is influencing cellular processes, such as increased production of erythrocytes, rather than directly affecting DNA synthesis and causing a genotoxic event (Hayes *et al.*, 2013). Tweats *et al.* (2007), found when reviewing the literature that physiological disturbances could alter the induction of MN within the rodent BM. The review found that changes in the core temperature (hypo- and hyperthermia) caused an increase in MN formation. The *in vivo* BM, however, is a complex, 3D environment (as stated above), and may be the key to unlocking the true mechanisms behind pharmacological positives.

1.2.3. The protective role of the bone marrow microenvironment

The BM stroma is a metabolically competent system, and has been seen to express drug metabolising enzymes, including those of the CYP family involved in the oxidation, reduction, hydrolysis, hydration, conjugation, condensation or isomerisation of drug compounds and has been hypothesised as the cause of resistance and altered MN induction of compounds (Alonso *et al.*, 2015; Li *et al.*, 2016; Jeong *et al.*, 2009; McDonnell & Dang, 2013). The key cytochrome P450 enzymes expressed by the stroma include:

- CYP1A1: Involved in the oxidation of polycyclic aromatic hydrocarbons (PAH) to their carcinogenic state (Manzella *et al.*, 2018).
- CYP2B1: Involved in the hydroxylation of oxazaphosphorine such as CPM into the carcinogenic metabolite PM (Salazar *et al.*, 2018).
- CYP2D6: Metabolises and eliminates ~20% of over-the-counter drugs including codeine, amitriptyline, fluvoxamine, risperidone, fluoxetine, aripiprazole, paroxetine and dextromethorphan via hydroxylation, demethylation and dealkylation (Pan *et al.*, 2017).
- CYP3A4: Involved in the oxidative metabolism and mainly detoxification of ~30-40% of marketed drugs including antibiotics (erythromycin), antidepressants (diazepam) and steroids (testosterone). The expression of the enzyme has been seen to increase with the use of glucocorticoids (Fang *et al.*, 2017).

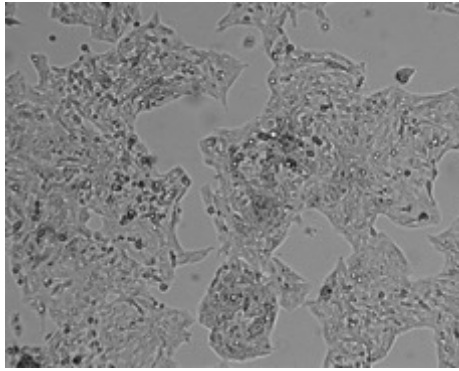
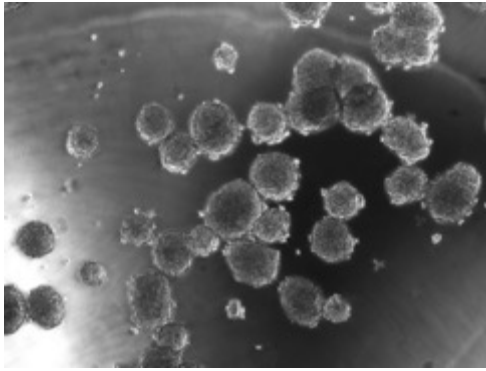
The cells used within the 2D *in vitro* MN assay (TK6 and L5176Y) do not express the CYP450 enzymes neither do they express the soluble cytokines and chemokines denoted previously within the BM (Revollo *et al.*, 2016). Therefore, in order to incorporate these soluble factors into a regulatory assay, to identify the mechanism behind alteration between the *in vitro* and *in vivo* results, a more *in vivo* relevant assay is required which combines MSC and HSC lineages upon an ECM as seen within the BM microenvironment.

1.3. The need for 3D modelling

1.3.1. 3D vs 2D cell culture

For over a decade, 2D platforms consisting of a monoculture of cells within a plastic flask, have been used in genetic toxicology to assess a compound's initial genotoxicity (Chaicharoenaudomrung *et al.*, 2019). These assays are easy to use, cheap, reproducible between laboratories and widely accepted by the governing bodies, however, they do not reflect the tissue architecture (e.g. ECM), cell-cell contact, change in oxygen content (hypoxia) and cellular necrosis seen *in vivo* (Riedl *et al.*, 2017; Lee *et al.*, 2019; Anton *et al.*, 2015). A 3D cell culture system is an artificial environment (fluidics and bioreactors) which was brought about to try to simulate the *in vivo* setting, where multi/co-cultured cells can interact with one another upon an artificial (hard or soft man-made)/ self-constructed (spheroid or organoid) scaffold in three dimensions (Huh *et al.*, 2011). The current published literature has shown that the morphology/ physiology, proliferation, drug exposure and gene expression of cells differ between simple 2D and 3D cultures (Rocha *et al.*, 2019) (Table 1-4).

Table 1-4. An overview of cellular characteristics seen in simple 2D and 3D cultures. Adapted from Edmondson *et al.* (2014), Soares *et al.* (2012) & Pickup *et al.* (2019).

Cellular Characteristics	2D	3D
Morphology	<p>Adherent cells form a mono-layer sheet along the bottom of the flask, they appear to be stretched and irregular when compared to the <i>in vivo</i> environment.</p> 	<p>Cells have begun to proliferate into a natural, spheroid structure around the aggregate.</p> <p>Cells are less stretched and appear more like the <i>in vivo</i> counterpart.</p> 
Proliferation	Cells will proliferate faster, as the culture conditions are kept stable for all cells (5% CO ₂ , 36°C) and medium can flow freely.	Cells proliferate at a reduced rate due to differing niches developing within the culture (hypoxic/ vascular) and access to medium.
Exposure	As the cells are sitting as a monolayer or free floating, every cell is equally exposed to the medium/ drug.	The medium/ drug may not be distributed to all cells especially in large spheroid cultures where the core is tightly surrounded.
Sensitivity	As the compound is applied directly to the cells the drug can be seen as extremely effective.	As the drug cannot reach all cells within the culture its effects are reduced, this is similar to responses found <i>in vivo</i> .
Expression (Gene/ Protein)	Cells have a change in the expression of genes related to adherence and morphology compared to <i>in vivo</i> .	Gene and protein expression directly correlate with that seen in the <i>in vivo</i> setting.

In a traditional 2D assay, adherent cells form a monolayer on a flat plastic surface. These cells are allowed to spread, only hindered by the size of the plastic surface, therefore increasing dramatically in size compared to their *in vivo* counterparts. This morphology allows a greater surface area of cells to receive homogenous amounts of nutrients, growth factors and compound (Jensen & Teng, 2020). Conversely within a 3D system, cells are diffused throughout with cellular projections wrapped around an artificial matrix. The distribution throughout the 3D system can reduce oxygen levels leading to hypoxic regions as is the case *in vivo*. This can change gene expression, with hypoxic cells upregulating genes in aerobic glycolysis, lactic acid production and E-cadherin whilst in the same culture as normoxic cells (Nath & Devi, 2016). This change in morphology impacts the organisation and distribution of structures within the cell affecting secretion, cell signalling, cell cycle and response to external stimuli (Kapałczyńska *et al.*, 2018; Lee *et al.*, 2019). This gradient of factors throughout the system leads to cells of differing stages of lineage, unlike 2D, with upregulation of stemness markers such as *CD133*, *Oct4*, *Sox2*, *Nestin*, *MSH1*, *MSI2*, *BMI-1* and *c-Myc* which have a marked effect on proliferation (Bodgi *et al.*, 2019; Jia *et al.*, 2018).

In static 2D culture, the monolayer of cells will only proliferate to the size of the vessel they are in. Proliferation will then cease once contact-inhibition has developed, unlike 3D, where the scaffold on which the cells sit has a larger surface area for expansion and hence allows for a longer culture time (Khurshid *et al.*, 2018; Li *et al.*, 2017). The expression of N-cadherin has a marked increase in 3D compared to 2D signifying a greater cell-cell interaction (Zhou *et al.*, 2017). However, due to the larger surface area and distribution of factors throughout 3D cellular cultures, the proliferation rate decreases compared to 2D, signified by a decreased expression of the proliferating cell nuclear antigen protein marker, but this decrease in proliferation rate aligns with the *in vivo* environment (Souza *et al.*, 2018; Edmondson *et al.*, 2014). This reduction in proliferation has been found to increase integrins such as $\beta 1$ and $\beta 4$ which serve as *in vivo* markers of polarisation and differentiation (Duval *et al.*, 2017; Zhou *et al.*, 2017). The change in morphology, distribution and proliferation affects the exposure and how sensitive a cell is to a compound.

As already mentioned, the distribution of cells throughout a 3D system and use of an artificial matrix (ECM) has an effect on a compound's toxicity, showing an increased resistance to such drugs as dacarbazine and cisplatin (Fontoura *et al.*, 2020). The bioavailability of the compound to cells throughout the system appears as a key source of

resistance and can be greatly increased by several factors (Lee *et al.*, 2018). Firstly, depending on the artificial matrix or the introduction of flowing medium, the compound can be taken up and retained, irreversibly, by the matrix reducing the concentration delivered to cells (Casey *et al.*, 2016). Secondly, those cells closest to the core of an artificial matrix have little to no uptake of the compound, unlike the outer layer of cells and those grown in 2D, which have a direct high dose (Kim *et al.*, 2019). Finally, within a 3D co-culture system, cellular enzymes such as the CYP450 family have an upregulation in detoxification genes such as *GJB6*, *AKR1C1*, *CYP1A1* and *IB1* reducing a compound's toxicity before it reaches the cells of interest similar to that seen within the *in vivo* BM (Langhans, 2018; Schmidt *et al.*, 2016).

The changes in morphology/ physiology, proliferation, drug exposure and gene expression between a 2D and 3D culture can be seen above, with the method of 3D culturing being the fundamental factor in the changes seen between 3D and 2D.

1.3.2. Common 3D culture methods used within supplementation systems

Within 3D culture systems several differing methods are used in order to create a 3-dimensional platform for which the cells can adhere and interact. These include, but are not limited to, scaffold free self-constructing spheroids, soft hydro-gels, prefabricated hard scaffolds (Table 1-5) and 3D bioprinting.

Table 1-5. Overview of current matrices for 3D culture. Extracellular matrix (ECM).

Scaffold	overview	Advantages	Disadvantages	Example	References
Spheroids	<ul style="list-style-type: none"> - Cells cultured into a 3D spheroid with cells proliferating out from a central core. - Can be achieved utilising the hanging drop method, multi-well plates, spinner flasks and matrix embedded. 	<ul style="list-style-type: none"> - Can recreate specific organ functions (liver). - Can be used for cancer modelling. - Easy to produce even in high throughput. - Can be recreated in a wide range of adherent cell types. 	<ul style="list-style-type: none"> - Drug may not reach the centre in larger spheroids. - Hypoxic core in large spheroids. - No ECM for cells to adhere and interact with. - Studies limited by spheroid size. 		<p>Fennema <i>et al.</i> (2013) Verjans <i>et al.</i> (2017) Lin & Chang (2008) Chen <i>et al.</i> (2019)</p>
Hydrogels	<ul style="list-style-type: none"> - Material with >99% water by volume. - Contains a diluted polymer and cross-linking agent. - Structure given by the induction of intermolecular crosslinks. - Can be found in nature (collagen, Matrigel, alginate) or be synthetic. 	<ul style="list-style-type: none"> - Fluid environment can protect cells and drug. - Mimics ECM. - Gel can be infused with cells/ cytokines etc. - If the gel is naturally found in the body (collagen) more <i>in vivo</i> relevant. - Can be chemically degraded to retrieve cells. 	<ul style="list-style-type: none"> - Can be mechanically weak if not adequately crosslinked. - Hard to manipulate. - Time consuming due to loading cells into the gel itself. - Difficult to sterilise. - Cells can die if cross-linker concentration is too strong. 		<p>Worthington <i>et al.</i> (2015) Weber <i>et al.</i> (2006) Chirani <i>et al.</i> (2015) Kovisto <i>et al.</i> (2019)</p>
Solid Scaffolds	<ul style="list-style-type: none"> - Fabricated from a wide range of materials such as metal, ceramic, glass and polymers (PCPU) each with differing properties. 	<ul style="list-style-type: none"> - Strong rigid scaffold which is easy to handle and sterilise. - Mimics ECM. - Each scaffold is uniform to the next as microspores aren't chemically induced. 	<ul style="list-style-type: none"> - Hard to get all cells out of the scaffold. - Scaffold could chip or break. - Cells cannot be incorporated into the scaffold itself. 		<p>Knight & Przyborski (2015) Campuzano & Peeling (2019)</p>

1.3.2.1. The use of scaffold free spheroids for 3D culture

The spheroid is a self-assembling aggregate of adherent cells, binding together to form a 3D structure without the need for an artificial scaffold at its core (Zuppinger, 2019). Due to the cell-cell contact and morphology formed within a spheroid, alterations in metabolism and signalling pathways are unaltered, unlike in a 2D culture where cells are spatially separated and flat against the plate. Spheroids can be manufactured using several different methods as indicated by Sant & Johnston (2017):

- Matrix embedded/ encapsulated: A small aggregate core of cells is suspended into a medium such as agarose, Matrigel or hydrogel and allowed to proliferate over time around the core.
- Ultra-low attachment plates: Cells are added to culture plates with a non-adherent surface to prevent them adhering to the plate, they instead adhere to one another. Similar to a spinner flask, a gyrating plate can be used to ensure that cells only adhere to one another.
- Hanging drop: A cellular population in medium is added as a single drop to a plate. The plate is then inverted or forced through a micropore creating a hanging drop. This drop utilising gravitation force to congregate the cells at the tip, with nothing to adhere to, cells instead adhere to one another.

The most common spheroid in use utilises human hepatocytes (HepG2 cells) in order to form an artificial liver structure. The liver spheroid has been found to have increased expression of CYP450 enzymes, which is maintained over a 35-day period, when compared to that of the 2D counterpart (Kozyra *et al.*, 2018). However, spheroid size needs to be tightly controlled depending on the eventual outcome needed from the assay. A 48 hour long culture can generate a small spheroid (200µm in diameter) of a uniform size and homogeneity, a culture time of > 4 days will generate a large heterogeneous spheroid (>500 µm in diameter). As cells expand from the core and the spheroid becomes larger, the gradient of oxygen and nutrients reduces to the core. Larger spheroids (>500 µm in diameter) become hypoxic and then necrotic at the core producing a spheroid consisting of cells of different proliferation kinetics, thereby making these suitable for pathophysiological studies only (Nath & Devi,

2016). Due to the limit on cell number and size required with spheroids, the use of artificial scaffolds has been seen as more beneficial but still with limitations.

1.3.2.2. The use of hydrogels and prefabricated hard scaffold for 3D culture

Hydrogels are soft and elastic structures, typically made of 98-99% aqueous media, consisting of a dilute polymer or naturally occurring protein which is crosslinked to form a rigid scaffold (Anderson *et al.*, 2015). Hydrogels can be produced using many differing materials, depending on the assay, including but not limited to:

- Gelatin-methacryloyl (GelMA): GelMA is a hydrogel obtained by the derivatisation of biocompatible gelatine with methacrylic anhydride, resulting in modification of lysine and hydroxyl residues with methacrylamide and methacrylate side groups. The GelMA hydrogel is then subjected to ultraviolet light (UV) which initiates polymerisation resulting in covalent crosslinks producing a gel which is transparent and stable at physiological temperatures. However, due to the use of UV light, cells cannot be incorporated into the gel before crosslinking (Pepelanova *et al.*, 2018)
- Matrigel: Matrigel is a natural, reconstituted basement membrane-derived extract secreted from the Engelbreth-Holm-Swarm mouse sarcoma tumour. Cells are incorporated into the matrix and left to proliferate over time however, due to its soft gelatinous nature Matrigel is hard to manipulate long term (Nguyen-Ngoc *et al.*, 2014)
- Alginate: Alginate, naturally found in the cell walls of brown algae, is a linear polysaccharide. It can be crosslinked via chelation of divalent cations such as calcium chloride and can also be fully dissolved. The resulting hydrogels can encapsulate cells, without damage, for long term cell culture (Armstrong *et al.*, 2016).

The new field of bioprinting can incorporate these hydrogels, in the form of bioinks, with and without the inclusion of cells, growth factors and signalling molecules into a scaffold with exact pore sizes in any design or shape to suit the assay needs (Kim *et al.*, 2019). Hydrogel materials, before crosslinking, such as gelatine, collagen, HA and alginate, are added as semi-solid bioinks into the 3D printer (Jia *et al.*, 2016). The bioink is then deposited

onto the printing bed layer-by-layer utilising a micro-extrusion printing nozzle (Berg *et al.*, 2018). The bed is heated to 37 °C so that the bioink semi-solidifies on contact before the addition of further layers. Once printed the semi-solid structure can be crosslinked with the relevant agent (Cidonio *et al.*, 2019). As hydrogels require some form of reaction to create a rigid structure and the structure may not last prolonged culture, prefabricated solid scaffolds have also been seen as an alternative 3D matrix.

Prefabricated solid scaffolds do not require chemical or enzymatic crosslinking in order to create a scaffold, instead they are usually made out of solid, man-made materials and arrive ready to use. Due to this, cells cannot be incorporated into the scaffold itself but only adhere to it. However, as these are mass manufactured from man-made materials, pore-size, total size and rigidity is kept constant (Salerno *et al.*, 2019). These types of scaffold can be made utilising, but not limited to, materials such as hydroxyapatite (ceramic calcium phosphate composite) which is poured into moulds as a slurry and left to set, nanofibres (electrospun to mimic the ECM), polycarbonate polyurethane-urea (PCPU), glass and metal (Koski *et al.*, 2018; Wang *et al.*, 2017; Zhang *et al.*, 2016). Each scaffold above has the capacity to allow cells to adhere and proliferate in a 3D environment. However, an appropriate system to deliver medium supplementation and simulate the *in vivo* conditions is required.

1.3.3. 3D culture supplementation systems

A 3D culture supplementation system is required to simulate the *in vivo* environment as close as possible, *in vitro*, by controlling temperature, pH, medium flow rate, oxygen, nutrient supply, and waste metabolite removal for cells residing on the scaffold. The selection of a culture system requires an analysis of what produces an *in vivo* environment but is also easily reproducible and cheap for any laboratory to use. Current 3D culture systems can be broadly defined as static or fluidic.

A static culture system involves the incorporation of a 3D scaffold into a flask or well plate, covered in medium containing cells and left to incubate. This system is easy to replicate between laboratories, requires no other external pumps or filtration systems and thus is cheaper to set up than modern fluidic systems (Kutscher *et al.*, 2019). However, as there is no movement of the medium within the system, cells are exposed to a constant drug dose, accumulation of waste products and metabolites throughout the entirety of the study (Tsai *et al.*, 2019). This can be combated with regular medium changes with or without a rocker

system for a gentle flow, but this could alter cellular communication established within the culture and requires further expense.

A fluidic system, unlike a static, requires some form of medium movement, which can be created in a number of ways, such as pumps, rotation, mixing in an effort to simulate the sheer force seen within the *in vivo* environment. However, if the sheer force is too great cells will be removed from the scaffold or apoptose, and if sheer force is too small, it won't recreate the force necessary to express the associated growth and signalling pathways (Khurshid *et al.*, 2018). Several systems have been used within the published literature to recreate this, including but not limited to, bioreactors and microfluidics. The bioreactor has been adapted for 3D culture and has precise control of all factors mentioned above. Bioreactors fall into four categories rotating wall vessel, direct perfusion, mechanical force and spinner flasks each inducing a fluidic environment (Anton *et al.*, 2015; McKee & Chandhry, 2017; Izzo *et al.*, 2019; Schmid *et al.*, 2018)

Similar to direct perfusion bioreactors, microfluidic systems provide a constant stream of nutrients, oxygen and sheer force to cells through micro-channels (100 nm-500 μm) in some cases removing waste products (Chen *et al.*, 2018). This system still requires the use of a medium reservoir, pump and polydimethylsiloxane tubing (used for its ease of use, gas permeability and low cost) to create the fluidic system. Due to their relatively small size, microfluidic devices can be integrated into downstream analytical devices such as electrochemistry and spectroscopy without altering cellular processes (Castiaux *et al.*, 2019). Recently, microfluidics has been used to try to create an organ/ human-on-a-chip. These culture systems try to simulate the structure, function, physiology and pathology of that specific organ *in vitro* by combining cell culture and microfluidics. The eventual goal of this combination is to connect each organ together for pharmacodynamic and pharmacokinetic study (Bein *et al.*, 2018). However, there are many setbacks that individual organ chips can overcome, unlike a whole-body system, as cells within differing organs require different media supplementation, multiple pumps and tubing which is costly and cells of differing organs require changes in sheer pressure (Kimura *et al.*, 2018). Every culture system has their advantages and disadvantages but how complex and expensive does a 3D system need to be to gain results similar to that seen *in vivo*?

1.3.4. Current 3D models of the bone marrow for genetic toxicology testing.

Research into the use of 3D cell cultures within the toxicology industry has grown exponentially over the past decade as increasing publications highlight the similarities between cells cultured in an *in vitro* 3D model and those within an *in vivo* animal/ human. The current literature highlights the advanced development of static toxicity models of the liver, brain, kidney and skin, combining conventional toxicology assays with cutting edge 3D scaffolds and culture systems (Duque-Fernandez *et al.*, 2016; Reisinger *et al.*, 2018; Fizesan *et al.*, 2019; DesRochers *et al.*, 2015; Salama *et al.*, 2018; Zhou *et al.*, 2019).

The field of BM toxicology specifically genetic toxicology, however, seems to be lacking for such a crucial organ. The current literature, in an effort to replicate the delicate microenvironment seen within the *in vivo* BM, first employs the use of primary human MSC monocultures in static models upon simple scaffolds such as Matrigel, collagen, hydroxyapatite, gelatine and scaffold free spheroids (Yeung *et al.*, 2019; Inglis *et al.*, 2019; Yu *et al.*, 2018). Further research utilises primary MSCs as a feeder layer upon the scaffolds previously mentioned. Primary human/ animal HSCs from both normal and diseased states (e.g. multiple myeloma) are then co-cultured within bioreactors and microfluidics in order to gauge the response of drug treatments, including pro-drugs, without the need for S9 as MSC derived cells have been seen to be metabolically competent (Elango *et al.*, 2019; Braham *et al.*, 2018; Fairfield *et al.*, 2019). These types of multi/ co-culture have shown drug response and differentiation into both lymphoid and myeloid lineages similar to that of the *in vivo* setting but with varying degrees of reproducibility from assay to assay (Sieber *et al.*, 2018; Sun *et al.*, 2011). Human primary cells, those directly isolated from the *in vivo* tissue, retain their morphological and functional characteristics of the multicellular tissue, thus, seem like a good start in recreating an *in vivo* relevant *in vitro* model. However, primary cells can differentiate naturally which can hinder reproducibility of an assay between cultures and laboratories due to their heterogeneity. As they are directly taken from the tissue of interest, primary cell cultures are more costly compared with their cell line alternative (Paster *et al.*, 2010; Stacey, 2006). The use of primary cultures in a 3D environment has become extremely useful but due to a lack of reproducibility and the high cost of bioreactors and microfluidic systems, these are not a viable option for routine genotoxicity studies of new compounds.

To combat the lack of reproducibility and to decrease overall cost whilst still providing a 3D environment for cellular cultures, the use of cell lines has gained increasing interest. Cell lines, unlike primary cultures, are cells which have been taken from the tissue of interest and genetically immortalised, either through viral or cancerous manipulation, at a specific stage in differentiation. This allows long term culture of cells which have homogeneity with each sub-culture at a greatly reduced purchase cost. However, due to this genetic manipulation, cell lines may not accurately depict the primary cells from which they were taken (Kaur & Dufour, 2012). The human bone marrow stromal cell line HS-5, virally transformed by the human papilloma virus, has been used routinely as a surrogate for primary MSC-derived fibroblasts. The HS-5 cell line, when seeded onto artificial scaffolds in static cultures, has similar gene expression and resistance to drugs such as melphalan compared to primary fibroblasts (Kabrah *et al.*, 2016; Limongi *et al.*, 2020; Windus *et al.*, 2013). This cell line, however, has only been used in combination with normal or cancerous primary HSC (Belloni *et al.*, 2018; Bartnicka *et al.*, 2018; Karimpoor *et al.*, 2018).

In commercial 2D MN genotoxic assessment of compounds, the human TK6 or mouse L5176Y lymphoblastoid cell line is used to replace the erythroblast/ erythroid cells assessed for MN within the *in vivo* assay due to their proliferation rate. However, as mentioned previously TK6 do not express cytokines, chemokines and metabolic enzymes seen within the *in vivo* BM microenvironment. To predict the response *in vivo*, the *in vitro* assay must simulate the necessary components of the BM to uncover the mechanism behind this alteration between *in vivo* and *in vitro* results. As the TK6 cell line has been routinely used for regulatory genetic toxicology due to its proliferation time and sensitivity to genotoxic compounds, it has an archive of historical data for comparison. Therefore, these appear to be a suitable foundation for the addition of BM cell lines and ECM in an effort to simulate the *in vivo* environment, as an *in vitro* model.

1.4. The focus of this current study

This research will aim to develop a reproducible, 3D *in vitro* physiologically relevant model of the human BM *in vivo* using a co-culture of commercial cell lines (HS-5 and TK6) for MN assessment of compounds. The results gained from this *in vitro* model will be compared to those gathered from standard *in vitro* and historical *in vivo* testing to ascertain whether our model is more *in vivo* relevant than conventional 2D testing.

1.5. Aim

1. To develop a static *in vitro* model of the human BM, utilising a co-culture of cell lines which are viable and proliferating upon a novel commercially available scaffold.
2. To expose the model to known positive genotoxic compounds, negative compounds, and pharmacological positive compounds and compare these results to historical *in vivo* and 2D MN data.
3. To characterise the model's expression of phase 1 and 2 metabolic enzymes, seen *in vivo*, and HS-5's ability to metabolise the pro-drug CPM into its cytotoxic form without the use of S9.

1.6. Objectives

To meet aim one

- Prefabricated solid scaffolds and hydrogels will be evaluated for relevant morphology and ease of manipulation.
- HS-5 culture conditions such as seeding density, culture time, retrieval of cells and proliferation index will then be assessed and optimised for the addition of TK6 cells, to model the current *in vitro* MN testing.
- TK6 in co-culture with HS-5 cells, upon the scaffold, will be assessed and optimised for seeding density, culture time, retrieval of cells and proliferation index for compound dosing during the exponential phase of TK6 cell growth for MN production.
- Analysis of markers residing on TK6 only will be identified for separation of TK6 cells from HS-5 for MN assessment.

To meet aim two

- Known positive, negative and pharmacological positive genotoxic compounds will be assessed in a 2D *in vitro* MN assay, utilising TK6 for MN induction at a range of concentrations spanning an RPD of >50% and <50%.
- The optimised 3D co-culture model, utilising TK6 and HS-5 cells, will be exposed to each compound concentration tested within the 2D *in vitro* MN assay, to elucidate

if 3D can identify MN production seen with historical *in vivo* data not identified within 2D.

To meet aim three

- HS-5 cells grown in a 2D monoculture, 2D well insert co-culture (with TK6), 3D scaffold monoculture and 3D co-culture (with TK6), will be extracted for RNA and analysed via qPCR for the expression of genes relating to phase 1 and 2 metabolic enzymes.
- TK6 with and without co-cultured HS-5 cells or S9 will be exposed to CPM for changes in cytotoxicity.

Chapter Two

Materials and Methods

2. General Methods

2.1. Materials

All reagents, unless otherwise stated, were purchased from Sigma-Aldrich (Poole, UK). To align experimental approaches and normalise data between University of the West of England (UWE) and AZ, for the purposes of comparing outcomes in the 3D BM model with historical data, several experiments were conducted at both AZ and UWE and where relevant will be highlighted.

2.2. Tissue culture

All cell cultures were seeded into T-75 vented flasks and incubated at 37°C, 5% CO₂ in a humidified chamber. All cultures were grown in RPMI 1640 supplemented with 10% heat inactivated foetal bovine serum, L-glutamine (2 mM), penicillin (100 U/ml) and streptomycin (100 µg/ml) and will be referred to as complete medium. The human bone marrow stromal cell line, HS-5, was acquired from American Type Culture Collection (ATCC) (LGC standards, Bury) and grown as an adherent monolayer at an initial seeding density of 1.3×10^4 cells/cm². Medium was demi-depleted every two days and cells passaged every four days at a density of 4×10^3 cells/cm². Culture time did not exceed passage 6. As the surface area of the scaffolds was unknown, once the HS-5 adherent monolayer was trypsinised, HS-5 cells were seeded as cells/scaffold not cells/cm². The human lymphoblastic B cell line, TK6, was acquired from AZ (Cambridge, UK) and grown in suspension at an initial seeding density of 3×10^5 cells/ml. These cells were originally purchased by AZ from the European Collection of Cell Cultures (cell number 95111735). Cultures were maintained at a concentration between 3×10^5 and 9×10^5 cells/ml. Culture time did not exceed four weeks to reduce the accumulation of mutations through prolonged culture. The human liver carcinoma cell line, HepG2, was acquired from ATCC (LGC standard, Bury) and grown as an adherent monolayer at an initial seeding density of 1.3×10^4

cells/cm². A 50% medium change was conducted every two days and cells passaged every four days, at a density of 4x10³ cells/cm². Culture time did not exceed passage 11.

2.2.1. Cell count and viability

Cell counts at UWE were assessed using a haemocytometer chamber and Luna-FL™ automated fluorescence cell counter (Labtech International Ltd, East Sussex, UK). Cell counts at AZ were conducted using the Beckman Coulter Counter (Beckman Coulter, Indianapolis) and Countess II (ThermoFisher Scientific, Loughborough). Counts were compared between UWE and AZ for consistency between the two laboratories. Cell count and viability was determined using trypan blue (TB) utilising the Luna-FL™ automated fluorescence cell counter at UWE and Countess II at AZ. TB enters cells that have a compromised membrane, using a 1:1 dilution (10µl of sample and 10µl of TB). The Beckman coulter counter does not assess cell viability but only particles and thus was only used for the 2D micronucleus assay at AZ, as this is done routinely within the company.

2.2.2. Identifying TK6 exponential phase in 2D

The TK6 cell line was cultured utilising the method outlined in section 2.2 for a seven-day period. The cells were seeded into T175 flasks at a seeding density of 5x10⁴ or 1x10⁵ cells/ml in 25 ml of medium and grown over a five-day period with samples taken at 11am and 5pm each day. At each sampling point the flask was gently mixed and an aliquot (10 µl) was taken from each flask to assess cell number and viability using TB. Population doubling (PD) was calculated using the following equation from the OECD guideline 487 (2016):

$$PD = \frac{\text{Time between samples} \times \log 2}{\log (\text{count two}) - \log (\text{count one})}$$

2.2.3. Cryopreservation and thawing of cell lines

All cell lines were batch cultured at low passages (1-3) before being cryopreserved. Cells were counted, collected by centrifugation (300 xg, 7 minutes) and the pellet resuspended in FBS (50%) rich culture medium and ice-cold freezing medium containing DMSO (20%) in

a 50:50 ratio to a density of 1×10^6 cells/ml. Cells (1ml) were transferred to 2 ml cryovials, frozen for 24 hours at -80°C before being transferred to liquid nitrogen. Cell lines were thawed using 5 ml of warmed complete medium, added dropwise until the cell pellet was resuspended. Cells were collected by centrifugation (300 xg, 7 minutes) and resuspended in T75 cm^2 flasks in 20 mls of complete medium.

2.2.4. Trypsinisation of adherent cells

When adherent cell lines (HS-5 and HepG2) reached a confluence of 80 – 90%, the medium was completely removed, cells washed twice with phosphate buffered saline (PBS) and 0.25% trypsin in EDTA added to cover the base of the flask. Flasks were incubated (37°C , 5% CO_2) for <10 minutes, until 100% of the cells had detached from the flask identified through light microscopy. Complete medium was added to a total volume of 15 ml to deactivate the trypsin, cell suspension harvested and centrifuged at 350 xg for 7 minutes. The cell pellet was resuspended in 1ml of complete medium and counted using the method described in section 2.2.3.

2.3. The finalised AlgiMatrix™ scaffold seeding protocol

2.3.1. Initial HS-5 seeding and long-term culture

HS-5 cells were seeded onto AlgiMatrix™ scaffolds at 2.5×10^5 cells in 500 μl of 50 % firming buffer, which was supplied by the manufacturer in order to solidify the AlgiMatrix™ scaffold, transferred to a 12 well plate, 3 ml complete medium added and left to incubate for 24 hours. After 24 hours a 100% complete medium change was conducted with scaffolds incubated for a further 144 hours with a 50% medium change conducted every 48 hours.

2.3.2. Addition of TK6 cells

After the initial seeding of HS-5 described in section 2.3.1, TK6 were then combined with each AlgiMatrix™ scaffold at an initial concentration of 0.5×10^5 cells/ml. A 50% medium change was conducted every 24 hours over a 72 hour period, compound dosing was then conducted on hour 72.

2.4. Flow cytometry

A brief overview of the fluorescent antibodies used within the body of work can be found in Table 2-1. The staining protocol for intracellular (Ki67), membrane bound and confocal staining (CD19 and CD20) differed, therefore reference to the location of these staining methodologies can also be found in Table 2-1. In order to assess the presence or absence of the fluorescent antibodies described in Table 2-1, a gating strategy was first employed to isolate single cells and exclude doublets and cellular debris. The criteria used to gate cells was adapted from Saskia (2015), utilising the side vs front scatter strategy seen in Figure 2-1. The population of interest was first identified using a side scatter (SSC) area vs forward scatter (FSC) area plot discarding debris or cellular remnants. This population was then further gated by granulation (SSC area vs SSC height) and then size (FSC area vs FSC height) to reduce contamination from doublets before assessing the population for the presence or absence of antibody fluorescence (for antibodies see Table 2-1). Flow cytometry was conducted on a Fortessa utilising the FACSDiva software at AstraZeneca and the Accuri C6, with accompanying software at UWE (Becton Dickinson (BD), New Jersey).

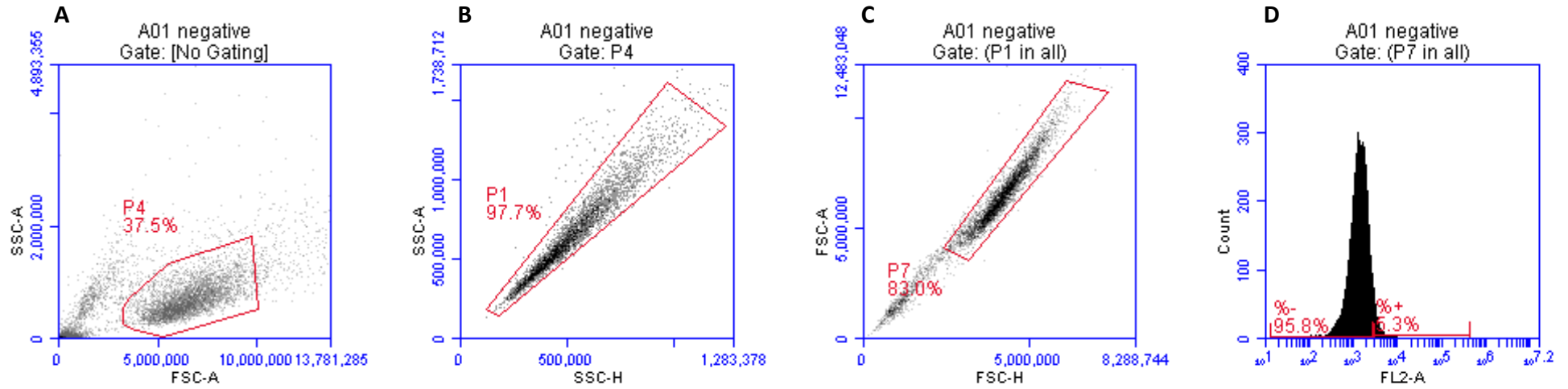


Figure 2-1. Flow cytometry gating strategy. The cellular population of interest was first identified using a side scatter (SSC) area vs forward scatter (FSC) area plot (A). This population was then further gated by granularity (SSC area vs SSC height) (B) and size (FSC area vs FSC height) (C) before assessing the population for the presence or absence of fluorescence (D).

Table 2-1. Details of the antibodies used for flow cytometry and confocal microscopy.

Marker	Description	Dilution antibody/ FACS buffer	Manufacturer and catalogue number	Location of staining methodology
Ki67 (flow cytometry)	Mouse anti-human, IgG ₁ , monoclonal to Ki67, PE conjugated, 5 µl/test.	1/20	ThermoFisher Scientific 12-5699-42	Section: 3.2.2.2.2
CD19 (flow cytometry and initial confocal work)	Mouse anti-human, IgG ₁ , monoclonal to CD19, FITC conjugated, 20 µl/test.	1/20	BD 555412	Section: 3.2.2.2.4
CD20 (flow cytometry and initial confocal work)	Mouse anti-human, IgG _{2b} , monoclonal to CD20, PerCP-cy 5.5 conjugated, 5 µl/test.	1/20	BD 560736	Section: 3.2.4.1.2
CD19 (confocal)	Primary: Mouse anti-human, IgG _{2a} , monoclonal to CD19, unconjugated, 100 µl. Secondary: Goat anti-mouse, IgG, polyclonal, Alexa Fluor® 488 conjugated, 500 µg.	Primary: 1/250 Secondary: 1/200	Abcam, Cambridge Primary: ab31947 Secondary: ab150113	Section: 3.2.4.1.3
CD20 (confocal)	Primary: Mouse anti-human, IgG _{2a} , monoclonal to CD20, unconjugated, 200 µl. Secondary: Goat anti-mouse, IgG, polyclonal, Alexa Fluor® 488 conjugated, 500 µg.	Primary: 1/50 Secondary: 1/200	Abcam Primary: ab9475 Secondary: ab150113	Section: 3.2.4.1.3

FACS (fluorescence-activated cell sorting buffer)

2.5. Microscopic examination

Light and phase contrast microscopy was used to assess the morphology, distribution and identification of cellular colonies, spheroids and MN within sample populations. As light was able to pass through the AlgiMatrix™ scaffold, cellular morphology, distribution and identification of cellular colonies was also conducted with those cells residing on the scaffold. Microscopic images were taken utilising a Nikon Eclipse TE300 microscope with an attached Nikon Coolpix 950 camera.

2.6. Screening of positive, negative and potential genotoxic compounds in 2D.

In order to make a comparison between 2D and 3D *in vitro* MN results, each compound was assessed using the *in vitro* MN assay (IVM) following OECD 487 (2016) guidelines for MN induction. It was hypothesised that a higher concentration would be required when moving each compound into a 3D model. Therefore, a greater concentration of each compound was tested using the IVM to assess cytotoxicity.

2.6.1. Industrial *in vitro* micronucleus assay

TK6 cells in exponential phase (3×10^5 - 9×10^5), identified in section 2.5.1.1 were seeded into T25cm² flasks at 1×10^5 cells/ml and a baseline cell count recorded to confirm the seeding density. Following culture for 24 hours, cells in ‘baseline flasks’ were counted to ensure that TK6 cells were within the exponential phase (3×10^5 - 9×10^5) and thus are actively proliferating. Cells were treated with the vehicle control of <1% DMSO or drug for 24h. After treatment, the cells were collected by centrifugation (300 x g, 5 minutes, room temperature (RT)), washed once in fresh complete medium before being counted and adjusted to 3×10^5 cells/ml. Cells were maintained for a further 24 hours to allow them to complete cell cycle, counted and an RPD calculated. Utilising the OECD guideline 487 (2016):

RPD was determined as:

$$\frac{\text{number of population doublings in treated cultures}}{\text{number of population doublings in control cultures}} \times 100$$

Where population doubling (PD) is calculated:

$$\frac{[\log(\text{post treatment} / \text{initial cell number})]}{\log 2}$$

Cell cultures with an RPD of $>50\% \pm 5\%$ (OECD, 2016) were adjusted to 1×10^5 cells/ml ready for addition to cytofunnels. Cells were spun onto the glass slides utilising a cytospin 3 (Shandon, ThermoFisher) at 800 rpm for 8 minutes, fixed in 100% methanol (10 minutes, RT), stained for 1 minute with acridine orange (AO) (12mg/ 100ml phosphate buffered saline (PBS), RT), washed once for 10 minutes in PBS then washed again in fresh PBS for a further 15 minutes.

To keep in-line with regulatory bodies, the OECD guideline 487 (2016) was utilised in performing the MN assay at both UWE and AZ. The main criteria adopted within this guideline are as follows:

1. A dose which can be scored for MN induction must have an RPD of $>50\% \pm 5\%$; an RPD lower than this cannot be scored as MN induction cannot be clearly differentiated from apoptosis.
2. At least one dose per compound must induce an RPD of $50\% \pm 5\%$, this shows that the compound has been tested to its cytotoxic limit.
3. Four doses must be scored per compound (excluding the negative and positive control) for the MN result to be accepted.
4. A total of 2000 mononucleated cells per culture must be scored for the presence of MN, for a concentration to be deemed as “scored”.
5. If all other criteria are met, a positive result for a compound can be called if the MN induction is at least double that of the negative control.
6. When reporting results, concentration of compound should be expressed as ng/ml and/or nM.

These OECD guidelines were followed closely when identifying a greater concentration of each compound for use in the 3D model. However, as the RPD $<50\% \pm 5\%$ (guideline 1), MN could not be differentiated away from apoptotic cells, therefore scoring was not conducted.

2.6.2. Scoring of micronuclei

The criteria utilised for scoring of MN and mononucleated cells was adapted from the Fenech (2003) paper and was as follows:

1. MN has a diameter of less than one third of the main nucleus, any bigger is considered a binucleated cell.
2. MN have a round or oval morphology.
3. MN will not refract light unlike other artefacts within the culture.
4. MN cannot be counted if they are connected to the main nucleus.
5. A clear boundary must be seen between the main nucleus and the MN to be counted.
6. Those cells going through mitosis will not be counted.
7. MN will have a similar colouration and fluorescent intensity as the main nucleus

Common morphologies seen when assessing the presence of MN can be seen in Figure 2-2.

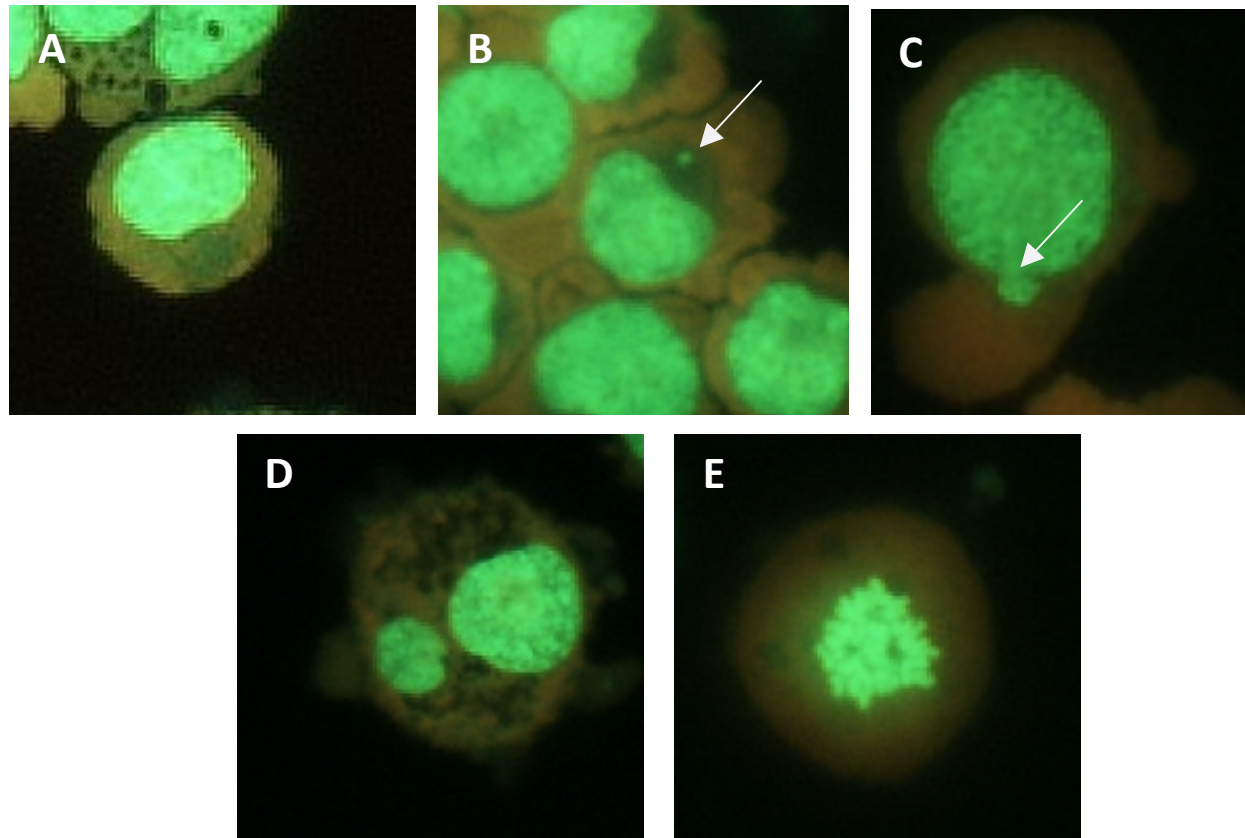


Figure 2-2. Photomicrographs of the characteristic morphologies identified when scoring MN. The addition of acridine orange identifies nucleic material as fluorescent green and cytoplasm as light orange. A mononucleated cell (A), micronucleated cell with micronucleus (arrowed) (B), mononucleated cell with attached micronuclei (arrow) (C), binucleated cell (D) and mitotic cell (E). All images at x 40 magnification.

2.7. Statistical Analysis

All values are presented as mean \pm standard deviation (SD) of 3 biological repeats, unless otherwise stated. All statistical analysis and graphical illustrations were conducted using raw data inputted into GraphPad Prism 7.0 software. Firstly, all samples were analysed for normal distribution using the Shapiro-Wilk test. A Two-Way ANOVA was used to compare samples in chapter 3 and 4 for simple effects within rows, followed by a Dunnett's test to identify pairs with significant differences. A One-Way ANOVA, followed by a Dunnett's test was also used in chapter 4 to identify significant increases in micronuclei from the vehicle control. Within chapter 5, statistical comparisons between results obtained with CPM were performed using a Two-Way ANOVA followed by a Tukeys test to correct for multiple comparisons. The difference between means within the qPCR data was calculated based on a Student's t-test of the replicate $2^{(-\Delta CT)}$ values for each gene in the control group and treatment groups. A p-value of ≤ 0.05 was considered significant. Graphical symbols of significant difference were identified as (*) $p < 0.05$, (**) $p < 0.01$, (***) $p < 0.001$, (****) $p < 0.0001$.

Chapter Three

3. Developing a 3D model of the bone marrow using commercial cell lines

3.1. Introduction

The development of a 3D physiologically relevant model of the BM, which truly reproduces the interaction between cellular groups seen *in vivo*, for use in genotoxicity testing is the eventual aim of this research. The complexities seen within the BM, such as the interaction between haematopoietic, mesenchymal stem cells and ECM (Jagannathan-Bogdan & Zon, 2013) isn't seen in a monolayer 2D environment currently adopted by the pharmaceutical industry. This harmonisation between compartments of the BM, discussed within chapter 1, has been attributed to changes in compound interaction, stromal mediated protection and altered genotoxicity (Torisawa *et al.*, 2014; Ciciarello *et al.*, 2019). However in order to evaluate the influence that these cellular interactions might have on a compound's genotoxicity in producing inconsistency between *in vitro* and *in vivo* study, the production of a 3D BM microenvironment *in vitro* is required.

The development of a more *in vivo* relevant, *in vitro* BM model has been ongoing for the past decade, with each model increasing in complexity in order to identify the true response and mechanism to new and existing compounds (Ham *et al.*, 2019). The utilisation of culture systems (fluidic, bioreactor etc), cells (primary, cell lines) and ECMs (soft, hard etc), each with their own advantages and limitations, discussed in chapter 1, has increased our understanding of the *in vivo* response to compounds (Ravi *et al.*, 2015; Hoch *et al.*, 2017). However, is this level of complexity required for reproducible testing of compounds for genotoxicity, whilst replicating an *in vivo* environment *in vitro*?

In brief, three artificial scaffolds were chosen, from those identified in Table 1-5, as potential surrogate ECMs for the addition of each cell line. These scaffolds consisted of the biocompatible polycarbonate polyurethane-urea scaffold, Biomerix, commercial hydrogel scaffold AlgiMatrix™ and in-house alginate hydrogel documented in the Armstrong *et al.*

(2016) paper. The Biomerix scaffold was chosen as it was already in use at UWE with successful initial seeding of the HS-5 stromal cell line. The commercial scaffold AlgiMatrix™ made primarily of crosslinked alginate, was chosen due to its ability to encapsulate cells within, which can then be dissolved allowing their retrieval after compound dosing. As it was made by a large commercial manufacturer, batch to batch reproducibility was granted. Finally, the in-house alginate hydrogel was chosen as, unlike the similar AlgiMatrix™ scaffold, it had known components which could be assessed for toxicity and influence on scaffold morphology in comparison to the AlgiMatrix™ scaffold. The in-house alginate hydrogel could also be used in conjunction with a bioprinter for the production of bespoke scaffolds.

The human stromal HS-5 and lymphoblastoid cell line TK6 were chosen for eventual addition to each scaffold. The HS-5 cell line was chosen as it is the only non-cancerous human BM stromal cell line currently on the market (Adamo *et al.*, 2020). The TK6 cell line was chosen as it is routinely used in *in vitro* genetic toxicology due to its proliferation rate, p53 competency and sensitivity to compounds (section 1.3.4). As a protocol was already in place at UWE for the seeding of HS-5 cells onto Biomerix scaffolds, the reproducibility of this seeding method was first assessed and optimised in an effort to maintain an increased density of HS-5 on the scaffold. However, optimisation of the hydrogel scaffolds was required before the addition of either cell line.

The hydrogel scaffolds both in-house and commercial (AlgiMatrix™), unlike the pre-constructed Biomerix, required solidification with either a firming buffer (AlgiMatrix™) or CaCl₂ solution creating divalent crosslinks. The percentage of either firming buffer (10, 25 and 50%) or CaCl₂ (100 - 1000 mM) would alter the mechanical properties and structure of the finalised scaffold. Therefore, increasing concentrations of firming buffer or CaCl₂ was evaluated for its ability to simulate the mechanical properties and structure of the *in vivo* BM. Each firming concentration was also assessed for cytotoxicity in HS-5 cells, as these would be directly exposed when incorporated into the scaffold. As each scaffold could be dissolved either with a prediluted dissolving buffer or 55 mM EDTA (Armstrong *et al.*, 2016), both solutions were evaluated for their ability to dissolve each scaffold and any cytotoxicity they may induce. Those concentrations which gave a scaffold with similar mechanical and structural properties to the *in vivo* BM, were then assessed for their effect on viability, proliferation and cell cycle for long term culture of HS-5 cells. Once a long

term culture protocol had been established which supported the primary addition of HS-5 cells, the addition of TK6 was optimised to maintain them in their exponential phase for the addition of compound. The construction of a bioprinter for the extrusion of the in-house alginate gel was also conducted in addition to the main body of work. This bioprinter once constructed was evaluated for its potential use in the printing of bespoke scaffolds using the in-house alginate gel. Finally, in order to identify TK6 from those HS-5 which had not been included into the scaffold itself, evaluation of appropriate markers was assessed.

The Biomerix scaffold was evaluated first, with the AlgiMatrix™ and bespoke hydrogel scaffold evaluated concurrently for comparison between alginate scaffolds.

3.2. Materials and methods

All reagents and equipment were purchased from Sigma-Aldrich (Poole, UK) unless otherwise stated. All reagents were of the correct chemical, molecular and cell culture grade.

3.2.1. Biomerix™ (hard) scaffold seeding development

3.2.1.1. Original seeding of HS-5 onto a Biomerix™ scaffold

Passage 2 - 6 HS-5 cells were grown to confluence and seeded at a density of 5×10^5 cells in 20 μ l of complete medium directly onto the centre of a sterilised Biomerix™ scaffold (Cellon, Edinburgh) within a 12 well plate, made of a biocompatible polycarbonate polyurethane-urea compound. Sterilisation of the Biomerix™ scaffolds was achieved by several compression-decompression cycles in 70% EtOH to expel all air from the scaffold, followed by incubation (20 mins) and 2 x 10 minute washes in PBS. Scaffolds were left for 2 hours (37°C, 5% CO₂) for cells to adhere after which a further 2 ml of complete medium was added and baseline counts taken of cells within the medium, scaffold and adhered to the plate after this initial incubation. To ascertain cell number within the scaffold and plate, each was washed separately with PBS 2 x 10 minute washes, 1 ml of 0.25% trypsin in EDTA added, incubated for 5 minutes, collected by centrifugation (300 x g, 7 minutes) and counted using the Luna-FL™ Counter as described in section 2.2.1. Remaining wells were incubated for a further 72 hours with cell counts of the medium, plate and scaffold taken every 24 hours.

3.2.1.2. Optimisation of HS-5 initial seeding time and density

HS-5 cells were grown until confluence and seeded at a concentration of 5×10^5 , 1×10^6 or 1.5×10^6 cells/scaffold in 20 μ l of complete medium onto the centre of a sterilised Biomerix™ scaffold. Each scaffold was either compressed then decompressed, drawing the cell suspension into the centre of the scaffold, or left for the cells to find their own way into the scaffold. Cells were allowed to adhere for 2, 4, 5 or 24 hours after which 2 ml of complete medium was added. Immediately, cell number from the medium, plate and scaffold was ascertained as described previously. This experimentation concludes that a cell density of

1×10^6 , and adherence time of 24 hours was found to be optimal and selected for all future experiments.

To assess long term culture within the Biomerix™ scaffolds, 1×10^6 total HS-5 cells in 20 μ l complete medium were seeded onto each sterile Biomerix™ scaffold, either left to adhere naturally or compressed then decompressed; both conditions incubated for 24 hours at 37°C, 5% CO₂ after which 2 ml of complete medium was added and incubated for a further 72 hours. Scaffolds and medium were then harvested every 24 hours over the 72 hour period for assessment of cell number and viability as described previously in section 2.2.1.

3.2.1.3. Evaluation of trypsinisation efficiency

The RealTime-Glo™ MT assay (Promega, Southampton) determines the number of viable cells in a culture through the reduction of a pro-substrate to a substrate, which is converted to a luminescent product by a NanoLuc luciferase enzyme, producing a luminescent signal relative to cell number, for a maximum of 72 hours. Therefore, HS-5 cells were seeded onto sterile Biomerix™ scaffolds at a concentration of 0, 5×10^5 , 1×10^6 or 1.5×10^6 cells/scaffold in 20 μ l of complete medium and maintained for 2, 4, 5 or 24 hours. The RealTime-Glo™ MT assay reagent was then added to each condition, following the manufacturer's protocol, before and after trypsinisation. Reagent was also added to a blank scaffold to assess background luminescence. Luminescence was then read for each sample on a FLUOstar Omega (BMG Labtech, Buckinghamshire) at an integrated time of 0.25 - 1 second per well.

3.2.2. AlgiMatrix™ (gel) model development

3.2.2.1. Identification of AlgiMatrix™ internal structure

Dry AlgiMatrix™ scaffolds (ThermoFisher Scientific, Loughborough) were suspended in 500 μ l of either a 50, 25 or 10 % solution of AlgiMatrix™™ firming buffer: complete medium (with/without 2.5×10^5 HS-5 cells/ scaffold) for approximately 5 minutes. The rehydrated scaffolds were washed with 1 ml of complete medium before analysis by light microscope for cellular distribution and structural arrangement. Rehydrated scaffolds without HS-5 cells, were also analysed via scanning electron microscopy (SEM), which was conducted by Dr D Patton of UWE, for pore size at differing firming concentrations. In order

to image via SEM, each scaffold was placed on lint free tissue overnight to draw out any moisture within the scaffold. The dehydrated scaffold was then placed on a carbon conductive tab on pin stubs (TAAB, UK), sputter coated with gold utilising a SC 500 Emscope sputter coater (BIO-RAD, Watford). Imaging of pore size was then achieved using a FEI Quanta 650 field emission SEM.

3.2.2.2. AlgiMatrix™ optimisation of cellular seeding and retrieval

3.2.2.2.1. The effect of 55mM EDTA and dissolving buffer on HS-5 cells

The AlgiMatrix™ is supplied with a dissolving buffer (ThermoFisher Scientific) which, when added to firm AlgiMatrix™ scaffolds, will dissolve the scaffold allowing the collection of cells encapsulated within. An alternative method of dissolving each scaffold was identified using 55 mM EDTA as a chelating agent for the divalent ions within the AlgiMatrix™ scaffold. To identify if either 55mM EDTA or commercial dissolving buffer had a cytotoxic effect on cells, HS-5 cells were grown to confluency in a 75cm² flask, trypsinised and aliquoted at a concentration of 1.5×10^6 cells in 1ml of either 55mM EDTA or commercial dissolving buffer. HS-5 cells were left for 0, 10, 20 or 30 minutes within each solution, washed and assessed for viability and total cell number utilising the Luna-FL™ counter with acridine orange (AO) and propidium iodide (PI) counter stain.

3.2.2.2.2. Proliferation index of HS-5 with/ without an AlgiMatrix™ scaffold present

To assess how the size, growth area and medium volume of 25 cm² flask, 24 or 12 well plate affected the growth of HS-5 seeded within, HS-5 cells were grown to confluency, trypsinised and counted as previously described in section 2.2.1. HS-5 cells were then seeded at the same initial density of 6×10^3 cells/cm² into a T25 cm² flask, 24 and 12 well plate with 10, 2 and 3 mls of complete medium added respectively. Each condition was incubated for 216 hours, with 50% medium change every 48 hours and sampled every 24 hours. Separate HS-5 cells were also seeded into 50% firm AlgiMatrix™ scaffolds, placed in a 12 well plate, at a density of 2.5, 5, 7.5 and 10×10^5 cells/ scaffold with 3 mls of fresh complete medium added. Each condition was incubated for an initial 24 hours, 100% medium change

conducted and incubated for a further 312 hours. Scaffolds underwent a 50% medium change every 48 hours and select scaffolds harvested at 48 hour time points over this 312 hour period.

In order to assess the affect each culture vessel had on HS-5 cells each experimental condition above was analysed for cell number, viability, presence of Ki67 and stages of cell cycle. Each sample, mentioned above, was split into 3, one sample was analysed for cell number and viability using the Luna-FL™ counter, samples 2 and 3 were washed and resuspended in around 10 µl of medium. A 1 ml working solution of Foxp3 fixation/permeabilisation solution, using the manufacturer's instructions, was added to samples 2 and 3 and left to incubate on ice for 30 minutes. A 2 ml working stock of permeabilization buffer was immediately added to both before centrifugation at 600 x g for 5 minutes with the supernatant discarded. Samples 2 and 3 were resuspended in approximately 100 µls of medium, 5 µl of Ki67 (Table 2-1) was added to sample 2. Samples 2 and 3 were then vortexed and incubated for 30 minutes at room temperature in the dark. A further 2 ml of 1x permeabilization buffer was immediately added to both samples before centrifugation at 600 x g for 5 minutes with the supernatant discarded. A 500 µl working solution of PI (50 µg/ml PI, 100 µg/ml RNase, 2 mM MgCl₂ made up to 1 ml in PBS) was added to sample 3 for 20 minutes in the dark to assess stages of cell cycle. A 500 µl aliquot of fluorescence-activated cell sorting (FACS) (1% bovine serum albumin (BSA) in PBS) buffer was added to sample 2 before both sample 2 and 3 were analysed on the Accuri C6 Plus flow (BD) cytometer for 50,000 events after initial gating (Figure 2-1).

3.2.2.2.3. Washing regimen for increased cellular viability

HS-5 cells were grown to confluency, trypsinised and counted as previously described in section 2.2.1, seeded in either 50, 25 or 10% firming buffer in complete medium, at a concentration of 5×10^5 cells/ml. Dry AlgiMatrix™ scaffolds, in a 24 well plate, were rehydrated with 500 µl of each firming condition (50, 25 or 10%), containing a total cell number of 2.5×10^5 cells per scaffold and left for approximately 5 minutes. The rehydrated scaffolds were either washed with complete medium or left before being transferred into 12 well plates, 3 ml of complete medium was then added and scaffolds incubated for an initial 24 hours, after which, scaffolds underwent either a 100, 50 or 0% complete medium change, incubated and process repeated every subsequent 48 hours. At 24 hour intervals, HS-5

incubated scaffolds were transferred into a 15ml centrifuge tube, 2 ml of AlgiMatrix™ dissolving buffer added and left for <30 minutes with gentle agitation every 2 minutes until the scaffold had dissolved. Cells were collected by centrifugation (300 x g, 7 minutes), supernatant removed, fresh medium added, and an aliquot taken for cell number and viability as described in section 2.2.1. This experiment identified, in conjunction with the results obtained from section 3.3.3.3, an optimised seeding regime (section 2.3.1) of HS-5 cells encapsulated within an AlgiMatrix™ scaffold for the addition of TK6. Therefore, this method will be used for further studies.

3.2.2.2.4. Proliferation index of TK6 cells in co-culture with HS-5 cells.

HS-5 cells were grown to confluency, trypsinised and counted as previously described in section 2.2.1 and cultured within AlgiMatrix™ scaffolds as described in section 2.3.1. After 144 hours, TK6 cells were added directly to the scaffold at 0.5, 1 or 3.5 x 10⁵ cells/ml in complete medium, mixed by pipetting and left to incubate for 102 hours. A 50 or 0% medium change was conducted every 0, 24 or 48 hours over this 102 hour period. Twice a day, six hours apart, cells were collected from the medium and dissolved scaffolds and counted as described in section 2.2.1. Cells were then washed with PBS, a 1:20 dilution of CD19 (section 2.4, Table 2-1) in 100 µl of FACS buffer, mixed and incubated on ice for 45 minutes. Following incubation, samples were collected (300 x g for 7 minutes) before the addition of 500 µl's of FACS buffer. Flow cytometry of percentage positive cells was assessed after initial gating (section 2.4, Figure 2-1). This experiment identified the optimal culture conditions for the addition of TK6 outlined in section 2.3.2 and therefore will be used for further study.

To identify if the viability of HS-5 increased with the addition of TK6 after the initial incubation described in section 2.3.1, the addition of TK6 cells seeded into a 0.25µ well inserts, at a concentration of 0.5 x 10⁵ cells/ml, were added into wells containing HS-5 seeded AlgiMatrix™ scaffolds cultured as described in section 2.3.1. The well insert was used to distinguish HS-5 cells from TK6. A 50% medium replacement was then conducted at either 24 or 48 hour intervals over the remaining 96 hour period. Well inserts were removed, and AlgiMatrix™ scaffold dissolved every 48 hours, HS-5 cells within were counted (as described in section 2.2.1) stained with the fixable viability dye, eFluor 520

(ThermoFisher,), and assessed via flow cytometry for 50,000 events (gating described in section 2.4, Figure 2-1). A negative dead (HS-5 incubated at 100°C for 10 minutes), positive live (HS-5 cells at a viability of >90%) and 50:50 (positive: negative) control for percentage positivity was also assessed. The percentage positive and total cell number was then used to calculate the total number of live HS-5 cells.

3.2.3. 3D printing of in-house Alginate scaffolds

3.2.3.1. Modification of a 3D printer for use with bioink and design of an *in vivo* relevant bone marrow scaffold.

To accurately extrude the bioink into a 3D soft hydrogel structure, a Mendlemax 3 3D printer (Makers tool works, California) was purchased and constructed according to the manufacturer's guidelines. The Mendlemax is built to extrude a hard plastic (polylactic acid; PLA) when heated to 220 °C which is layered to make a structure. To prove that the Mendelmax 3 can print accurate 3D scaffolds, SEM images of the BM were converted into 3D structures using the online software selva 3D. This was then manipulated using the online software TinkerCad so that it could be converted into a STL. file (3D file which is recognised by the printer) and printed in PLA.

In order for the Mendlemax to extrude unheated bioink, not PLA, the Mendlemax required conversion into a 'bioprinter'. The bioprinter uses a needle of differing gauge to guide the bioink onto the surface, unlike the heated nozzle currently fitted. The conversion required the Mendlemax to first print off its own parts in PLA from donated STL. files; notably the syringe driver, motor holder and pusher before the conversion could take place. These files, along with new firmware for the Mendlemax were kindly donated by Mr T Richardson (University of Bristol). The software Arduinino was used to upload the firmware onto the Mendlemax. This firmware would control the rate at which the bioink would be extruded from the needle, as it would consider differing pressures not present with the original heated nozzle.

3.2.3.2. Experimentation of a non-commercial bespoke hydrogel scaffold

A bespoke hydrogel (60% sodium alginate, 32% pluronic F127 and 8% medium) was constructed (to compare with the previously described Biomerix™ solid scaffold) utilising the protocol in Armstrong *et al.* (2016) to create a scaffold with differing pore sizes. A 100 µl aliquot of bioink (a combination of cells, alginate, pluronic F127 and medium) was extruded into a 24-well plate and 1 ml of either 100 mM or 1 M calcium chloride (CaCl₂) solution (CaCl₂ and complete medium) was added at RT to crosslink the gel thus hardening it. Visual examination of the structure was conducted every 5 minutes for a total of 30 minutes. The CaCl₂ solution was then removed and replaced with a 5 mM CaCl₂ solution (CaCl₂ and complete medium) to stop the scaffold from degrading over time. The crosslinked hydrogel was then examined via SEM for pore size as described in section 3.2.2.1.

3.2.3.3. The effect of calcium chloride on bioink and HS-5 cells

HS-5 cells were grown to confluence, trypsinised and seeded onto a 12-well plate at a density of 1×10^5 cells in 400 µl complete medium and left to adhere for 2 hours (37 °C, 5% CO₂). Medium was then removed from the cells and 400 µls of either 0, 100, 300, 500, 700 or 1000 mM CaCl₂ solution was added for 10 minutes (37 °C, 5% CO₂). After 10 minutes the medium was removed, cells were washed with PBS, trypsinised, counted and viability assessed using an acridine orange/ propidium iodide stain.

3.2.4. Identification of a single cell type in a co-culture

3.2.4.1. Identification of TK6 within a co-culture system.

Within the model described in section 2.3, cells need to be distinguished from HS-5 in order to count micronuclei in the ‘haematopoietic’ compartment of the model. The conventional method of AO staining cannot distinguish either cell line morphologically. The staining of TK6 only would allow the quantification of MN in the “haematopoietic” element of the model whilst allowing both cell types to be in contact with each other.

3.2.4.1.1. Use of the nanocrystal technology Qtracker 655

The Qtracker 655 labelling kit (ThermoFisher Scientific) delivers Qdot™ nanocrystals into the cytoplasm of living cells which has a stable fluorescence emission of 655 nm over six generations. The Qtracker 655 reagents were incubated following the manufacturer's protocol and added to a density of 1×10^6 TK6 cells, incubated at 37 °C for 60 minutes then washed twice with complete medium. The stained TK6 were combined with unstained HS-5 cells at a ratio of 100:0, 75:25, 50:50, 25:75 or 0:100 at a final density of 1×10^5 cells in 1 ml of complete medium. Cells were either cytospun onto a glass slides using a utilising a Shandon cytospin 3 (ThermoFisher) at 800 rpm for 8 minutes, for identification of TK6 stained cells by florescent microscopy or pelleted and 500µl of FACS buffer added for flow cytometry analysis (section 2.4, Figure 2-1) of 50,000 events.

3.2.4.1.2. Flow cytometry of TK6 specific markers.

According to the European Collection of Authenticated Cell Cultures (ECACC), 100% of TK6 cells express the membrane bound cluster of differentiation (CD) marker 19 (B cell lineage), 50% express CD20 (pro-B cell stage) and a small population express CD22 (mature B cells). HS-5 cells, however, do not express these CD markers as they do not reside within the B cell lineage. TK6 and HS-5 cells were grown as described in section 2.2, trypsinised (HS-5 cells) and counted as described in section 2.2.1. Cells were mixed in a ratio of 100:0, 75:25, 50:50, 25:75 and 0:100 TK6:HS-5 cells at a concentration of 1×10^5 cells/ml. Cells were washed with PBS, a 1:20 dilution of CD19 or CD20 (section 2.4, Table 2-1) either alone or in combination in 100 µl of FACS buffer was added, mixed and incubated on ice for 45 minutes. Following incubation, samples were collected (300 x g for 7 minutes), 500 µl of FACS buffer added before being gated (section 2.4, Figure 2-1) and analysed for 50,000 events on an Accuri C6 Plus flow cytometer (BD).

3.2.4.1.3. Immunofluorescent differentiation of TK6 from HS-5 cells

TK6 and HS-5 cells were grown as described in Section 2.2, trypsinised (HS-5 cells) and counted as described in section 2.2.1. Cells were mixed in a ratio of 100:0, 75:25, 50:50, 25:75 and 0:100, TK6:HS-5 cells at a total concentration of 1×10^5 cells/ml. 200 μ l of each ratio was cytopspun onto a glass slide using a Shandon cytospin 3 (ThermoFisher) at 800 rpm for 8 minutes, and once dry, fixed in 100% methanol (15 minutes, RT). To stain, slides were washed once with PBS for 1 minute, 200 μ l of blocking buffer (1% BSA in PBS) added and slides incubated at room temperature for 30 minutes. The primary antibody for CD19 and CD20 (section 2.4, Table 2-1) were then diluted in blocking buffer, 200 μ ls added to each slide and incubated for 1 hour at room temperature. Each slide was washed in PBS (3 x 5 minutes), 200 μ ls of secondary antibody added (section 2.4, Table 2-1) and incubated for 1 hour at room temperature in the dark before being washed in PBS (3 x 5 minutes). To visualise the nuclear material, 10 μ ls of DAPI (4',6-diamidino-2-phenylindole) (2 μ g/ml in PBS) was added to each slide and incubated for 10 minutes at room temperature in the dark, washed in PBS (3x 5 minutes) and left to dry, then 200 μ l of Prolong Gold antifade mounting medium (ThermoFisher) added to each slide and covered with a cover slip. Each sample was analysed on a Leica SP8 confocal microscope (Leica, Newcastle Upon Tyne). This was also trialled with primary antibodies conjugated with FITC (CD19) and PerCy5.5 (CD20) (section 2.4, Table 2-1).

3.3. Results

3.3.1. Biomerix™ scaffold seeding development

3.3.1.1. The seeding of HS-5 onto Biomerix™ using a previously published method

To assess the reproducibility of a previous work conducted within UWE, HS-5 grown to confluence were seeded onto a Biomerix™ scaffold and 2 mls of fresh complete medium added. Each scaffold was left for a 96 hour incubation period with scaffolds harvested every 24 hours (Figure 3-1). The datum shows that following a 2 hour incubation of cells with the scaffold, cell counts show 75% of cells reside in the medium or have attached to the plate surface, and only 25% have adhered to the scaffold. This finding occurs throughout the experiment with a significant increase in cells residing on the plate compared to the scaffold occurring at 96 hours. This result shows that HS-5 cells will not adhere to the scaffold in large numbers with this seeding density or incubation time, therefore, optimisation of the initial seeding density and time should be conducted.

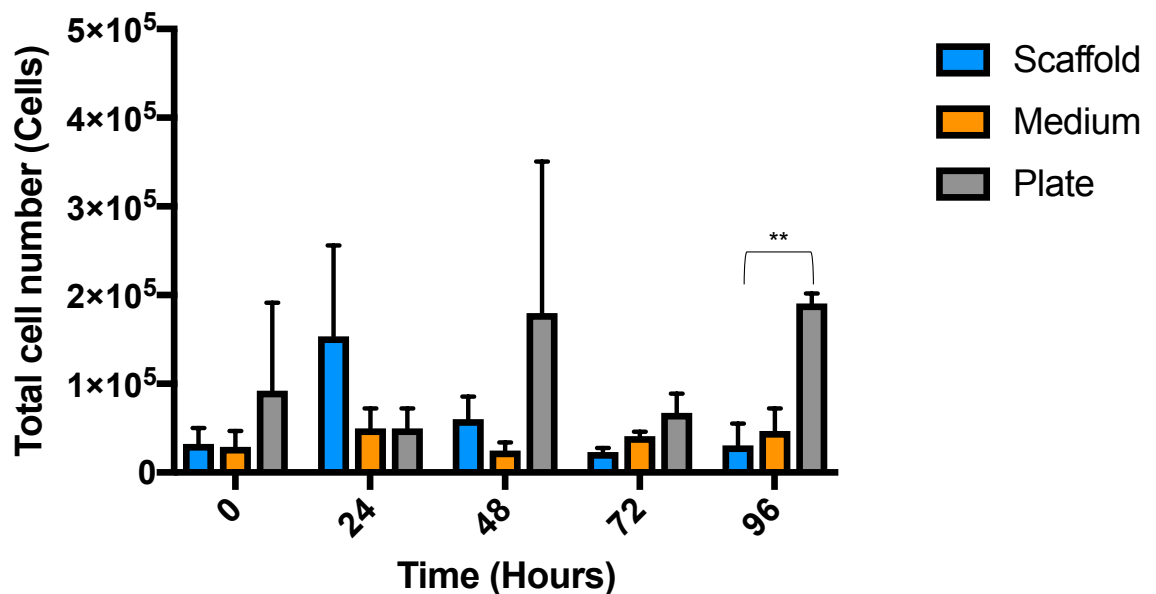


Figure 3-1. Growth of HS-5 cells seeded onto Biomerix™ scaffolds at a density of 5×10^5 cells/ scaffold using a previously established method. Cells were added to Biomerix™ scaffolds and incubated for 2 hours. Cells were retrieved from the plate and Biomerix™ scaffold via trypsinisation every 24 hours over a 96 hour period. Cell number was established using trypan blue. (n=3). Significant differences between samples were calculated using a Two-Way ANOVA followed by a Dunnett's test. The p value is indicated by ** ($p < 0.01$), actual p values can be found in appendix 1.

3.3.1.2. Optimisation of initial seeding density

In order to retain a larger proportion of cells within the scaffold compared to the medium and /or plate surface, an optimisation of the initial seeding concentration and time were conducted. An initial seeding concentration of 5×10^5 (Figure 3-2) and 1×10^6 (Figure 3-3) of HS-5 cells in 20 μ ls were added to each scaffold and left to adhere naturally for either 2, 4 (Figure 3-2 A, Figure 3-3A), 2, 5 or 24 (Figure 3-2B, Figure 3-3B) hours, or scaffolds were compressed-decompressed before a 5 or 24 (Figure 3-2C, Figure 3-3C) hour incubation. In both initial seeding concentrations (5×10^5 and 1×10^6), irrespective of compression of the scaffold 2, 4 and 5 hour incubations resulted in a significant increase in total cells within the medium compared to that of the scaffold. The mean total cell count was also $>75\%$ in the medium compared to the scaffold. In both initial seeding concentrations (5×10^5 and 1×10^6), scaffolds that were not compressed (Figure 3-2 B, Figure 3-3 B) showed no significant difference between scaffold and medium at 24 hours. However, those scaffolds seeded with 1×10^6 total cells (Figure 3-3 B), were found to have a higher mean total cell number of 3.25×10^5 cells upon the scaffold, unlike those seeded with 5×10^5 , which only reached 2.9×10^5 cells over the same period.

To ensure that the scaffolds had been fully harvested of cells, RealTime-Glo assay reagents were added to loaded scaffolds before and after trypsinisation along with a cell free scaffold as a negative control (Figure 3-2D, Figure 3-3D). In each condition the RLU of the scaffold containing cells reduced by $>98\%$ when compared to trypsinised scaffold, with the negative control giving a consistent result of 0 RLU confirming a complete harvest of the scaffold.

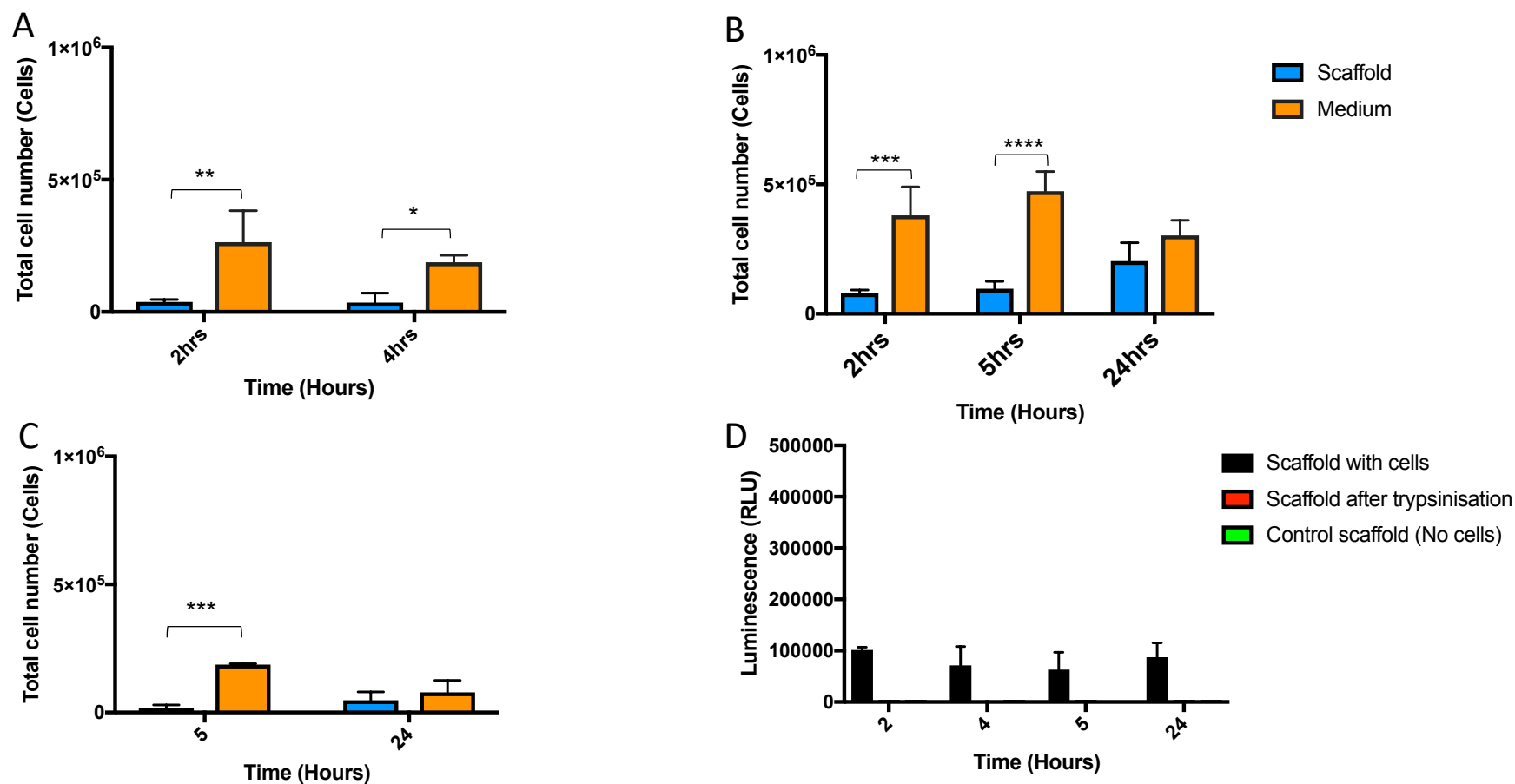


Figure 3-2. Initial adherence time of HS-5 cells seeded onto Biomerix™ scaffolds at a concentration of 5×10^5 . Biomerix™ were either left to naturally adhere (A+B) or compressed-decompressed (C) before addition of 20 μ l of cell suspension. Cells were incubated for 2 & 4 (A), 2, 5 & 24 (B) or 5 & 24 hours before trypsinisation and cell count via trypan blue. Confirmation of complete evacuation of cells from the scaffold using trypsin was established using the RealTime-Glo assay from Promega (D). (n=3). Significant differences between samples were calculated using a Two-Way ANOVA followed by a Dunnett's test. The p value is indicated by * ($p < 0.05$), ** ($p < 0.01$), *** ($p < 0.001$), **** ($p < 0.0001$), actual p values can be found in appendix 1.

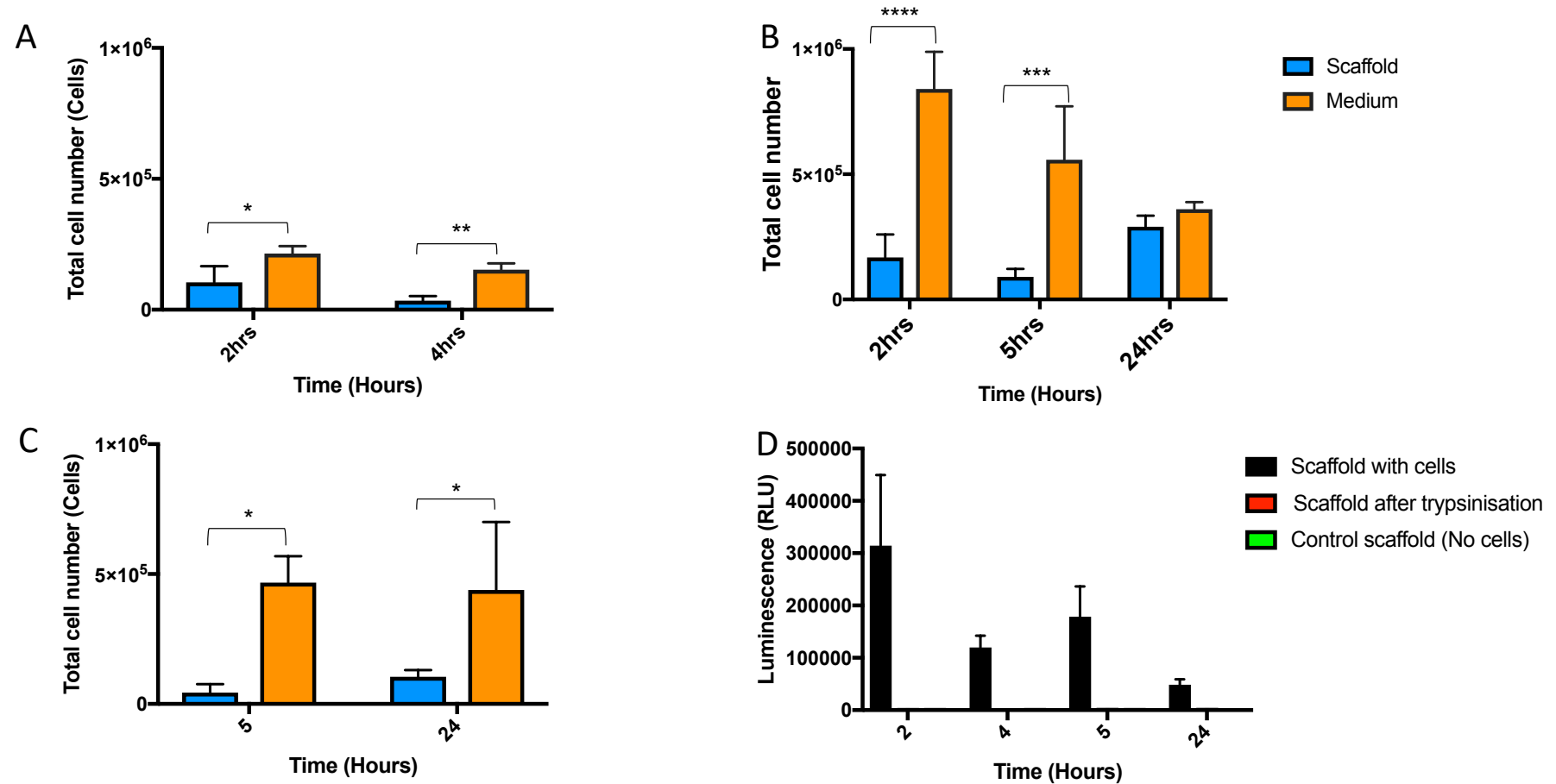


Figure 3-3. Initial adherence time of HS-5 cells seeded onto Biomerix™ scaffolds at a concentration of 1×10^6 . Biomerix™ were either left to naturally adhere (A+B) or compressed-decompressed (C) before addition of 20 μ l of cell suspension. Cells were incubated for 2 & 4 (A), 2, 5 & 24 (B) or 5 & 24 hours before trypsinisation and cell count via trypan blue. Confirmation of complete evacuation of cells from the scaffold using trypsin was established using the Real Time Glo assay from Promega (D). (n=3). Significant differences between samples were calculated using a Two-Way ANOVA followed by a Dunnett's test. The p value is indicated by * ($p < 0.05$), ** ($p < 0.01$), *** ($p < 0.001$), **** ($p < 0.0001$), actual p value can be found in appendix 1.

As an initial seeding density of 1×10^6 cells in 20 μ ls of complete medium, added to a sterile Biomerix™ scaffold for 24 hours has shown to yield a greater number of cells on the scaffold, the effects of long-term culture were investigated using this initial seeding method with the addition of compression (Figure 3-4 A) or natural adhesion to the scaffold (Figure 3-4 B). It can be seen that in both conditions a statistical increase in cells within the medium compared to the scaffold was seen. However, cells exposed to an initial compression (Figure 3-4 A) had increased cell numbers in the scaffold ($2 \times 10^5 - 4 \times 10^5$ cells) and decreased ($9 \times 10^5 - 5 \times 10^5$ cells) in the medium between the 48 - 96 hour period, with the combined number of cells in the scaffold and medium reaching 9×10^5 cells which was lower than the initial seeding density of 1×10^6 cells. The results from this section show that the HS-5 cell line will not adhere in a high enough density for future culture, therefore new scaffold were investigated which encapsulates the HS-5 cells, retaining a larger population.

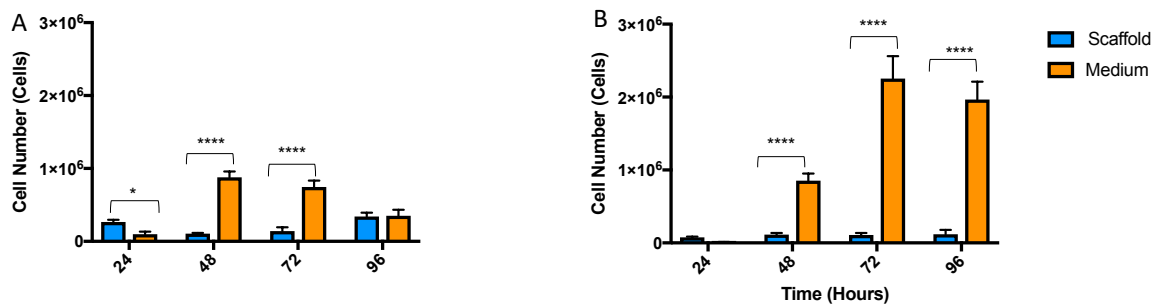


Figure 3-4. Growth of HS-5 cells seeded onto Biomerix™ scaffolds at a concentration of 1×10^6 . Cells were seeded onto either compressed (A) or natural Biomerix™ scaffolds (B) and incubated for an initial 24 hours before the addition of medium. Cells were retrieved from the Biomerix™ scaffold via trypsinisation every 24 hours over a 96 hours period. Cell number was established using trypan blue. (n=3). **Significant differences between samples were calculated using a Two-Way ANOVA followed by a Dunnett's test. The p value is indicated by * ($p < 0.05$), **** ($p < 0.0001$), actual p values can be found in appendix 1.**

3.3.2. AlgiMatrix™ model development

In an effort to maintain a higher proportion of cells within the scaffold compared to that of the medium and maintain reproducibility between scaffolds, investigation into the use of a new, soft hydrogel instead of Biomerix™ was investigated. The commercial scaffold AlgiMatrix™, a hydrogel made of biologically inactive alginate, was used for its ability to incorporate and retrieve cells within the scaffold itself.

3.3.2.1. Optimisation of initial solidifying and eventual dissolving of AlgiMatrix™ scaffolds.

The commercial AlgiMatrix™ scaffold arrives as a freeze-dried alginate solution, which is rehydrated with differing concentrations of firming buffer dependent on the internal structure required. AlgiMatrix™ scaffolds were subjected to 10, 25 or 50% firming buffer in complete medium with the internal and external structure assessed by light microscopy (Figure 3-5). The internal (Figure 3-5 B, E and H) and surface structure (Figure 3-5 C, F and I) showed little to no difference in structure using light microscopy in either 10, 25 or 50% firming conditions. However, the external appearance and mechanical structure of a 10% scaffold (Figure 3-5 A) was much more gelatinous than that of 25 (Figure 3-5 D) or 50% (Figure 3-5 G) scaffolds and fell apart when manipulated. The scaffolds solidified with 25 or 50% firming solution held their shape when manipulated and resembled the consistency of the hard Biomerix™ scaffold.

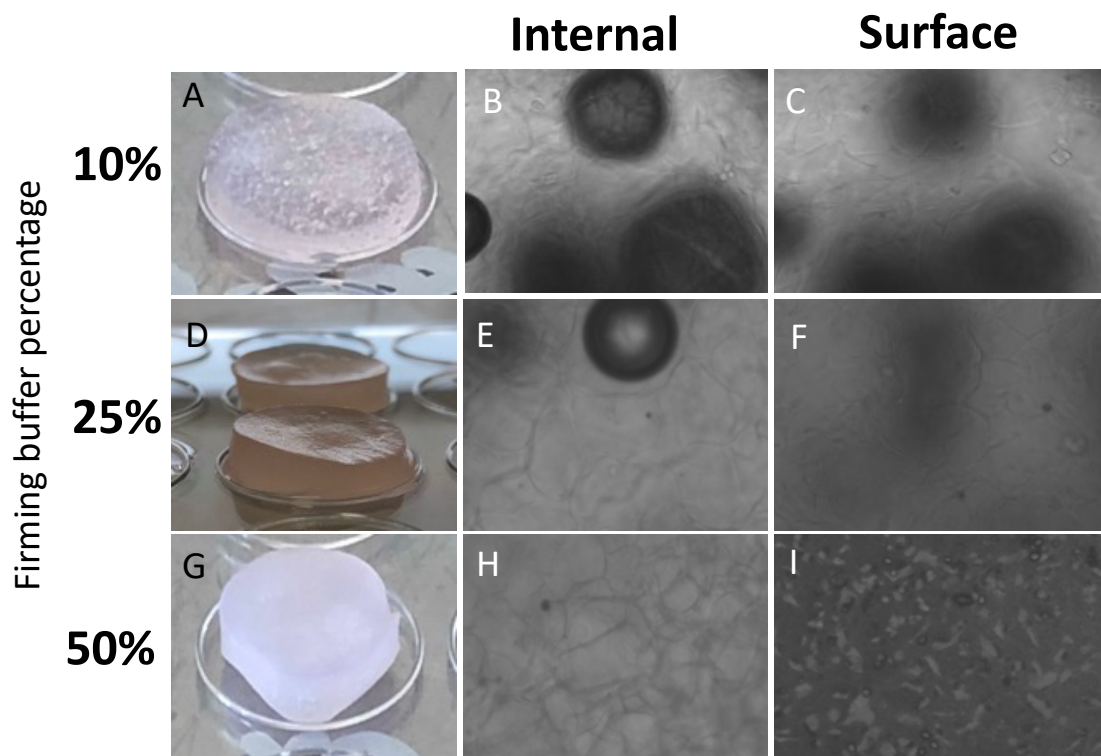


Figure 3-5. Images depicting the physical structural difference seen with increasing firming buffer concentration of AlgiMatrix™ scaffolds. A 10, 25 or 50% solution of firming buffer and medium was added to each dry AlgiMatrix™ scaffold for >5 minutes for solidification. The external appearance of each scaffold can be seen in A (10%), D (25%) and G (50%). Light microscopy (10x magnification) was then used to look at the internal (B, E and H) and surface (C, F and I) of each solid scaffold.

Due to the lack of differentiation between internal structures using light microscopy, SEM was used to identify structural changes at $>150\times$ magnification (Figure 3-6). Dried AlgiMatrix™ scaffolds were once again solidified with 10, 25 or 50% (Figure 3-6 A, B and C) firming solution before being assessed by SEM. A 10% firming solution (Figure 3-6 A) produced a structure with no visible pores. However, those scaffolds solidified with a 25% firming solution (Figure 3-6 B) gave pore sizes of $25\ \mu\text{m}$ and a 50% firming solution (Figure 3-6 C) gave a uniform pore size of approximately $120\ \mu\text{m}$.

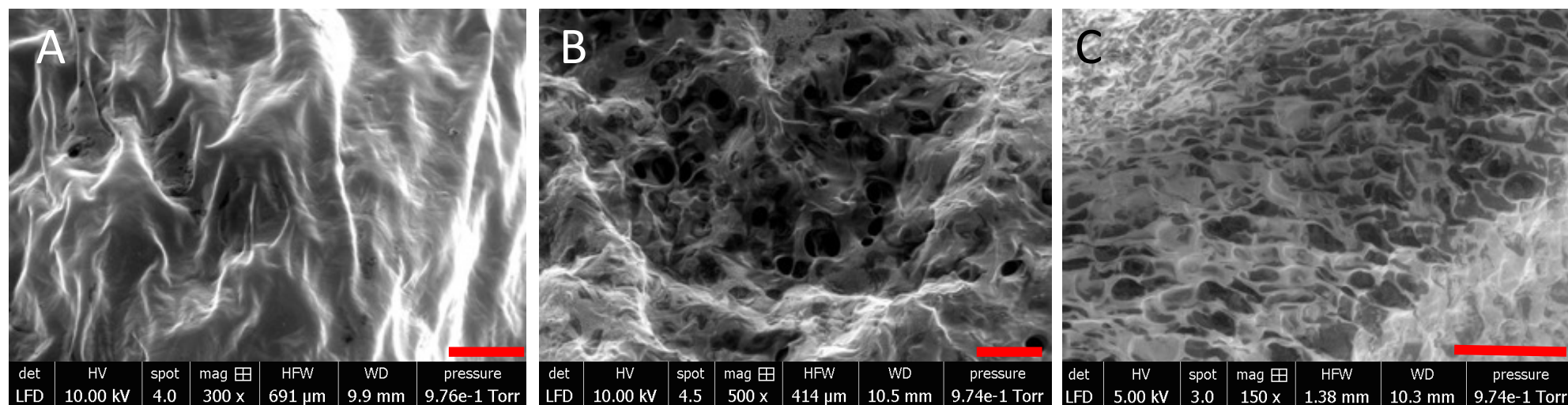


Figure 3-6. Scanning electron microscopy (SEM) images of AlgMatrix™ scaffolds hardened with a 10, 25 or 50% firming buffer. A 10% (A), 25 (B) or 50% (C) solution of firming buffer and medium was added to each dry AlgMatrix™ scaffold for >5 minutes, allowed to air dry for 24 hours before being placed on lint free tissue. Once residual medium had been drawn out, the scaffold was then pressurised within the SEM to evaporate further moisture before images were taken. A. 300x mag, B. 500x mag and c. 150x mag. Scale bars are indicated by the red bar and represent 100 μ m (A), 50 μ m (B) and 300 μ m (C).

The AlgiMatrix™ kit was initially chosen as each scaffold, once solidified, can be fully dissolved using either the supplied dissolving buffer or 55 mM EDTA, enabling the retrieval of the residing cells for cellular assessment. It can be seen, that neither the 55 mM EDTA (Figure 3-7 A) or the commercial dissolving buffer (Figure 3-7 B) had any statistical effect on the viability or cell number of HS-5 cells over a 30 minute period. The viability, measured using a PI/AO stain, produced a viability >95% in both cases, with cell number consistently producing a mean of approximately 1.3×10^5 cells. These results suggest that there is no detrimental effect of using wither 55 mM EDTA or dissolving buffer.

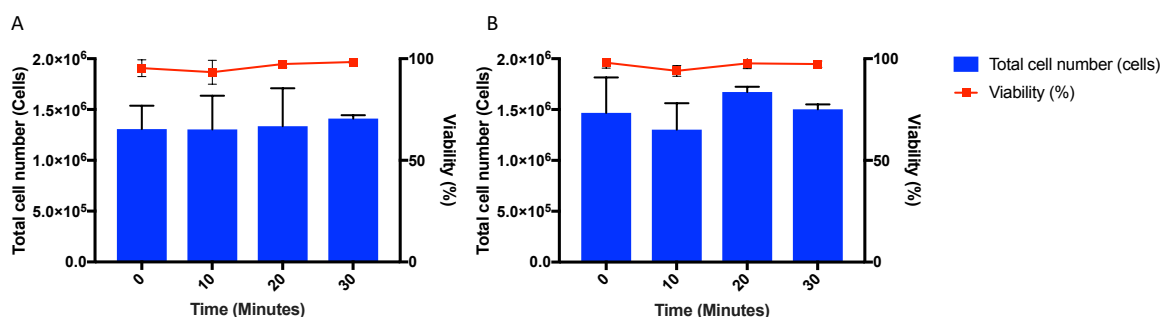


Figure 3-7. The effect of 55mM EDTA (A) and commercial dissolving buffer (B) on the viability (line) and total cell number (bar) of HS-5 cells. HS-5 cells at a concentration of 1.5×10^6 in either 55 mM EDTA or commercial dissolving buffer, incubated for 0, 10, 20 or 30 minutes, washed and assessed for viability and total cell number using an acridine orange and propidium iodide stain (n=3).

The effects of both the 55 mM EDTA and commercial dissolving buffer on AlgiMatrix™ scaffolds, bathed in 50% firming buffer for 5 minutes before being replaced with 55 mM EDTA and commercial dissolving buffer, can be seen in Figure 3-8. In both cases 3 mls of the dissolving solution was added and incubated for 5 minutes. Light manipulation of the scaffolds, to break them up, was carried out every minute with a Pasteur pipette. It can be seen that the EDTA (Figure 3-8 B), after a 5 minute incubation, did not dissolve the scaffold completely with some residue remaining on the surface. However, the dissolving buffer (Figure 3-8 C), after a 5 minute incubation, still has some remnants of the scaffold but less than that of the EDTA. This result suggests that a prolonged bathing period of the scaffold in either solution is needed to achieve complete disassociation.

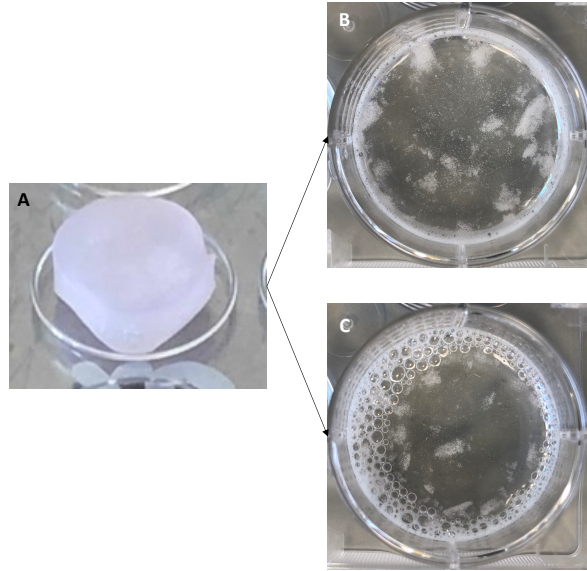


Figure 3-8. The effect of 55mM EDTA (B) and commercial dissolving buffer (C) on an Algimatrix™ 50% scaffold. Algimatrix™ scaffolds were solidified in 50% firming solution for <5 minutes (A), washed and then bathed in 3 either 55 mM EDTA (B) or commercial dissolving buffer (C) for 5 minutes. The scaffolds were gently broken up with a Pasteur pipette over the 5 minute period.

3.3.2.2. Effect of firming buffer on incorporated HS-5 cells and optimisation of long-term culture conditions

The concentrations of AlgiMatrix™ firming buffer, evaluated for physical structure in section 3.3.2.1, was able to accommodate cells for inclusion into each scaffold whilst solidification occurred. However, the effect that the firming buffer had on HS-5 cells had not yet been evaluated, therefore the effect on viability and cell number of each contraction was assessed. This was achieved by introducing firming solution containing HS-5 to the freeze-dried scaffold and incubating for <5 minutes. Therefore, the effect of incorporating HS-5 cells into the scaffold itself with either a 10, 25 or 50% firming solution was investigated (Figure 3-9). Once seeded, each scaffold contained 2.5×10^5 total HS-5 cells and had 2 mls of fresh medium added, then were incubated and had either a 0, 50 or 100% medium change on day 2, with cell number and viability identified using an AO/PI stain. It can be seen, that those scaffolds treated with either 25 or 50% firming buffer resulted in a statistically significant decrease in cell number (Figure 3-9 A, C, E) and viability (Figure 3-9 B, D, F) within the first 24 hours. However, HS-5 incorporated into a 10% scaffold remained >90% viable; reductions in cell number can be seen before a 0 or 100% medium change in the same firming condition (Figure 3-9 A & E). Once a 0, 50 or 100% medium

change had occurred on day 2, the scaffold was incubated for a further 3 days. Those scaffolds which hadn't had a medium change (Figure 3-9 A & B) saw an increase in cell number from day 2- 5 in scaffolds treated with a 10, 25 and 50% firming solution.

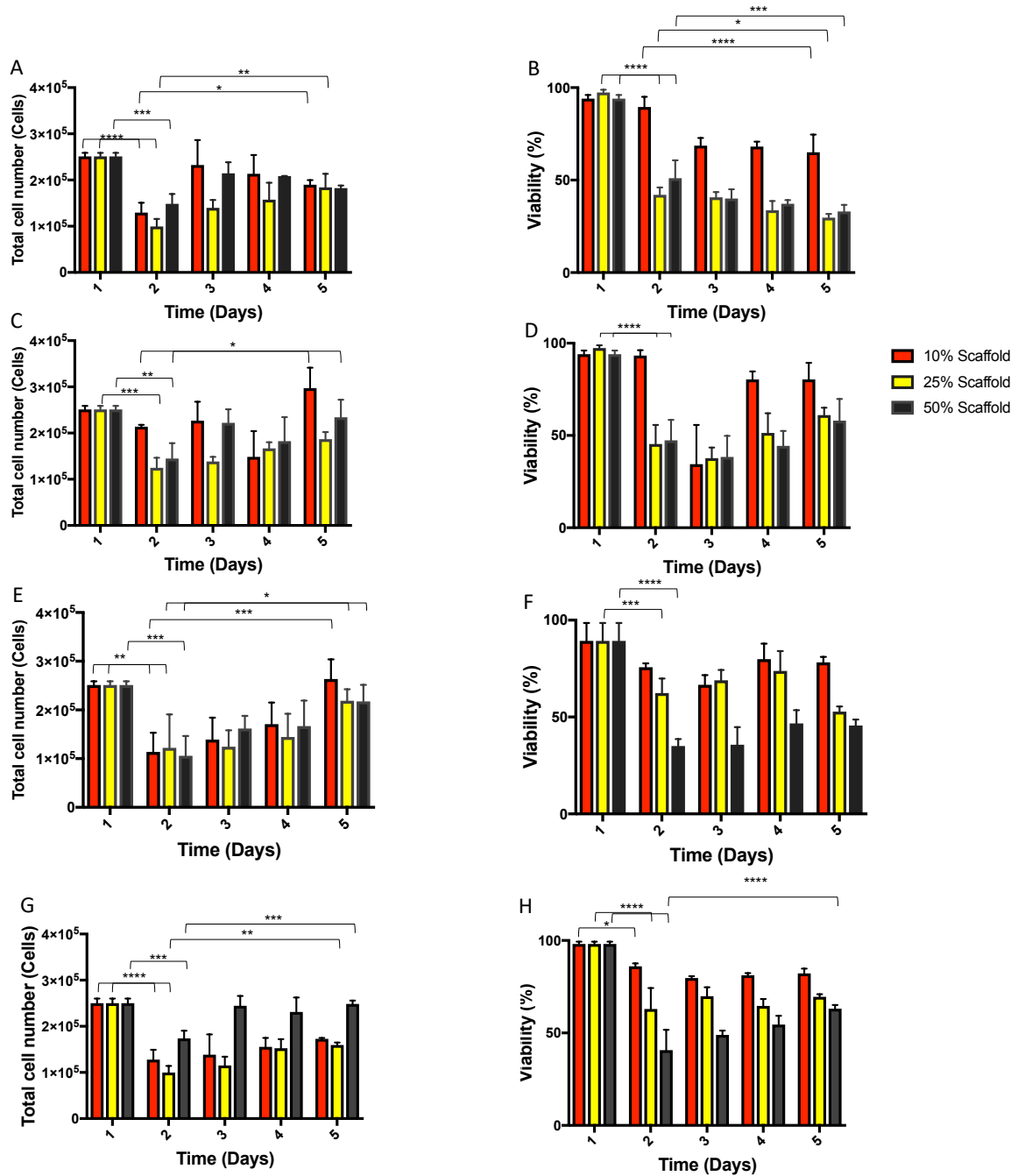


Figure 3-9. Cell number and viability of HS-5 cells seeded at a concentration of 2.5×10^5 onto AlgMatrix™ scaffolds. The Cell number (A, E, C) and viability (B, D, F) of HS-5 cells seeded at a concentration of 2.5×10^5 onto AlgMatrix™ scaffolds, incubated for 5 days with a 0% (A, B), 50% (C, D) or 100% (E, F) medium change on day 2. Cell number (G) and viability (H) were also taken for cells that underwent a 100% medium change on day 2 and a 50% medium change on day 4. In all experiment's HS-5 cells were seeded in a 10, 25 and 50% solidified AlgMatrix™ scaffold for <5 minutes before the addition of fresh medium. At each time point scaffolds were dissolved with viability and cell number assessed using an acridine orange and propidium iodide stain. (n=3). **Significant differences between samples were calculated using a Two-Way ANOVA followed by a Dunnett's test. The p value is indicated by *(p < 0.05), ** (p < 0.01), *** (p < 0.001), **** (p < 0.0001), actual p values can be found in appendix 1.**

However, there was a statistical reduction in viability over the same time period in all conditions. Scaffolds which underwent a 50% medium change on day 2 (Figure 3-9 C & D), resulted in a statistical increase in cell number within the 10 and 50% firming solution groups. However, over the same time period (day 2- 5), there was no statistical increase in viability in all firming conditions. Finally, those cells which underwent a 100% medium change on day 2 (Figure 3-9 E & F) had statistical increases in cell number in all firming conditions over the 3-day period. In the same period, however, no increase in viability was seen in any of the firming conditions. This infers that the initial addition of firming buffer had detrimental effect on HS-5 viability however, the addition of a medium change on day 2 reduced this effect.

To increase the longevity and viability of cells within the scaffold the addition of a medium change on day 4 was investigated (Figure 3-9 G & H). Scaffolds were treated in the same way as described above but on day 4 a further 50% change was performed. This protocol produced a statistical increase in cell number of those cells treated with a 25 or 50% firming solution between days 2- 5. However, only those cells within 50% treated scaffolds resulted in a statistical increase in viability over the same period.

The results from this section identified that a 50% firming solution, 100% medium change on day 2 and a 50% change on day 4 gave a robust scaffold with maintenance of total cell number $>2.5 \times 10^5$ and viability $>50\%$. Therefore, this protocol was used to assess the optimal initial seeding density of HS-5 onto AlgiMatrix™ scaffold for long term co-culture.

3.3.2.3. Identifying the optimal seeding density of HS-5 cells within AlgiMatrix™ scaffolds.

In order to identify the optimum seeding density required for prolonged growth in an AlgiMatrix™ scaffold, the growth of HS-5 cells in differing 2D well areas were investigated and compared to that of a routinely used 25cm² flask. The cell number, viability and presence of Ki67 (Figure 3-10A, B and C) was assessed in a 25cm² flask, 24 and 12 well plate at a starting seeding concentration of 6×10^3 cells/cm². Throughout the 168 hour incubation (7 days) cell number, viability and Ki67 was significantly reduced in the 24 well plate compared to that of both the 25cm² flask and 12 well plate with a viability constantly $<60\%$. The 24 well plate did increase in cell number (4.2×10^4 cells) and Ki67 percentage (41%) at

168 hours, but not to the level of the 12 well (6.7×10^5 cells and 58%) and 25 cm² flask (9.2×10^5 cells and 84%). A significant decrease was seen in the 12 well plate compared to the 25cm² flask at 168 hours in both Ki67 percentage and cell number. Total cell number was also reduced between 168 and 216 ($6.7 \times 10^5 - 4.8 \times 10^5$ total cells) in the 12 well plate, however, this did not result in a significant change in viability or Ki67 compared to the 25cm² flask. Cell cycle was also assessed for 25cm² flasks, and 24 and 12 well plates (Figure 3-10D, E, F) but no significant difference was seen between culture vessels. However, all culture vessels maintained a high level of cells with the G0/G1 transition. These results indicate that a 12 well plate has comparable growth to a 25cm² flask, up to 168 hours and should be used for AlgiMatrix™ addition.

The growth of differing initial total cells seeded onto an AlgiMatrix™ and their effects on long term culture was then investigated. Scaffolds were seeded in a 12 well plate with either 2.5, 5, 7.5 or 10×10^5 total HS-5 cells and assessed for cell number, viability and the presence of Ki67 over a 312 hour period (Figure 3-11 A, B and C). It can be seen that after an initial incubation of 24 hours 5, 7.5 and 10×10^5 seeding densities decreased in cell number, viability and Ki67 with no significant difference between each. However, those scaffolds seeded at 2.5×10^5 total cells, did not have a reduction in cell number but did decrease in viability and Ki67 during the same time period. The following 144 hours saw only a statistical increase in viability (42%-70%) and Ki67 (38%-65%) in those cells initially seeded at 2.5×10^5 total cells, with total cell number over this period remaining approximately 2.5×10^5 total cells. The rise in viability continued in the 2.5×10^5 group but coincided with a decrease in Ki67. Those scaffolds initially seeded at 7.5×10^5 total cells did see a spike in cell number (1×10^6 cells) at 120 hours, but this decreased over the remaining time along with both viability and Ki67. Cell cycle was also assessed for 2.5, 5, 7.5 and 10×10^5 cells/ scaffold (Figure 3-11, Figure 3-10 D, E, F, G) but no significant difference was seen between culture vessels. However, once again as in 2D, all culture vessels maintained a high level of cells with the G0/G1 transition. These results indicate that a starting seeding density of 2.5×10^5 total HS-5 cells left to incubate over a 168 hour period, would be beneficial for the addition of TK6.

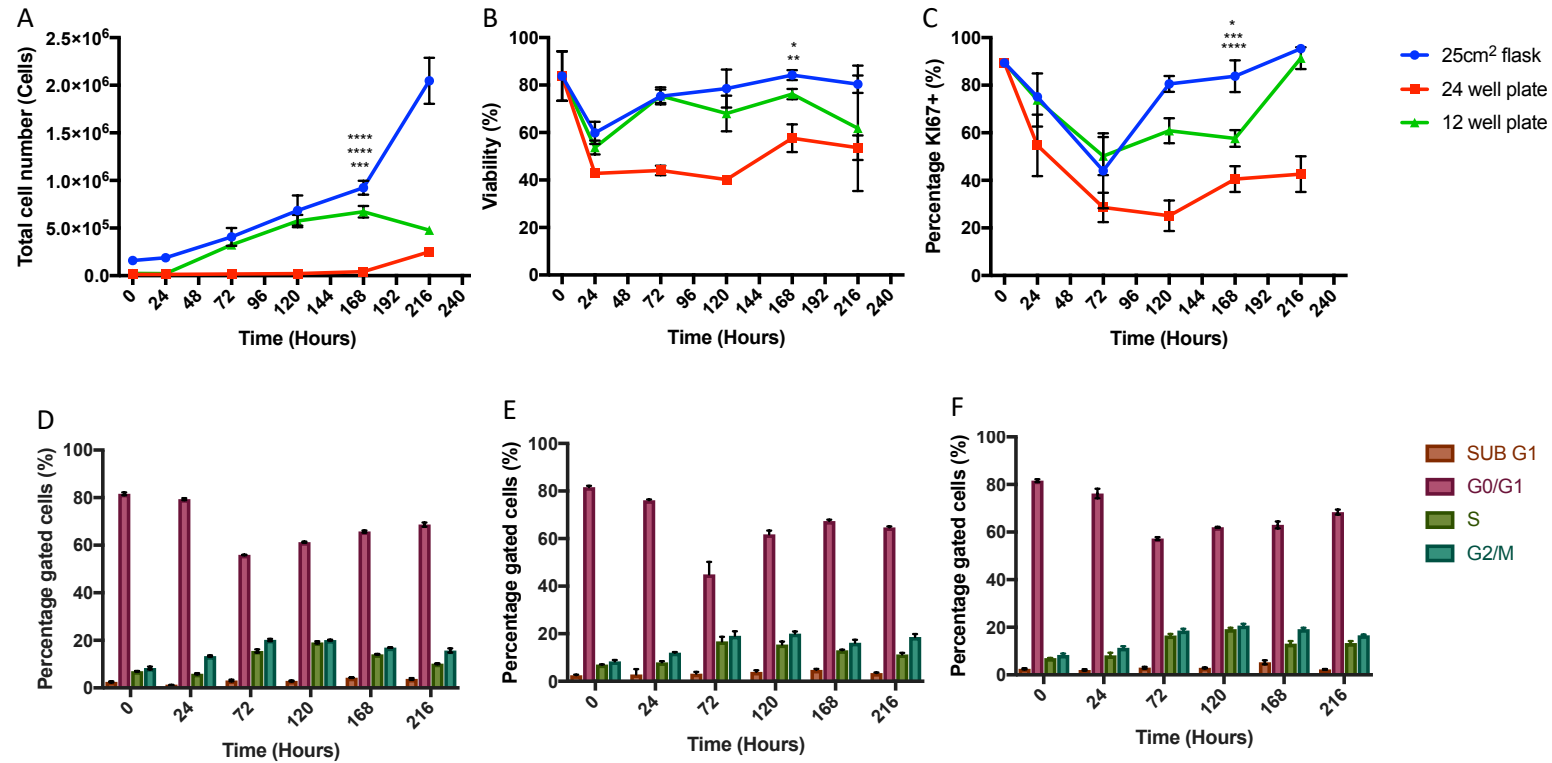


Figure 3-10. The growth of HS-5 cells in a 25cm² flask, 24 and 12 well plate at an initial seeding density of 6x10³ cells/cm². HS-5 cells were seeded at a density of 6 x 10³ cells/cm² into either a 25 cm² flask, 24 or 12 well plate, incubated for 24 hours, complete medium change undertaken, incubated for a further 192 hours with a 50% medium change conducted every 48 hours. At each 48 hour time point, cells were harvested and assessed for total cell number (A) viability (B) and the presence of Ki67 (C). Cells within a 25 cm² flask (D), 24 well plate (E) or 12 well plate (F) were also analysed for cell cycle over the same period. (50,000 events) (n=3) **Significant differences were calculated using a Two-Way ANOVA followed by a Dunnett's test. Significant differences between A. 25 vs 24 ****, 12 vs 24 **** & 25 vs 12 *** B. 12 vs 24 * & 25 vs 12 ** C. 12 vs 24 *, 25 vs 12 *** & 25 vs 24 **** were * p < 0.05, ** p < 0.01, *** p < 0.001, **** p < 0.0001, actual p values can be found in appendix 1.**

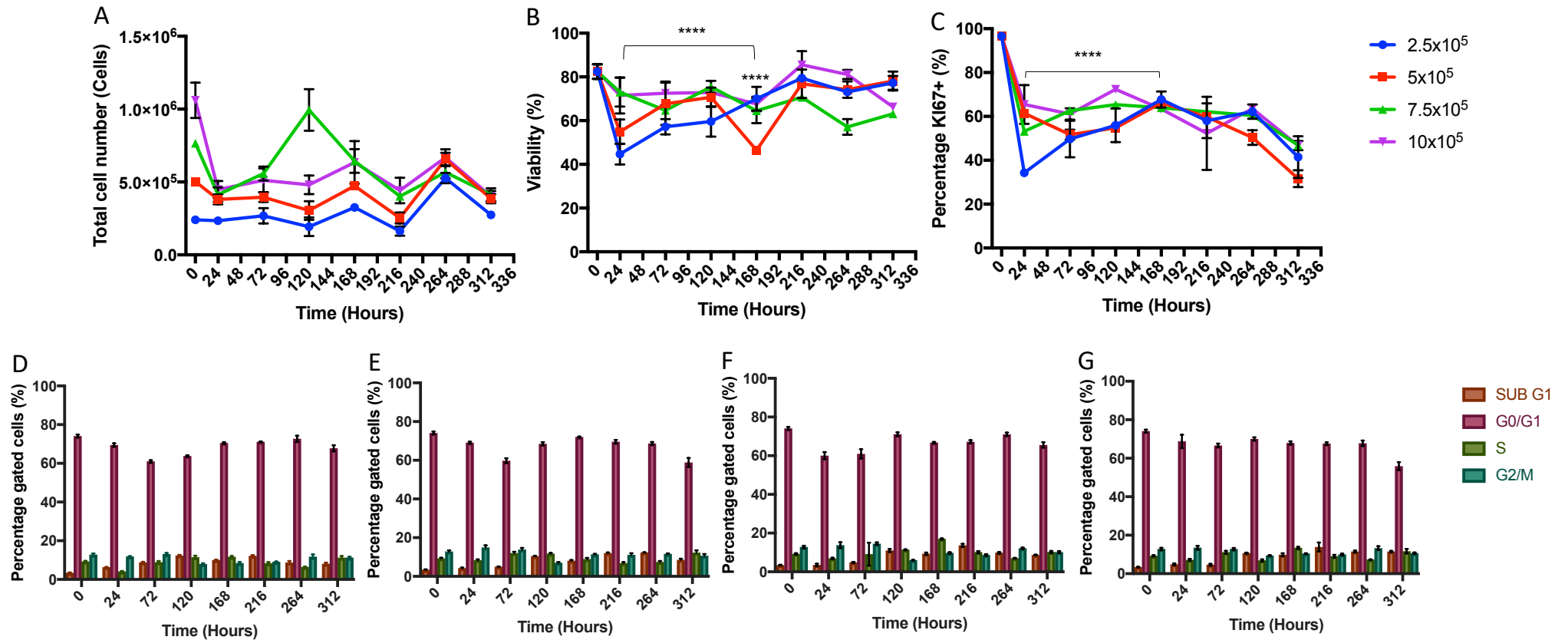


Figure 3-11. The growth of HS-5 cells seeded at 2.5, 5, 7.5 and 10 x 10⁵ cells onto an AlgiMatrix™ scaffold. HS-5 cells were seeded at a density of 2.5, 5, 7.5 and 10 x 10⁵ cells onto AlgiMatrix™ scaffolds, transferred to a 12 well plate, incubated for 24 hours, complete medium change undertaken and incubated for a further 312 hours with a 50% medium change every 48 hours. At each 48 hour time point, cells were harvested and assessed for total cell number (A) viability (B) and the presence of Ki67 (C). Cells at a starting seeding density of 2.5 (D), 5 (E), 7.5 (F) and 10 x 10⁵ (G) cells were also analysed for cell cycle over the same period. (50,000 events) (n=3). **Significant differences were calculated using a Two-Way ANOVA followed by a Dunnett's test. Significant differences between B. 24 hour 2.5 vs 168 hour 2.5 **** & 2.5 vs 5 **** C. 24 hour 2.5 vs 168 hour 2.5 **** were **** p < 0.0001, actual p values can be found in appendix 1.**

3.3.2.4. Identification of TK6 cells utilising florescent CD markers

In order to identify TK6 from HS-5 in future co-culture experimentation, the use of fluorescent antibodies of TK6 specific CD markers was investigated. The CD19 and 20 membrane markers were investigated for their presence on TK6 and HS-5 cells. It can be seen that HS-5 cells stained with each marker only produced one peak with the isotype control when analysed via flow cytometry (Figure 3-12 A). However, when TK6 were analysed, a sharp peak which has shifted to the right of the isotype control can be identified in Figure 3-12 A for CD19, whereas a broader peak can be seen with CD20 as fewer TK6 cells express this. As the presence of CD19 and 20 can clearly be identified, a total mixture of 3×10^5 TK6 and HS-5 cells in ratios of 100:0, 75:25, 50:50, 25:75, 0:100 were stained with CD19 and analysed by flow cytometry for the actual number of CD19 positive cells and percentage of TK6 vs HS-5 (Figure 3-12 B and C). Utilising percentage positive cells and the total cell number counted using trypan blue, the true number of TK6 successfully stained in each ratio can be seen compared to HS-5 (Figure 3-12 B). At 100% or 3×10^5 TK6 cells, 2.9×10^5 cells were stained and detected. At 50% or 1.5×10^5 TK6 cells, 1.9×10^5 cells were stained and detected with no cells detected at 0% or 0 TK6 cells. These total cell numbers were then converted into a percentage compared to the original trypan blue cell number. Figure 3-12 C shows the comparison between the original ratio and the actual percentage of TK6 in each sample. There is no significant difference between the estimated and actual percentage at 100, 75 and 0%. However, the actual percentage was statistically decreased compared to the estimated percentage at 50 and 25% TK6.

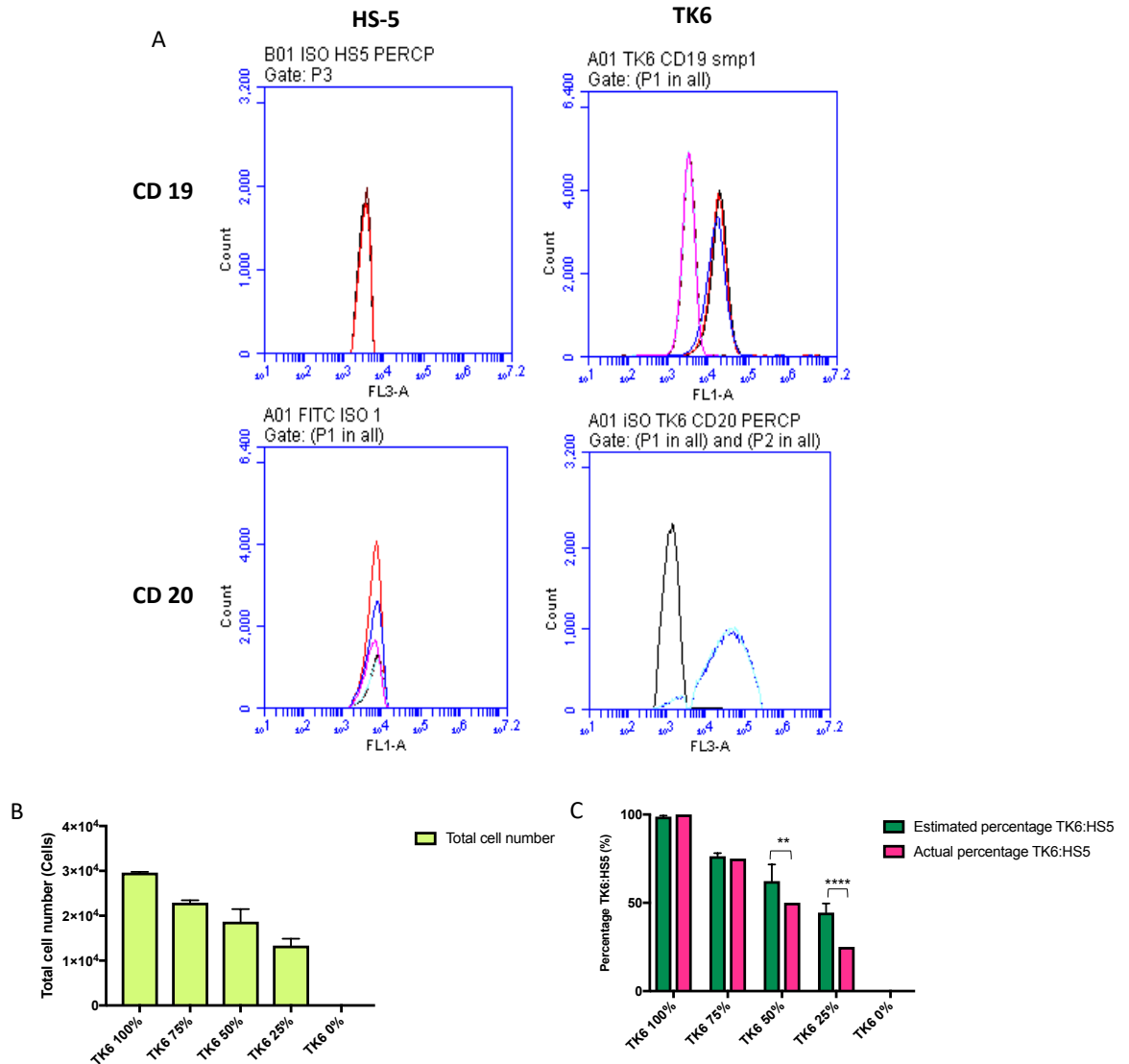


Figure 3-12 Histogram plot of CD19 and CD20 expression in TK6 and HS-5 cell lines. The expression of CD19 and CD20 (A) in TK6 and HS5 cells. Bar chart showing the total number (B) and percentage (C) of TK6 cells expressing CD19 in differing ratios with HS-5 (50,000 events, n=3). Significant differences between samples were calculated using a Two-Way ANOVA followed by a Dunnett's test. The P values are indicated by ** (p < 0.01), **** (p < 0.0001), actual p values can be found in appendix 1.

3.3.2.4.1. Identifying an initial concentration of TK6 and optimal long-term co-culture condition.

To investigate the required initial seeding density and exponential phase of TK6 cells for dosing of actively proliferating cells, HS-5 cells were seeded onto AlgiMatrix™ and incubated using the protocol described in section 2.3.1. TK6 cells were then directly added to each scaffold at an initial seeding density of 0.5, 1 and 3.5 x 10⁵ cells/ml. A medium change was then not conducted or conducted every 24 or 48 hours over a 102 hour period.

As identified in section 3.3.2.4 TK6 express CD19 unlike HS-5, this marker was used to distinguish TK6 from HS-5 in co-culture via flow cytometry, therefore, TK6 will now be identified as CD19+ and HS-5 CD19- in Figure 3-13.

Those scaffolds seeded with an initial concentration of 3.5×10^5 cells/ml, saw combined CD19+ and CD19- from the scaffold and medium increase over an initial 24 hour period (Figure 3-13 C) to a combined density of 2.7×10^6 cells. However, after a further 6 hours, the combined CD19+ cell population decreased whilst CD19- cells surpassed that of CD19+. Due to this shift in CD19+ and CD19- cells the experiment was terminated, and a medium change was not conducted. This result indicated that a lower seeding density of TK6 was required for culture past 24 hours.

A seeding density of 1×10^5 cell/ml was then trialled (Figure 3-13 F), which once again showed a steady increase in CD19+ cells, entering into an exponential phase at 24 hour up to a total cell number of 1.4×10^6 at 54 hours, over the same time period CD19- cells stayed $<2.5 \times 10^5$. However, after a further 24 hours of culture, the combined CD19- cell population increased and surpassed that of a decreasing CD19+ population. The shift in CD19 was seen for the remainder of the experiment, with CD19+ cells constantly decreasing from 1.4×10^6 - 5×10^5 cells between 54- 96 hours but CD19- cells remaining approximately 1.3×10^6 . As this result was also previously identified in Figure 3-13 C and no medium change had occurred in either, the introduction of a medium change was then investigated. As an initial seeding density of 1×10^5 cell/ml extended the experiment by 30 hours, compared to 3.5×10^5 cells/ml, this was used as the initial seeding density before a 50% medium change was conducted at 24 hours (Figure 3-13 G). This medium change increased the duration that CD19+ cells proliferated (0-30 hours), compared to 3.5×10^5 cells/ml (0-24 hours), with CD19- remaining $<2.5 \times 10^5$ and the start of an exponential phase of CD19+ cells identified between 6-24 hours. However, a medium change at this time point (24 hours) caused a decrease in CD19+ and increase in CD19- cells, at approximately 30-48 hours, a reduction from the 54-72 hours seen in Figure 3-13 F. This result seemed to indicate that a lower seeding density would be necessary but with added medium changes.

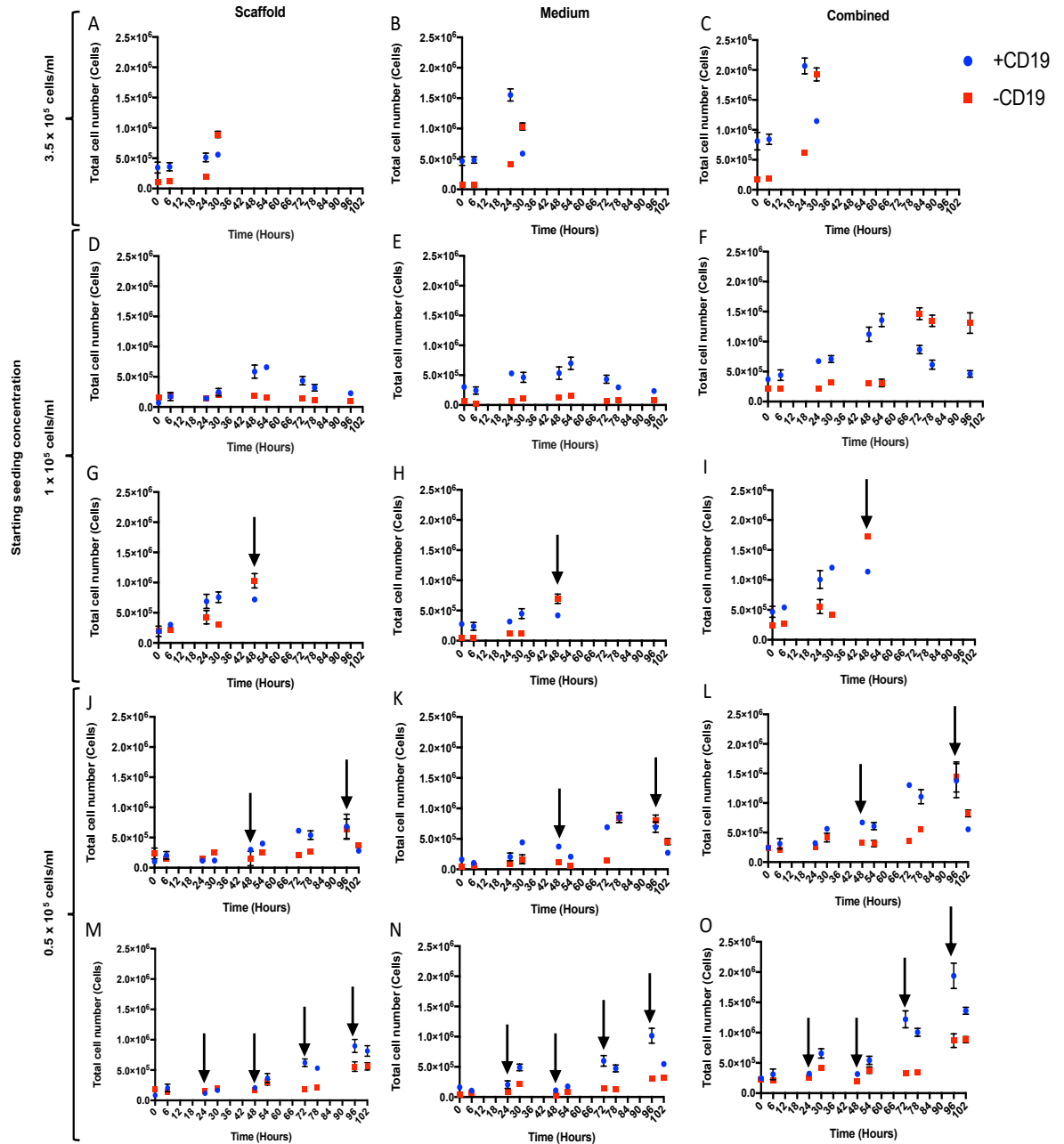


Figure 3-13. Initial seeding density and long-term culture of TK6 (CD19+) cells, co-cultured with pre-cultured AlgiMatrix™ scaffold. HS-5 (CD19-) cells seeded onto AlgiMatrix™ scaffolds at a density of 2.5×10^5 , incubated for 24 hours, complete medium change conducted, incubated for a further 144 hours with a 50% medium change every 48 hours. TK6 were then combined at an initial concentration of 3.5 (A, B, C), 1 (D, E, F, G, H, I) or 0.5×10^5 cells/ml (J, K, L, M, N, O). A 0% (A, B, C, D, E, F) or 50% (G, H, I, J, K, L, M, N, O) medium change was conducted every 0 (A, B, C, D, E, F), 24 (M, N, O) or 48 (G, H, I, J, K, L) hours over a 102 hour period. highlighted with an arrow. Twice over 24 hours, six hours apart, cells were collected from the medium (B, E, H, K, N) and dissolved scaffold (A, D, G, J, M), counted and stained separately with CD19 antibody. Percentage positive of cells was assessed by flow cytometry for total CD19+ and CD19- in the scaffold and medium giving a combined total for cells in the well (C, F, I, K, O). (50,000 events) (n=3).

As 1×10^5 cell/ml increased the longevity of the experiment, compared to 3×10^5 cell/ml, an initial seeding density of 0.5×10^5 cell/ml then investigated with a medium change every 24 hours (Figure 3-13 M). It can be seen that the CD19+ cells remain under 7×10^5 cells until hour 54, at this point an exponential phase can be seen between 54- 96 hours (5×10^5 - 2×10^6 total cells) with CD19- cells remaining $< 5 \times 10^5$ up to 96 hours. At 102 hours, CD19+ cells reduced and CD19- cell increased in cell number, but didn't surpass. The introduction of a medium change every 48, not 24 hours, was also trialed (Figure 3-13L) but once again CD19+ cells decreased at 96 hours, surpassed by CD19-. However, it was noted that the start of the exponential peak occurred at the same period (54- 96 hours) as a medium change every 24 hours. In all cases, before surpassing CD19+ cells, CD19- cells remained $> 5 \times 10^5$ total cells in the medium and scaffold. The proliferation of TK6, CD19+ cells, in the medium and scaffold was at the same rate despite the compartment they resided in. However, an increase in TK6 within the scaffold was required before an exponential increase in the medium was seen. Given this result, TK6 seeded at an initial density of 0.5×10^5 cell/ml and a 50% medium change every 24 hours identified an exponential peak, fit for compound dosing, between 54 and 96 hours (Figure 3-13 O).

In an effort to ensure that each well had been fully harvested of TK6 and HS-5 cells, light microscopy investigation of the well surface before and after TK6 addition was assessed (Figure 3-14). It can be seen that after 168 hours of incubation, a small population of HS-5 cells reside upon the well surface not on the scaffold (Figure 3-14 A). After the addition of TK6, and a 24 hour incubation, this small population of HS-5 seem to draw and adhere to the TK6 cells causing them to become immobile (Figure 3-14 B). However, after the medium and scaffold are removed and well surface washed, only a small population of both TK6 and HS-5 cells reside upon the well surface (Figure 3-14 C). This result highlights three cellular environments within each well, which includes the scaffold, medium and well surface. The role of each of these environments should be considered when administering compound.

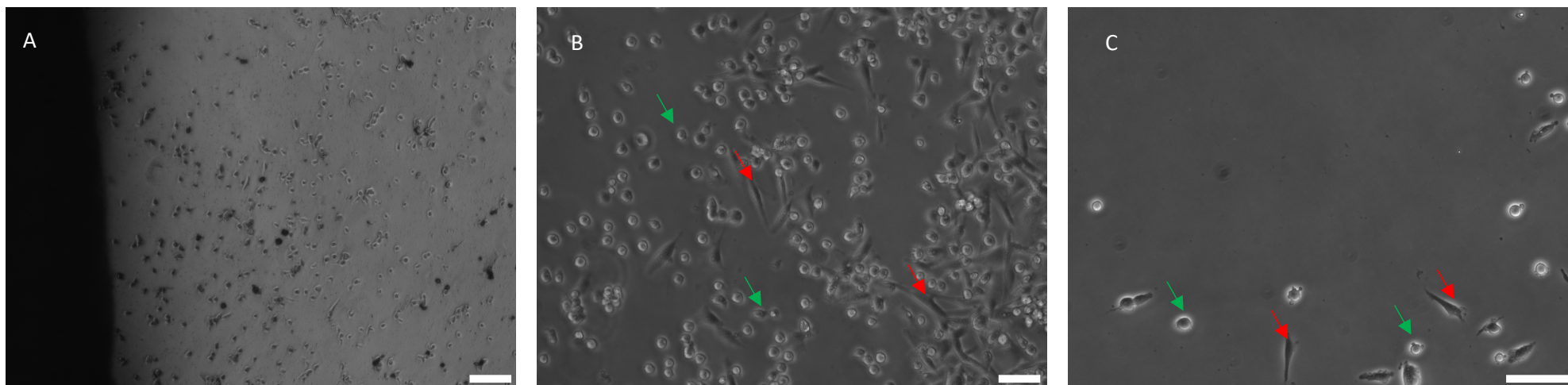


Figure 3-14. Light microscopy images of the bottom of a 12 well plate containing a seeded AlgiMatrix™ scaffold. HS-5 cells seeded onto AlgiMatrix™ scaffold at a density of 2.5×10^5 , incubated for 24 hours, complete medium change conducted, incubated for a further 144 hours with a 50% medium change conducted every 48 hours. (A) HS-5 cells residing on the bottom of the 12 well plate after 144 hour incubation of the AlgiMatrix™ scaffold, before the addition of TK6 at 0.5×10^5 cells/ml (4x magnification). (B) The bottom of a 12 well 168 hours after initial AlgiMatrix™ seeding and 24 hours after the addition of TK6 (10x magnification). (C) The surface of a 12 well plate after the removal of AlgiMatrix™ and TK6, 24 hours after TK6 initial seeding (20x magnification). Green arrows indicate TK6 cells, red arrows indicate HS-5 cells. Scale bar A. $100 \mu\text{m}$ B & C. $50 \mu\text{m}$.

The establishment of an initial seeding density and protocol for the longevity of both cell lines, allowed the investigation into the effects of TK6 and medium change on HS-5 viability and cell number (Figure 3-15). It can be seen that after an initial incubation (168 hours) of HS-5 onto the AligiMatrix scaffold, the viability, identified by flow cytometry, of HS-5 cells remained approximately 80% (Figure 3-15 A). TK6 in a well insert was then added at 5×10^4 cells/ml and left to incubate. After a 24 hour incubation, a 50% medium change of each well was conducted in the 24 hour group. An additional 24 hour incubation resulted in the viability dropping within the 48 hour group but staying approximately 80% within the 24, a medium change was then conducted in both the 24 and 48 hour groups and incubated for a further 24 hours. At this point a third 50% medium change was conducted on the 24 hour group and incubated a further 24 hours. Those HS-5 which received a 50% medium wash every 24 hours after addition of TK6 within a trans-well insert, remained at approximately 80% viability. However, the viability of those who received a medium change every 48 hours reduced to approximately 50%.

The viability recorded using flow cytometry (Figure 3-15 A), combined with the total cell number identified via TB, gave a total live cell figure for each time point (Figure 3-15 B). It can be seen that the live cell number did not change between 0 and 168 hours. However, after the addition of TK6 and a 24 hour medium change (24 hour group only), cells in both the 24 and 48 hour groups increased in live cell number from 1.6×10^5 live cells to 1.7×10^5 (24 hour group) and 2.4×10^5 (48 hour group). After a further 48 hour incubation, the live cell number increased again in the 24 hour group (1.7×10^5 - 2.2×10^5), however, a decrease in live cell can be seen in the 48 hour group below the initial count (2.4×10^5 - 1.5×10^5). These outcomes reinforce previous results in identifying the need for a medium change every 24 hours.

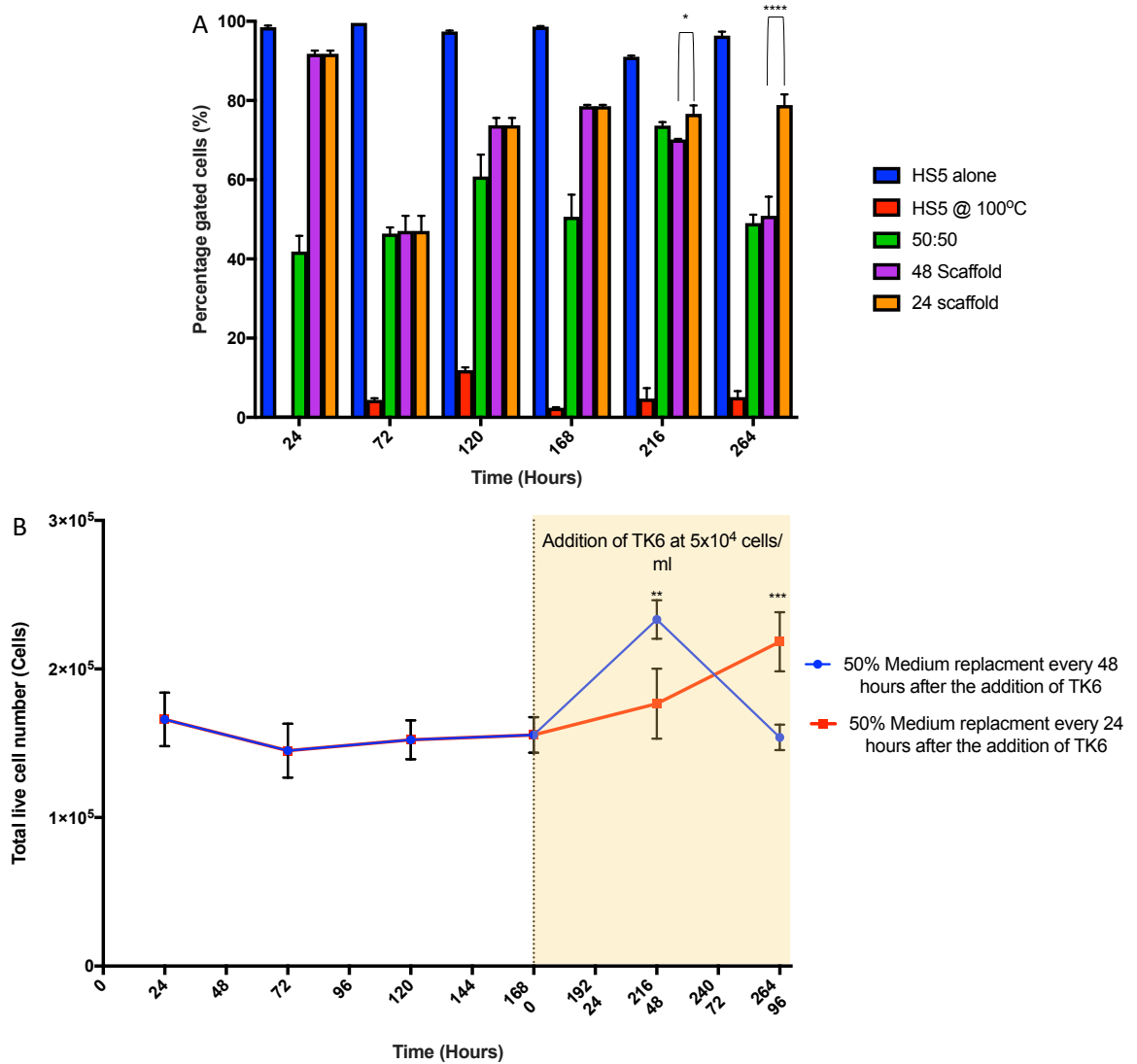


Figure 3-15. Viability of HS-5 cells seeded onto an Alginate™ scaffold with the addition of TK6. HS-5 cells seeded onto Alginate™ scaffolds at a density of 2.5×10^5 , incubated for 24 hours, complete medium change conducted, incubated for a further 144 hours with a 50% medium change conducted every 48 hours. At each 48 hour time point, scaffolds were harvested and assessed for total cell number (TB) and viability. After 168 hours of incubation, TK6 cells were added at a concentration of 5×10^4 cells/ml into a $0.25 \mu\text{m}$ well insert residing within each scaffold well. A 50% medium change conducted ever 24 or 48 hours. Each time point was compared to a dead (HS-5 incubated at 100°C for 10 minutes), live (HS-5 cells at a viability of $>90\%$) and 50:50 (dead: live) control for percentage positivity (A). This percentage positivity was then used to calculate the total number of live HS-5 cells in each condition (B). (50,000 events) ($n=3$). Significant differences between samples were calculated using a Two-Way ANOVA followed by a Dunnett's test. The P values are indicated by ** ($p < 0.01$), *** ($p < 0.001$), **** ($p < 0.0001$), actual p values can be found in appendix 1.

3.3.3. 3D printing of an in-house Alginate scaffold

3.3.3.1. Optimisation of a bespoke hydrogel for 3D printing and culture

A bespoke hydrogel (60% sodium alginate, 32% pluronic F127 and 8% medium) was constructed (to compare with the previously described Biomerix™ and AlgiMatrix™ scaffold) utilising the protocol in Armstrong *et al.* (2016). This hydrogel remains semi-fluidic at room temperature and partially solidifies at 37 °C, therefore, can be shaped into any form chosen. This hydrogel, Like the AlgiMatrix™, can incorporate cells into the scaffold itself reducing the need to layer cells upon a solid scaffold. However, once extruded into its final shape, this hydrogel must be crosslinked with varying concentration (100-1000 mM) of CaCl₂, dependant on the eventual application, and maintained in 5 mM CaCl₂ in order to gain the long-term structural integrity seen in the AlgiMatrix™ and BM ECM.

To assess the effect of CaCl₂ on viability, HS-5 cells were directly exposed for 10 minutes to differing concentrations of CaCl₂ (Figure 3-16). The results in Figure 3-16 show that when seeded into a 12-well plate, not scaffold, the viability decreases from 95% (0 mM) to 85% (100 mM) to 55% (500 mM) to 20% (1000mM) after the 10 minutes of exposure. These results infer that 1 M CaCl₂ is extremely toxic to cells due to a 65% reduction in viability. However, a lower concentration of 100 mM gave a viability >80%. Therefore, a concentration of 100 mM was investigated for its use in solidifying each hydrogel.

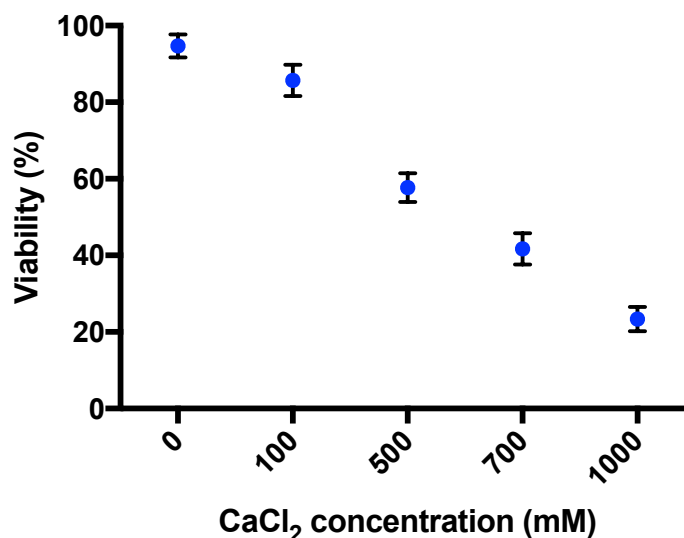


Figure 3-16. Viability of HS-5 cells after 10 minute exposure to 100, 500, 700 and 1000 mM CaCl₂. The graphs show HS-5 seeded at 1×10^5 cells into a 12 well plate, incubated for 2 hours before the addition of a concentration of CaCl₂ for 10 minutes. Each well was washed with PBS before the addition of trypsin. Cell viability was assessed using acridine orange / propidium iodide stain (n=3).

To test this, a hydrogel was recreated using the Armstrong *et al.* (2016) published protocol. These hydrogels were then crosslinked with 100 mM CaCl₂ in complete medium for 10, 15, 20, 25 and 30-minute as seen in Figure 3-17. An additional concentration of 1 M CaCl₂ was also tested (Figure 3-17). Once the hydrogel had formed the medium was removed and fresh 5 mM CaCl₂ in complete medium was added. This protocol should produce a tight hydrogel structure like the ECM of human BM for HS-5 to spread and interact, with uniform pores across the hydrogel suitable for cytokines and other cellular signalling molecules to flow. As can be seen in Figure 3-17 the 1 M hydrogel has formed a solid, opaque ball which light will not pass through. This 1M hydrogel took 10 minutes to develop, which when taken out of the medium and squeezed with tweezers sprang back to its initial structure. The addition of 100 mM, as seen in Figure 3-17 for 10, 15, 20 and 25 minutes gave a slightly transparent hydrogel which disassociated when manipulated with tweezers. It wasn't until 30 minutes of incubation that the hydrogel represented the mechanical properties of that seen with 1M. Due to the similar mechanical properties of the 1 M and 100 mM (30 minutes) hydrogels, these were taken forward to assess, via SEM, if pore size had been affected by increased exposure.

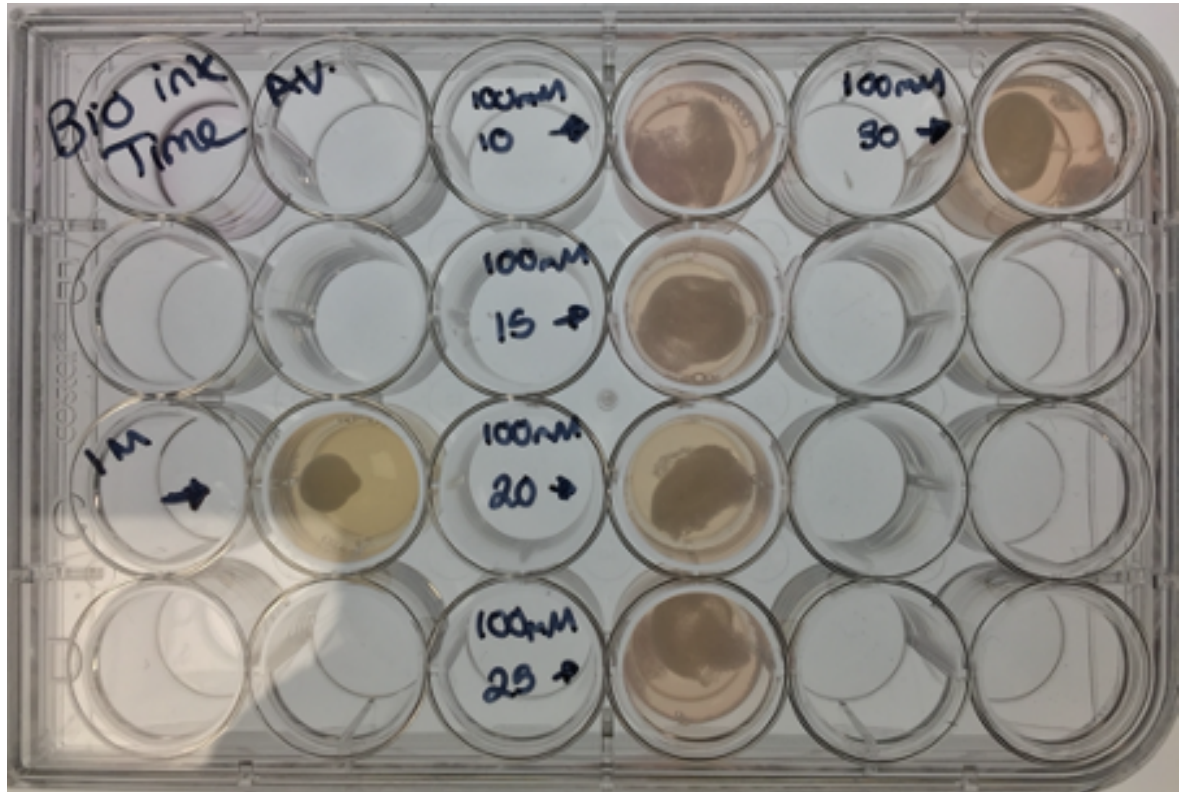


Figure 3-17 Image of crosslinked hydrogels after a 30 minute period to 100 mM or 1 M CaCl_2 in medium. Image shows the hydrogel formed after 10, 15, 20, 25 and 30 minute bioink exposure to 100 mM CaCl_2 . The image also shows a 10 minute exposure to 1 M CaCl_2 . At each time point the 100 mM/1 M CaCl_2 was replaced with 5 mM CaCl_2 to maintain the gel's structure.

The hydrogels were subjected to SEM at a magnification of x1000 (Figure 3-18 A) and x600 (Figure 3-18 B). The 1 M hydrogel can be seen in Figure 3-18 A and shows a very compact, uniform construction with pores no bigger than approximately 1 μm being visible throughout. The 100 mM hydrogel seen in Figure 3-18 B, however, shows a very loose construction with varying pore sizes across the area (approximately 1- 50 μm approximately). These results show that a concentration of 1 M would be beneficial in the production of a scaffold which HS-5 cells could be layered upon, but 100 mM could be used for the inclusion of cells into the scaffold itself. This hydrogel, due to its semi-fluidic nature at room temperature, could be used within cutting edge 3D biological printers as a bioink which could be extruded into any shape necessary. Therefore, the use of this hydrogel as a bioink in a 3D biological printer was investigated.

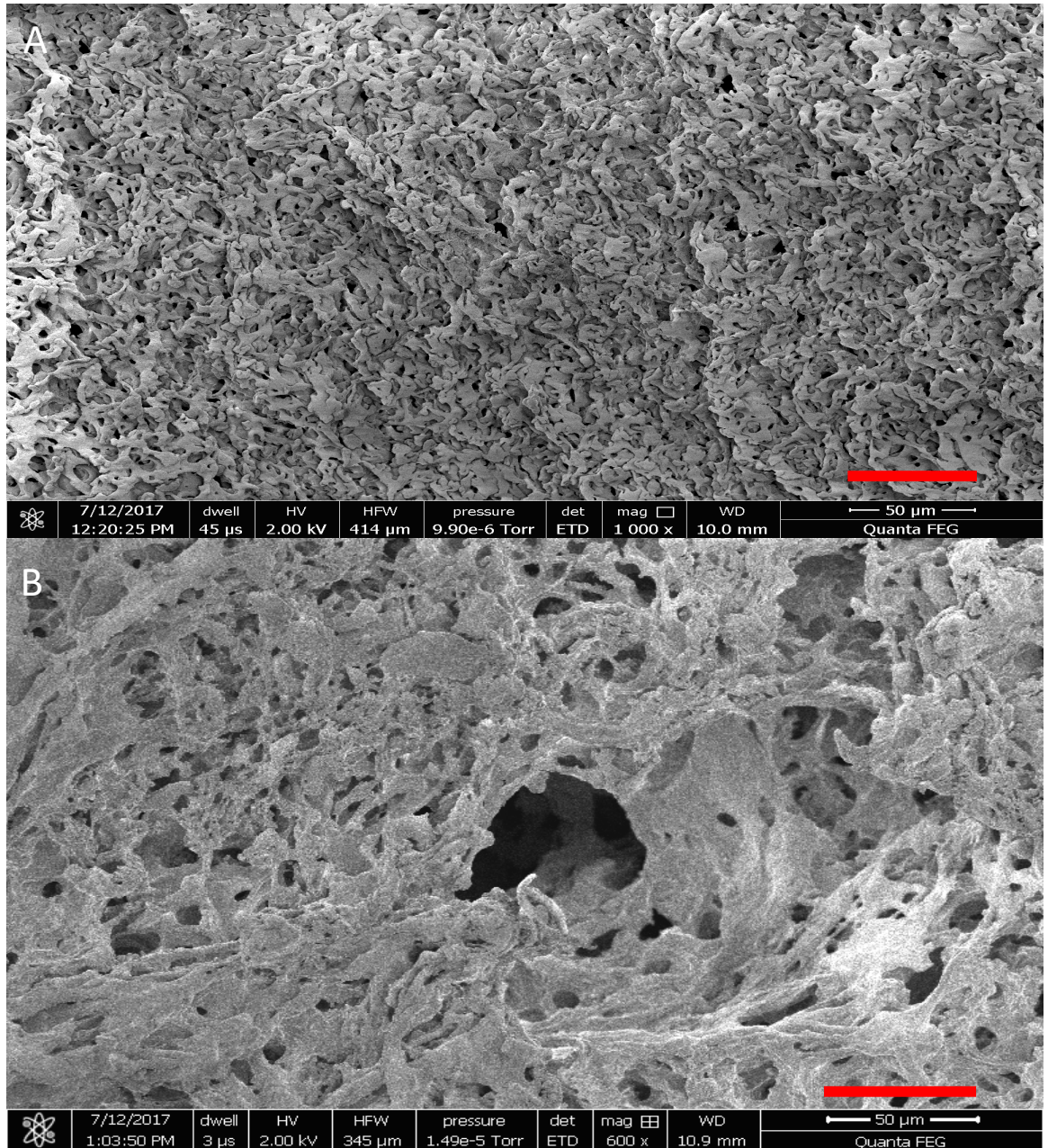


Figure 3-18 Scanning electron microscope (SEM) images of the bespoke alginate hydrogel. Hydrogels were crosslinked with either 1 M (A) or 100 mM (B) CaCl_2 until the gel had solidified adequately to undergo SEM. Scaffolds were left to dry overnight on lint free tissue before being processed for SEM. A. 1000x magnification of a crosslinked hydrogel with 1 M CaCl_2 for 10 minutes. B. 600x magnification of a crosslinked hydrogel with 100 mM CaCl_2 for 30 minutes. Scale bars indicate 50 µm.

3.3.3.2. Conversion of a polylactic acid 3D printer to extrude biological material

To construct a 3D hydrogel ECM, a personal communication with Richardson and Perriman of the University of Bristol led to the idea of converting a conventional 3D printer into a biological one which could print bioink. Richardson and Perriman suggested using the Mendlemax 3D printer as this could be modified easily with parts printed on the machine itself. Richardson and Perriman had used the 3D printer before and agreed to allow UWE access to the conversion data required. The converted 3D printer would allow the extrusion of bioink forming a bespoke scaffold of varying size and shape produced using online software.

Figure 3-19 of the 3D printer shows how it was bolted together (Figure 3-19 A) using an online manual from Makertoolbox (the supplier of the printer). The motherboard, motors, power supply and fans were then wired into the shell to produce a fully functioning 3D printer (Figure 3-19 B). To show that the printer can print a platform of our choice, a bespoke scaffold was designed (Figure 3-19 C- G). Firstly, a SEM image of human BM was traced in black and white (Figure 3-19 C) so that the online software Selva could differentiate the pores from the ECM when converting the 2D trace into a 3D stl. file (Figure 3-19 D). The converted, single plain 3D trace was then uploaded into the online software Tinkercad where it was duplicated, turned on its axis and collated to form a completed bespoke scaffold (Figure 3-19 E). This completed scaffold was then uploaded to the 3D printer software Mattercontrol (Figure 3-19 F) and printed in PLA thermoplastic. The resulting successfully printed scaffold (G) showed that it was possible to print a scaffold of our choice, thus the conversion into a 3D bioprinter began. The 3D stl. conversion files (pusher, motor holder and mounting bracket) were kindly donated by Richardson and printed out in PLA using the Mendlemax 3D printer (Figure 3-19 H). Due to the differing constraints the bioink, but not the solid PLA, would have on the printer, firmware (computer code) was uploaded to the Mendlemax using the programme Arduino (Figure 3-19 I). The printer was then ready for the extrusion of the hydrogel bioink in a constant, uniform pattern as seen in Figure 3-19 J. However, the inclusion of cells into the bioink before extrusion was unmanageable due to long printing times and lack of sterility. The printing time was reduced with optimisation, but due the sheer force on the pump motors, produced from printing a viscous fluid, this time could not be reduced to <1 hour for the simple structure seen in Figure 3-19 J. The issue of time was not a problem with structures printed without HS-5 inclusion, but a scaffold that

could retain these cells was ultimately required. Due to time restraints caused by increased printing times and further optimisation of the gel itself, which had already been conducted with the similar commercial AlgiMatrix™ scaffold, this hydrogel was side-lined for future work in favour of the AlgiMatrix™ scaffold.

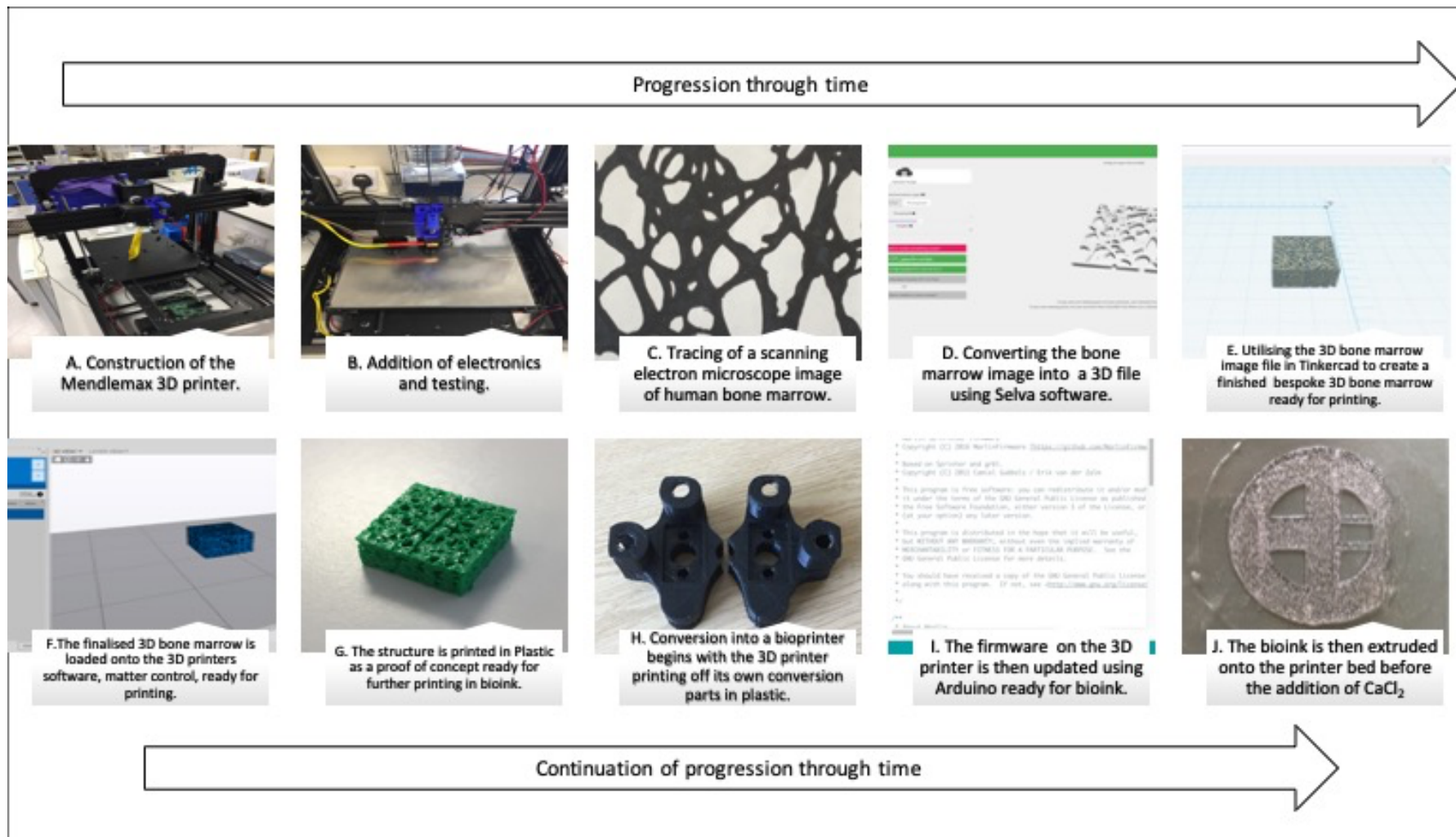


Figure 3-19 Process of building and converting a 3D printer whilst also creating a bespoke scaffold from scratch. The process follows the chronological order as depicted by A, B, C, D, E, F, G, H, I and J

3.3.4. Identification of a single cell type within a co-culture

3.3.4.1. Identification of TK6 cells from HS-5

In order to identify micronuclei within either the HS-5 or TK6 co-cultured population, the nanocrystal dye, Qtracker, was evaluated. The Qtracker dye, using manufactures guidance, was added to TK6 and mixed with unstained HS-5 cells in ratios of 0:100, 25:75, 50:50, 75:25, 100:0 (Figure 3-20 A-E respectively). It can be seen, under fluorescent microscope, that as the ratio of TK6 to HS-5 increases, the Qtracker dye also is seen to increase. These seeding ratios were also analysed using flow cytometry (gating strategy Figure 2-1) (Figure 3-20 H), with percentage Qtracker stained cells vs percentage positive events equating to 100% = 91%, 75% = 67%, 50% = 49%, 25% = 20 and 0% = 0%. However, when TK6 cells in isolation were counterstained with either DAPI (Figure 3-20 F) or Hoescht (Figure 3-20 G), the Qtracker dye was unable to identify individual cellular membrane boundaries for the detection of micronuclei.

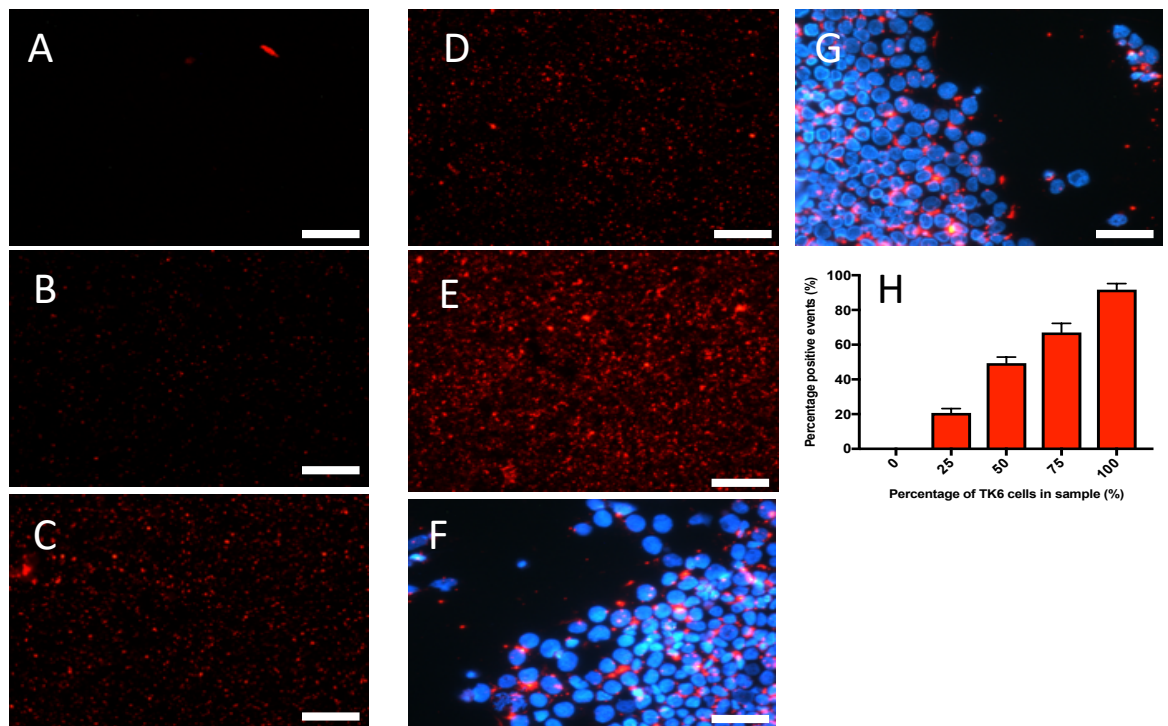


Figure 3-20 Fluorescent microscopy images of TK6 cells stained with Qtracker combined in differing ratios with unstained HS-5 cells TK6 cells were incubated with Qtracker dye (10 nM). The stained TK6 cells were then mixed in differing ratios with unstained HS-5 cells A: 0:100, B: 25:75, C: 50:50, D: 75:25, E: 100:0 (40x magnification). The nucleic stains DAPI (F) and Hoescht (G) were then added to Qtracker stained TK6. Bar chart (H) showing the number of events positive for Qtracker when analysed via flow cytometer (50,000 events) (n=3). Scale bars indicate 50 μ m.

The use of CD19 and 20, identified in section 3.3.2.4, were evaluated for their use as a membrane marker for the identification of micronuclei in TK6 cells (Figure 3-21). A ratio of TK6 to HS-5 cells (total cell number of 3×10^5 total cells) at 100:0, 50:50 and 0:100 were first stained with CD19 and 20 conjugated antibodies (FITC and PerCy5.5) and subsequently counterstained with DAPI (Figure 3-21 A, B and C). The combination of antibodies and DAPI produced an image which was unable to differentiate TK6 from HS-5 cells or clearly identify nucleic acid material. Utilising the same ratio of cells, a primary, unconjugated antibody of CD19 and 20 was first incubated with each culture, a secondary Alexa Fluor 488 fluorophore was then incubated before the addition DAPI. This staining combination produced images in which the ratio of TK6 to HS-5, membrane and nucleic acid material can be clearly seen (Figure 3-21D, E and F) and would be used in further studies.

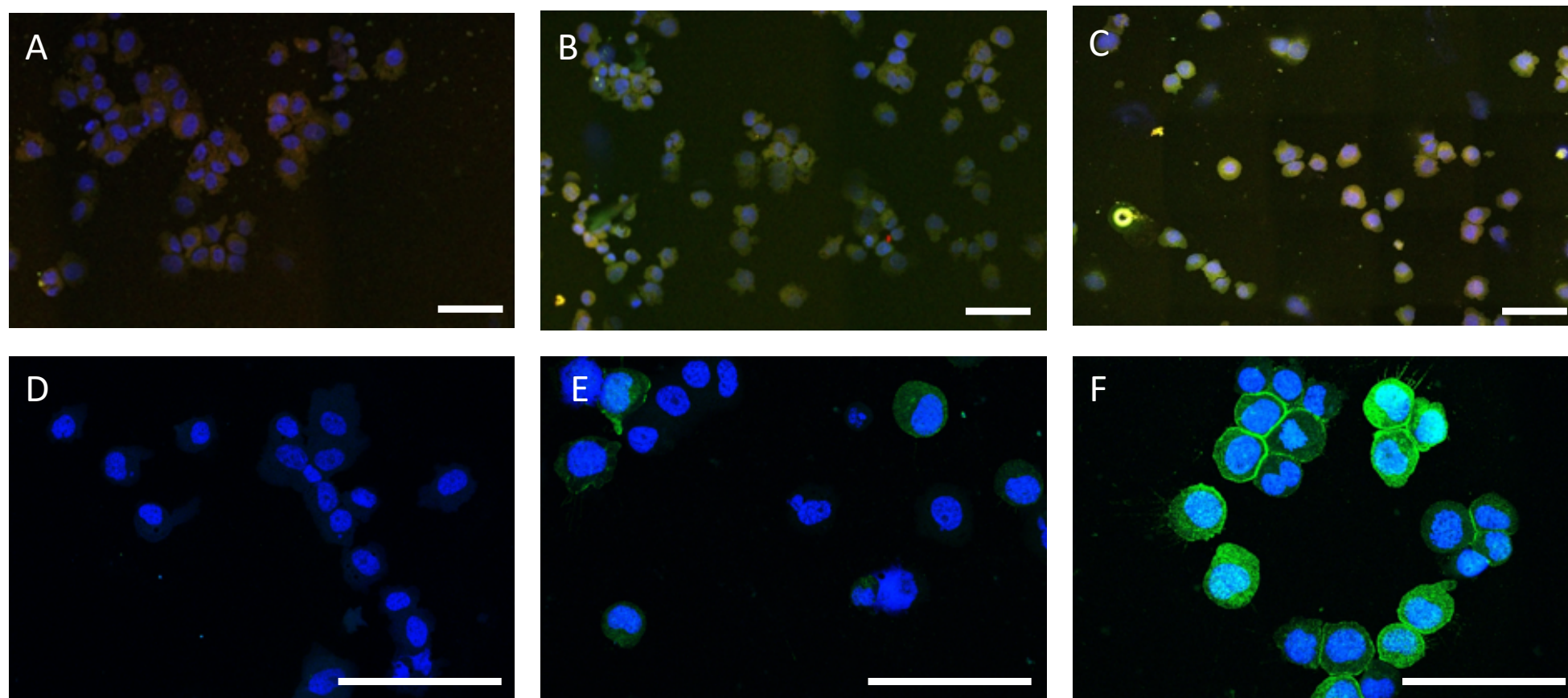


Figure 3-21 Fluorescent confocal microscopy images of TK6 and HS-5 cells stained with CD19, CD20 and DAPI in differing ratios. TK6 and HS-5 were combined in differing ratios A, D: 0:100, B, E: 50:50, C, F: 100:0 before being spun down onto slides for staining. Cells were either stained with conjugated CD19, CD20 (A, B, C) or unconjugated CD19 and CD20 with an Alexa Fluor 488 secondary (D, E, F) before the addition of DAPI and progold antifade. A, B, C 40x magnification D, E, F 60x magnification. Scale bars indicate 50 μm .

3.4. Discussion

The aim of this chapter was to establish an *in vitro* model of the BM, which simulated the *in vivo* environment, for the proliferation and expansion of co-cultured cells for the future addition of compound. The results presented within this chapter show the successful selection, optimisation and long-term culture of a simple, reproducible, *in vitro* 3D model of the BM, utilising cell lines and a static dissolvable ECM which simulated the structure of the *in vivo* environment. This model was also able to maintain the TK6 cell line in its exponential phase.

3.4.1. 3D Scaffold assessment

3.4.1.1. The Biomerix™ hard scaffold already in use at UWE

A model already in development at UWE was first trialled for its ability to simulate the microenvironment of the BM. This model utilised the commercially manufactured, hard, polyurethane based Biomerix™ scaffold. This scaffold was initially identified as a candidate as it has been used in regenerative medicine, in combination with primary MSCs, due to its biocompatibility and interconnecting pores, of around 100 to 250 μm , which closely corresponded with the structure of the *in vivo* BM (Gniesmer *et al.*, 2019; Encalada-Diaz *et al.*, 2011). These matrices were then cultured with an initial layer of the cell line, HS-5. The HS-5 cell line has a fibroblast morphology which is used as a stromal layer due to its secretion of large quantities of cytokines. The cytokines released imitated that seen in the human BM, driving differentiation of haematopoietic stem cells to maturation (Ramakrishnan *et al.*, 2013; Aqmasheh *et al.*, 2017). The HS-5 cell line differs however, from the primary MSCs within the human BM as they are less adherent which could explain the lack adherence to the Biomerix scaffold seen in Figure 3-1, 3-2, 3-3 and 3-4 (Adamo *et al.*, 2020).

The results from Figure 3-1 show that after using the original seeding protocol of a 2 hour incubation of 5×10^5 cells upon the Biomerix™ scaffold, before the addition of fresh medium, cells evacuated the scaffold and adhered to the surrounding plate. This result can be justified primarily via adherence time, cell-cell contact and surface area. Work conducted by Salzig *et al.* (2016) found that primary MSCs adhered within 4 hours when seeded at a concentration of 7×10^3 - 1×10^4 cells cm^2 in a six-well plate. However, work by Vasibuh *et*

al. (2010) found that when utilising at a seeding density of 1×10^6 cells per scaffold, primary cells needed 24-48 hours to adhere with cells still leaving the scaffold when flushed. The work conducted on HS-5 cells by Wang *et al.* (2007) and Mraz *et al.* (2011), found that at a seeding concentration of 5×10^4 cells per well 24-48 hours was the minimum time needed for successful adhesion to a 96/24 well plate. The first conclusions made from this evidence is that a lower seeding density is needed when seeding in plates ($7 \times 10^3 - 5 \times 10^4$ cells), compared to Biomerix™ (1×10^6), due to the maximum surface area available to the cells in the latter. The Biomerix™ has a greater surface area, so required a greater initial seeding density for close cell-cell communication when adhering. The initial seeding density of 5×10^5 cells used in Figure 3-1 was thus too low, and cells evacuated the scaffold to adhere on the plate where there was less surface area. The second conclusion that can be drawn from the evidence above is that primary MSCs, which are more adherent than HS-5, need around 4-24 hours incubation, with HS-5 needing at least 24 hours (Adamo *et al.*, 2020). The initial 2 hour incubation utilised in Figure 3-1 thus was too short.

The conclusion, that an initial 2 hour incubation was too short for successful adherence, were then rectified using time lines within the literature. The initial adherence time was increased to 4, 5 and 24 hours, with initial seeding densities of 5×10^5 and 1×10^6 cells/ scaffold tested. Scaffolds were left for cells to adhere naturally, or scaffolds were compressed-decompressed after addition of cells, as this was hypothesised to bring a higher proportion of cells to the centre of the scaffold increasing cell-cell contact. In line with the previously mentioned literature, a higher seeding density of HS-5 (1×10^6 cells/ scaffold) combined with a prolonged initial seeding time of 24 hours, increased the cells remaining within the scaffold. Conversely, scaffolds that were compressed-decompressed retained less HS-5 than those left to adhere naturally. This finding suggests that the internal surface area of the Biomerix™ was still too large, even with increased cell number, and that cells that naturally adhered to the external structure of the Biomerix™ were in closer proximity and thus remained attached. However, even when using the increased initial seeding time (24 hours) and cell number (1×10^6 cells/scaffold), regardless of the manipulation of the scaffold, HS-5 cells still evacuated the scaffold during long term culture as can be seen in Figure 3-4. This finding could, in part, be due to the small amount of medium used to initially adhere the HS-5 onto the scaffold. In all experimentation, HS-5 were added to scaffolds in 20 µls of medium before a 2, 4, 5 or 24 hour incubation. This amount of medium was seen as sufficient initially, due to a 48 hour doubling time of HS-5. but work by Kosol *et al.* (2019) found that a reduction in medium supplementation caused a considerable reduction in cellular processes,

such as adherence of stromal cells similar to HS-5. However, the study also suggested that even with larger volumes of medium, cells still may not adhere and instead prefer to reside in the medium or plate due to cell-cell contact, and surface area described previously. Work by Bruce *et al.* (2015) found that in human BM stromal cells, the use of microfluidic systems increased cells residing within the scaffold. It was suggested that the constant shear force and circuit of flow, reduced the adherence to the plate, thus cells remained in the medium. This medium was then constantly forced through the scaffold allowing cells to only adhere to the scaffold itself. It was concluded from this evidence, that the Biomerix culture protocol could work in a microfluidic system. However, due to the increased cost and complexity of microfluidics, which was beyond the scope of the project, investigation into an alternative scaffold, which would encapsulate and or adhere the HS-5 in place in a static system, would be more beneficial in developing a cheap, reliable, easy to use assay in any laboratory.

3.4.1.2. Establishing a new model for 3D co-culture

Reviewing the current literature and conversing with collaborators at University of Bristol and AstraZeneca, it was decided that an alginate hydrogel model would best suit the needs of this research, as they have been used in regenerative and tissue engineering of the BM due to its bio-mechanical properties (Hernández-González *et al.*, 2020). Alginate, a lineal hydrophilic polysaccharide, can be dissolved into complete medium, with/ without cells, to make a thick honey-like liquid. This can then be crosslinked with a divalent cation, such as CaCl_2 , to form a rigid hydrogel with pores of differing sizes depending on the concentration of the divalent cation, encapsulating cells within. The alginate hydrogel can then be dissolved using a chelating agent such as EDTA for retrieving the cells within (Stagnaro *et al.*, 2018). The Algimatrix™ scaffold, once solidified, can also be dissociated using the dissolving buffer supplied by the manufacturer. As this category of hydrogel would negate the issues seen with the Biomerix™, as cells would be encapsulated into the hydrogel, two differing alginate hydrogels were selected, including the commercial Algimatrix™ and hybrid in-house hydrogel constructed by Armstrong *et al.* (2016). The Algimatrix™ system consists of a freeze-dried scaffold, containing alginate, which is then rehydrated with a firming buffer with/ without cells (Godugu & Singh, 2016). However, the in-house hybrid gel required the combination of alginate, pluronic F127 and medium, with/ without cells, which was then bathed in CaCl_2 to form a rigid structure. This selection allowed the comparisons between a hydrogel with known constituents (hybrid), versus one that we did not (Algimatrix™), for the ability to create an *in vitro* environment similar to that of the *in*

vivo BM. In both cases, a solution of either CaCl₂/ firming buffer was needed to solidify either the hybrid gel or freeze-dried scaffold, the concentration of which, in either case, determined the pore size and mechanical properties of the final structure.

The Algimatrix™ firming buffer was investigated for its effect on HS-5 cells. A firming solution of either 10, 25 or 50%, firming solution: medium, was added to the freeze-dried scaffold and incubated for 5 minutes before fresh medium added. It can be seen in Figure 3-5 B, C, E, F, H and I that there is no difference in internal or surface structure under light microscopy. However, the overall mechanical structure differs greatly. Those scaffolds solidified in 10% firming buffer (Figure 3-5 A) fell apart under light manipulation, whereas 25 and 50% (Figure 3-5 B & C) retained its structure when manipulated. As there wasn't any visible alteration in the internal or external structure of each scaffold, SEM was conducted. The SEM images (Figure 3-6) show that at concentrations of 10%, no pores were seen, at 25% pores of 25 µm were seen and at 50% pores of 100-150 µm were seen. The mechanical and internal structure is as a result of diluted cation within the firming buffer. Studies such as Zhang *et al.*, (2020), Watanabe *et al.*, (2019), Çelik *et al.*, (2016) and Agulhon *et al.*, (2014) found similar results when setting alginate scaffolds. These studies found that at lower concentrations of cations such as Mn²⁺ Co²⁺, Cu²⁺, Ca²⁺, Mg²⁺ and Sr²⁺, penetration to the centre of the scaffold was not achieved, leaving an alginate hydrogel of poor mechanical structure and smaller internal pore size, similar to the scaffold seen at 10 and 25%. At low concentration, the cation solution is depleted through chelation with (1-4)-β-D- mannuronic acid and α-L-guluronic acid subunits, before it can reach the centre. Therefore, this was overcome by saturating the scaffold in a high level of cation solution, similar to solidifying each scaffold in 50% firming buffer, so that crosslinking can occur throughout the entire scaffold. This same observation was also seen with the in-house hybrid gel. The protocol set out in the Armstrong *et al.* (2016) paper required the alginate, pluronic F127 and medium solution to be crosslinked with 100 mM CaCl₂ for 10 minutes. However, as Figure 3-17 shows the hydrogel did not solidify and instead fell apart. If the gel was solidified in 100 mM for 30 minutes a structure which could be manipulated was achieved. If the concentration of CaCl₂ was increased to 1 M, scaffolds became solidified in only 10 minutes, to the same degree as 100 mM for 30 minutes. Once again, SEM was conducted on both 1 M scaffolds (10 minute incubation) and 100 mM (30 minute incubation) (Figure 3-18), in line with the literature and the Algimatrix™ scaffold result, small pores of around 1 µm, with a 100 mM solution, and larger 25 µm, with 1 M CaCl₂ were achieved. As previously stated in section 4.1.1, the human BM consists of pores around 100 to 250 µm,

and it has been found that pore size has a considerable impact on cellular differentiation and proliferation of the cellular compartments within the BM (Chen *et al.*, 2020). A study by Gupte *et al.* (2018) identified that smaller pore sizes (<50 μm) would enhance differentiation of human BM stromal cells down the chondrogenic lineage compared to large pore scaffolds. It was also found that a small pore size reduced interconnectivity and medium flow, therefore, promoting capillary formation to enhance this. Conversely, Brennan & Hoey, (2019) found that pores of 100- 200 μm was beneficial for cellular morphology, proliferation and osteogenic differentiation of human MSCs, signifying that the pore size produced within a 50% solidified scaffold of 100 and 150 μm , would be *in vivo* relevant.

It can be concluded from these results, a CaCl_2 solution of 1 M (hybrid) or a firming solution of 25 or 50% (AlgiMatrix™) is required to produce pores which will aid in proliferation, differentiation and morphology similar to the *in vivo* environment. However, does this level of CaCl_2 or firming buffer cause detrimental effects to the cells which require incorporation into the hydrogel or scaffold?

Calcium is fundamental to controlling cell life, hormone secretion, gene expression, immune response and apoptosis (Rimessi *et al.*, 2008). As calcium is fundamental to cell life/death, Armstrong *et al.* (2016) utilised a very small dose (100 mM) to set the hydrogel for 10 minutes with little detriment to the human MSCs within. However, as previous experimentation has shown, a concentration of 1 M CaCl_2 is necessary for adequate pore size and mechanical structure. The results in Figure 3-16 show that when HS-5 cells were directly exposed to 1 M CaCl_2 , viability dropped by 80% with a concentration of 500 mM reducing viability by around 50%. Work by Cao *et al.* (2012) on Schwann cells, with reduced susceptibility to calcium compared to BM, looked at crosslinking hydrogels with 100 mM, 500 mM and 1 M CaCl_2 for 5, 10 and 30 minutes. They found that in all cases, direct exposure to calcium had triggered an apoptotic response which had reduced the cell viability by 50% compared with that of the control. Cao *et al.* (2012) noted that when cells were indirectly (within the hydrogel) exposed to levels of CaCl_2 , the cell viability was >60% even at a 1 M concentration. The cells within the hydrogel seem to be protected from the CaCl_2 thus a higher concentration had a reduced effect on the cells. Similar work by Acri *et al.* (2019), found that a concentration of 20 mM CaCl_2 or below, added directly to human BM MSCs, was required for a reduction in toxicity and unaltered gene expression.

In conclusion, given the viability and structural data produced with CaCl₂, it is not possible to incorporate cells into this hybrid alginate hydrogel. This protocol would be beneficial if the hydrogel was extruded from a biological printer, seen in Figure 3-19, to form a specific structure, crosslinked followed by the addition of HS-5 cells; however, the lack of adherence may occur as seen with the Biomerix™. Due to these complications, the use of the hybrid alginate scaffold was ceased in favour of the Algimatrix™ system.

The solidified Algimatrix™, as mentioned previously, can be dissociated with the supplied dissolving buffer. The constituents of this buffer are unknown, therefore, the toxicity to HS-5 was conducted, in parallel with an investigation into similar dissolving solutions. As seen in the hybrid gel, a divalent cation was used to crosslink alginate subunits to create a solidified structure. When mechanical and structural properties were compared to that of the solidified AlgiMatrix™ scaffold, several similarities were seen. Since both scaffolds seem to be constructed using a divalent cation, a chelating agent such as EDTA could be the main component of this commercial dissolving buffer, and therefore would be used as a comparison. The AlgiMatrix™ protocol for dissolving buffer requires bathing each solidified scaffold in 3 mls of solution for 5-10 minutes, depending on the percentage firming buffer used, with manipulation to break up the scaffold entirely. The firming buffer, with increased percentage, introduces more of these crosslinks which require a longer period of time to chelate (Grijalvo *et al.*, 2019).

As can be seen in Figure 3-7, when 3 mls of 55 mM EDTA or dissolving buffer was added directly to HS-5 cells, there was no difference between solutions in cell number or viability over the initial 5-10 minute period required within the protocol. The experiment was extended to 30 minutes as this was the maximum time, indicated by the manufacture, needed to dissolve an AlgiMatrix™ scaffold with dissolving buffer therefore, if there was no detrimental effects up to this point then solutions were determined as non-toxic and, as shown, there was no reduction in viability or cell number over this time period. As the time required for dissolving was dependent on the firming buffer percentage used, a 50% scaffold was bathed in each solution for 5 minutes. A 50% AlgiMatrix™ scaffold was included as firming with this solution, which provided the required pore size and mechanical structure identified *in vivo* have the maximum subunits to chelate, therefore should require an increased time to dissociate. As can be seen in Figure 3-8, after a 5 minute incubation, in either solution, the scaffold hasn't dissolved, with more remnants within the EDTA solution

than dissolving buffer, therefore, a >5 minute incubation in either solution would dissolve a scaffold solidified with a firming solution <50%.

Given the results obtained, it can be concluded that both the dissolving buffer and 55 mM EDTA are non-toxic to HS-5 cells and that the dissolving buffer's main constituent appears to be a chelating agent similar to EDTA, but possibly more concentrated, as AlgiMatrix™ scaffolds were dissolved more rapidly in the dissolving buffer. Now that the dissolving buffer has been seen as non-toxic and requires >5 <30 minutes to dissolve a scaffold, the successful retrieval of cells, without loss of viability, can be conducted, and the effects of the firming buffer on HS-5 seeded within the scaffold was investigated.

The AlgiMatrix™ firming buffer produced scaffolds which, when compared to the hybrid alginate gel, seemed to resemble structures created by a divalent cation such as CaCl₂. As seen with previous work within section 3.3.3.1, CaCl₂ had a detrimental effect on directly treated HS-5 cells, however, it seemed from the literature, that cells within a scaffold are less affected by the cation compared to those treated with a direct dose. Since the firming buffer appeared to include a divalent cation, the toxicity of this buffer was investigated. Utilising the protocol put forward by the manufacturer, HS-5 cells were seeded in 10, 25 or 50% firming buffer, at a total count of 2.5×10^5 cells/scaffold into dry AlgiMatrix™ scaffolds; once set new complete medium was added and then scaffolds left to incubate. Even though results in Figure 3-6 showed that a 10% scaffold did not produce a structure that simulated the *in vivo* setting, it was still included for comparison of toxicity with dose escalation conducted with CaCl₂. It can be seen from Figure 3-9 B, that after a 24 hour period the viability of HS-5 cells fell below 50% in the scaffolds treated with 25 and 50% firming buffer, but not with an initial 10%. However, over the remaining period, viability continued to drop in the 25 and 50% scaffold and began to decrease steadily in the 10% group. Once again, this result reinforced the use of a cation, like CaCl₂, within the firming buffer as at 100 mM, in a similar manner to a 10% firming solution, HS-5 did not reduce in viability. However, when a 500 mM solution of CaCl₂ was added to HS-5 cells, viability dropped to around 50% when compared to the control, similar to the results seen with a 50% firming buffer solution. The continuous drop in viability over the remaining time period can be explained, in part, by the paper produced by Armstrong *et al.* (2016). In this paper it is concluded that a small level of divalent cation (5 mM CaCl₂) is required to stay within the medium to maintain the long-term structure of an alginate scaffold. However, at low levels, (<5 mM in the case of CaCl₂), human or rat MSCs do not turn on their respective ion pumps,

therefore an accumulation of compound occurs, causing apoptosis and loss of viability (Yener. 2013; Scherzad *et al.*, 2016; Leonard *et al.*, 2019). These data suggest, that even with a direct, acute, low dose of divalent cation (20-100 mM), further dilution is required for long term culture of HS-5. As the level of divalent cation perceived to be the main component of the firming buffer is unknown, an investigation into the level of dilution, whilst still maintaining scaffold structure and HS-5 viability, was conducted. It was found, that if a 50% medium change was conducted on day 2 (Figure 3-9 C and D), hence diluting the cation solution by 50%, an initial decrease in total cell number and viability was still seen in all three concentrations (10, 25 and 50%). However, if a 100% medium change (Figure 3-9E and F), hence diluting the cation solution by ~90% as some residual medium remained in the scaffold, no initial dip in viability was seen at day 3, whilst maintaining the structure. Conversely, at day 4, 10% and 50% scaffold viability levelled off and 25% reduced in viability. This result was not due to the level of cation in the solution but instead the supplementation in the medium. As previously mentioned, HS-5 have a doubling rate of 48 hours in 2D flasks and it can be seen in Figure 3-9 E and G that over the same time period, HS-5 cell numbers are increased within the 25% group, after an initial reduction on day 2, back to 2.5×10^5 total cells. At this cell number, the supplementation with the 3 mls of medium within the well may not be adequate, therefore, a 50% medium change was added on day 4 to accommodate this higher number. This increase in HS-5 number appeared to be the cause of the lowered viability as, when this medium change was added, viability (Figure 3-9H) continued to increase in a 50% scaffold between day 4 and 5 instead of plateauing. It can also be seen that cell number (Figure 3-9G) seems to plateau at 2.5×10^5 total cells in the 50% scaffold at day 3, whereas 10 and 25% scaffolds only reach half this total number at day 4. Given the previous evidence on cell-cell contact and the surface area's impact on viability within the Biomerix™ scaffold, the reduction in cell number on day 2 of the 10 and 25% is too large, creating a greater space around cells, even with the optimised medium regime. This reduction is not as apparent within the 50% AlgiMatrix™ scaffolds on day 2 and hence a greater increase in cell number and viability occurs, until it appears, the surface area is entirely accommodated with a total cell number of $<5 \times 10^5$, allowing cells to continue to increase in viability. This low density of cells residing on the scaffold, does concur with the literature, as it can be seen *in vivo* that BM stromal MSCs make up 1 in every 3×10^4 cells (Wexler *et al.*, 2003).

The conclusions that can be drawn from these results are that, even though a preliminary drop in viability associated with the concentration of CaCl_2 , is seen after initial seeding, this

can be increased by diluting the firming solution by 90% on day 2 combined with a medium change 48 hours later to accommodate the expanding cell number. However, over the 5 day period, viability only reached between 60-70% which infers a increased incubation period of initial HS-5 culture on the scaffold is required. Given the evidence put forward in this chapter on increased number, viability, pore size and bio-mechanical structure of the differing scaffolds, it was decided that a 50% AlgiMatrix™ scaffold simulated the *in vivo* ECM more closely, and therefore was utilised for further study.

The initial reduction in HS-5 cell number and viability seen in Figure 3-9 G and H, even with an optimised medium regime, was still disconcerting with a drop of 50% seen in both cell number and viability in the 50% scaffold. The starting seeding density used in this study was 2.5×10^5 total cells/ scaffold in a 24 well plate, therefore, an investigation into the seeding density and vessel of initial HS-5 culture on an 50% AlgiMatrix™ scaffold was assessed. Firstly, HS-5 cells were seeded in a 25 cm² flask, 24 and 12 well plate at the same starting seeding density, to assess the initial growth parameters of HS-5 without an AlgiMatrix™ present. The HS-5 cell line is routinely cultured for 7-8 days at starting concentration of 6×10^3 cells/cm² in a 25 cm² flask before use in further assays. It can be seen in Figure 3-10 that HS-5 seeded in a 25 cm² flask, increased in cell number (A) and viability (B) over this period, therefore, would act as the control to assess other culture vessels. The freeze-dried AlgiMatrix™ scaffolds arrive in a 24 well plate which, when cells are seeded on the AlgiMatrix™, only allow for the addition of 2-3 mls of fresh culture medium, with the latter reaching the vessel lid which could introduce contamination. As previous study had been conducted within the 24 well plate, an empty 24 well plate was used to assess how the HS-5 would react to this reduction in medium. As illustrated in section 3.3.2.3, a medium volume of 3 mls is required for long-term culture and increased viability of HS-5 upon an AlgiMatrix™ scaffold, therefore, a 12 well plate, which can accommodate 3 mls was also seeded with HS-5. The same culture protocol outline in section 3.3.2.2, for 3D culture, was used for this 2D experiment, with HS-5 in separate wells, trypsinised every 48 hour and assessed for cell number, viability, cell cycle and the presence of Ki67. The nuclear protein, Ki67, was used as it is routinely deemed as a marker of proliferation. When the cell is proliferating, the marker is transferred from the internal nuclear membrane to the outer nuclear membrane and is present in all phases of cell cycle apart from G0 or quiescence (Sun & Kaufman 2018; Yang *et al.*, 2018; Menon *et al.*, 2019; Bosch). This can then be correlated with viability and cell cycle to gain an indication of cell health and indicate the optimal time for seeding of a secondary cell line. However, as can be seen in Figure 3-10,

the viability of the 25cm² and 12 well are maintained above 50% viability after an initial drop at 24 hours. This level of viable cells and steady increase in cell number, over this time, would indicate that cells were proliferating, conversely, the presence of Ki67 doesn't increase at the same rate. This could be explained utilising the cell cycle analysis seen in Figure 3-10D, E and F, as in all culture vessels, cells appear to gather in the G0 or quiescence stage of cell cycle, which would infer that cells were not proliferating even with the cell number and viability data. Work by Miller *et al.* (2018) confirmed the Ki67 finding, as they found that the longer cells are in G0, regardless of the cause of entry, Ki67 would degrade and is highly heterogeneous between cell cultures. However, work by Rumman *et al.* (2018), Cherry *et al.* (2014) and Morikawa *et al.* (2009) found that primary BM stromal stem cells, even though viable, remain in G0 in the *in vivo* BM to enhance self-renewal and wouldn't pass into G1 routinely until HSCs were present. If BM stromal stem cells don't have contact with HSCs, they will begin to reduce in viability and cell number to conserve a small population. This finding suggests that even without an AlgiMatrix™ scaffold, the HS-5 cell line may be simulating the BM stromal stem cell population not previously seen in the literature. It was concluded by using these markers of cell cycle, viability and cell number, the change in Ki67 expressions were true and comparable between all samples, therefore, taking this into account, along with medium and space required for the AlgiMatrix™ scaffold, a 12 well plate overall maintained HS-5 cells similar to that of the routinely used 25 cm² flask, and therefore was used in future AlgiMatrix™ study.

Now that an appropriate culture vessel had been identified, the required total cell seeded onto the AlgiMatrix™ was investigated. Hence cells were seeded at a total density of 2.5, 5, 7.5 and 10 x 10⁵ cells/scaffold before being transferred to a 12 well plate. The seeding densities were chosen because, as previously mentioned in section 3.3.2.3, the AlgiMatrix™ scaffold seems to hold <5 x 10⁵ total cells, which correlated with the *in vivo* literature. However, at this density the firming buffer had a detrimental effect on the HS-5 cells and as noted with the bespoke hydrogel scaffold, a higher number of cells seemed to dilute the effects of the firming buffer, therefore a higher seeding density was also chosen. The results seen in Figure 3-11 A reinforce this result, as there is a sudden drop in cell number between 0 and 24 hours in the 7.5 and 10 x 10⁵ samples, to around 5 x 10⁵, but not 2.5 or 5 x 10⁵ which remain at the same density throughout the experiment, inferring that the scaffold can only hold a maximum of 5 x 10⁵ total cells. Unfortunately, as previously mentioned, the freeze-dried scaffold arrives in a 24 well plate and cannot be removed until firming has occurred. This movement from one vessel to the next could explain this initial loss, as too

high a density of cells were initially seeded and couldn't reside within the scaffold, therefore, the excess may be lost to the medium when transferring across to the 12 well plate.

However, unlike in 2D, Ki67 does correlate with viability over a 168 hour period, although a high proportion of cells were still remaining in the G0 stage of cell cycle throughout. Within the previous 2D experiment each well was trypsinised; trypsinisation has been seen to be detrimental to cells, altering cell size, shape, markers (such as Ki67) and gene expression which has not been seen or noted in the literature when using the AlgiMatrix™ firming buffer (Shin *et al.*, 2017). This change in retrieval of cells, therefore, seems to also have an impact on the final result, with a firming buffer allowing cells to maintain their 3D morphology. Conversely, each density, after a 168 hour period, increased cell number, plateaued/ decreased viability and decreased Ki67 expression. As previous literature has highlighted, regarding the stall of BM cells within G0, if BM stromal cells don't have contact with HSCs for an extended period, they will reduce in viability and cell number to conserve cellular numbers in dwindling supplementation. In conclusion, the original, lower seeding density of 2.5×10^5 total cells seeded onto an AlgiMatrix™, seems to correlate with the current *in vivo* BM literature, with a maximum seeding time of 168 hours before the introduction of a secondary HSC cell line.

The human B lymphoblastoid cell line, TK6, is used routinely in 2D genotoxicity studies within the pharmaceutical industry. This cell line is used due to its proliferation index (12-15 hour doubling time), p53 competency, human origin and ease of culture allowing a rapid 7 day analysis of potential therapeutic compounds (Hintzsche *et al.*, 2018). This cell line is used in the single culture 2D MN assay, as a predictor of the potential genotoxic damage that could occur in erythroblasts *in vivo* (Hayashi *et al.*, 2016). As this cell line is routinely used within the pharmaceutical industry, it was decided that due to its ease of use and ability to compare between MN induction in 2D, our 3D model and the *in vivo* result, this would be the best candidate for addition to the AlgiMatrix™ cultured HS-5.

As mentioned previously, work by Rumman *et al.*, (2018), Cherry *et al.* (2014) and Morikawa *et al.* (2009) found that BM stromal stem cells remained in a quiescent state until the addition of HSCs which then increased the MSC's viability, proliferation and cell number. The model's ability to simulate this *in vivo* behaviour, was once again reinforced with the addition of TK6, in a 0.2 µm pore culture insert, to HS-5 seeded onto AlgiMatrix™ scaffolds for seven days as seen in Figure 3-15. This result infers that just the addition of

soluble factors, not just cell-cell contact, induces an increase in HS-5 similar to the *in vivo* literature. A 0.2 μm pore insert was used to separate cell lines as literature by Ngo *et al.* (2019) and Cardoso *et al.* (2015) had found that a 15 μm TK6 or HS-5 could not pass through a 0.4 μm pore, therefore, a 0.2 μm pore would ensure that only the HS-5 were counted when analysing cells residing on the scaffold. However, both cell lines were cultured in RPMI-1640, as mentioned in chapter 2 section 2.2.1, but HS-5 have been routinely cultured in Dulbecco's modified Eagle's medium. Nevertheless, a study by Deynoux *et al.* (2020) found that RPMI-1640 had no effect on HS-5 cells and conversely produced a HS-5 cell more morphologically similar to the *in vivo* BM fibroblast.

The *in vitro* and *in vivo* MN assay requires the active proliferation of the HSC compartment for the formation of micronuclei. Therefore, a method of differentiating cell lines from each other must be established, so that the proliferation and initial seeding density of TK6 can be established for future compound addition. The results in Figure 3-12 show that TK6 cells, unlike HS-5, are CD19 positive which aligns with the literature (Krüger *et al.*, 2014) and can be used to differentiate TK6 via flow cytometry for proliferation, and confocal microscopy for identification of MN (Figure 3-21). A marker for TK6 only was selected as, mentioned in section 3.3.2.4, the harvest of HS-5 seems to alter their surface markers, and this study is especially interested in the genotoxic events occurring in the TK6 for comparison to the 2D and *in vivo* setting. As CD19 was found to be present in >98% of cells this was used to assess the proliferation and optimal initial seeding density of TK6 onto AlgiMatrix™ cultured HS-5.

Utilising this CD marker, TK6 were added to AlgiMatrix™ cultured HS-5 and assessed for their ability to proliferate over a 5 day period, similar to that of the *in vitro* MN. As can be seen in Figure 3-13, regular medium changes were needed every 24 hours to accommodate the increasing number of cells within the well, concurrent with previous evidence on medium supplementation in section 3.3.2.2. An exponential phase, without the loss of CD19, can be seen in Figure 3-13 D between 54 and 96 hours, which closely corresponds with the timeframe seen in the *in vitro* MN assay, allowing for the comparison between 2D and 3D MN induction *in vitro*. The loss of CD markers indicates membrane degradation of dead or dying cells through reduction in medium supplementation not necessarily an increase in CD19- HS-5 cells (Lin *et al.*, 2013).

The initial lack of proliferation of TK6 between hour 0-54 (Figure 3-13) is indicative of the cell-cell interaction seen *in vivo*. As previously stated, HS-5 begin to increase in cell number when TK6 are added in a well insert. This expansion *in vivo*, facilitates the release of chemokines into the surrounding medium, such as SDF-1, homing the HSCs to the stromal MSCs, which will slowly proliferate until they are in cell-cell contact, and lineage defined (Wei & Frenette, 2018; Emmons *et al.*, 2016). Hence, this apparent lack of proliferation could indicate TK6 cells homing from the medium into the scaffold, before increased expansion of the TK6 can occur. This change can be seen in Figure 3-13, as TK6 cells within the scaffold are required to increase before an exponential increase of those in the medium. The introduction of a medium change also influenced this initial lack of proliferation, as 50% of the medium is discarded every 24 hours, reducing cells within and reducing the accumulating cellular signalling molecules. Additionally, the initial low seeding density would have an effect on proliferation as mentioned previously with HS-5 proliferation in 3D. Therefore, a 0.5×10^5 total initial seeding density of TK6 cells onto AlgiMatrix™ cultured HS-5, produced a finalised model which simulates the *in vivo* environment within an *in vitro* MN time frame.

3.5. Conclusion

A co-culture model of HS-5 and TK6 has been developed, with optimised conditions for the long-term (270 hour) *in vitro* culture of both cell types, which closely simulates the *in vivo* BM stromal and haematopoietic compartments closely, whilst being able to discriminate cell lines from each other. The *in vitro* model developed, provides a physiologically relevant platform to investigate the effects of new and existing compounds in a more *in vivo* relevant setting, for genotoxicity and changes in gene expression.

These data clearly demonstrate the importance of selecting an optimal initial seeding density, medium change, culture vessel and ECM for the co-culture of two diverse cell lines. These results have shown that HS-5 stromal cells are not able to adhere fully to Biomerix™ scaffolds. However, by incorporating 2.5×10^5 total cells into a solidified Algimatrix™ scaffold, using a 50% firming buffer, HS-5 proliferated and expanded in a similar manner to human primary *in vivo* stromal cells. The addition of TK6 at 0.5×10^5 cells/ml, at day seven, continued to closely replicate the expansion and environment mentioned within the *in vivo* BM literature. Therefore, in all subsequent experiments, the optimised *in vitro* co-culture model described in this chapter (outlined in section 2.3.1) was used.

Chapter Four

4. Screening of positive, negative and potential genotoxic compounds in 2D and 3D systems.

4.1. Introduction

Genetic toxicology testing is routinely performed by pharmaceutical companies on therapeutic compounds to identify potential carcinogens. A battery of assays is recommended by the ICH, so that a compound will meet the criteria set out by the regulatory body of that region, such as the Food and Drug Administration (FDA) in America and the European Medicines Agency (EMA) in Europe (Koutsilieri *et al.*, 2020). The ICH recommends a battery of assays, described in section 1.2.2, with the pharmaceutical company AZ including in their battery, the Ames and *in vitro* MN assay before moving the compound into animals utilising the *in vivo* BM MN assay.

The compound's interaction within the *in vitro* MN assay, is meant to be predictive of the *in vivo* BM environment. However, the complexities described previously with the differing compartments of the BM, cannot truly be represented with the single cell culture used *in vitro*. This has led to compounds (termed pharmacological positives), known to be non-genotoxic in the clinic, showing a positive result in the *in vivo* but not the *in vitro* MN assays (Hayes *et al.* 2013). Therefore, new compounds may infer a negative result *in vitro*, which are then positive *in vivo* wasting time, money, animal life with an uncertainty which compound is a true positive/ negative for genotoxicity. Conversely, the stromal layer of the BM, has been seen to provide protection to the haematopoietic cells through metabolism and absorption, reducing the genotoxicity of compounds, giving a negative result *in vivo* but positive *in vitro* (Jaroch *et al.*, 2018). These problems highlight the need for a more *in vivo* relevant multicellular model *in vitro*, to isolate these compounds and identify their mechanism before being assessed *in vivo*.

Work in the previous chapter has demonstrated a simple, optimised, *in vitro*, co-culture model of cell lines, upon an ECM, which aligns with the BM *in vivo* environment noted in the literature. The aim of this chapter was to evaluate the outcome of known positive, negative and pharmacological positive compounds for genotoxicity, within this developed

model, and compare these results to those seen within the regulatory *in vitro* and *in vivo* MN assay. To achieve this aim, three stages were conducted: (1) A series of baseline 2D *in vitro* MN assays were then conducted, on known compounds which induce genotoxicity, to standardise the scoring of MN between AZ and UWE. (2) A secondary 2D *in vitro* MN assay was then conducted, solely at UWE, of known positive, negative and pharmacological positive compounds which induced cytotoxicity (RPD) $<50\% \pm 5\%$ or reached a 1 mM concentration, which is noted as the highest dose necessary without genotoxicity to call a compound non-genotoxic. This increase in dose was essential, as *in vivo* a higher concentration of compound is required due to a reduction in bioavailability and detoxification (Shan *et al.*, 2018). (3) Finally, a range of doses from each compound tested within the 2D *in vitro* MN assays, were then assessed using the 3D model optimised in chapter 3 for comparison between *in vitro* and *in vivo* results.

4.2. Methods

4.2.1. Identification of the exponential phase of TK6 cells in 2D culture

Identification of the exponential phase in TK6 cells was conducted at UWE utilising the method described in section 2.2.2.

4.2.2. The regulatory *in vitro* 2D micronucleus assay

The 2D *in vitro* MN assay was conducted for the initial baseline doses of MMC, 4NQO, etoposide and paclitaxel at UWE and AZ. Those slides scored at AZ were then scored at UWE to ensure that scoring was comparable between each laboratory. Additional doses, for use in future 3D analysis, of MMC, 4NQO, etoposide and paclitaxel were then tested at UWE, with relevant doses of dexamethasone, prednisolone and caffeine also identified. All 2D *in vitro* MN assay were performed as previously described in section 2.6 whilst satisfying the criteria laid out within the section 2.6.1. All assays for each compound, except MMC, included a positive control of MMC at 30 and 40 nMol/L.

4.2.3. Selection and concentration of known positive, negative and pharmacological positive compounds.

The final concentrations, added to TK6 within the regulatory *in vitro* 2D MN assay, of known positive (MMC, 4NQO, etoposide and paclitaxel), pharmacological positives (dexamethasone and prednisolone) and non-genotoxicant (caffeine) can be seen in Table 4-1, Table 4-2, Table 4-3 respectively with those inducing an RPD score $<50\% \pm 5\%$ highlighted. A range of doses for each compound was initially tested for induction of a $50\% \pm 5\%$ RPD, this range was then increased to identify doses which gave an RPD $<50\%$. Those compounds that did not reach an RPD of $50\% \pm 5\%$ at a dose of 1 mM, were deemed as non-genotoxic and dose ranges were terminated at this point. The final concentrations identified and tested within the multicellular 3D model, of known positive (MMC, etoposide and paclitaxel), pharmacological positives (dexamethasone and prednisolone) and non-genotoxicant (caffeine) can be seen in Table 4-4, Table 4-5, Table 4-3 respectively. However, doses of 4NQO were not advanced to the 3D MN assay.

Table 4-1. Concentration of known genotoxic compounds used in the 2D in vitro micronucleus assay in assessing the correct dose to induce a <50% RPD score in TK6 cells. Concentrations are given in both ng/ml and nmol/L as stipulated in OECD guideline 487 (2016) in section 2.6.1. Those concentrations highlighted in yellow gave an RPD <50%.

4-nitroquinoline- <i>N</i> -oxide (4NQO)		Etoposide		Mitomycin C (MMC)		Paclitaxel	
Vehicle control <1% DMSO		Vehicle control <1% DMSO		Vehicle control <1% DMSO		Vehicle control <1% DMSO	
ng/ml	nmol/L	ng/ml	nmol/L	ng/ml	nmol/L	ng/ml	nmol/L
0.01	0.06	0.1	0.2	1.7	5	0.3	0.4
0.02	0.13	0.3	0.5	2.3	7	0.7	0.8
0.04	0.19	0.6	1	3.3	10	0.9	1
0.21	1.1	2.9	5	6.7	20	3.4	4
0.4	2.09	6	10	10	30	6.8	8
0.68	3.59	12	20.4	11.7	35	8.5	10
0.83	4.39	14.9	25.4	13.4	40	14.5	17
0.93	4.91	18	30.6	16.7	50	17.1	20
1.08	5.7	24	40.8	20.1	60	17.9	21
1.2	6.29	29	49.3	23.4	70	20.5	24
1.45	7.61	35	59.5	26.7	80	22.2	26
1.64	8.6	38	64.5	30.1	90	28.2	33
1.81	9.51	41	69.7	33.4	100	30.7	36
1.9	10	47	79.9	40.1	120	38.4	45
2.09	11	53	90.1	46.8	140	47	55
2.47	13.01	59	100.2	53.5	160		
5	26.3	72.9	123.9	60.2	180		
7.4	38.9	88	149.5	66.9	200		
10	52.6	120	203.9	73.6	220		
15	78.9	150	254.9	80.2	240		
17	89.4	160	271.8				
20	105.2						
25	131.5						
30	157.8						
35	184.1						
40	210.3						
45	236.6						
50	262.9						
55	289.2						
60	315.5						
65	341.8						
70	368.1						

Table 4-2. Concentration of pharmacological positive compounds used in the 2D in vitro micronucleus assay in assessing genotoxicity of TK6 cells in 2D. Concentrations are given in both ng/ml and nmol/L as stipulated in OECD guideline 487 (2016). Concentrations are quoted as per the OECD guidelines in section 2.6.1. Doses with these compounds did not induce an RPD score of <50% in the 2D in vitro MN assay. Therefore, testing with doses higher than 1 mM was not undertaken.

Dexamethasone Vehicle control <1% DMSO		Prednisolone Vehicle control <1% DMSO	
ng/ml	nmol/L	ng/ml	nmol/L
2.4 x 10 ⁴	6 x 10 ⁴	1.8 x 10 ⁴	5 x 10 ⁴
3.9 x 10 ⁴	1 x 10 ⁵	4.5 x 10 ⁴	1.25 x 10 ⁵
1.2 x 10 ⁵	3 x 10 ⁵	9 x 10 ⁴	2.5 x 10 ⁵
2 x 10 ⁵	5 x 10 ⁵	1.8 x 10 ⁵	5 x 10 ⁵
3.1 x 10 ⁵	8 x 10 ⁵	2.7 x 10 ⁵	7.5 x 10 ⁵
3.9 x 10 ⁵	1 x 10 ⁶	3.6 x 10 ⁵	1 x 10 ⁶

Table 4-3 Concentration of a negative genotoxic compound used in the 2D and 3D in vitro micronucleus (MN) assay in assessing genotoxicity of TK6 cells. Concentrations are given in both ng/ml and nmol/L as stipulated in OECD guideline 487 (2016). Concentrations are quoted as per the OECD guidelines in section 2.6.1 Doses with these compounds did not induce an RPD score of <50% in the 2D in vitro MN assay. Therefore, testing with doses higher than 1 mM was not undertaken, with all 2D doses utilised in 3D.

Caffeine			
Regulatory 2D MN assay Vehicle control sterile H ₂ O		The multicellular 3D MN assay Vehicle control sterile H ₂ O	
ng/ml	nmol/L	ng/ml	nmol/L
97	5 x 10 ²	97	5 x 10 ²
9.71 x 10 ²	5 x 10 ³	9.71 x 10 ²	5 x 10 ³
9.710 x 10 ³	5 x 10 ⁴	9.710 x 10 ³	5 x 10 ⁴
9.7 x 10 ⁴	5 x 10 ⁵	9.7 x 10 ⁴	5 x 10 ⁵
1.5 x 10 ⁵	7.7 x 10 ⁵	1.5 x 10 ⁵	7.7 x 10 ⁵

Table 4-4 Concentration of known genotoxic compounds used in the 3D in vitro micronucleus assay in assessing genotoxicity of TK6 cells within the model. Concentrations are given in both ng/ml and nmol/L as stipulated in OECD guideline 487 (2016). Concentrations are quoted as per the OECD guidelines in section 2.6.1. Those concentrations highlighted in yellow gave an RPD <50% in the 2D in vitro micronucleus (MN) assay.

Mitomycin C (MMC)		Etoposide		Paclitaxel	
Vehicle control <1% DMSO		Vehicle control <1% DMSO		Vehicle control <1% DMSO	
ng/ml	nmol/L	ng/ml	nmol/L	ng/ml	nmol/L
2.3	7	0.6	1	0.9	1
11.7	35	24	40.8	14.5	17
20.1	60	38	64.5	17.9	21
30.1	90	59	100.2	28.2	33
46.8	140	120	203.9	38.4	45

Table 4-5. Concentration of pharmacological positive compounds used in the 3D in vitro micronucleus (MN) assay in assessing genotoxicity of TK6 cells within the model. Concentrations are given in both ng/ml and nmol/L as stipulated in OECD guideline 487 (2016). Concentrations are quoted as per the OECD guidelines in section 2.6.1. Doses with these compounds did not induce an RPD score of <50% in the 2D in vitro micronucleus (MN) assay. Therefore, testing with doses higher than 1 mM was not undertaken.

Dexamethasone		Prednisolone	
Vehicle control <1% DMSO		Vehicle control <1% DMSO	
ng/ml	nmol/L	ng/ml	nmol/L
3.9×10^4	1×10^5	1.8×10^4	5×10^4
1.2×10^5	3×10^5	9×10^4	2.5×10^5
2×10^5	5×10^5	1.8×10^5	5×10^5
3.1×10^5	8×10^5	2.7×10^5	7.5×10^5
3.9×10^5	1×10^6	3.6×10^5	1×10^6

4.2.4. Genotoxicity and cytotoxicity of known positive, negative and pharmacological positive compounds within a 3D multicellular model.

The HS-5 cell line was initially seeded onto an AlgiMatrix scaffold™ for 7 days before the addition of the TK6 cell line. The TK6 cell line was then allowed to proliferate in contact with HS-5 for a further 54 hours, in accordance with the method described in section 2.3.2 before MN assessment was carried out (Figure 4-1.).

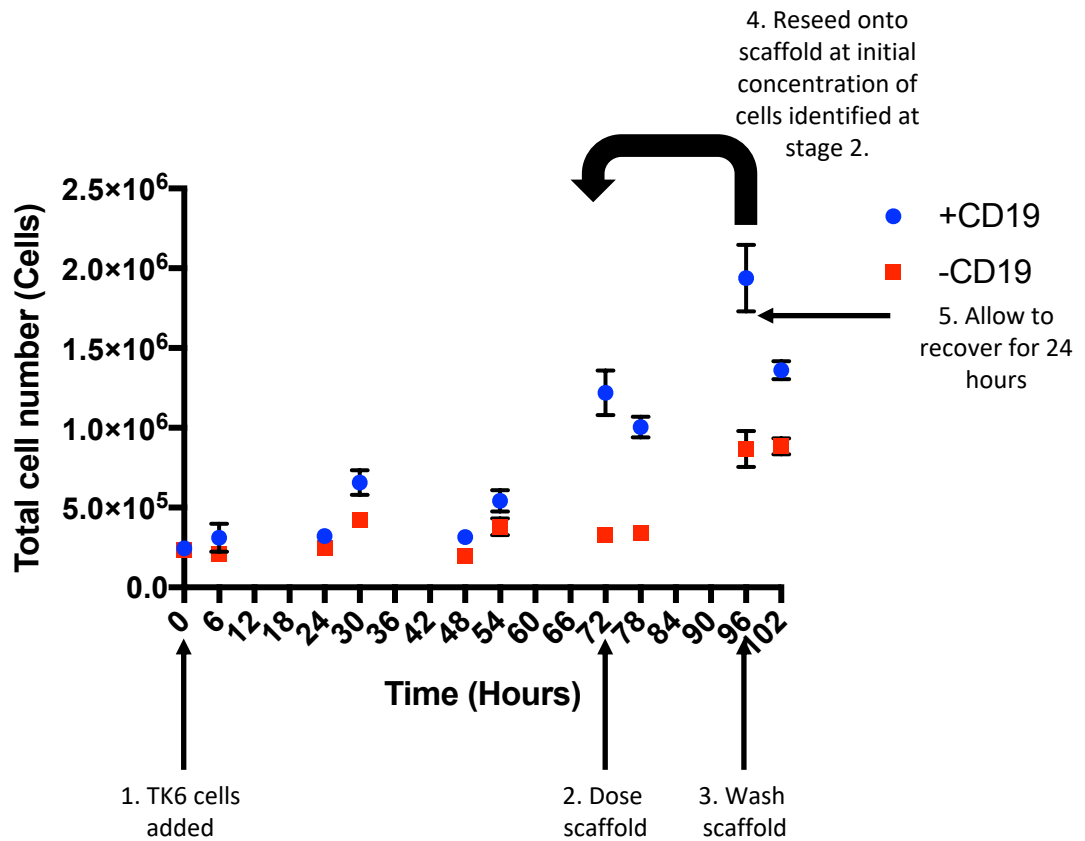


Figure 4-1. Planned protocol, utilising the proliferation of cells in 3D, for micronucleus assessment of known positive, negative and pharmacological positive genotoxicants. HS5 (CD19-) cells were incubated on AlgiMatrix™ scaffolds for 168 hours before the addition of TK6 (1). After a 72 hour incubation, scaffolds were dosed with compound (2), incubated, cells washed of compound (3), cells reseed onto the scaffold (4), incubated for a further 24 hours and harvested for MN and cell number assessment.

At the 54 hour time point (-24 hours before dosing), baseline seeded scaffolds (4 technical repeats) were harvested for cell number within the medium and scaffold, with the remaining treatment scaffolds, left to incubate for an additional 24 hours. At hour 72 (0 hours), a further 4 baseline seeded scaffolds were harvested for cell number within the medium and scaffold, with the remaining treatment scaffolds undergoing a 50% depletion (1.5 mls) of medium. Each compound was then added directly in 1.5 mls of medium to the scaffold according to the schematic seen in Figure 4-2, including a positive and vehicle control evenly spaced across each plate reducing plate location bias, mixed using a 1 ml pipette and left to incubate for a further 24 hours. After a 24 hour (+24 hours after dosing) incubation, medium from each scaffold and well was mixed with a 1 ml pipette, collected, washed and counted. Scaffolds still containing low amounts of medium, were moved to fresh 12 well plates whilst their original well was washed with 3 mls of PBS.

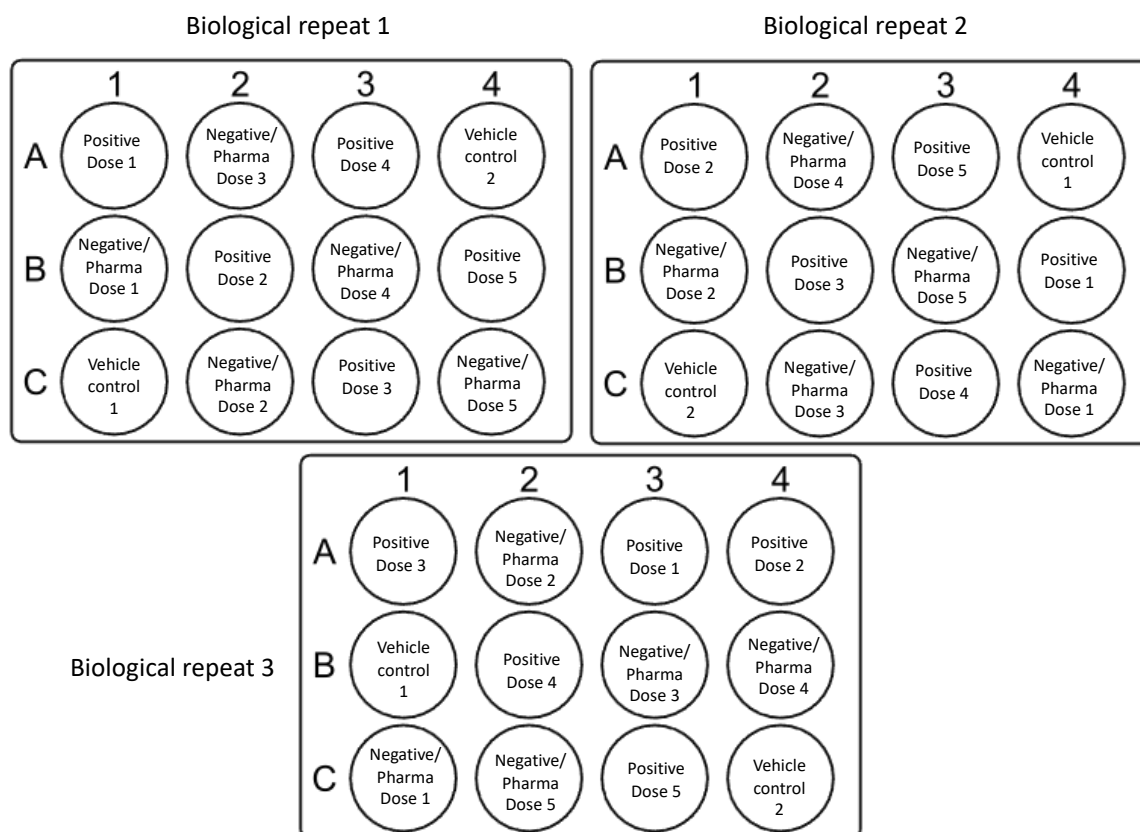


Figure 4-2. Schematic representation of the plate layout of AlgiMatrix™ scaffolds for 3 biological repeats of compound dosing. Each plate consisted of one positive, negative, pharmaceutical genotoxicant, and a vehicle control evenly spaced across the plate. Each sample location was altered with each biological repeat to reduce location bias.

Scaffolds were then placed back into their original, now washed wells, for the addition of their corresponding cells from the medium, seeded at the density at which they were dosed, mixed with a 1 ml pipette and left to incubate for an additional 24 hours. After this incubation (+48 hours after dosing), the medium for each well was mixed with a 1 ml pipette, collected, scaffolds harvested, both well and scaffold assessed for cell number using TB and MN assessed individually for each scaffold and corresponding well using the protocol described in section 2.6.2. This was then compared to the results seen in the regulatory 2D MN assay for each corresponding compound. The percentage increase from 2D to 3D MN induction, was then conducted using the following calculation where V2 equals the final value and V1 equals the initial value:

$$\frac{(V2 - V1)}{V2} \times 100$$

4.3. Results

4.3.1. Identifying the exponential phase of TK6 at UWE

The MN assay assesses the genotoxic potential of a compound and requires the cells to be actively turning over. Cells which are not actively turning over (in lag phase) will not take the compound up and thus no genotoxic event will occur. To assess the optimal times to dose TK6 cells (exponential phase) a growth curve was performed on differing starting concentrations. Cells were sampled at 11am and 5pm for 102 hours on an automated Luna counter. The initial seeding density differed, starting at 5×10^4 and 1×10^5 cells/ml (Figure 4-3).

The results seen in Figure 4-3 shows the exponential phase for both seeding densities starts at around 3×10^5 - 3.5×10^5 at around 24-30 hours into the 102 hour period. The exponential phase then reaches a plateau between 1.3×10^6 - 1.4×10^6 at around 100-102 hours. A PD time was calculated for both seeding densities to be 14.57 hours. These results conclude that TK6 cells should be allowed to proliferate for around 24 hours after seeding before being dosed. The cell count at this stage should be at around 3×10^5 cells/ml which suggests that the cells are actively turning over and taking up the drug. The exponential phase lasts for a period of 78 hours thus encompasses the 48 hour treatment period needed for the MN assay.

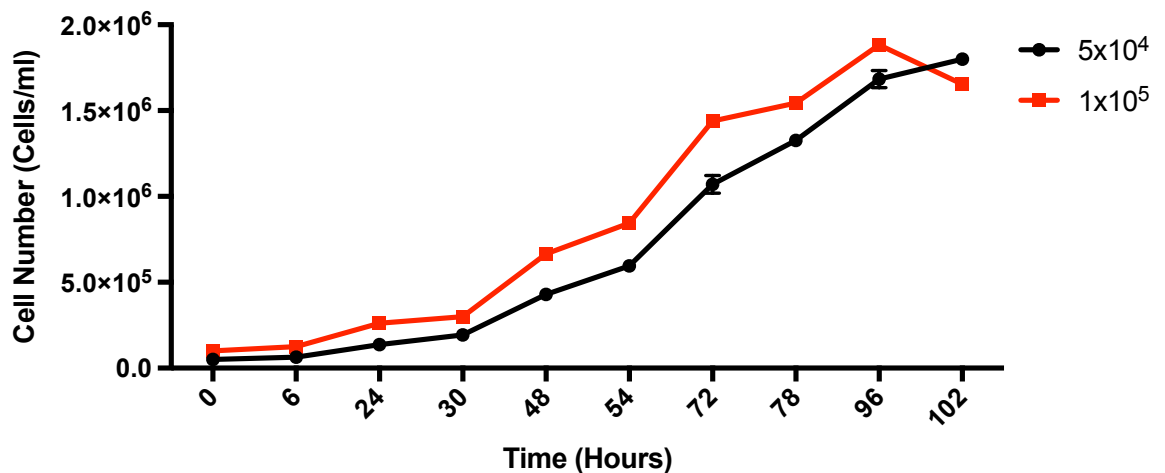


Figure 4-3. TK6 growth curve over 102 hour period. The graph illustrates the lag and exponential phase of two differing starting seeding densities (5×10^4 and 1×10^5 cells/ml) in the TK6 cell line. Cell counts were taken at 11am and 5pm every day for a five-day period. The cell doubling time was calculated at 14.57 hours for both ($n=3$)

4.3.2. An initial dose range of known genotoxic positive compounds conducted at AZ

The following MN assays (Figure 4-4) were conducted at AZ with MMC, etoposide, 4NQO and paclitaxel for alignment of scoring and expansion of dose concentration at UWE. The criteria set out in section 2.6 were followed so that alignment can take place once testing has been re-conducted at UWE. Where the toxicity meant RPD exceeded $50\% \pm 5\%$, experiments were repeated to ensure enough doses were available to demonstrate 50% cytotoxicity, as well as have 4 doses for scoring MN. This set of experiments was utilised as a dose range finder, to glean an RPD of $50\% \pm 5\%$ testing the compound to its limits. Each experiment consisted of a 48hr treatment (24 hour with drug, 24 hour recovery without drug) to allow the completion of cell cycle. Further to the data in section 4.3.1, cells were dosed 24 hours after seeding at a density of around 3×10^5 cells/ml. All compounds were tested with a negative (vehicle control), and the assays for etoposide, 4NQO and paclitaxel utilised MMC as a positive control.

The results in Figure 4-4 A show that MMC induced an RPD of 53% and 46% at 50 nmol/L and 70 nmol/L respectively. MN induction was found to be 81 and 55 MN/ 1000 mononucleated cells for these doses. However, it can also be seen that the RPD progresses from 53% at 50 nmol/L to 58% at 60 nmol/L then to 46% at 70 nmol/L. As the 50 nmol/L and 70 nmol/L have an RPD nearer to the $50\% \pm 5\%$ criterion we have to reject the result obtained at 60 nmol/L. These results conclude that, 50 nmol/L gave the highest, scorable induction of MN during dose finding at AZ for future validation at UWE. The results also showed that 30 nmol/L and 40 nmol/L gave an RPD of 74% and 62%. Since these scores show a cytotoxic affect, at an RPD $>50\% \pm 5\%$, they will be used as the positive in the following experiments.

The results in Figure 4-4 B show that etoposide induced an RPD of 52% and 44% at 69.7 nmol/L and 79.9 nmol/L respectively. MN induction was found to be 97 MN/ 1000 mononucleated cells for 69.7 nmol/L but was not scored at 79.9 nmol/L due to high cytotoxicity. This result concludes, that 69.7 nmol/L gave the highest, scorable induction of MN during dose finding at AZ for future validation at UWE. Additionally, the positive control (MMC) has exceeded more than double that of the negative with around 50 MN/ 1000 mononucleated cells, so can be confirmed as positive.

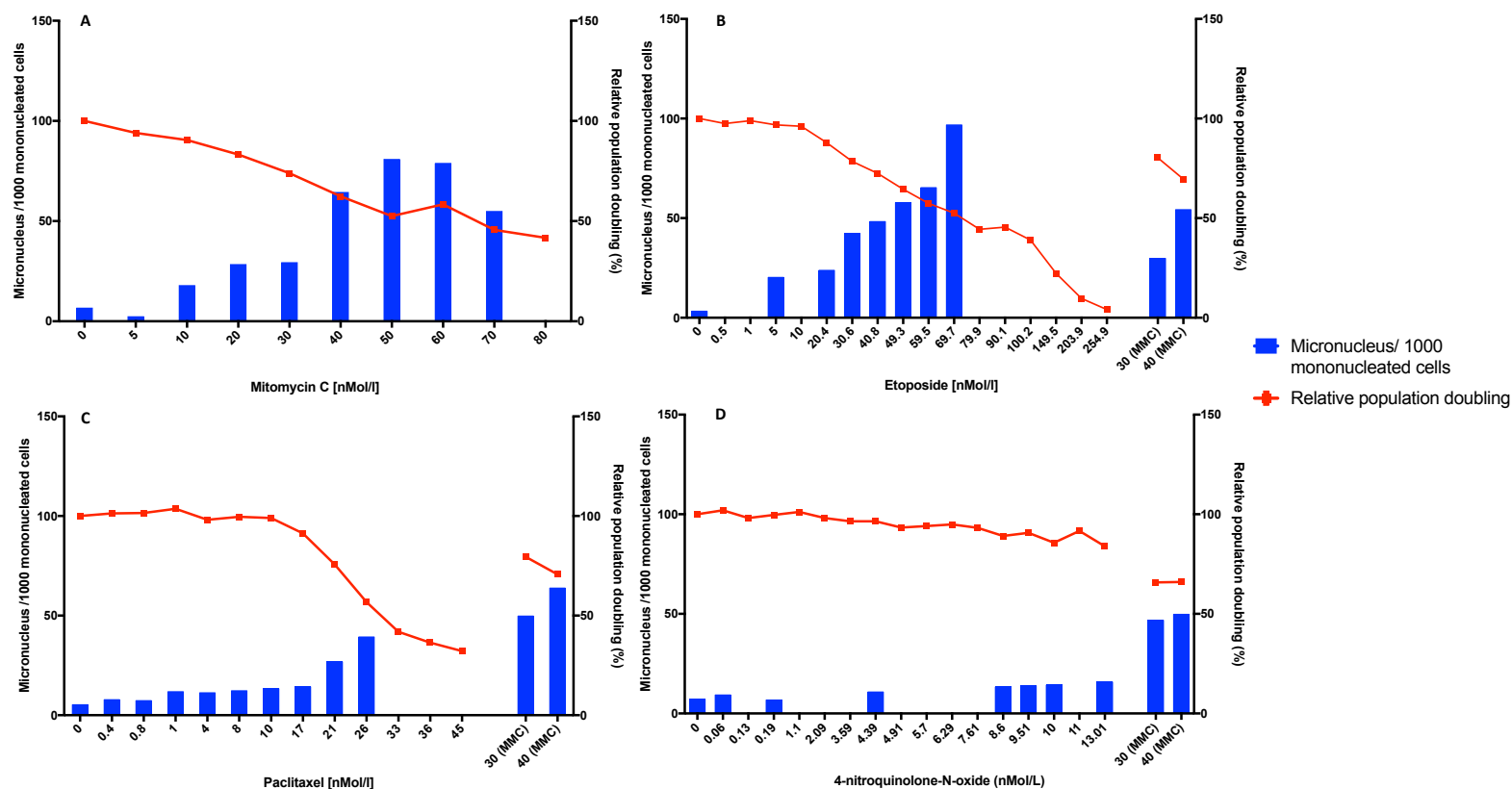


Figure 4-4. Baseline relative PD (RPD) and MN induction following 24 hour treatment with mitomycin C, etoposide, paclitaxel and 4-nitroquinolone-N-oxide at AstraZeneca for initial dose discovery. The total number of MN scored per 1000 mononucleated cells and RPD induced over a 48 hour period (24 hour treatment + 24 hour recovery) by mitomycin C (A), etoposide (B), paclitaxel (C) and 4-nitroquinolone-N-oxide (D). Those concentrations without a result for MN were not scored as they passed below the 50% \pm 5% RPD regulatory guidelines (2.6.1). A positive mitomycin C control was run alongside etoposide (B), paclitaxel (C) and 4-nitroquinolone-N-oxide (D) to ensure that the assay had successfully worked. A minimum of 2000 mononucleated cells were scored (n=1).

The results seen in Figure 4-4 C shows that paclitaxel induced an RPD of 57 % at a concentration of 26 nmol/L. MN induction at this dose was found to be 40 MN/ 1000 mononucleated cells more than twice the negative which only gained 6 MN/ 1000 mononucleated cells. The MMC controls can also be called positive as they are twice the negative at 50 and 64 MN/ 1000 mononucleated cells. These results conclude that a dose of 26 nmol/L paclitaxel has an induction of MN twice that of the negative, so can be called positive. However, since an RPD of $50\% \pm 5\%$ wasn't identified, a further extension of the dose range will be required at UWE to identify its cytotoxic limit.

The results seen in Figure 4-4 D show that 4NQO induced an RPD $>80\%$ at every dose tested. The last concentration of 13.01 nmol/L gave an RPD of 84% which was the closest dose to 50% tested. The MN score at this dose was 16 MN/ 1000 mononucleated cells, more than twice the negative control which produced only 7. The results conclude that since 13.01 nmol/L showed an induction of MN twice that of the negative, in conjunction with a positive MMC induction of MN, it can be called a positive genotoxic dose. However, since an RPD of $50\% \pm 5\%$ wasn't identified, not meeting the criteria in section 2.6.1, once again a further dose range will be required at UWE to identify its cytotoxic limit.

4.3.3. Comparison of micronucleus induction at AZ and UWE for alignment of scoring

To assess if scoring of MN was comparative between AZ and UWE for validation of future 2D and 3D study, the regulatory 2D MN assay was conducted at AZ for MMC, etoposide, 4NQO and paclitaxel as described in section 2.6, spun onto slides and counted for MN at AZ. Each slide was counted blind at AZ using a coding system to reduce experimenter bias, with dose and compound not revealed until after counting. These slides were then transported to UWE, re-coded and scored again to ensure that counting was reproducible between laboratories of the same sample.

The results seen in Figure 4-5 show that, for these compounds and doses, the number of MN in each sample were comparable between the two laboratories. These results conclude that scoring between the two laboratories is comparable, therefore an increase in range finding of doses for each compound can be conducted utilising the baseline counts identified at AZ.

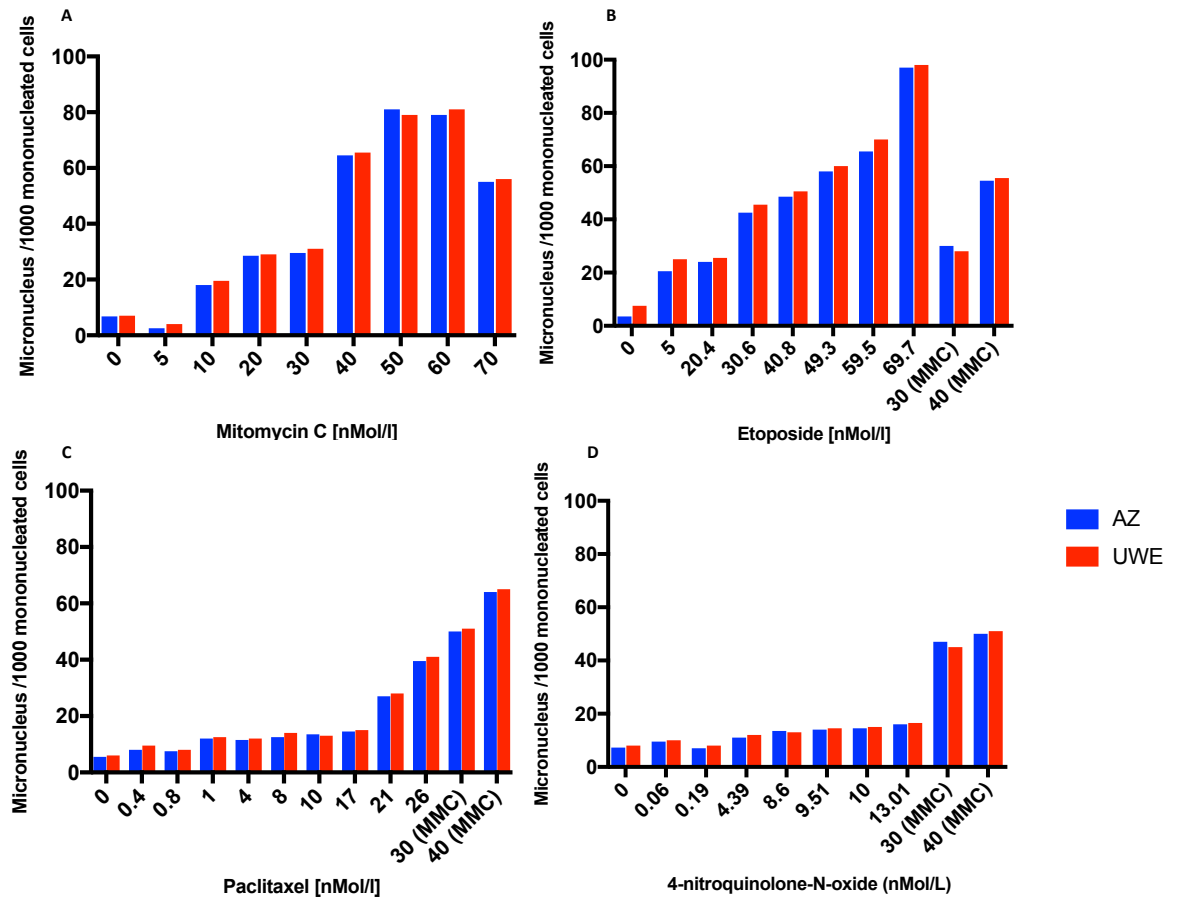


Figure 4-5. Comparison of micronucleus scoring between AZ and UWE, utilising the same individual scoring, within TK6 cells dosed with mitomycin C (A), etoposide (B), paclitaxel (C) and 4-nitroquinolone-N-oxide (D). The original *in vitro* micronucleus assay and initial scoring was conducted at AZ by Mr A Vernon. These slides were then transported to UWE and scored again by Mr A Vernon for comparison of scoring at the two laboratories. Each slide was coded to reduce bias with each concentration or compound not disclosed until all slides had been scored.

4.3.4. Extended dose range of known positive genotoxicants conducted at UWE, utilising an initial range from AZ

The following MN assays (Figure 4-6) were conducted at UWE with MMC, etoposide, 4NQO and paclitaxel for alignment with the baseline dose range identified at AZ and expansion into a range which gave an RPD of <50%. Once again, the regulatory MN assay, set out in section 2.6, was followed so that alignment can take place once re-testing has been conducted. Each experiment consisted of a 48 hour treatment (24 hour with drug, 24 hour recovery without drug) to allow the completion of cell cycle. Further to the data in section 4.3.1, cells were dosed 24 hours after an initial seeding concentration of around 3×10^5 cells/ml. All compounds were tested with a negative (vehicle control), with the assays for etoposide, 4NQO and paclitaxel utilising MMC as a positive control. The results of the expansion of dose concentration to identify an RPD <50%, would allow a wide range of doses for use in a 3D multicellular culture system, in case of possible increases/ decreases in cytotoxicity occurring in 3D culture systems.

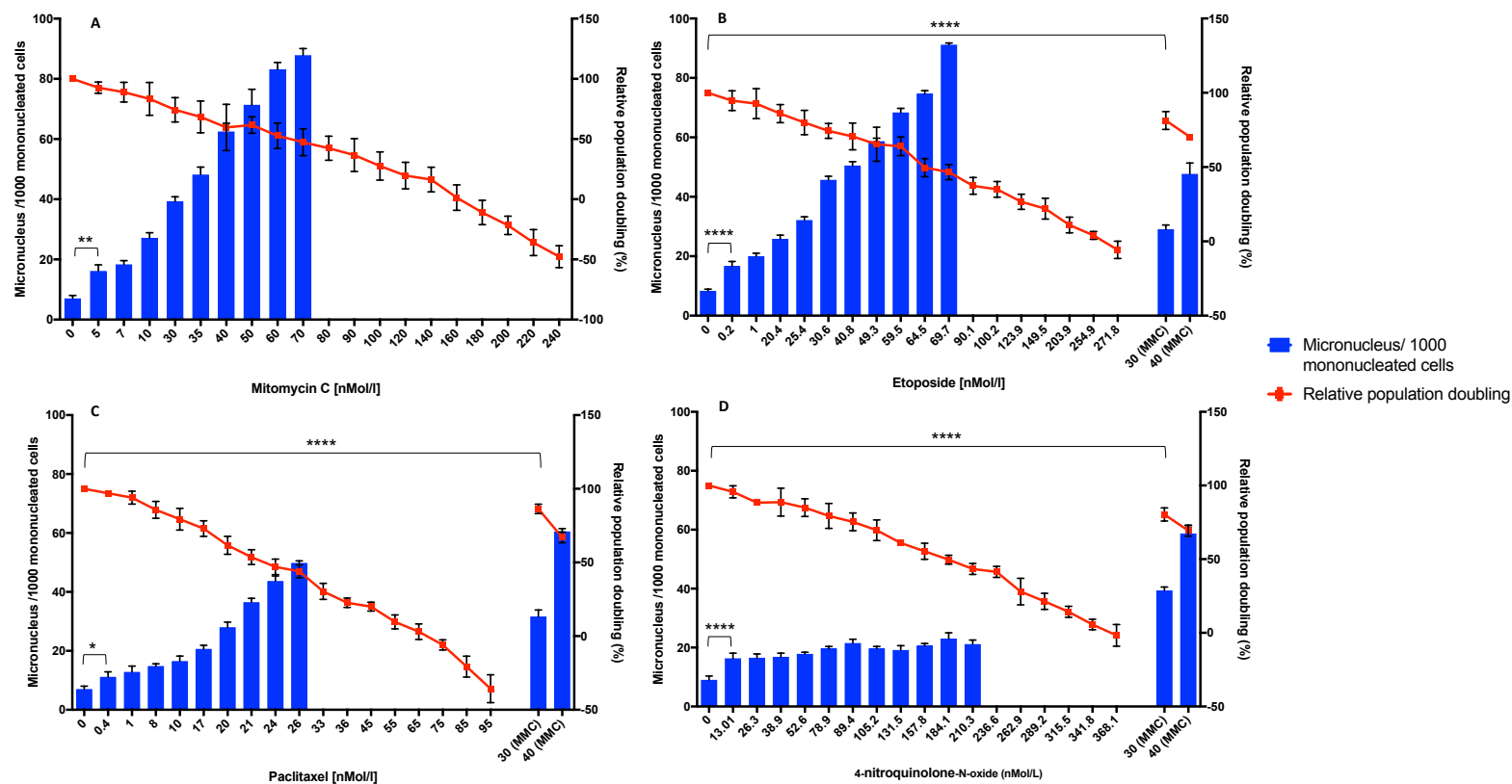


Figure 4-6. Extended dose range finder at UWE, identifying the relative PD (RPD) and micronucleus induction, of TK6, following a 24 hour treatment with mitomycin C, etoposide, paclitaxel and 4-nitroquinolone-N-oxide. The dose range included those doses which were identified at AZ as well as those which exceeded the regulatory guidelines. The total number of MN scored per 1000 mononucleated cells and RPD induced over a 48 hour period (24 hour treatment + 24 hour recovery) by mitomycin C (A), etoposide (B), paclitaxel (C) and 4-nitroquinolone-N-oxide (D). Those concentrations without a result for MN were not scored as they passed below the $50\% \pm 5\%$ RPD regulatory guidelines (2.6.1). A positive mitomycin C control was run alongside etoposide (B), paclitaxel (C) and 4-nitroquinolone-N-oxide (D). A minimum of 2000 mononucleated cells were scored ($n=3$). **Significant differences between samples were calculated using a One-Way ANOVA followed by a Dunnett's test. The P values are indicated by * ($p < 0.05$), ** ($p < 0.01$), **** ($p < 0.0001$), actual p values can be found in appendix 1.**

The results in Figure 4-6 A show that MMC induced an RPD of 53 and 47% at 60 and 70 nmol/L respectively. MN induction was found to be 83 and 87 MN/ 1000 mononucleated cells for these doses in a clear dose dependent increase. However, during the baseline dose range at AZ, an RPD of 53 and 46% were found at 50 and 70 nmol/L respectively with MN induction, found to be 81 and 55 MN/ 1000 mononucleated cells for these doses. This result shows that even though the baseline range identified at AZ was correct, that 70 nmol/L dose induces a RPD around 47%, three biological replicates were needed for accurate assessment of the level of cytotoxicity induced by 50 and 60 nmol/L. This result concludes that a dose of 70 nmol/L gave the highest, scorable induction of MN. Using 70 nmol/L as a starting dose, which gave $50\% \pm 5\%$ cytotoxicity, the dose range was increased to a maximum dose of 240 nmol/L. The results show that at an RPD of 36%, 16% and 1.3% was induced with 90, 140 and 160 nmol/L respectively. MN was not counted at these doses as genotoxicity could not be differentiated from cytotoxicity (section 2.6.1). Further doses did follow a dose dependent trend which induced an RPD $<0\%$, however, past this point the RPD calculation is inadequate due to 'minus' RPD values. It can be suggested from these results that a dose range, to be used in 3D culture, should include 7, 35, 60, 90 and 140 nmol/L which induce an RPD of around 100-80%, 80-60%, 60-40%, 40-20%, 20-0% providing a wide dose range for possible increase/ decrease of cytotoxicity in 3D.

The results in Figure 4-6 B show that etoposide induced an RPD of 49 and 46% at 64.5 and 69.7 nmol/L respectively. MN induction was found to be 74 and 91 MN/ 1000 mononucleated cells for these doses in a clear dose dependent increase. However, during the baseline dose range finding at AZ, an RPD of 52% was found at 69.7 nmol/L, with MN induction found to be 97 MN/ 1000 mononucleated cells for this dose. This result shows that there was a decrease in cytotoxicity by 6% and increase in MN by 6 MN/ 1000 mononucleated cells seen at UWE compared to AZ. However, this result still concludes that 69.7 nmol/L gave the highest, scorable induction of MN at an RPD around 50%. Utilising 69.7 nmol/L as a starting dose, which gave $50\% \pm 5\%$ cytotoxicity, the dose range was increased to a maximum dose of 271.8 nmol/L. The results show that an RPD of 35, 11 and 4% was induced with 100.2, 203.9 and 254.9 nmol/L respectively. MN were not counted at these doses as genotoxicity could not be differentiated from cytotoxicity. A further dose did follow which induced an RPD $<0\%$, however, past this point the RPD calculation is inadequate due to 'minus' RPD values. It can be suggested from these results that a dose range, to be used in 3D culture, should include 1, 40.8, 64.5, 100.2 and 203.9 nmol/L which induce an RPD of around 100-80%, 80-60%, 60-40%, 40-20%, 20-0% providing a wide

dose range for possible increase/ decrease of cytotoxicity in 3D. Additionally, the positive control (MMC) has exceeded more than double the MN than that of the negative, so can be confirmed as positive and the assay successfully completed.

The results in Figure 4-6 C show that paclitaxel induced an RPD of 53 and 47% at 21 and 24 nmol/L respectively. MN induction was found to be 36 and 43 MN/ 1000 mononucleated cells for these doses in a clear dose dependent increase. However, during the baseline dose range finding at AZ, an RPD of 57 % at a concentration of 26 nmol/L with MN induction of 40 MN/ 1000 mononucleated cells was found for this dose. As 26 nmol/L induced an RPD of 44%, below the $50\% \pm 5\%$ threshold, at UWE it should not be scored, however, given the previous score at AZ this dose was scored inducing 50 MN/ 1000 mononucleated cells. This result shows that a higher level of cytotoxicity and genotoxicity was seen, with 3 biological repeats, at UWE than at AZ. Given these results, it can be concluded that 24 nmol/L gave the highest, scorable induction of MN at an RPD around 50%, not 26 nmol/L as first suggested at AZ. Utilising 24 nmol/L as a starting dose, which gave $50\% \pm 5\%$ cytotoxicity, the dose range was increased to a maximum dose of 95 nmol/L. The results show that an RPD of 30, 20 and 3% was induced with 33, 45 and 65 nmol/L respectively. MN were not counted at these doses as genotoxicity could not be differentiated from cytotoxicity. A further dose did follow which induced an RPD $<0\%$, however, past this point the RPD calculation is inadequate due to 'minus' RPD values. It can be suggested from these results that a dose range, to be used in 3D culture, should include 1, 17, 21, 33 and 45 nmol/L which induce an RPD of around 100-80%, 80-60%, 60-40%, 40-20%, 20-0% providing a wide dose range for possible increase/ decrease of cytotoxicity in 3D. Additionally, the positive control (MMC) has exceeded more than double the MN than that of the negative so can be confirmed as positive and the assay successfully completed.

The results in Figure 4-6 D show that 4NQO induced an RPD of 50% at 184.1 nmol/L with a MN induction of 23 MN/ 1000 mononucleated cells. However, during the baseline dose range finding at AZ, an RPD of $50\% \pm 5\%$ was not achieved, with the highest dose at AZ of 13.01 nmol/L giving an RPD of 84%. Given these results it can be suggested that 184.1 nmol/L is required to give the highest, scorable induction of MN at an RPD of 50%. Utilising 184.1 nmol/L as a starting dose, which gave 50% cytotoxicity, the dose range was increased to a maximum dose of 368.1 nmol/L. The results show that a dose dependent decrease in RPD did occur, conversely, over the scorable doses, MN did not increase. The positive control (MMC) did exceed more than double the MN than that of the negative so can be

confirmed as positive and the assay successfully completed. Due to the lack of MN induction within this dose range and the selection of two clastogens (MMC and etoposide) which did give a dose dependent increase in MN, 4NQO was not chosen for further study within the 3D multicellular model.

4.3.5. Dose range of known negative and pharmacological positives conducted at UWE.

The use of known negative and pharmacological positive compounds was not assessed at AZ. However, as the regulatory 2D MN assay was comparable between UWE and AZ for the known positives (section 4.3.3), this assessment was only carried out at UWE. To assess a dose of each compound which gave an RPD of $50\% \pm 5\%$ or, as these were known non-genotoxicants, a maximum dose of 1×10^6 nmol/L without an RPD of $50\% \pm 5\%$ at these concentrations, to use in the 3D multicellular model the following MN assays (Figure 4-7 Figure 4-8) were conducted. Once again, the regulatory MN assay, set out in section 2.6, was followed so that alignment can take place with both an MMC positive and vehicle control.

The results in Figure 4-7 A show that the pharmacological positive compound, dexamethasone, did not induce an RPD of $50\% \pm 5\%$ at the top dose of 1×10^6 nmol/L, with an actual RPD of 60%. A dose dependent increase in cytotoxicity can be seen with dexamethasone but MN induction remained around 18 MN/ 1000 mononucleated cells. This induction of MN was not twice that of the vehicle control of 10 MN/ 1000 mononucleated cells; therefore, can be classed as negative. The positive control of MMC did induce more than twice as many MN than that of the negative control and ensures that the negative result is true. In conclusion, the results suggest that all concentrations tested within the regulatory MN should be taken forward into the 3D multicellular system.

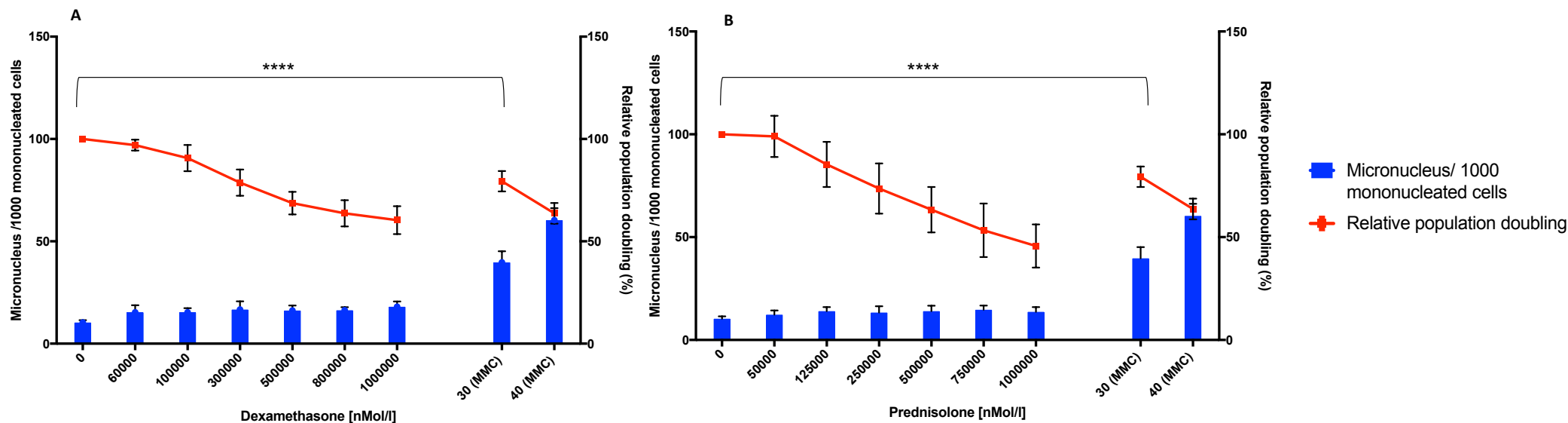


Figure 4-7. Dose range finder of pharmacological positive compounds at UWE, identifying the relative PD (RPD) and micronucleus induction, of TK6, following a 24 hour treatment with dexamethasone and prednisolone. The graphs illustrate the total number of MN scored per 1000 mononucleated cells and RPD induced over a 48-hour period (24 hour treatment + 24 hour recovery) by dexamethasone (A) and prednisolone (B). The dose range didn't induce an RPD score <50%, up to and including 1×10^6 nMol/l (1 mM) therefore, was identified as non-genotoxic as stated in section 2.6.1. A positive mitomycin C control was run alongside dexamethasone (A) and prednisolone (B). A minimum of 2000 mononucleated cells were scored (n=3). **Significant differences between samples were calculated using a One-Way ANOVA followed by a Dunnett's test. The P values are indicated by **** ($p < 0.0001$), actual p values can be found in appendix 1.**

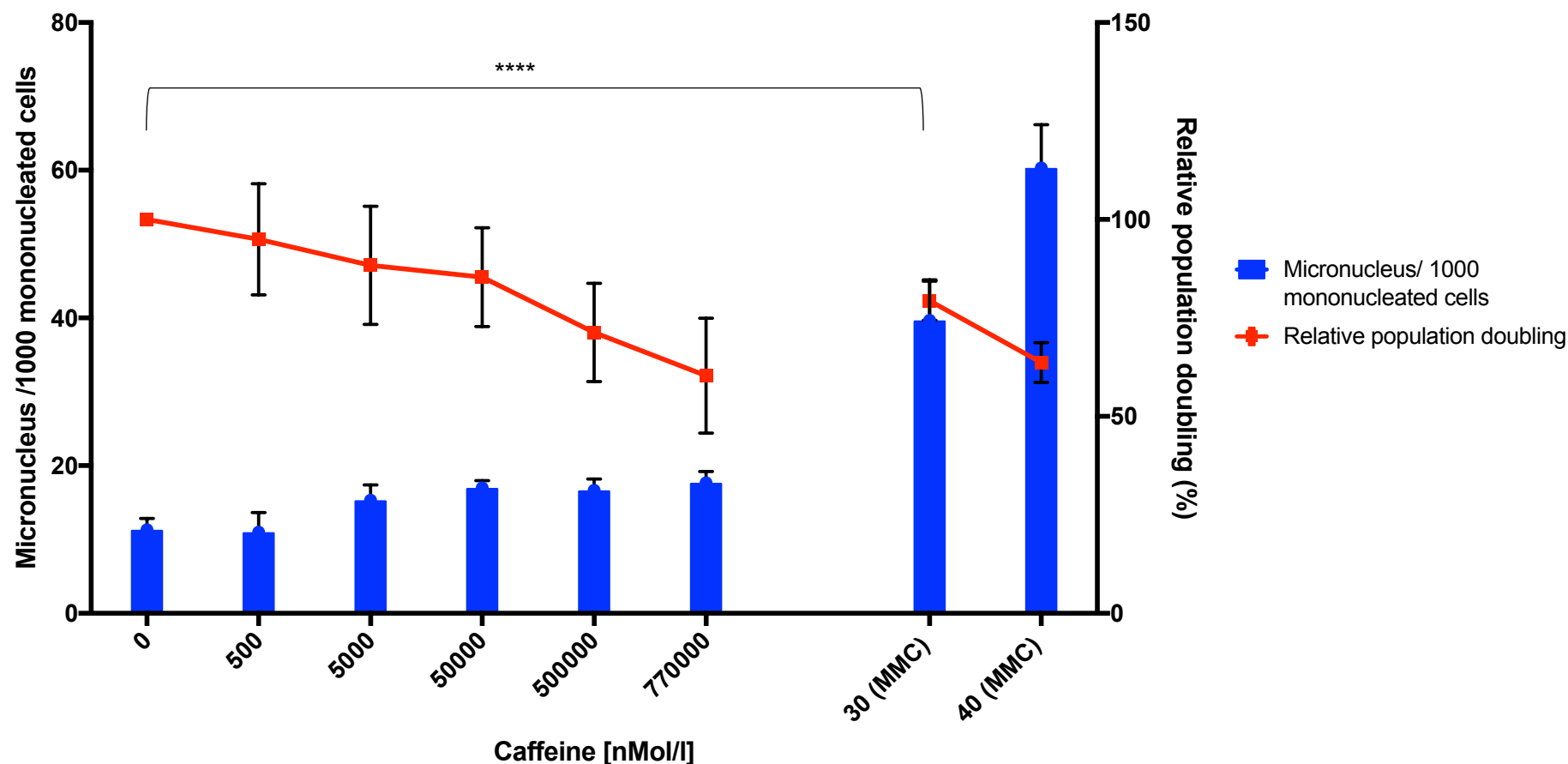


Figure 4-8. Dose range finder of a known negative compound at UWE, identifying the relative PD (RPD) and micronucleus induction, of TK6, following a 24 hour treatment with caffeine. The graph illustrates the total number of MN scored per 1000 mononucleated cells and RPD induced over a 48-hour period (24 hour treatment + 24 hour recovery). The dose range didn't induce an RPD score <50%, up to and including the maximum soluble concentration of 7.7×10^5 nMol/l, therefore, was identified as non-genotoxic as stated in section 2.6.1. A positive mitomycin C control was run alongside to ensure that the assay had successfully worked. A minimum of 2000 mononucleated cells were scored (n=3). **Significant differences between samples were calculated using a One-Way ANOVA followed by a Dunnett's test. The P values are indicated by **** ($p < 0.0001$), actual p values can be found in appendix 1.**

Unlike dexamethasone, the results shown in Figure 4-7 B for prednisolone, an alternative glucocorticoid which has also been classed as a pharmacological positive compound, did induce an RPD of 46% at the top dose of 1×10^6 nmol/L. Even though this top dose was cytotoxic, (and cytotoxicity increased in a dose dependent manner), the top dose was not genotoxic as MN induction did not increase above 14 MN/ 1000 mononucleated cells, less than twice the vehicle control; therefore, can be classed as negative. The positive control of MMC did induce more than twice as many MN than that of the negative control and ensures that the negative genotoxic result is true. In conclusion, the results suggest that all concentrations tested within the regulatory MN should be taken forward into the 3D multicellular system.

The results in Figure 4-8 show that the known negative compound, caffeine, did not induce an RPD of $50\% \pm 5\%$ at the top dose of 7.7×10^5 nmol/L, with an actual RPD of 60%. However, the SD did infer that this level of caffeine can induce an RPD of 44%. The dose of caffeine did not reach 1×10^6 nmol/L as it was insoluble at this concentration; therefore the top dose used of 7.7×10^5 nmol/L was now used as the maximum dose necessary following the guidelines in section 2.6.1. Even though an RPD of $50\% \pm 5\%$ was only reached by the error bars at this dose, a dose dependent decrease can be seen throughout. This trend cannot be seen with MN induction with the top dose of 7.7×10^5 nmol/L inducing 17 MN/ 1000 mononucleated cells, less than twice the vehicle control at 11 MN/ 1000 mononucleated cells. The positive control of MMC did induce more than twice as many MN than that of the negative control and reinforces the use of caffeine as a known negative genotoxic control. In conclusion, the results suggest that all concentrations tested within the regulatory MN should be taken forward into the 3D multicellular system.

4.3.6. Genotoxic assessment of positive, negative and pharmacological positive compounds within a multicellular, *in vitro*, 3D model of the bone marrow.

As described in section 1.2.2.1 the HSC compartment or TK6 cells in the developed 3D model, is required to be actively proliferating before the addition of compound. The HS-5 cell line was seeded onto AlgiMatrix™ scaffolds and cultured as described in section 2.3.1, TK6 cells were then added to each scaffold and cultured for a 54 hour period. At this point, to ensure that the TK6 cells were actively dividing, pre-treatment baseline counts of the medium and corresponding AlgiMatrix™ were taken 24 hours before and on the day of dosing with compound, counted with TB and compared to the proliferation of cells seen

during optimisation of the model seen in Figure 3-13 to assess the alignment between the two.

The results in Figure 4-9 show that 24 hours before dosing with compound, cell number within the pre-treatment (baseline) medium, scaffold and total for the well were 2.5, 4.6 and 7.1×10^5 total cells respectively. However, the total cell number of cells seen during optimisation of the model (Figure 3-13 M, N and O), were at a lower level than that of the medium, scaffold and total for the pre-treatment, baseline wells, gleaning results of 1.4, 3.7 and 5.1×10^5 total cells, but these results didn't induce a significant difference.

The results in Figure 4-9 show that on the day of dosing, unlike 24 hours before, total cell number within the pre-treatment (baseline) medium, scaffold and well were at 7.3, 7.7 and 15×10^5 total cells, similar to the proliferation of cells seen within the model optimisation (Figure 3-13 M, N and O) at 6.9, 8.1 and 15×10^5 total cells which once again did not produce a significant difference between the two samples. Utilising the calculation in section 2.6.1, PD between the total cell number in the 24 hour period, in the pre-treatment, baseline group was 1.06 compared to the original proliferation of cells within the model (Figure 3-13 M, N and O) which was 1.54. The PD within the pre-treatment, baseline medium and scaffold was 1.54 and 0.65 respectively, with PD of the original proliferation of cells (Figure 3-13 M, N and O) in the medium and scaffold being 2.37 and 1.11 respectively.

These results conclude that both the pre-treatment (baseline) and original proliferation of cells in the model (Figure 3-13 M, N and O) had successfully gone through at least one PD before the addition of compound, inferring that both cultures were proliferating. However, it can be seen that the pre-treatment (baseline) group has a lower PD than the original proliferation in the model, but this is still above 1 within the combined scaffold and medium. Therefore, any addition of compound would induce a response within the exponential phase of the cells in co-culture.

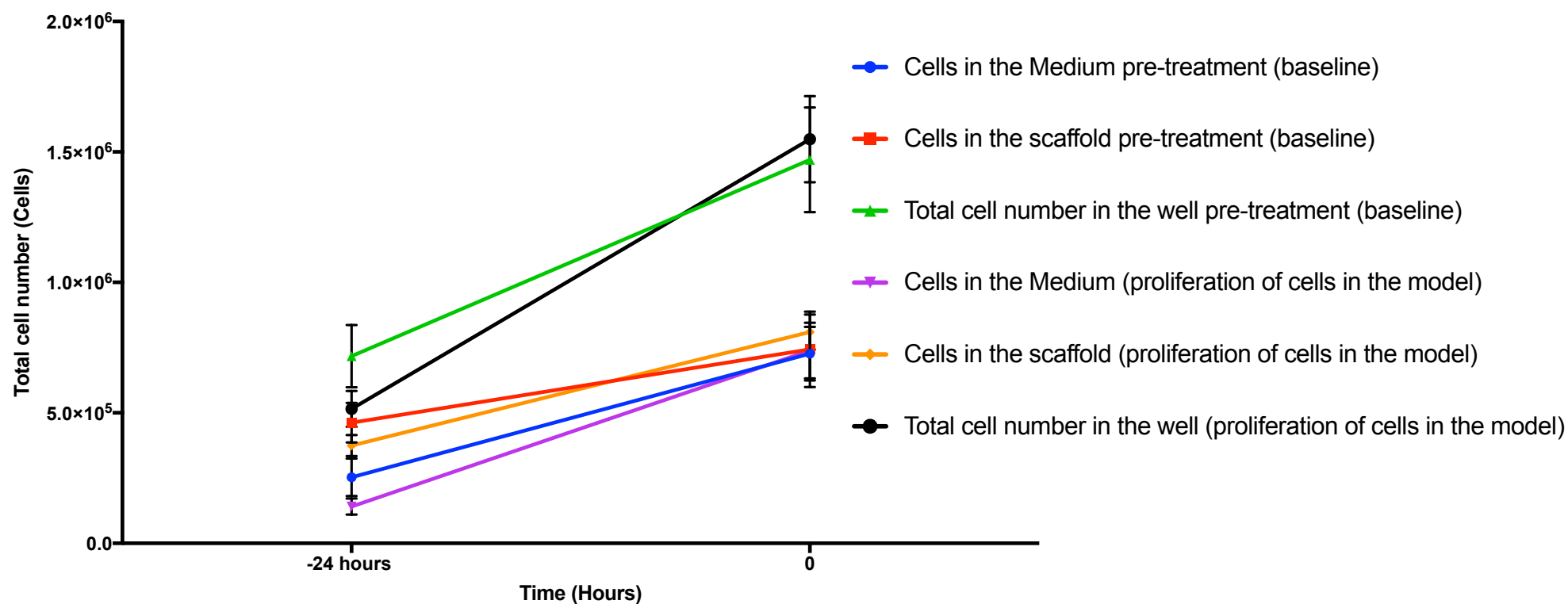


Figure 4-9. Baseline counts taken from the medium and well of TK6 and HS-5 seeded AlgiMatrix™ scaffolds, 24 hours before and on the day of compound dosing. Pre-treatment baseline counts, were then compared to the same parameters previously seen within Figure 3-13 M, N and O, to establish the consistent initial growth between the two studies. HS-5 cells were seeded onto AlgiMatrix™ scaffold, left to incubate for 24 hours, complete medium change conducted, incubated for a further 144 hours with a 50% medium change conducted every 48 hours. TK6 were then combined with each scaffold and incubated for a further 54 hours. Baseline AlgiMatrix™ scaffolds (four technical repeats) and corresponding medium were then harvested at -24 hours before and on the day of dosing (0 hour), with total cell number assessed via trypan blue, compared to the proliferation of cells found previously within the model (Figure 3-13 M, N and O).

Having established a dose range suitable for use in the multicellular model (section 4.3.5, 4.3.6), a dosing period (Figure 4-1) confirming that cells within the model are proliferating, comparable to previous optimisation, treatment of the AlgiMatrix™ scaffolds was conducted. The HS-5 cell line was seeded onto AlgiMatrix™ scaffolds, incubated, TK6 introduced and the co-culture left to incubate as described in section 2.3. At 0 hour time point, compound was added to the centre of the scaffold, mixed and incubated. After a 24 hour incubation, cells from the medium were harvested, counted and reseeded at the cell density established at time point 0 hour from the baseline counts onto their corresponding AlgiMatrix™ scaffold, and the scaffold returned to washed wells, for a further 24 hour incubation. Total cell number residing on the AlgiMatrix™ scaffold was not established at this point, as to not disturb the cells residing within. After a period of 48 hours after initial dosing, cells were harvested from the AlgiMatrix™ scaffold and medium and counted using TB. The results in Figure 4-10, show the total cell counts for two clastogens (MMC and etoposide), one aneugen (paclitaxel), two pharmacological positives (dexamethasone and prednisolone) and one known negative genotoxicant (caffeine) over the 48 hour period after dosing.

The results in Figure 4-10 A and B show the total cell counts for the two clastogens MMC and etoposide. On the day of dosing (0 hour) both MMC and etoposide wells, have 7.3×10^5 total cells in the medium and 7.4×10^5 total cells within the AlgiMatrix™ scaffold. After a 24 hour incubation, those cells within the medium of MMC treated AlgiMatrix™ scaffolds, at all concentrations were 1×10^6 total cells, which were then washed and reseeded onto their corresponding AlgiMatrix™ scaffold at 7.3×10^5 total cells. However, those cells harvested from the etoposide treated AlgiMatrix™ scaffold saw a dose dependent increase in total cell number with 1, 40.8, 64.5, 100.2 and 203.9 nMol/L achieving 1, 1.4, 1.4, 1.5 and 1.9×10^6 total cells respectively but weren't significant between each concentration. Once again, cells were washed and reseeded onto their corresponding AlgiMatrix™ scaffold at 7.3×10^5 total cells and left to incubate for a further 24 hours.

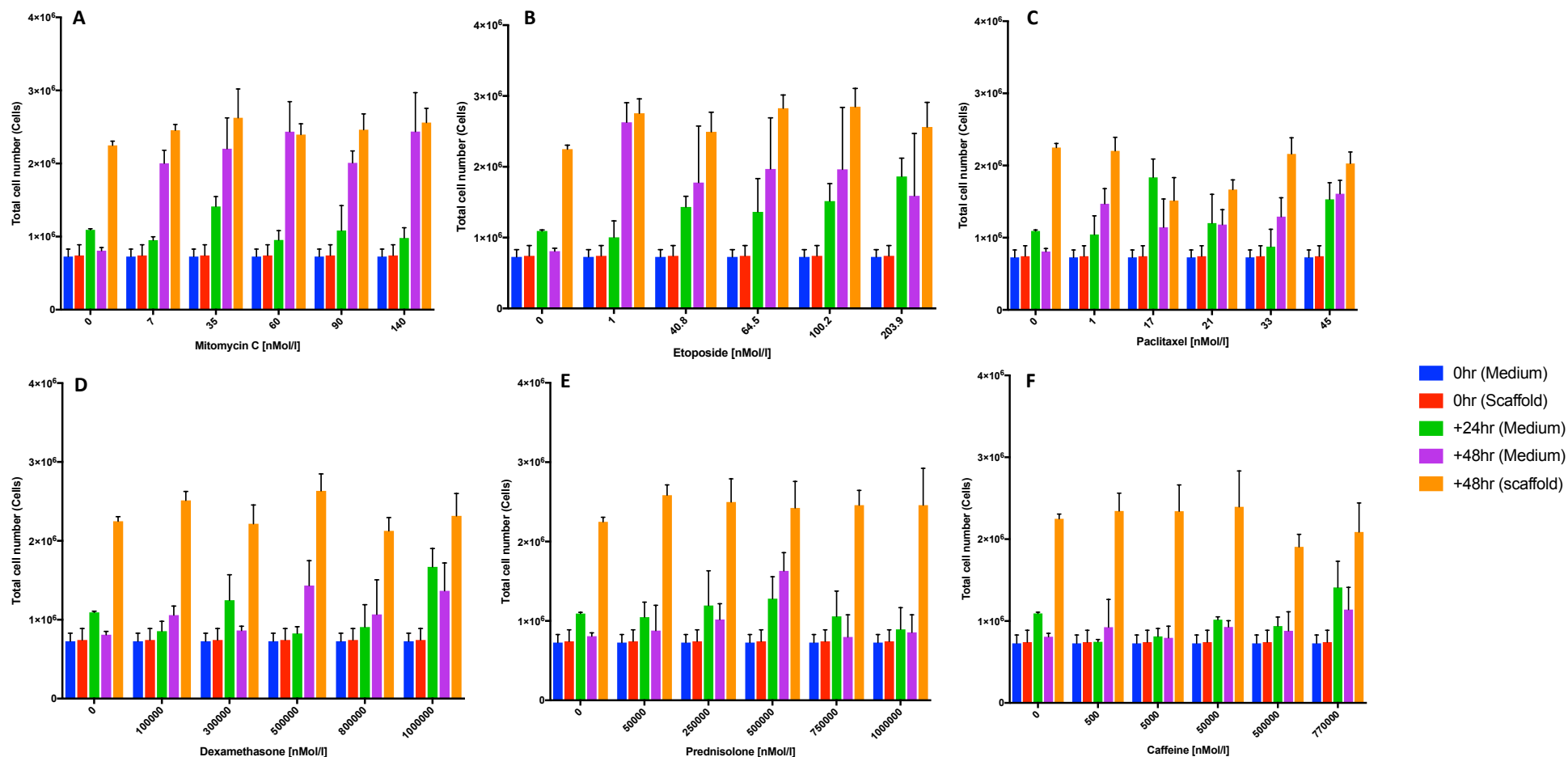


Figure 4-10. Total cell number of cells harvested from the medium and AlgiMatrix™ scaffold after dosing with compound. HS5 cells seeded onto AlgiMatrix™ scaffolds, incubated for 24 hours, complete medium change conducted, incubated for a further 144 hours before the addition of TK6 cells. After a 72 hour incubation, concentration of mitomycin C (A), etoposide (B), paclitaxel (C), dexamethasone (D), prednisolone (E) and caffeine (F) were added, incubated for 24 hour (+24 hours after initial dosing), medium washed, cells reseeded, incubated for a further 24 hours (+48 hours after initial dosing) before the medium and scaffold were harvested and assessed for total cell number via trypan blue (n=3)

After this second 24 hour incubation, the MMC vehicle control (0 nMol/L) resulted in a total cell number within the medium of 8×10^5 and a total cell number of around 26×10^5 in the AlgiMatrix™ scaffold. The total cell number within the AlgiMatrix™ scaffold remained constant at all concentrations. However, total cell number within the medium increased from 8×10^5 to around 20×10^5 in all concentrations, inducing a 2.5 fold increase in total cells. Etoposide showed a similar result, with cells in the vehicle control (0 nMol/L) resulting in a total cell number of 8×10^5 within the medium and a total cell number of around 25×10^5 in the AlgiMatrix™ scaffold. The total cell number within the AlgiMatrix™ scaffold remained constant at all concentrations. However, similar to MMC, the total cell number within the medium increased from 8×10^5 to around 26×10^5 , inducing a 3.3 fold increase in all remaining concentrations.

The results in Figure 4-10 C show the total cell counts for the aneugen paclitaxel. On the day of dosing (0 hour), in all wells there was a total cell number of 7.3×10^5 in the medium and 7.4×10^5 within the AlgiMatrix™ scaffold similar to MMC and etoposide. After a 24 hour incubation, those cells within the medium of treated AlgiMatrix™ scaffolds, saw an increase in total cell number at 17 and 45 nMol/L to around 18×10^5 with the remaining concentrations inducing a total cell number of around 12×10^5 . Cells within the medium of all concentrations were washed and reseeded onto their corresponding AlgiMatrix™ scaffold at 7.3×10^5 total cells and left to incubate for a further 24 hours. After this 24 hour incubation, similar to MMC and etoposide, the vehicle control (0 nMol/L) resulted in a total cell number within the medium of 8×10^5 and a total cell number of around in the AlgiMatrix™ scaffold. The AlgiMatrix™ scaffold which had received a dose of compound did see an increase in cells within the medium from 8×10^5 to around 15×10^5 total cells, a fold increase of 1.9. However, unlike MMC and etoposide, there was no significant difference in total cells within the AlgiMatrix™ scaffold or medium within all concentrations excluding the vehicle control.

The results in Figure 4-10 D and E show the total cell counts for the pharmacological positive compounds dexamethasone and prednisolone. On the day of dosing (0 hour) both dexamethasone and prednisolone, in all wells, had 7.3×10^5 total cells in the medium and 7.4×10^5 total cells within the AlgiMatrix™ scaffold, similar to the known genotoxic positives above. After a 24 hour incubation, those cells within the medium of dexamethasone treated AlgiMatrix™ scaffolds, saw an increase in total cell number, compared to the vehicle control, at 3×10^5 and 10×10^5 nMol/L with 12 and 17×10^5 total cells recorded. However,

there was no change in the total cell number residing in the medium of AlgiMatrix™ scaffolds treated with concentrations of prednisolone. Cells within both compound dose ranges, were washed and reseeded onto their corresponding AlgiMatrix™ scaffold at 7.3×10^5 total cells and left to incubate for a further 24 hours.

After this second 24 hour incubation, the vehicle control (0 nMol/L) in both dexamethasone and prednisolone, resulted in a total cell number within the medium of 8×10^5 and a total cell number of around 22×10^5 in the AlgiMatrix™ scaffold. The total cell number within the AlgiMatrix™ scaffold, as previously seen in the known genotoxic positives above, remained around the cell number identified within the vehicle control, for all concentrations. However, the total number of cells within the medium increased from the vehicle control to 14×10^5 at 5×10^5 and 10×10^5 nMol/L concentrations of dexamethasone, a fold increase of 1.8. In a similar manner, prednisolone remained at constant total cell number, similar to the vehicle control, for all concentrations with an increase only observed at 5×10^5 nMol/L to 16×10^5 total cells; a fold increase of 2.

The results in Figure 4-10 F show the total cell counts for the known negative caffeine. On the day of dosing (0 hour), in all wells, there was a total cell number of 7.3×10^5 in the medium and 7.4×10^5 within the AlgiMatrix™ scaffold similar to the results seen above. After a 24-hour incubation with compound, those cells within the medium of treated AlgiMatrix™ scaffolds, saw a decrease from the vehicle control (11×10^5 total cells) at 5×10^2 and 5×10^3 nMol/L (7.5 and 8.1×10^5 total cells). Further doses at 5×10^4 and 5×10^5 nMol/L remained around the total cell number seen with the vehicle control, with a dose of 7.7×10^5 nMol/L increasing cell number to 14×10^5 . Once again, cells within the medium of all concentrations were washed and reseeded onto their corresponding AlgiMatrix™ scaffolds at 7.3×10^5 total cells and left to incubate for a further 24 hours. After a second 24 hour incubation, those cells within the medium of treated AlgiMatrix™ scaffolds, saw an increase in total cell number, compared to the vehicle control (8×10^5 total cells), at 7.7×10^5 nMol/L to 11×10^5 total cells, inducing a fold increase of 1.4. The total cell number within the AlgiMatrix™ scaffolds, similar to previous results, remained around 24×10^5 with a drop only seen at a concentration of 5×10^5 nMol/L to 20×10^5 total cells.

It can be concluded from these results, that the introduction of known genotoxic and pharmacological positive compounds, will induce an increase in total cell number compared to the vehicle control, in the medium only. This would infer that MMC, etoposide, paclitaxel,

dexamethasone and prednisolone, at these concentrations, are not cytotoxic. However, caffeine appears to be cytotoxic at low concentrations. As the 24 hour cell counts within the AlgiMatrix™ scaffolds were not assessed, to maintain the cellular environment within, cytotoxicity within the scaffold and thereby within each well cannot be completely concluded. However, to truly assess the cytotoxicity of each compound, the RPD outlined by the OECD, should be calculated from the identified PD's within the medium on each day to assess if cells remain in a proliferating state.

As the total cell number within the medium was ascertained for MMC, etoposide, paclitaxel, dexamethasone, prednisolone and caffeine over the 48 hour treatment period, PD used for eventual RPD, was calculated (Table 4-6). Those cells treated with the vehicle control only, in all compound groups achieved a PD of 0.6 within 0-24 hours of dosing. Within the same time period during the original seeding growth curve, the PD within the medium was 0.8. Doses of MMC (7, 60 and 140 nMol/L), etoposide (1 nMol/L), paclitaxel (1 and 33 nMol/L), dexamethasone (1, 5 and 8×10^5 nMol/L), prednisolone (1×10^6 nMol/L) and caffeine (5×10^2 , 5×10^3 , 5×10^4 and 5×10^5 nMol/L) resulted in a PD below 0.6 inferring a reduction in proliferation at these concentrations. However, doses of MMC (35 nMol/L), etoposide (40.8, 64.5, 100.2 and 203.9 nMol/L), paclitaxel (17, 21 and 45 nMol/L), dexamethasone (3 and 10×10^5 nMol/L), prednisolone (2.5 and 5×10^5 nMol/L) and caffeine (7.7×10^5 nMol/L) gave a PD >0.6 inferring that these concentrations increased proliferation.

Table 4-6. The population doubling of cells within the medium of the 3D in vitro multicellular model when exposed to mitomycin C, etoposide, paclitaxel, dexamethasone, prednisolone and caffeine. The table shows the population doubling (PD) of cells exposed to each compound for 24 hour (0-24 hours) and recovery after compound is removed (24-48 hours). PD was only achieved in the medium as, 24 hours after dosing, cell number within the AlgiMatrix™ scaffold were not assessed in order to maintain cellular interaction within scaffold.

Population doubling								
Mitomycin C (nMol/L)	0-24 hours	24-48 hours	Etoposide (nMol/L)	0-24 hours	24-48 hours	Paclitaxel (nMol/L)	0-24 hours	24-48 hours
0	0.6	0.2	0	0.6	0.2	0	0.6	0.2
7	0.4	1.5	1	0.5	1.8	1	0.5	1
35	0.9	1.6	40.8	0.9	1.3	17	1.3	0.6
60	0.4	1.7	64.5	0.9	1.5	21	0.7	0.7
90	0.6	1.5	100.2	1.0	1.5	33	0.3	0.8
140	0.4	1.7	203.9	1.4	1.1	45	1	1.1
Dexamethasone (nMol/L)	0-24 hours	24-48 hours	Prednisolone (nMol/L)	0-24 hours	24-48 hours	Caffeine (nMol/L)	0-24 hours	24-48 hours
0	0.6	0.2	0	0.6	0.2	0	0.6	0.2
100000	0.2	0.6	50000	0.6	0.3	500	0	0.4
300000	0.7	0.2	250000	0.7	0.4	5000	0.2	0.1
500000	0.2	1	500000	0.8	1.1	50000	0.5	0.4
800000	0.3	0.6	750000	0.6	0.1	500000	0.4	0.3
1000000	1.2	1	1000000	0.3	0.3	770000	1	0.6

The medium was then harvested and reseeded at 7.3×10^5 total cells onto the corresponding AlgiMatrix™ scaffolds and incubated for a further 24 hours. As the cells had been reseeded at the same density as they had been dosed at 24 hours earlier, the PD should remain the same at 0.6. However, between the 24-48 hour time point, the PD within the vehicle control medium, reduced to 0.2 in all compound groups. This was not the case for those cells dosed with MMC or etoposide, as in all concentrations, cells doubled more than once. An increase >0.2 in PD was also seen with doses of paclitaxel (1, 17, 21, 33 and 45 nMol/L), dexamethasone (1, 5, 8 and 10×10^5 nMol/L), prednisolone (5×10^4 , 2.5, 5 and 10×10^5 nMol/L) and caffeine (5×10^2 , 5×10^4 , 5×10^5 and 7.7×10^5 nMol/L) inferring that all of these concentrations increased the proliferation of the cells within the medium. These results once again conclude that at these concentrations, compounds are not cytotoxic and seem to be increasing proliferation. However, the PD was not calculated for cells within the AlgiMatrix™ scaffold itself. Therefore, the PD for total cells within the AlgiMatrix™ scaffold and medium combined cannot be ascertained. At this dose range, concentrations do

not seem to be cytotoxic and an RPD is normally needed to be calculated to agree with OECD guidelines, in order for the genotoxicity of each dose to be investigated.

Once the AlgiMatrix™ scaffold had been exposed to each concentration of compound, within the 48 hour treatment period, AlgiMatrix™ scaffolds were harvested along with their corresponding medium and assessed for MN utilising AO staining. The cells harvested from the AlgiMatrix™ scaffold were scored separately to those cells in the medium. The results in Figure 4-11, show the MN induced in 1000/ mononucleated cells in the medium, scaffold and the combined MN of both, which have been exposed to differing concentrations of MMC, etoposide, paclitaxel, dexamethasone, prednisolone and caffeine. The percentage change between the total MN induced in the regulatory 2D MN assay, compared to the combined total MN of the scaffold and medium within the multicellular 3D model was also calculated. In all concentrations, regardless of compound, there was no significant difference between the number of MN within the scaffold and medium in the multicellular 3D model.

The results seen in Figure 4-11 A show that the combined total MN for MMC exceed twice the number in the vehicle control (15 MN/1000 mononucleated cells) at 60 nMol/L (59 MN/1000 mononucleated cells), inferring a genotoxic compound at this concentration and higher. This level of MN induction, within the 2D regulatory assay, was seen between 35-60 nMol/L. A lower concentration of 7 nMol/L was seen to exceeded twice the vehicle control of 7 MN/1000 mononucleated cells, which gave a MN induction of 25 MN/ 1000 mononucleated cells. There is a significant increase in MN between the vehicle control of the 2D and 3D assay, with 7 MN / 1000 mononucleated cells identified in 2D but 15 MN / 1000 mononucleated identified in 3D a percentage incerse of 53%. As the concentration of MMC increases within both the 2D and 3D assays, the number of MN/ 1000 mononucleated cells in the 2D assay surpasses that induced by 3D model at a concentration of 35 nMol/L, continuing this for the following concentration. The final two doses of MMC (90 and 140 nMol/L) weren't scored in the 2D assay, as they induced an RPD of $<50\% \pm 5\%$ in previous study (Figure 4-6).

The results seen in Figure 4-11 B, identify that the combined total MN for etoposide exceed twice the number of the vehicle control (15 MN/1000 mononucleated cells) at a concentration of 40.8 nMol/L (32 MN/1000 mononucleated cells), inferring a genotoxic compound at this concentration and above. This level of MN induction, within the 2D

regulatory assay, was seen with a concentration of between 1-40.8 nMol/L. A lower concentration of 1 nMol/L was found to be genotoxic induction 20 MN/ 1000 mononucleated cells, twice that of the vehicle control (8 MN/1000 mononucleated cells). A significant increase in MN between the vehicle control of the 2D and 3D assay, with 8 MN / 1000 mononucleated cells identified in 2D but 15 MN / 1000 mononucleated identified in 3D a percentage increase of 44%. The number of MN/ 1000 mononucleated cells induced by etoposide in the 2D assay, surpasses that induced by 3D model at a concentration of 40.8 nMol/L, continuing to increase in MN for the following concentration. The final two doses of etoposide (100.2 and 203.9 nMol/L) weren't scored in the 2D assay, as they induced an RPD of $<50\% \pm 5\%$ in previous study (Figure 4-6).

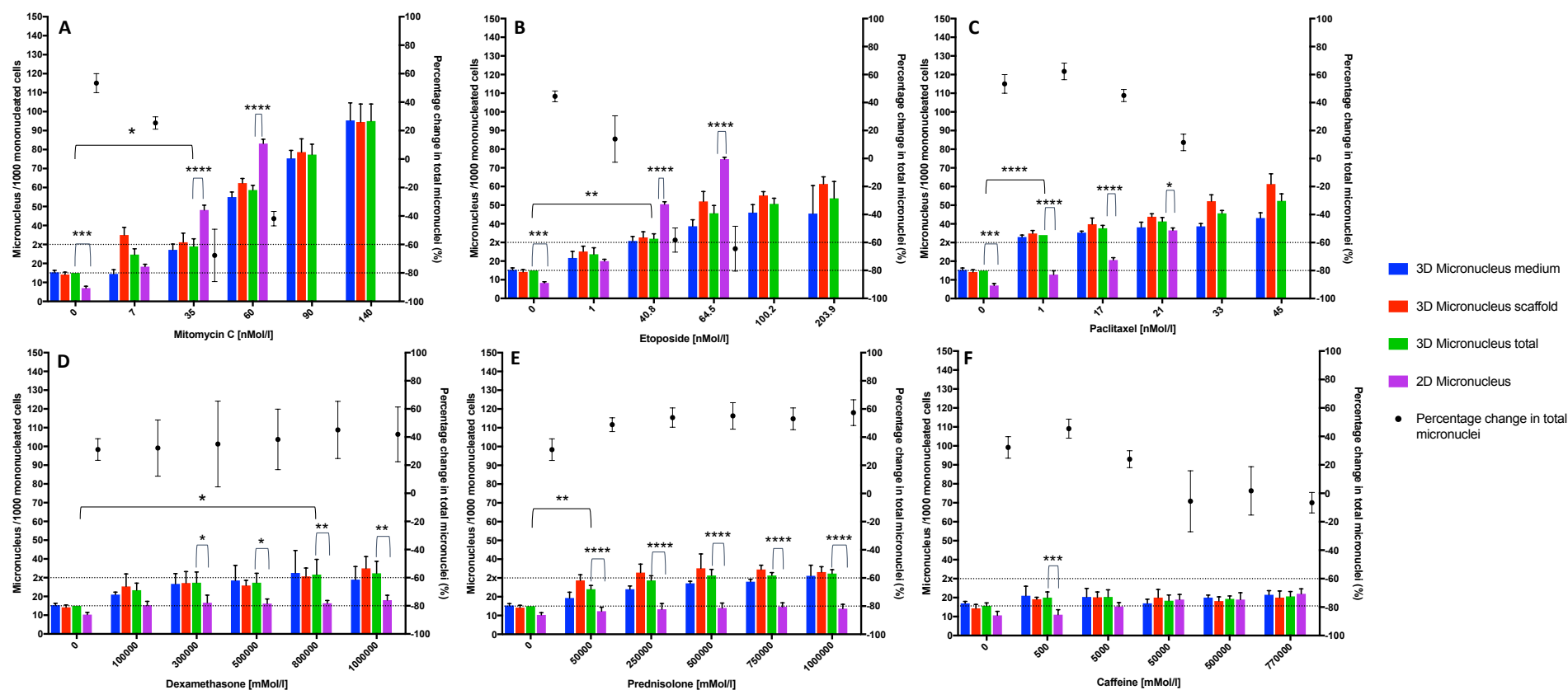


Figure 4-11. MN induction in cells within the medium and scaffold, harvested from a 3D model after dosing with compound. HS5 cells seeded onto AlgiMatrix™ scaffolds incubated for a 168 hours before the addition of TK6 cells. After a 72 hour incubation, concentration of mitomycin C (A), etoposide (B), paclitaxel (C), dexamethasone (D), prednisolone (E) and caffeine (F) were added, incubated for 24 hours, medium washed, cells reseeded, incubated for a further 24 hours before the medium and scaffold were harvested and assessed for MN using an AO stain. The combined total MN was then compared to that found within the regulatory 2D *in vitro* MN assay, with percentage change in total micronuclei (percentage increase from 2D to 3D) also assessed. Lines indicate vehicle control and 2x vehicle control MN counts within the 3D assay. Those concentrations without a 2D MN count induced a RPD of >50% ± 5% and weren't counted. A minimum of 2000 mononucleated cells were assessed for micronuclei (n=3) **Significant differences between samples were calculated using a Two-Way ANOVA followed by a Dunnett's test. The P values are indicated by * (p < 0.05), ** (p < 0.01), *** (p < 0.001), **** (p < 0.0001), actual p values can be found in appendix 1.**

The results for the two clastogenic compounds MMC and etoposide conclude, that even though a higher percentage of MN are induced for the 3D model within the vehicle control in comparison to the 2D regulatory assay, a higher concentration of MMC and etoposide is needed in the 3D model to replicate the equivalent MN induced within the 2D regulatory assay. This would infer that MMC and etoposide are less genotoxic in the 3D model than in 2D but are still genotoxic.

The results seen in Figure 4-11 C show the MN induction and percentage change for the known positive genotoxic compound paclitaxel. The combined total MN for paclitaxel saw an induction of 34 MN/ 1000 mononucleated cells, twice the number in the vehicle control (15 MN/1000 mononucleated cells), at a concentration of 1 nMol/L in 3D, inferring a genotoxic compound at this concentration and above. However, this level of MN induction was seen between 17-21 nMol/L within the 2D regulatory assay, with a concentration of 17 nMol/L of paclitaxel required to induce a positive genotoxic response (21 MN/1000 mononucleated cells). There is a significant increase in MN induced between the vehicle controls of the 2D and 3D assays, with a percentage increase of 53%. The level of MN induction in 3D appears to plateau between a concentration of 1 and 45 nMol/L with around 40 MN/1000 mononucleated cells. The final two concentration of paclitaxel (33 and 45 nMol/L), within the 2D regulatory assay, weren't scored as they induced an RPD of <50% \pm 5% in (Figure 4-6). These results conclude that paclitaxel requires a concentration of around 1 nMol/L in the 3D model, to induce a MN score twice that of the vehicle control inferring a positive genotoxic compound. A concentration higher than this has no significant effect on the induction of MN. It can also be concluded that paclitaxel is more genotoxic in the 3D model than the 2D regulatory assay.

The results seen in Figure 4-11 D and E show the MN induction and percentage change for dexamethasone and prednisolone. The concentrations of either compound, within the 2D assay was found to be non-genotoxic as MN did not exceed twice that of the vehicle control (15 MN/1000 mononucleated cells). The combined total MN for both dexamethasone at a concentration of 8×10^5 nMol/L and prednisolone at 5×10^5 nMol/L saw an induction of 32 and 31 MN/ 1000 mononucleated cells respectively, exceeding twice the number in the vehicle control (15 MN/1000 mononucleated cells), inferring a weak positive genotoxic compound at these concentrations. However, once either compound had reached its respective genotoxic concentration, further increases in concentration didn't induce a higher level of MN; instead, MN remained at the level stated earlier. The maximum induction of

MN/ 1000 mononucleated cells in the 2D assay was around 16 and 14 for dexamethasone and prednisolone. There was no statistical difference between the 3D and 2D vehicle controls for either compound. The percentage increase of MN between 3D and 2D for dexamethasone and prednisolone remained around 35 and 50% respectively for all concentrations tested. These results conclude that within a 3D multicellular model, concentrations of $>8 \times 10^5$ and $>5 \times 10^5$ nMol/L of dexamethasone and prednisolone, induced an increase in MN, thereby inferring a genotoxic concentration, in what is seen as a non-genotoxicant in the 2D regulatory assay. These data offer an important outcome within this research and supports the validity of the 3D model in bridging the gap between 2D and *in vivo* testing. The data presented here align with previous 2D work (demonstrating non-genotoxic), as well as outcomes for *in vivo* animal testing (weak genotoxic positive) with these compounds.

The results seen in Figure 4-11 F show the MN induction and percentage change for known negative compound caffeine. Within both the 2D regulatory assay and 3D multicellular model, at all concentrations, an induction of MN twice that of the vehicle control was not achieved reinforcing the use of caffeine as a negative genotoxic control. There was no significant difference in MN between 2D and 3D within the vehicle control. However, at low concentrations (5×10^2 and 5×10^3 nMol/L) a percentage increase can be seen in MN between the 3D and 2D of 45% and 24% respectively. This increase then plateaus at 5×10^4 nMol/L for the remainder of the concentrations. In conclusion, these results show that caffeine is non-genotoxic at all concentrations tested, therefore, reinforcing its use as a negative control.

4.4. Discussion

As stated in the previous chapter, the eventual aim of this research was to develop a physiologically relevant model of the *in vivo* BM, for use in genotoxicity testing. The genotoxicity of new compounds is routinely undertaken within the pharmaceutical industry, using a battery of tests as mentioned in section 1.2.2. The pharmaceutical company AZ utilises the bacterial AMES assay, before progressing each compound into the single 2D culture *in vitro* regulatory MN assay. The *in vitro* regulatory MN assay is intended to predict the genotoxic capability of a compound when advanced to *in vivo* studies. However, it has been documented that known non-genotoxic compounds, such as the glucocorticoid receptor agonists dexamethasone and prednisolone, are negative utilising the *in vitro* MN assay and within the clinic but marginally positive when progressed *in vivo* and thus have been named pharmacological positives (Hayes *et al.*, 2013). A compound-related disturbance in the rodent which increases the MN within the BM, but which is not genotoxic, such as changes in core body temperature and increased erythropoiesis, has been postulated as the mechanism behind these pharmacological positives (Tweats *et al.*, 2007, Pontén *et al.*, 2013). Even though we have an understanding regarding the mechanisms by which dexamethasone and prednisolone cause this weak increase in MN, other new compounds may produce the same outcome with no *in vivo* human and or rodent data to reassure that they are safe, possibly shutting down further development of an otherwise valuable resource. Therefore, the use of an *in vitro*, multicellular model of the BM, which mimics to the outcomes of compounds identified within the *in vivo* setting to confirm the 2D result, would be a useful tool in investigating the exact mechanisms and true genotoxicity of compounds before moving *in vivo*.

In this chapter an optimised, *in vitro* model of the BM containing both MSC derived (HS-5) and TK6 cell lines, upon an artificial ECM, which acted in a similar manner to that seen *in vivo* (Figure 4-1), was used to assess the cellular characteristics and genotoxicity of compounds with known positive, negative and 'pharmacological positive' genotoxic outcomes in relation to both rodent and human data within the literature. A series of regulatory 2D MN assays were initially undertaken at AZ and UWE for comparative scoring to ensure the transfer of assay and conditions between the laboratories. The compound dose range identified through these experiments which gave an RPD of $50\% \pm 5\%$, were then expanded to incorporate a toxic dose ($<50\% \pm 5\%$ RPD) for use within the 3D model. This chapter also reports on the MN induction and cellular changes of cells within the 3D model,

as a result of exposure to a dose range of known positive, negative and 'pharmacological positive' genotoxic compounds.

4.4.1. Genotoxicity of known positive, negative and pharmacological positive compounds within the *in vitro* regulatory 2D micronucleus assay.

In the present work, the 2D regulatory *in vitro* MN assay was used to identify a compound dose range of genotoxic (MMC, etoposide, 4NQO and paclitaxel), negative (caffeine) and pharmacological positive (dexamethasone and prednisolone) compounds which gave an RPD $>50\% \pm 5\%$. The four positive genotoxic compounds MMC, etoposide, 4NQO and paclitaxel were first assessed at AZ for MN induction and RPD, which was then carried out again at UWE for comparison of scoring. The results seen in Figure 4-5 show that for the same slide, scoring of MN between UWE and AZ was the same. However, when the range finding was conducted at UWE, with the concentration first identified at AZ, there was a difference in RPD and MN production at the same scorable dose which gave an RPD $>50\% \pm 5\%$.

When tested at AZ, MMC, etoposide and paclitaxel identified the highest scorable dose with an RPD $>50\% \pm 5\%$ at 70 (46%), 69.7 (52%) and 26 (57%) nmol/L with MN/1000 mononucleated cells at 55, 97 and 40 respectively. However, at UWE, the same doses of MMC, etoposide and paclitaxel gleaned an RPD of 47, 46 and 44% with MN/1000 mononucleated cells at 87, 91 and 50 respectively. This change in RPD and MN can be attributed to the number of biological repeats conducted at UWE and AZ. As this was only a preliminary study at AZ, an N number of one ($n=1$) was conducted. However at UWE three biological repeats were conducted per compound. It has been found that there can be a 10% shift in RPD and MN induction between the same dose of compound with differing biological repeats (Fellows *et al.*, 2008). Work by Smart *et al.*, (2020) Brüsehäfer *et al.* (2014), Thougard *et al.*, (2014), Hashimoto *et al.* (2012) and Dollapudi *et al.* (2019) in TK6, agreed with MN frequency and RPD induction found for MMC, etoposide and paclitaxel, with a maximum scorable dose within a 10% shift of those found at UWE.

The fourth positive genotoxic compound, 4NQO, did not identify a maximal scorable dose of $50\% \pm 5\%$ at AZ. However, at UWE, an RPD of 50% was found at a concentration of 184.1 nMol/L (35 ng/ml) with a MN induction of 23. The MN induction did not increase in a dose dependent manner, unlike RPD and the other three genotoxic compounds, and

appeared to remain around 23, which had increased from the negative control of 11 MN. A study by Brüsehafer *et al.* (2016) on TK6 cells, found that a concentration of 30-50 ng/ml was required to cause an increase in MN from the negative control. However, this study found that even at a dose of 157.8 nMol/L (30 ng/ml) at an RPD of 60%, MN formation had not increased from the first escalation after the negative control. This compound was still deemed positive as in both the Brüsehafer paper and at UWE it exceeded twice that of the negative control, with the positive also gleaming a score twice that of the negative control.

The initial dose range of MMC, etoposide, 4NQO and paclitaxel, found at UWE, was then expanded to include concentrations for each compound that induced an RPD $<50\% \pm 5\%$. It has been shown that higher concentrations of compound are required within 3D models and *in vivo* than in conventional 2D assay, due to reduction in bioavailability, detoxification and exposure of the compound (Nudischer *et al.*, 2020; Mathews *et al.*, 2016). However, as compounds are only tested to identify an RPD of $50\% \pm 5\%$, the literature does not reveal the MN and RPD of compounds above this. This study, therefore, is the first to identify the cytotoxicity of MMC, etoposide, 4NQO and paclitaxel ranging from an RPD of 100- 0%. However, the literature cited for the initial dose of each compound did see a dose dependent decrease in RPD, which if continued would correlate with the findings of the dose range expansion at UWE.

The pharmacological positive compounds dexamethasone and prednisolone, along with the genotoxic negative caffeine, were then assessed for genotoxicity at UWE only. In accordance with OECD guidelines, each compound was tested to a maximum dose of 1 mM or highest concentration that was still soluble. At a 1 mM dose of dexamethasone, an RPD of 60% was identified with a MN induction of 18, which did not reach twice that of the vehicle control at 10. At a 1 mM dose of prednisolone an RPD of 46% was found. However, at this dose MN induction was only 14, four more than the vehicle control. This inferred that even though both compounds were non-genotoxic, as they did not induce a MN score twice that of the vehicle control, both induced some level of cytotoxicity. It has been noted that glucocorticoids of this nature are cytotoxic to cells of the immune system such as lymphocytes and, therefore, could cause some cytotoxicity to TK6 without being genotoxic (Lee *et al.*, 2018). Work by Bryce *et al.* (2013) and Wilde *et al.* (2017) found that in TK6 cells, both dexamethasone and prednisolone at 1 mM did not have an increase in MN twice that of the vehicle control. However, they did find a reduction in RPD over the selected

concentration similar to that found at UWE, with 1 mM dexamethasone producing an RPD score of 60% and prednisolone 50%.

The non-genotoxic, but known cytotoxic compound caffeine was then assessed, with increasing concentrations up to a top dose of 7.7×10^5 nmol/L which was the maximum concentration that was soluble. At the highest dose, caffeine produced an RPD of 60% with a MN induction of 17, less than twice the vehicle control of 11. This level of cytotoxicity aligns with the literature as Chapman *et al.*, (2020), found that TK6 dosed with 7.7×10^5 nmol/L of caffeine in a 24 hour treatment - 24 hour recovery MN assay, an RPD of 60% and a MN frequency of 1.2% of the vehicle control was established. However, within UWE the MN frequency was 1.5% but as previously addressed, concentrations can fluctuate by 10% between biological repeats and laboratories.

4.4.2. Genotoxicity of known positive, negative and pharmacological positive compounds within the multicellular 3D model.

Following the findings of MN induction and relative RPD within the 2D MN assay, five concentrations of MMC, etoposide, paclitaxel, dexamethasone and prednisolone were identified for use in the 3D model. These five concentrations spanned an RPD of 100-80, 80-60, 60-40, 40-20, 20-0% for MMC, etoposide and paclitaxel. However, the five concentrations of dexamethasone and prednisolone ranged from 100 to 50%, as a lower RPD was not acquired within the 2D dose range finder. Owing to the lack of induction of MN with the compound 4NQO and the selection of two other clastogenic compounds (MMC and etoposide) 4NQO was not taken forward for 3D assessment.

Each concentration of compound was added directly to the centre of the scaffold on day 0 and allowed to perfuse out of the scaffold over the following 24 hours. This inferred a dynamic dosing regimen which doesn't occur within the 2D MN assay as cells are dosed directly. Dynamic dosing allows a change in compound concentration over time as bioavailable compound, which hasn't adhered to proteins or the scaffold, perfuses out into the surrounding medium. The addition of the drug directly to the scaffold also allows the BM stromal cells, already noted as being metabolically competent, to metabolise the compound. This type of dosing is seen within the *in vivo* environment (LaBonia *et al.*, 2016). However, within the *in vivo* setting a low but constant flow of blood facilitates the transportation of bioavailable compound into and out of the BM microenvironment, instead

of perfusion as seen with the scaffold (Torisawa *et al.*, 2016). To tackle this lack of flow within this 3D static model, once compound was added, the medium surrounding the scaffold was forced through the centre of the scaffold. This allowed the distribution of compound throughout the well and scaffold. The high level of sheer force produced from this method of compound distribution has been shown to alter gene expression and remove cells from the scaffold entirely, disrupting the microenvironment which has been developed (Prabhakarpanthian *et al.*, 2011). However, by distributing the compound for a small amount of time (<5 minutes), this would infer that the level of sheer force wouldn't alter the cellular adherence or gene expression but would distribute the compound to the whole well not just the scaffold.

After a 24 hour direct exposure to the compound, medium was removed from the well surrounding the scaffold. In order to maintain the microenvironment within the scaffold that had developed, the scaffold was not washed with medium, so the scaffold is likely to still contain remaining compound (and possibly metabolites). The half-life of MMC (50 mins), etoposide (1.5 hours), paclitaxel (13 hours), dexamethasone (190 mins), prednisolone (60 mins) and caffeine (5 hours) are shorter than the 24 hour period the drug had been within the system (McKenna *et al.*, 2012, Fang *et al.*, 2018, Gerson *et al.*, 2018, Wang *et al.*, 2011, Cevc & Blume, 2004, Bindreither *et al.*, 2014 & Alsabri *et al.*, 2018). As previously explained, the bioavailability, perfusion into the surrounding medium and potential metabolism by the stromal layer would greatly reduce the concentration of each compound over the initial 24 hour period. Therefore, the residual medium left within the scaffold would likely have had low, if any active compound.

The lack of wash did mean that the cellular contents of the scaffold could not be identified, unlike the surrounding medium which was counted and reseeded at the concentration at which the well was dosed. Furthermore, reseeded cells were reintroduced into the centre of the scaffold and mixed 3 times encouraging non-adhered cells within the scaffold out into the medium. This reintroduction of washed cells to the centre of the scaffold, displaced unwashed medium from the centre to the surrounding medium. Furthermore, cytokines and signalling molecules within the scaffold, could be reintroduced to the fresh surrounding medium, at a reduced concentration than that which had been removed through washing, , allowing a level of cellular communication to be maintained. As the cellular components of the scaffold weren't harvested in order to maintain the microenvironment, reintroducing cells in medium through the scaffold would likely increase the expected final cell

concentration within the well. This was accounted for by only reintroducing cells through the scaffold at the density measured in the medium when dosing, not the concentration of the well as a whole. The well of each scaffold was also washed, as it was seen that both HS-5 and TK6 cells resided on the well surface. Each culture was then left for a further 24 hours for a recovery period.

Once the recovery period had concluded, the scaffold and medium were harvested separately in order to count the cell number and MN in each compartment. The scaffold was removed first and then the surrounding medium, which had been washed across the surface of the well to collect any cells remaining on the surface. As the scaffold was removed first, the action of removal could have introduced (or removed) more cells to/from the scaffold surface, hence the total MN in each well was also calculated from the individual compartments. The identification of MN within the TK6 only, using the staining protocol of CD19 and CD20 identified in section 3.3.4.1 was the initial aim, with those MN residing with the DAPI only stained HS-5 also of interest. However, when the CD markers were stained, TK6 were not identifiable away from the HS-5 as shown in section 3.3.4.1. It has been noted that mutations, caused through de novo or chemical alteration in the genetic sequence of the CD marker, can cause the loss or abnormal expression of that CD marker (Shahrabi et al., 2020). The loss of these CD markers in 2D compound treated cells has not been documented in the literature'. However, as previously mentioned, the co-culture of cells can alter gene expression without chemical alteration.

As these CD markers were present during preliminary 3D study, the addition of compound, especially those that have detrimental effect on the genome, may have been the cause of this loss. Therefore, AO was used to identify MN within each compartment but was unable to differentiate TK6 from HS-5. A study by Sharma *et al.*, (2015) identified that stromal cells, when treated with compound in 2D culture, did not induce a high level of MN compared to that of the vehicle control. Even though, this study was conducted within a 2D environment it implies that the MN seen within our study would be predominately induced within the TK6.

As the 3D static model used within this study is meant to be representative of the *in vivo* human and/ or rodent, the comparison and explanation of MN induction and cellular alterations using the compounds mentioned previously, was achieved utilising the literature of pharmacokinetic profiles of each compound in both the human and rodent. Due to the novel aspect of this model, utilising *in vivo* data seemed more appropriate than comparing

this model with other *in vitro* models within the literature which differed in cell type, scaffold use and medium supplementation. As described previously, the concentration of each compound in the model would not be the final concentration biologically available to the cells, due to binding to proteins, scaffold and detoxification from the stromal layer.

4.4.2.1. The addition of known genotoxic compounds

The total cell number acquired for the two clastogenic compounds MMC and etoposide, after the 48 hour treatment period, appear to be higher in the treated wells compared to that of the negative control DMSO. As previously mentioned, cells were reseeded onto the scaffold after washing, at a reduced concentration (i.e. initial seeding density) to maintain the TK6 in their exponential phase, and yet cells within the medium were more than double that of the control for both compounds. When looking at the PD in 3D, after dosing (0-24 hours after addition of compound) cells within the medium do not have at least one PD, unless treated with high levels of etoposide. However, once reseeded, the cells within the recovery stage (24-48 hours) have more than 1.5 PDs compared to the control which was only at 0.2.

The increase in cell number over this timeframe could be explained by the dose range provided. It was found that in humans with non-small cell lung cancer, given a clinical dose of 6 mg/ m² or sub-clinical dose of 50 ng/ m² of MMC, an unbound plasma concentration of 440 ng/ml and 126ng/ml respectively was found within the bloodstream (Higley *et al.*, 2006). Within the 2D assay, the highest dose used which gave an RPD of 16%, was 46.8 ng/ml added directly to the model. As described previously, this concentration added to the model would signify the total, not unbound plasma concentration. The reduced concentration used within the model gives reason for the lack of cell death seen. However, this does not explain why the cellular concentration was increased so dramatically from the DMSO control.

To explain this increase in cell number we must turn to the *in vivo* rodent MN assay. When Swiss albino mice were given 1 mg/ kg intravenously of MMC, the unbound plasma concentration was found to be 45 ng/ ml, similar to the top concentration added to our model. At this low dose, the erythrocyte population in the blood stream declined. However, erythrocytes and erythroblasts found within the bone marrow increased; this was postulated to be because they were homed to

the BM to aid in repair and if repair couldn't be achieved, the production of new erythroblasts from HSCs in the BM niche was required (Yang *et al.*, 2019). This would infer that the TK6 cells within our model, once dosed, homed to the scaffold for repair (or perhaps protection from the HS-5), resulting in a depletion of cells within the medium after 24 hours of direct treatment. As the TK6 had migrated to the scaffold, the cell number within the medium after 24 hours was not representative of the actual cell number within the well as a whole. The cells that had migrated to the scaffold which hadn't been washed or counted, may have evacuated out of the scaffold with the reintroduction of washed cells. This would in some way explain the increase in cell number in the medium after 48 hours. However, with all compounds not just MMC, the level of cells within the scaffold, after 48 hours remain at the same level, inferring that a population of cells at around 2.5×10^5 cells remained adhered to the scaffold. Unfortunately, due to the lack of discrimination in staining, it cannot be stated the concentration of TK6 or HS-5 within this population.

Furthermore, studies by Niikawa *et al.*, (2001) & Bowen *et al.*, (2011) also found similar findings when treating both Swiss albino mice and rats with 1 mg/ kg of MMC over a 3 day or 7-day dosing period. At this dose the unbound plasma concentration was thought to be around 45 ng/ ml, and once again an erythrocyte population was slightly increased from 47.9 to 47.92% after dosing. At this concentration an 8 to 16-fold increase in MN was scored within the polychromatic erythrocytes. However, within the 3D system, at a concentration of 46.8 ng/ml, only a 6-fold increase from the vehicle control was seen. However, within the rodent, the constant flow from the circulatory system reduces the compound gradually, unlike our model which has a complete wash 24 hours after dosing. This extended dosing period, seen in each study could have attributed to the increase in MN. The 2D MN assay at the maximum scorable dose of 20.1 ng/ ml gave a 7- fold increase in MN from the vehicle control, highlighting the overestimation of genotoxicity of MMC at this dose.

The increase in cell number within the etoposide treated wells was likely due to factors similar to that of MMC. Within human treatment regimens, a clinical dose of 26.8 mg/kg gives a total unbound plasma concentration of 10,000 ng/ ml (Duong *et al.*, 2019). The highest concentration administered in the current model was 120 ng/ ml, which was significantly less than that seen in humans, giving reason for the lack of cytotoxicity. However, within the 2D MN assay this concentration gave an RPD of 11%

showing a high level of cytotoxicity at this concentration. Unlike MMC, etoposide had higher levels of cells within the medium after 24-hours of direct treatments and was attributed to the concentration of compound added to the model. The highest total concentration of MMC was 10-fold lower than that found in the human's unbound plasma, with the highest concentration of total etoposide used here equating to an 83-fold lower concentration compared to human plasma. This reduced level of compound (relative to clinically measured concentrations) thus did not cause equivalent cytotoxicity in the model, within the first 24 hours.

This explanation of lack of cytotoxicity with etoposide was also highlighted within the rodent *in vivo* MN assay. Sprague-Dawley rats intravenously administered with 3 kg/ mg resulted in an unbound plasma concentration of 30,000 ng /ml, 3x more than the human levels and 250x more than the maximum concentration administered within our model (Li & Choi 2009). A level of cytotoxicity was only seen at a high concentration of 20 mg/ kg, administered to Swiss albino mice, resulting in a small decrease of polychromatic erythrocytes from 6248 to 6153 (Choudhury *et al.*, 2004). Due to the lower concentrations of etoposide within the current model, unlike MMC, TK6 did not migrate to the BM as they did not appear to accumulate damage. Hence when washing and reseeded occurred, less cells in comparison to the MMC treated wells were evacuated into the medium. This gives further evidence to the decrease in cell number in the medium with increase in density after a 24 hour recovery period, as the number reseeded was more accurately depicting the well as a whole.

Once again, the addition of low concentrations of etoposide had an impact on MN production. The B62DF1 mouse was intravenously administered with 1 mg/ kg at an unbound plasma concentration of 10,000ng/ ml (Turner *et al.*, 2001). At this concentration a 25-fold increase in micronucleated polychromatic erythrocytes was found, unlike at the highest dose (120 ng/ ml) within our model of a 3-fold increase compared to the vehicle control. When looking at the results of the 2D MN, the highest scorable dose of 38 ng/ml gave an induction 11-fold higher, inferring overestimation of the genotoxicity of this concentration.

Similar to the two clastogenic compounds mentioned previously, paclitaxel has an increase in cell number within the medium of treated wells compared to that of the DMSO control. Once again, the highest concentration administered to the 3D model was lower compared to

that seen *in vivo*. In the treatment of metastatic breast cancer, a human clinical dose of 260 mg/ m² gave an unbound plasma concentration of 350 ng /ml, with patients at this concentration suffering from neutropenia, leukopenia, anaemia and thrombocytopenia. The highest concentration within our model was 38.4 ng/ ml; 9-fold less than the human clinically relevant dose. At this concentration within the 2D MN assay an RPD of 20% was recorded, showing a higher level of cytotoxicity *in vitro* than seen *in vivo*.

As the highest concentration of paclitaxel used within the model did not induce cytotoxicity, the genotoxicity of the compound within the model was investigated. Studies in mice found that when injected with 10 mg/ kg of paclitaxel, an unbound plasma concentration of 900ng/ ml was achieved and the erythrocyte's population declined rapidly (Li *et al.*, 2018). Once again this is higher than the concentration tested within the current model. However, when mice were tested with a therapeutic (0.6 mg/ kg), intermediate, (1.2 mg/kg) and high dose (1.8 mg/ kg) of paclitaxel, the unbound blood plasma concentration was 53, 113 and 150 ng/ ml respectively. At these concentrations, after a 24 hour incubation period, the MN induction slowly increased in a dose dependent manner, inducing around a 16-fold increase from the negative control (Zaid *et al.*, 2012 & Rabah *et al.*, 2010). This gradual increase in MN was seen within the current model at all concentrations above the vehicle control. However, only a 3-fold increase could be seen with even the highest concentration of paclitaxel, but as previously mentioned this could be a result of lower concentration of compound within the model. This gradual induction of MN was not seen within the 2D MN assay as induction increased rapidly from the vehicle control. At the highest scorable dose of 17.9 ng/ ml a 7-fold increase in MN could be seen, overestimating the level of genotoxicity.

4.4.2.2. The addition of pharmacological positive compounds

Unlike the known positive genotoxic compounds, dexamethasone and prednisolone did not induce the same increase in cell number within the medium or increased the PD over the 0-24 direct treatment or 24-48hour recovery period. Cell number within the two compounds fluctuated at each time point, with concentration of both dexamethasone and prednisolone causing an increase/ decrease in cell number after the direct and recovery treatment periods with no perceivable correlation. However, this fluctuation of cell number can be explained by looking within human studies, as compounds of this class have been noted as immunosuppressant and anti-emetic which are taken routinely through oral administration (Zabirowicz *et al.*, 2018).

A study by Jobe *et al.* (2020) showed, that when administering a 6 mg dose of dexamethasone to pregnant women to reduced morning sickness either intramuscularly or orally, the unbound blood plasma concentration peaked at between 95-100 ng/ml. The study found that at this concentration, T cell lymphocytes reduced 5-fold in cell number from the baseline line value to a nadir at 6 hours after administration. The concentration of T cells then returned back to baseline at 40-42 hours but continued to rise with a plateau 56 hours after initial treatment, 1.6-fold higher than the original baseline. This pattern also occurred within the basophil population. It was thought that this increase above and beyond the baseline was the remnant of a negative feedback loop, increasing the production of each to compensate for the initial loss. However, dexamethasone had the opposite effect on neutrophils; 24 hours after initial dosing the concentration of neutrophils increased 3-fold higher than the baseline, with concentrations returning and remaining at the baseline 46 hours after exposure.

The TK6 cell line used within the model is a B lymphoblast, unlike the T cell lymphocytes seen within the Jobe *et al.* (2020) study. The concentration of unbound dexamethasone found within (95-100 ng/ ml) the study was also far lower than the lowest dose used within the model (390,000 ng/ ml). However, as previously mentioned the concentration added to the model was unlikely the final concentration biologically available to the cells. Therefore, if one considers the highest dose of 390,000 ng/ ml, an increase in cell number after a 24 hour treatment or 48 hour recovery compared to the vehicle control was seen. The TK6 cell line has a doubling time of 14 hours unlike T cells which have a >24 hour cycle which would reduce the timeline seen *in vivo* (Macallan *et al.*, 2019). Therefore, the increase in cell number is not a lack of cytotoxicity, but the plateau above the baseline seen in humans with concentrations of dexamethasone <120,000 ng/ml representing those cells within the growth stage after initial reduction/inhibition.

This same occurrence can be used to explain the results seen with prednisolone. In a similar study, Magee *et al.* (2001) found that oral administration of 0.27 mg/ kg of prednisolone led to an unbound blood concentration of 100 ng/ml; 5x less than the bound concentration at 500 ng/ml. Once again, T cells declined to below the baseline to a nadir at 5 hours, which then increased past the baseline to a consistent plateau at around 18 hours post treatment. The neutrophil concentration also followed the same pattern as seen with dexamethasone, increasing post-treatment and returning to baseline 32 hours later.

Given the information on TK6 and T cell proliferation times above and the Magee *et al.* (2001) study, the results seen within the 3D model can also be attributed to a reduction in the *in vivo* timeline. As noted, prednisolone found a nadir at 5 hours post-treatment and plateaued above the baseline at 18 hours. This timeline was much longer with dexamethasone, with a nadir after 6 hours and increase above the baseline at 56 hours. This already reduced timeline and use of a more rapidly dividing cell line, is compounded by the concentration used within the model. As can be seen in Figure 4-10 E, the cell number at 24 and 48 hours after first exposure steadily increases in a dose dependent manner up to a concentration of 180,000 ng/ ml (500,000 nmol/L), 1800x higher than that used within humans. This would infer that the concentrations <180,000 ng/ ml corresponded with the increase in cell number up to a plateau seen at a concentration of 180,000 ng/ ml. Therefore, as concentrations >180,000ng/ ml did not increase in cell number, this is a sign of true cytotoxicity.

Given that the studies above suggested that the *in vitro* model was able to withstand concentrations of dexamethasone and low levels of prednisolone, in a similar manner to the *in vivo* setting, genotoxicity was then evaluated using data from the *in vivo* rodent BM MN assay. The total MN induction within the model for both dexamethasone and prednisolone exceeded that found in the corresponding 2D MN assay. A concentration greater than 800,000 (310,000ng/ ml) and 500,000 nMol/L (180,000ng/ ml) were found to induce a MN score twice that of the negative control. These concentrations are consistent with the proliferation past the baseline and plateau stages seen within Hayes *et al.* (2013). The level of MN within prednisolone plateaus with concentrations >180,000ng/ ml, correlating with the evidence that the cell number seen here is an indication of true cytotoxicity.

Within Swiss albino mice, given 8 mg/kg of dexamethasone, a peak unbound plasma concentration of 2300 ng/ ml was recorded (Li *et al.*, 2018). Utilising the same species, when dosed with 1, 5 or 10 mg/ kg, the unbound plasma concentration was 287.5, 1437.5, 2875 ng/ ml respectively. At these concentrations, the MN induced was 3, 3 and 5-fold higher than that of the vehicle control respectively (Singh *et al.*, 1994). Within our model a concentration of 310,000 ng/ ml, 107x higher than the highest concentration found within the rodent, gave a 2-fold induction of MN. This would infer that the biological, unbound concentration of dexamethasone was less than 287.5 ng/ ml within the model. This finding reinforces the increase in timeline due to increased proliferation of TK6 within the *in vitro* model,

compared to the human *in vivo* data, as this concentration is still 2.8x higher. However, at the same concentration used within the 2D MN there was less than a 1-fold increase in MN.

A concentration of 25mg/ kg of prednisolone administered to rats gave a peak bound, not unbound, plasma concentration of 80,000 ng/ml (Meno-Tetang *et al.*, 1990). Within the same species, a dose of 500, 1000 or 1500 mg/kg was administered and a 2-fold increase in MN compared to the vehicle control was seen. It was also noted that similar to the *in vivo* human, as concentration increased the level of white blood cells, lymphocytes and reticulocytes decreased and neutrophils increased in a dose dependent manner. Within the model a 2-fold increase in MN was seen with concentrations <180,000ng/ ml, which also correlated with the reduction in cell number seen within the *in vivo* rodent and human. This indicates that considering the level of prednisolone in conjunction with the increased cellular proliferation of TK6, it can be surmised that the concentration utilised *in vivo* was also administered within our model. However, at the same concentration used within the 2D MN, once again, there was less than a 1-fold increase in MN, highlighting the inability of the 2D MN assay to predict the outcome in rodent studies.

4.4.2.3. The addition of a negative genotoxic compound.

The negative genotoxic compound caffeine was the only drug, compared to the 5 previous compounds, which did increase cell number and PD, excluding the maximum dose of 7.7×10^6 nMol/L (1.5×10^5 ng/ ml). At each concentration the cell number remained similar to that found within the vehicle control of water. When investigating the effects within humans, White *et al.*, (2016), found that when participants orally ingested 0.32 mg/ ml of caffeine, the peak unbound plasma concentration was 3500 ng/ ml a 91-fold reduction with no determinantal effects to the participant. If this reduction was true within our model, the highest concentration of 150,000 ng/ ml would only give a biologically available concentration of 1648 ng/ ml and may explain the lack of cytotoxicity seen.

When rats were given orally administered 1 mg/ kg caffeine, a peak unbound plasma concentration of 350 ng/ ml was recorded, again with no detrimental effects to the rats (Noh *et al.*, 2015). It was found that at an increased concentration of 126 mg/ kg the level of MN remained <1-fold increase from the control (Bramebill *et al.*, 2013). This finding was consistent with the total MN production within the model and 2D MN assay. However, within the 2D assay a concentration of 150,000 ng/ ml gave an RPD of 60%, whereas there

was no effect on cellular number within the *in vivo* human and *in vitro* model, highlighting the overestimation of cytotoxicity within the 2D MN assay.

4.5. Conclusion

This study has shown the effects of a range of known positive, negative and pharmacological positive compounds within the 2D MN assay and 3D model, on the cell number and MN induction over a 48-hour treatment period. The 2D regulatory MN assay is meant to be predictive of the *in vivo* environment. However, findings from the 2D MN assay show that the results gleaned from positive genotoxic compound overestimates the level of cytotoxicity and underestimated the MN induction when compared to an *in vivo* environment. The use of pharmacological positive compounds had the opposite effect within the 2D assay, as both the level of cytotoxicity and genotoxicity was overestimated compared to the *in vivo* human and or rat.

The addition of each compound to the 3D model invoked an effect that was more *in vivo* relevant than that of the 2D MN assay. The cytotoxicity and genotoxicity more closely resembled that which was found within the literature for *in vivo* studies. However, a higher concentration of positive genotoxins and lower dose of the pharmacological positive compounds was required to fall in line with the clinically relevant, biologically available, doses seen within both human and rodents. Identifying the unbound concentration within the model would therefore be beneficial. However, the concentrations used within the 3D model were identified using OECD guidelines within a single cell culture and within a cytotoxic range, inferring that the addition of the HS-5 stromal line causes this change in effects, possibly via its metabolic competence. This result also sheds light on the suitability of OECD guidelines in the 21st century, and perhaps their need to be revisited.

In conclusion the addition of each compound to the 3D model provided a more *in vivo* genotoxic and cytotoxic response than that seen within the 2D MN assay. However, to identify the mechanism behind the change in genotoxicity and cytotoxicity with positive and pharmacological positive compounds, further investigation is needed into the role of the HS-5 stromal cell line when cultured within a 3D environment, both in isolation and with the addition of TK6.

Chapter Five

5. Assessment of the metabolic status of the 3D *in vitro* cell line model.

5.1. Introduction

The BM microenvironment is made up of differing cellular compartments consisting of haematopoietic and non-haematopoietic stromal cells such as osteoblasts, adipocytes and fibroblasts within a liquid compartment comprising of growth factors, cytokines, enzymes and chemokines (Lemaire *et al.*, 2011). It is this interaction between the stromal cells of the BM and the haematopoietic niche, that has been identified as the cause of drug detoxification and /or activation *in vivo*, leading to altered outcomes of drug interactions between *in vitro* and *in vivo* assays (Ria *et al.*, 2020; Chen *et al.*, 2020). The primary human stroma has been found to act in a similar manner to human hepatocytes, by expressing a variety of phase 1 and 2 metabolic enzymes (CYP450) as well as associated drug transporters (Alonso *et al.*, 2015 & Boutin *et al.*, 2020). Conversely, the human HSC compartment has low expression of drug metabolism enzymes and associated drug transporters (Chen *et al.*, 2019).

In order to assess the genotoxic capability of a pro-drug within the regulatory *in vitro* MN assay as haematopoietic cell lines such as TK6 do not express metabolic enzymes, the addition of the rat liver 9000 xg supernatant fraction (S9), extracted from rats pre-treated with drug metabolite enzyme inducers such as aroclor, is used to increase the expression of the phase I and II metabolic enzymes CYP1A1, 1A2, 2B1, 2B2, 2C6, 3A1 and 3A2 similar to that expressed by the liver (Kishino *et al.*, 2019). However, as previously mentioned cells of the haematopoietic niche do not express metabolic enzymes or contain the associated drug transporters noted within the *in vivo* stroma. The use of the rat S9 fraction, therefore, is only applicable to those compounds altered by the above family of CYP enzymes. In order to have a true representation of the genotoxicity of compounds, the addition of a cell line with a similar metabolic profile to that seen within *in vivo* stroma is required. Therefore, as HS-5 have been chosen as a cell line model of the *in vivo* BM stroma, it needs to be assessed for its ability to also express the equivalent enzymes *in vitro*, validating the current model.

The work in previous chapters has identified a method of co-culturing cell lines upon an artificial ECM (section 3.3.2.5), which when treated with known positive, negative and

pharmacological positive genotoxicity compounds induced a response similar to that seen *in vivo* (section 4.3.6). The aim of this chapter was to identify the metabolic profile of the HS-5 cell line, used as the stromal layer within the 3D model, in comparison to that seen within the *in vivo* BM. In brief, HS-5 cells were cultured as a 2D monolayer and within the 3D scaffold using a previously mentioned technique (section 2.3.1), with and without the addition of TK6 separated by a trans-well insert at a concentration identified in section 3.3.2.5. The HS-5 cell line from each culture was then harvested, RNA extracted, and quantitative polymerase chain reaction (qPCR) conducted for expression of phase I and II drug metabolic enzymes and associated drug transporters. This was then compared to HepG2 spheroids, cultured in-house, for comparison of relative expression. The HS-5 cell line was then cultured as a monolayer, before the addition of TK6 within a trans-well insert, to study the effects of the pro-drug cyclophosphamide with and without the addition of S9.

5.2. Materials and methods

5.2.1. Spheroid formation

As a positive control, HepG2 spheroids were generated using the protocol conducted within May *et al.*, (2012). Cells were grown for seven days as denoted in section 2.2, trypsinised and cells seeded into a 6-well plate at a concentration of 1×10^6 cells/ml in 3 mls of complete medium. Each plate was incubated on an orbital shaker at 37 °C, 5% CO₂ at 83 RPM for 24 hours and then 79 RPM for an additional 120 hours. A 50% medium change was conducted every 48 hours until maturation on day 6.

5.2.2. RNA extraction

HS-5 cells grown within an Algimatrix™ scaffold in 12 well plates (as described in section 2.3.1), were either harvested immediately or co-cultured with TK6 cells (separated by a 12-well 0.2 µm pore insert) for a further 48 hours (50% medium change every 24 hours), and then extracted for RNA. HepG2 spheroids were also collected as a positive control. RNA was extracted using the RNeasy Plus mini kit (Qiagen, Germany) following the manufacturer's guidelines using RNA free tips, pipettes and working area which had been sprayed down with RNase zap (Thermo Scientific, Loughborough).

Briefly, around 1×10^6 cells from each condition were collected by centrifugation (300 x g, 7 minutes), medium removed, 350 µl of RLT buffer (with addition of 2% 2 M dithiothreitol; DTT) added and mixed vigorously for 1 minute. The lysate was transferred into a QIAshredder (Qiagen) spin column in a 2 ml collection tube and centrifuged at 8000 x g for 2 minutes. The homogenized lysate was transferred into a gDNA Eliminator spin column (Qiagen) and spun at 8000 x g for around 30 seconds. A 1:1 ratio of 70% ethanol (100% molecular grade ethanol in RNase free water) to homogenized lysate was combined, mixed and 700 µl transferred to a RNeasy spin column. The column was then centrifuged for 15 seconds at 8000 x g and the flow-through discarded. Buffer RW1 (700 µl) was added to the RNeasy spin column and centrifuged at 8000 xg for 15 seconds with the flow-through discarded. RPE buffer (500 µl at working solution with 100% ethanol) was then added to the RNeasy spin column and centrifuged at 8000 x g for 15 seconds with the flow-through discarded; this step was then repeated for a second time. The RNeasy spin column was then transferred to a new 2 ml collection tube and centrifuged for 1 minute at 8000 x g to further

dry the membrane. The RNeasy spin column was transferred to a new 1.5 ml centrifuge tube, 10 μ l of RNase-free water added directly to the membrane and centrifuged for 1 minute at 8000 x g before the flow-through was placed back onto the membrane and centrifuged again for 1 minute at 8000 x g. The RNA sample was kept on ice or stored at -80 °C until quantification.

5.2.3. Assessment of RNA quality and concentration

RNA was assessed for concentration and purity using the Nanodrop 1000 spectrophotometer (Thermo Scientific, Loughborough). Each sample was analysed in duplicate with 2 μ l of extracted RNA. An absorbance ratio at $A_{260\text{nm}/280\text{nm}}$ was obtained for each sample with a ratio of around 1.8 denoting “pure” DNA and around 2.0 as “pure” RNA. A secondary absorbance ratio at $A_{260\text{nm}/230\text{nm}}$ was recorded; a value of >2.0 denotes “pure” nucleic acid, anything lower would indicate degradation or contamination of the RNA (Desjardins *et al.*, 2010). RNA quality was verified by 1% agarose gel electrophoresis containing 1x tris-acetate-EDTA (TAE buffer; 40 mM Tris acetate, 10 mM EDTA at pH 8.3) and 10 μ g/ml of ethidium bromide. RNA from each sample (around 700 ng) was combined with loading buffer (Bioline, UK) at a 5:1 ratio before loading along with a 1 Kb plus DNA ladder (ThermoFisher scientific) and electrophoresed at 100 V for 30 minutes. The 28s and 18s ribosomal RNA was then visualised by ultraviolet transilluminator to verify intact RNA.

5.2.4. Quantitative polymerase chain reaction of human drug metabolism components.

cDNA was synthesised using the recommended RT² first strand kit for use with the RT² profiler PCR array of human drug metabolism following the manufacturer’s instructions. In accordance with the kit handbook, all reagents were first thawed to RT and centrifuged for 15 seconds to collect the reagent in the bottom of the tube. To convert the RNA to cDNA using the RT² first strand kit, a genomic DNA elimination mix was prepared for each RNA sample in PCR tubes (RNA 0.5 μ g, GE buffer 2 μ l and brought to a total volume of 10 μ ls with RNase-free water), mixed by gentle pipetting, centrifuged to bring the components to the bottom of the tube and incubated on a thermocycler for 5 minutes at 42 °C. Once completed, the reaction was moved to ice for 1 minute whilst the reverse transcription mix was prepared (4% 5x buffer BS3, 1% control P2, 2% RE3 reverse transcription mix and 3% RNase-free water in a total volume of 10 μ l per sample). Reverse transcription mix (10 μ ls)

was added 1:1 to each PCR tube, mixed, incubated on a thermocycler for 15 minutes at 42°C then immediately heated to 95 °C for 5 minutes. An additional 91 µls of RNase-free water was then added to each reaction, mixed and placed on ice for use in the RT² profiler PCR array of human drug metabolism.

The gene expression of 84 associated drug metabolism genes including drug transporters (metallothioneins and p-glycoprotein family), phase 1 metabolic enzymes (CYP450 family phase 2 metabolic enzymes; carboxylesterases, decarboxylases, dehydrogenases, glutathione peroxidases, lipoxygenases, hydrolases, kinases, oxidoreductases, paraoxonases, glutathione S-transferases), 5 housekeeping genes, and 7 controls were assessed using the RT² profiler PCR array of human drug metabolism (Qiagen) following the manufacturer's instructions with each gene randomised across the plate (Table 5-1).

Briefly, reagents were thawed to RT whilst the PCR components mix was prepared in accordance with the kit handbook. PCR component mix (25 µls) was then added to each well using an 8-channel pipettor, sealed with an optical adhesive film, centrifuged at 1000 x g for 1 minute and run on a QuantStudio 12K Flex Real-time PCR system (Thermo Scientific) using the following programme: 1 cycle for 10 minutes at 95°C, 40 cycles of 95°C for 15 seconds, and 60°C for 1 minute. Three repeats per sample were conducted.

Table 5-1. The list of genes within the RT² profiler PCR array of human drug metabolism plate.

Position on plate	Symbol	Description
A01	<i>ABCB1</i>	ATP-binding cassette, sub-family B (MDR/TAP), member 1
A02	<i>ABCC1</i>	ATP-binding cassette, sub-family C (CFTR/MRP), member 1
A03	<i>ABP1</i>	Amiloride binding protein 1 (amine oxidase (copper-containing))
A04	<i>ADH1B</i>	Alcohol dehydrogenase 1B (class I), beta polypeptide
A05	<i>ADH1C</i>	Alcohol dehydrogenase 1C (class I), gamma polypeptide
A06	<i>ADH4</i>	Alcohol dehydrogenase 4 (class II), pi polypeptide
A07	<i>ADH5</i>	Alcohol dehydrogenase 5 (class III), chi polypeptide
A08	<i>ADH6</i>	Alcohol dehydrogenase 6 (class V)
A09	<i>AHR</i>	Aryl hydrocarbon receptor
A10	<i>ALAD</i>	Aminolevulinatase
A11	<i>ALDH1A1</i>	Aldehyde dehydrogenase 1 family, member A1
A12	<i>ALOX12</i>	Arachidonate 12-lipoxygenase
B01	<i>ALOX15</i>	Arachidonate 15-lipoxygenase
B02	<i>ALOX5</i>	Arachidonate 5-lipoxygenase
B03	<i>APOE</i>	Apolipoprotein E
B04	<i>ARNT</i>	Aryl hydrocarbon receptor nuclear translocator
B05	<i>ASNA1</i>	ArsA arsenite transporter, ATP-binding, homolog 1
B06	<i>BLVRA</i>	Biliverdin reductase A
B07	<i>BLVRB</i>	Biliverdin reductase B (flavin reductase (NADPH))
B08	<i>CES1</i>	Carboxylesterase 1
B09	<i>CES2</i>	Carboxylesterase 2
B10	<i>CES3</i>	Carboxylesterase 3
B11	<i>CHST1</i>	Carbohydrate (keratan sulphate Gal-6) sulphotransferase 1
B12	<i>COMT</i>	Catechol-O-methyltransferase
C01	<i>CYB5R3</i>	Cytochrome b5 reductase 3
C02	<i>CYP11B2</i>	Cytochrome P450, family 11, subfamily B, polypeptide 2
C03	<i>CYP17A1</i>	Cytochrome P450, family 17, subfamily A, polypeptide 1
C04	<i>CYP19A1</i>	Cytochrome P450, family 19, subfamily A, polypeptide 1
C05	<i>CYP1A1</i>	Cytochrome P450, family 1, subfamily A, polypeptide 1
C06	<i>CYP2B6</i>	Cytochrome P450, family 2, subfamily B, polypeptide 6
C07	<i>CYP2C19</i>	Cytochrome P450, family 2, subfamily C, polypeptide 19
C08	<i>CYP2C8</i>	Cytochrome P450, family 2, subfamily C, polypeptide 8
C09	<i>CYP2C9</i>	Cytochrome P450, family 2, subfamily C, polypeptide 9
C10	<i>CYP2D6</i>	Cytochrome P450, family 2, subfamily D, polypeptide 6
C11	<i>CYP2E1</i>	Cytochrome P450, family 2, subfamily E, polypeptide 1
C12	<i>CYP2F1</i>	Cytochrome P450, family 2, subfamily F, polypeptide 1
D01	<i>CYP2J2</i>	Cytochrome P450, family 2, subfamily J, polypeptide 2
D02	<i>CYP3A4</i>	Cytochrome P450, family 3, subfamily A, polypeptide 4
D03	<i>CYP3A5</i>	Cytochrome P450, family 3, subfamily A, polypeptide 5
D04	<i>EPHX1</i>	Epoxide hydrolase 1, microsomal
D05	<i>FAAH</i>	Fatty acid amide hydrolase
D06	<i>FBP1</i>	Fructose-1, 6-bisphosphatase 1
D07	<i>GAD1</i>	Glutamate decarboxylase 1
D08	<i>GAD2</i>	Glutamate decarboxylase 2
D09	<i>GCKR</i>	Glucokinase (hexokinase 4) regulator
D10	<i>GPI</i>	Glucose-6-phosphate isomerase
D11	<i>GPX1</i>	Glutathione peroxidase 1
D12	<i>GPX2</i>	Glutathione peroxidase 2
E01	<i>GPX3</i>	Glutathione peroxidase 3
E02	<i>GPX4</i>	Glutathione peroxidase 4
E03	<i>GPX5</i>	Glutathione peroxidase 5
E04	<i>GSR</i>	Glutathione reductase
E05	<i>GSTA3</i>	Glutathione S-transferase alpha 3
E06	<i>GSTA4</i>	Glutathione S-transferase alpha 4
E07	<i>GSTM2</i>	Glutathione S-transferase mu 2
E08	<i>GSTM3</i>	Glutathione S-transferase mu 3
E09	<i>GSTM5</i>	Glutathione S-transferase mu 5
E10	<i>GSTP1</i>	Glutathione S-transferase pi 1
E11	<i>GSTT1</i>	Glutathione S-transferase theta 1
E12	<i>GSTZ1</i>	Glutathione transferase zeta 1
F01	<i>HK2</i>	Hexokinase 2

F02	<i>HSD17B1</i>	Hydroxysteroid (17-beta) dehydrogenase 1
F03	<i>HSD17B2</i>	Hydroxysteroid (17-beta) dehydrogenase 2
F04	<i>HSD17B3</i>	Hydroxysteroid (17-beta) dehydrogenase 3
F05	<i>LPO</i>	Lactoperoxidase
F06	<i>MGST1</i>	Microsomal glutathione S-transferase 1
F07	<i>MGST2</i>	Microsomal glutathione S-transferase 2
F08	<i>MGST3</i>	Microsomal glutathione S-transferase 3
F09	<i>MPO</i>	Myeloperoxidase
F10	<i>MT2A</i>	Metallothionein 2A
F11	<i>MT3</i>	Metallothionein 3
F12	<i>MTHFR</i>	Methylenetetrahydrofolate reductase (NAD(P)H)
G01	<i>NAT1</i>	N-acetyltransferase 1 (arylamine N-acetyltransferase)
G02	<i>NAT2</i>	N-acetyltransferase 2 (arylamine N-acetyltransferase)
G03	<i>NOS3</i>	Nitric oxide synthase 3 (endothelial cell)
G04	<i>NQO1</i>	NAD(P)H dehydrogenase, quinone 1
G05	<i>PKLR</i>	Pyruvate kinase, liver and RBC
G06	<i>PKM2</i>	Pyruvate kinase, muscle
G07	<i>PON1</i>	Paraoxonase 1
G08	<i>PON2</i>	Paraoxonase 2
G09	<i>PON3</i>	Paraoxonase 3
G10	<i>SNN</i>	Stannin
G11	<i>SRD5A1</i>	Steroid-5-alpha-reductase, alpha polypeptide 1 (3-oxo-5 alpha-steroid delta 4-dehydrogenase alpha 1)
G12	<i>SRD5A2</i>	Steroid-5-alpha-reductase, alpha polypeptide 2 (3-oxo-5 alpha-steroid delta 4-dehydrogenase alpha 2)
H01	<i>ACTB</i>	Actin beta
H02	<i>B2M</i>	Beta-2-microglobulin
H03	<i>GAPDH</i>	Glyceraldehyde-3-phosphate dehydrogenase
H04	<i>HPRT1</i>	Hypoxanthine phosphoribosyltransferase 1
H05	<i>RPLP0</i>	Ribosomal protein large, P0
H06	HGDC	Human Genomic DNA Contamination
H07	RTC	Reverse Transcription Control
H08	RTC	Reverse Transcription Control
H09	RTC	Reverse Transcription Control
H10	PPC	Positive PCR Control
H11	PPC	Positive PCR Control
H12	PPC	Positive PCR Control

Blue: drug transporters, green: phase I metabolic enzymes, orange: phase II metabolic enzymes, yellow: 'associated genes', grey: housekeeping and white: controls.

5.2.5. Addition of cyclophosphamide to HS-5 cells for the assessment of pro-drug activation.

HS-5 cells were grown to confluency before trypsinisation and counting via trypan blue stain (Section 2.2). HS-5 cells were then seeded at 70 - 80% confluency into a 12 well plate ($7 - 8 \times 10^4$ cells/cm²) in 2 ml of medium and incubated at 37 °C, 5% CO₂ for 24 hours. TK6 cells, were then added into a 0.2 µm trans-well insert within a 12 well plate with or without HS-5 cells, at a concentration of 1×10^5 cell/ml in 3 mls. HS-5 cells alone was also included. Cells in all conditions were treated with a clinically relevant dose of cyclophosphamide (500 µM in DMSO <0.005%) ± S9 mix (20% S9, 19 mMol/L MgCl₂, 37.5 mMol/L potassium chloride, 0.11 mM sodium phosphate buffer (pH 7.4) 6.12 mMol/L mM glucose-6-phosphate and 4.7 mMol/L nicotinamide adenine dinucleotide phosphate) taken from Doherty (2012) at a final concentration of S9 at 1%. S9 mix alone, S9 mix + vehicle control,

vehicle control alone and untreated cells were included as controls. Cells were treated for 24 hours after which each sample was washed with PBS and assessed for cell number and viability via trypan blue staining on the Luna counter.

5.2.6. qPCR analysis

The difference between means within the qPCR data was calculated based on a Student's t-test of the replicate $2^{(-\Delta CT)}$ values for each gene in the control group and treatment groups. The p-value calculation used is based on parametric, unpaired, two-sample equal variance, two-tailed distribution. The cycle threshold (CT) value was identified for each plate, using the manufacturer's guidance whereby a positive PCR control (PPC) CT of 20 ± 2 and a reverse transcription control (RTC) of 22 ± 2 was required. Normalisation was achieved by calculating the geometric mean of the five housekeeping genes per plate (H01- H05). The geometric means from the biological repeats for each sample were then averaged to give an average geometric mean for normalisation. Once normalisation had been conducted, the results for HS-5 cultured in 2D was compared with HS-5 cultured within the model. HS-5 cultured within the model was then compared to HS-5 cultured within the model with the addition of TK6.

A threshold of 35 cycles, indicated by the manufacturer as the minimum detectable limit with the quantity of cDNA added to each well, was used with a CT value >35 indicating an extremely low level of expression and therefore negative for that gene, a CT of 40 indicated that the gene was undetectable. This threshold was only applicable if the human genomic DNA control was undetectable at a CT of >35 , PPC of 20 ± 2 and RTC of 22 ± 2 . The fold regulation (FR) was said to be biologically relevant if they resulted in a p value <0.05 and a FR >2 . FR represents the fold change but in a biologically meaningful manner with a negative value indicating a down-regulation and a positive indicating an up-regulation with a value of 1 or -1 indicating no change.

5.3. Results

5.3.1. Spheroid formation

As previously discussed, the stromal cells of the BM have the ability to act in a similar manner to hepatocytes of the liver in that they are metabolically competent. Therefore, a hepatocyte cell line would be beneficial as a positive control to identify the level of expression of metabolic enzymes between the developed 3D model and a known metabolically active cell. The hepatocellular carcinoma cell line HepG2 has been seen to express many genes similar to that seen within the liver. However, the expression of these genes is greatly reduced when cultured in a 2D flask as a monolayer, compared to that of a 3D spheroid (Ramaiahgari *et al.*, 2014). As expression of metabolic enzymes and associated drug transporters are reduced in 2D compared to 3D, the generation of HepG2 spheroids was conducted. The images in Figure 5-1 show the formation of HepG2 spheroids utilising the protocol set out by May *et al.*, (2012). HepG2 cells were grown to 80% confluency where a monolayer can be seen (Figure 5-1 A) before trypsinisation, reseeded in 3 mls of medium at a concentration of 1×10^6 cells/ml in a 6 well plate, incubated for 24 hours on an orbital shaker at 83 RPM, the speed reduced to 79 RPM, and incubated for a further 120 hour with a 50% medium change every 48 hours. After 3 days the formation of spheroids can be seen (Figure 5-1 B), with fully matured spheroids identified on day 6 (Figure 5-1 C).

5.3.2. RNA concentration and quality of each experimental condition.

The results in Table 5-2 show the concentration and absorption ratios of each experimental condition. Briefly, HS-5 cells were either seeded within a flask for 7 days with a 50% medium change every 48 hours, grown on a 50% firm Algimatrix™ scaffold for 7 days or grown on a 50% firm Algimatrix™ scaffold for 7 days before the addition of TK6 within a trans-well insert. HepG2 spheroids which were cultured for 6 days were also harvested and RNA extracted. As previously noted, the absorbance of each experimental condition at $A_{260\text{nm}/280\text{nm}}$ was around 2 indicating “pure RNA”. The absorption for each experimental condition at $A_{260\text{nm}/230\text{nm}}$ was >2 indicating a lack of contamination or degradation.

Table 5-2. The ng/ml and absorbance ratios for RNA extracted from HS-5 cultured in 2D, 3D, 3D with the addition of TK6 and HepG2 spheroids. An aliquot of 2 μl from each sample was analysed using the Nanodrop 1000 spectrophotometer for the concentration and purity of each RNA sample. Each sample number denotes a biological repeat.

Sample	ng/ μl	260/280	260/230
HS-5 alone in 2D 1	536.5	2.06	2.11
HS-5 alone in 2D 2	416.5	2.06	2.25
HS-5 alone in 2D 3	628.8	2.06	2.23
HS-5 seeded onto scaffold 1	328.8	2.07	2.26
HS-5 seeded onto scaffold 2	131.3	2.03	2.13
HS-5 seeded onto scaffold 3	207.6	2.04	2.06
HS-5 seeded onto scaffold + TK6 insert 1	476.5	2.06	2.16
HS-5 seeded onto scaffold + TK6 insert 2	621.9	2.02	2.21
HS-5 seeded onto scaffold + TK6 insert 3	670.6	2.02	2.19
HepG2 spheroid 1	146.4	2.05	2.20
HepG2 spheroid 2	187.3	2.08	2.18
HepG2 spheroid 3	276.3	2.09	2.19

To confirm that the extracted RNA was not degrading, visualisation of the ribosomal RNA 28s and 18s was conducted for each experimental condition utilising a 1% agarose gel. The results in Figure 5-2 show two clear bands for each experimental condition (around 700 ng of RNA per lane) and biological repeat at 1 kB (18s) and 2 kB (28s), thus demonstrating good quality RNA samples.

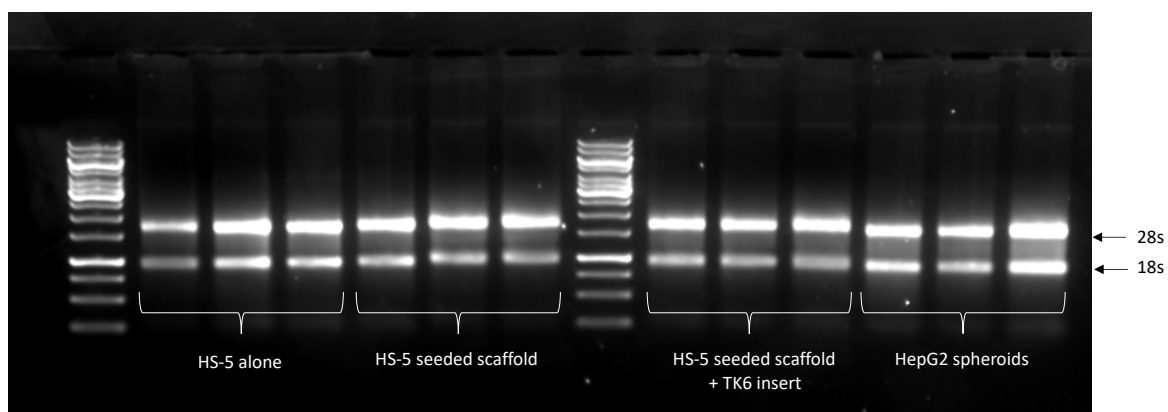


Figure 5-2. RNA integrity of each sample by agarose gel analysis. A 5 μ l aliquot, containing around 700 ngs of RNA was combined with 1 μ l of loading buffer and loaded along with a 1 kb DNA ladder into a 1% agarose gel stained with ethidium bromide. The gel was then run at 100 V for 30 minutes. Visualisation of the 28s and 18s ribosomal RNA was achieved via ultraviolet transilluminator.

5.3.3. QPCR analysis

Once RNA quality and concentration were identified, conversion of RNA into cDNA was conducted before analysis using qPCR. Each sample condition and biological repeat was analysed for CT value, normalised to the house-keeping genes, before being assessed for FR in gene expression.

5.3.3.1. Raw CT values

Once qPCR had been conducted on each sample, the threshold value was set in comparison to the known CT values of the Human Genomic DNA Contamination control (HGDC), PPC and RTC within each plate. The PPC gave a CT value at 20 ± 2 , HGDC >35 and RTC 22 ± 2 , with the same threshold value utilised for each plate. The results in Figure 5-3 shows the raw mean CT values for HS-5 grown in a 2D flask, an Algimatrix™ scaffold within and without the addition of TK6, and HepG2 spheroids for each gene. The HSGC, PPC and RTC CT gave justification to values >35 (red) indicating that this gene had extremely low presence, below the leave of detection, therefore was considered negative for that gene, whilst CT value <35 (green) indicated a presence of that gene.

ABCB1	32.8	35.1	37.3	25.3
ABCC1	26.0	26.3	26.5	25.8
AOC1	40.0	38.0	36.2	38.5
ADH1B	36.4	35.5	36.0	33.3
ADH1C	35.6	33.8	35.0	32.3
ADH4	37.6	36.9	36.7	27.5
ADH5	25.3	25.8	26.6	26.2
ADH6	35.5	30.7	31.7	25.3
AHR	25.3	25.7	27.5	24.3
ALAD	27.7	27.4	27.7	27.8
ALDH1A1	39.0	33.7	36.1	24.5
ALOX12	33.6	33.1	32.7	36.5
ALOX15	35.3	34.7	34.0	32.7
ALOX5	35.7	35.5	36.0	36.1
APOE	33.1	32.7	33.7	23.9
ARNT	29.3	29.2	28.6	30.2
ASNA1	24.2	24.9	25.7	25.7
BLVRA	25.0	26.2	27.0	25.5
BLVRB	25.5	25.7	25.9	27.3
CES1	28.1	29.3	30.3	24.2
CES2	26.7	26.6	27.7	25.9
CES3	35.2	30.2	29.9	29.7
CHST1	30.5	31.3	32.8	35.3
COMT	25.2	25.0	26.0	24.7
CYP5B3	23.4	24.5	25.1	24.5
CYP11B2	32.6	31.4	32.1	32.2
CYP17A1	33.2	33.8	32.8	32.9
CYP19A1	35.8	32.4	33.8	28.2
CYP1A1	31.8	30.7	32.2	31.8
CYP2B6	35.7	31.4	30.8	34.4
CYP2C18	35.6	37.9	38.5	37.3
CYP2C8	39.3	37.9	38.0	36.5
CYP2C9	40.0	40.0	40.0	39.6
CYP2D6	31.7	30.6	31.5	34.1
CYP2E1	31.4	30.7	32.0	37.0
CYP2F1	37.1	35.8	33.4	35.7
CYP2J2	29.5	31.7	34.2	30.8
CYP3A4	39.8	38.5	39.0	34.1
CYP3A5	33.3	33.0	33.3	31.5
EPHX1	26.5	26.9	28.1	25.5
FAAH	34.1	32.8	33.4	31.2
FBP1	37.5	36.2	35.1	32.5
GAD1	28.4	29.1	29.2	31.4
GAD2	39.1	37.3	36.5	36.2
GCKR	40.0	37.9	37.1	30.4
GPI	23.4	22.8	21.8	24.4
GPX1	22.1	23.1	23.9	24.4
GPX2	34.0	33.1	32.0	23.1
GPX3	28.9	29.3	31.7	25.4
GPX4	21.2	22.1	22.2	22.1
GPX5	36.4	35.3	35.2	35.3
GSR	29.4	29.3	30.9	29.2
GSTA3	35.3	33.4	34.3	33.4
GSTA4	29.6	30.2	30.7	28.2
GSTM2	28.3	30.5	32.0	31.5
GSTM3	25.3	25.9	27.6	26.8
GSTM5	36.0	35.6	34.8	34.4
GSTP1	21.7	21.6	22.4	34.7
GSTT1	28.0	29.0	30.4	24.7
GSTZ1	27.8	27.6	27.2	28.6
HK2	25.5	24.6	24.4	24.7
HSD17B1	32.2	31.0	32.3	30.7
HSD17B2	35.5	33.0	36.8	23.9
HSD17B3	35.8	35.0	36.3	35.5
LPO	38.2	36.0	36.3	36.3
MGST1	22.8	22.5	23.8	24.7
MGST2	29.8	29.6	30.7	22.9
MGST3	24.0	24.9	25.6	27.0
MPO	34.2	33.9	33.2	33.5
MT2A	30.3	23.2	21.6	25.3
MT3	34.6	33.6	32.4	32.2
MTHFR	29.3	29.5	28.7	30.5
NAT1	32.6	31.3	32.0	32.4
NAT2	31.4	32.1	31.4	32.3
NOS3	35.5	34.4	34.7	32.8
NQO1	23.6	24.1	25.7	23.0
PKLR	35.9	33.9	35.2	29.9
PKM	19.9	21.1	21.6	23.6
PON1	34.6	34.3	35.1	32.0
PON2	25.3	25.5	26.3	24.5
PON3	32.7	31.8	33.8	27.1
SNN	28.3	26.4	28.7	28.5
SRD5A1	28.2	28.2	28.3	29.8
SRD5A2	36.7	37.5	39.9	38.9
ACTB	17.2	17.8	18.5	20.3
B2M	20.4	20.4	19.9	22.7
GAPDH	18.3	19.4	19.1	21.1
HPRT1	25.2	25.2	25.6	26.1
RPLP0	17.8	17.6	17.7	18.3
HGDC	40.0	40.0	37.8	38.2
RTC	22.3	22.1	22.2	22.4
RTC	22.2	22.1	22.2	22.2
RTC	22.2	22.1	22.0	22.4
PPC	20.1	20.2	20.0	19.8
PPC	20.6	19.9	20.3	20.1
PPC	21.5	20.2	20.2	19.9

Figure 5-3. Raw CT values for each experimental condition. The raw mean CT values before normalisation of HS-5 seeded within a flask, AlgiMatrix™ scaffold with and without TK6 and HepG2 spheroids. Those results in red resulted in a mean CT value >35, with those in green gaining a mean CT value <35. The CT value can be found in each corresponding cell. Reverse Transcription Control (RTC), Positive PCR Control (PPC) and Human Genomic DNA Contamination control (n=3).

The results in Figure 5-3, highlighted in red, show those genes which resulted in a mean CT value >35, therefore would be considered for their use once normalised to the housekeeping genes had occurred. Those genes resulting in a mean CT value >35, for all four experimental groups included *CYP2C9*, *AOC1*, *CYP2C8*, *GAD2*, *LPO*, *SRD5A2*, *GPX5*, *ALOX5* and *CYP2C19*. Those genes which resulted in a CT value >35 for the HS-5 experimental groups only (not HepG2 spheroids) were *GCKR*, *CYP3A4*, *ADH4*, *FBP1*, and *ADH1B*. Those genes with a CT value >35 within the HS-5 2D experimental group, in addition to those mentioned above, were *ALADH1A1*, *CYP2F1*, *GSTM5*, *PKLR*, *CYP19A1*, *HSD17B3*, *CYP2B6*, *ADHIC*, *NOS3*, *ADH6*, *HSD17B2*, *ALOX15*, *GSTA3* and *CES3* with *AOC1*, *CYP2C9* and *GCKR* gaining a CT value of 40.

Those genes with a mean CT value >35 within the HS-5 AlgiMatrix™ without TK6 experimental group, in addition to those mentioned above, were *ABCB1*, *CYP2F1* and *GSTM5* with *CYP2C9* resulting in a CT value >40. Those genes with a CT value >35 within the HS-5 AlgiMatrix™ with TK6, in addition to those mentioned above, were *ABCB1*, *ALDH1A1*, *PKLR*, *HSD17B3*, *ADHIC*, *HSD17B2* and *PON1*, once gain *CYP2C9* resulted in a CT value of >40. Finally, those genes with a mean CT value >35 within the HepG2 spheroid experimental group were *CYP2F1*, *HSD17B3*, *ALOX12*, *CYP2E1* and *CHST1*. Out of the 87 genes associated with metabolism, 51 resulted in a CT value <35 in all four experimental conditions.

The housekeeping genes *ACTB*, *B2M*, *GAPDH*, *HPRT1* and *RPLP0* were present in all experimental conditions. The mean CT value for each housekeeping gene of the three HS-5 experimental groups had a SD of <1 cycle, with *ACTB*, *GAPDH*, *RPLP0* resulting in a CT value <20, *B2M* <25 and *HPRT1* >30. However, the SD of the mean CT values gleaned from the HepG2 spheroids for *ACTB*, *B2M* and *GAPDH* were between 1.2 and 1.3 cycles when compared to the three HS-5 experimental groups with a CT value between 20 and 25. This was not the case for *HPRT1* and *RPLP0* which had a SD <1 cycle between all. Out of the 84 genes assayed, those HS-5 cells cultured on a AlgiMatrix™ scaffold with/without cells resulted in 63 genes with a Ct <35. However, those cultured in 2D resulted in 56 genes with a Ct <35.

5.3.3.2. Fold regulation comparison between each experimental condition

The raw CT values were then normalised to the geometric mean of the housekeeping genes on each plate for comparison of FR of gene expression. The normalised gene expression ($2^{-(\Delta CT)}$) of the test sample was then divided by the normalised gene expression ($2^{-(\Delta CT)}$) in the control sample to calculate FR of each gene. The results in Figure 5-4, shows the FR between HS-5 cells grown on an Algimatrix™ scaffold compared to HS-5 seeded within a flask. The results also show the FR between HS-5 cells grown on an Algimatrix™ scaffold; compared to HS-5 cells grown on a Algimatrix™ scaffold with the addition of TK6. Those cells with a negative (red) value indicate a down-regulation. Conversely, those with a positive (green) value indicate an up-regulation in gene expression. A biological change was concluded if a ± 2 FR from the baseline was seen with a p value <0.005 . Genes which had resulted in a CT value of >35 for all 4 experimental conditions were excluded from the analysis, this included *AOC1*, *ADH1C*, *ALOX5*, *CYP2C19*, *CYP2C8*, *CYP2C9*, *CYP3A4*, *FBP1*, *GAD2*, *GCKR*, *GPX5*, *LPO* and *SRD5A2*.

When the FR of the gene expression was compared between HS-5 cells grown on a Algimatrix™ scaffold compared to those seeded within a flask, six genes had a biologically relevant change in gene expression including *ADH6* (FR=18.09, p=0.01), *CES3* (FR=28.41, p=0.0007), *CYP2B6* (FR=14.96, p=0.0003), *MT2A* (FR=165.42, p=0.0018), *SNN* (FR=4.76, p=0.0003) and *GSTM2* (FR=-3.48, p=0.0005). It was also seen that *AHR*, *EPHX1* and *GPX3* inducing a FR of -1 indicating no change in gene expression between the two samples.

The FR in gene expression between HS-5 cells grown on an Algimatrix™ scaffold; compared to those grown on a Algimatrix™ scaffold with the addition of TK6 resulted in the up-regulation of *GPI* (FR=2.06, p=0.0002) and down-regulation of *CES2* (FR=-2.06, p=0.01977), *GSR* (FR=-2.91, p=0.0326) and *GSTM2* (FR=-2.67, p=0.0452). It was also seen that *AOC1*, *ALOX5*, *CYP2C19*, *CYP2C9*, *CYP3A4*, *GAD1*, *GCKR*, *MPO*, *SRD5A1* and *SRD5A2* induced an FR of 1 indicating no change in gene expression between the two samples.

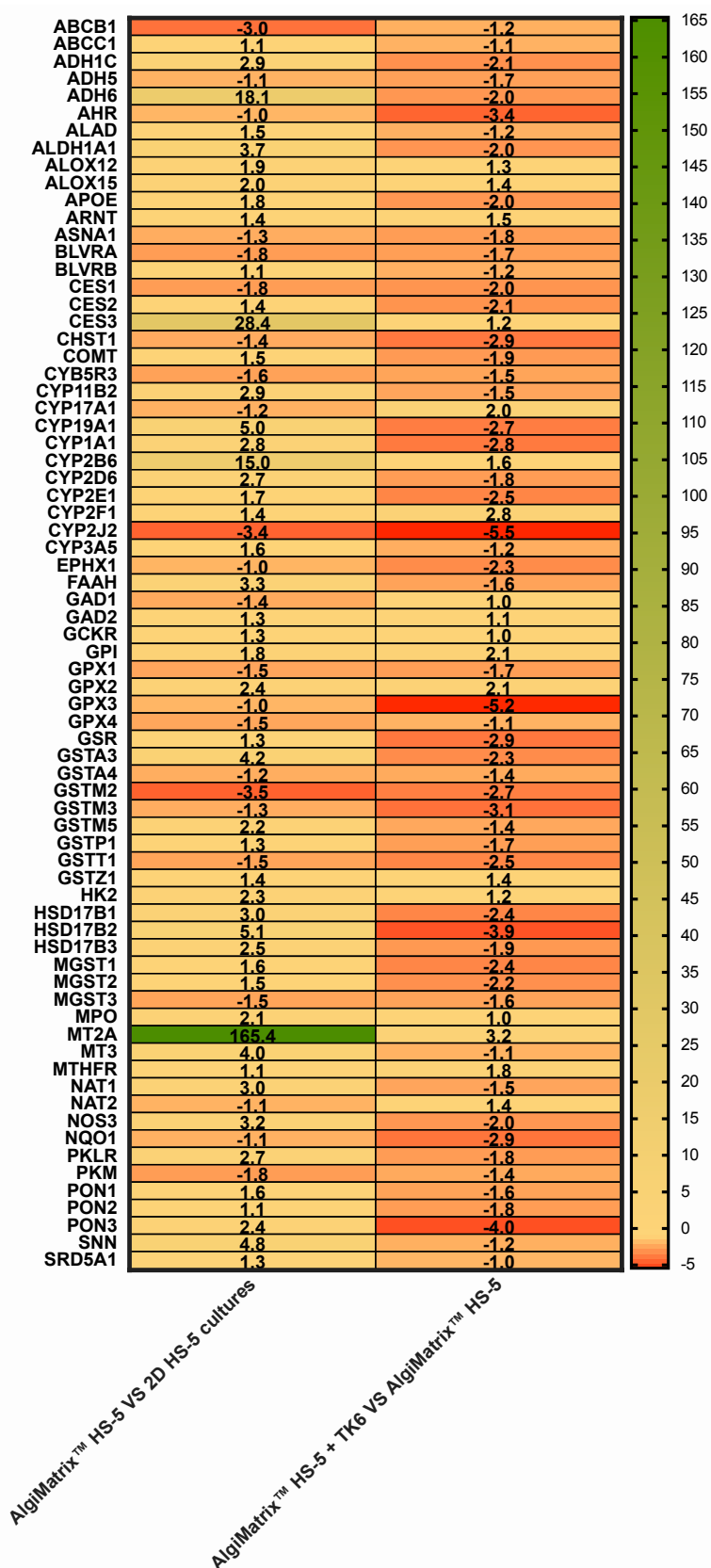


Figure 5-4. The comparisons of gene expression, through FR, of HS-5 experimental conditions following normalisation. After normalisation, HS-5 cells grown in Algimatrix™ scaffolds were compared to HS-5 seeded within a flask. Then the normalised values for HS-5 cells grown Algimatrix™ scaffolds were compared to those grown on Algimatrix™ scaffolds with the addition of TK6. Results in shades of red indicate a reduction in fold regulation, green increase in FR and orange no change. Genes which gave a CT value >35 and therefore were negative in all conditions, have been removed (n=3).

The mean gene expression of each HS-5 experimental condition was then compared to that of the positive HepG2 spheroid control. The results in Figure 5-5 show the change in mean gene expression of HS-5 cells seeded within a flask, Algimatrix™ scaffold with and without TK6 when compared to the mean gene expression of the HepG2 spheroid control. The results show that gene expression levels within HS-5 cells cultured in Algimatrix™ scaffolds with and without TK6 resulted in a FR of 1 for *SRD5A1*, *BLVRB* and *SRD5A1*, when compared to HepG2 spheroids indicating no change in gene expression. The expression of 11, 22 and 14 genes were found to have a FR <2/ <-2 (Table 5-3) when HS-5 cells seeded within a flask and Algimatrix™ scaffold with and without TK6 were compared to that of the HepG2 spheroids, showing similar gene expression levels between the samples.

However, as the HS-5 cell line is not of hepatic lineage and the BM has only been seen to express genes similar to a hepatic cell, the results in Table 5-3 show the high number of biologically relevant altered gene expressions between the HS-5 samples and HepG2 spheroids. Those genes that were exceptionally down-regulated (<-600) in all HS-5 conditions when in comparison to HepG2 spheroid's (Figure 5-5, Table 5-3) included *ABCB1*, *ALDH1A1*, *APOE*, *GPX2* and *HSD17B2*. Interestingly the gene *GSTP1* was up-regulated in all three HS-5 conditions when in comparison to HepG2 spheroid's with a FR of >1000. Out of the 84 genes associated with metabolic enzymes and drug transporters, 60 had a biologically relevant altered expression within the HS-5 experimental samples, compared to that of the HepG2 spheroids. A biologically relevant altered regulation was seen in 52, 39 and 47 genes when HS-5 seeded in a flask, Algimatrix™ with and without TK6, were compared to HepG2 spheroids. A total of 7, 5 and 5 genes were up-regulated with a FR of >2, with 63, 56 and 64 downregulated (FR <-2) in the same conditions inferring that metabolic expression is not as high in the HS-5 samples under any seeding conditions in comparison to the 3D HepG2 spheroids.

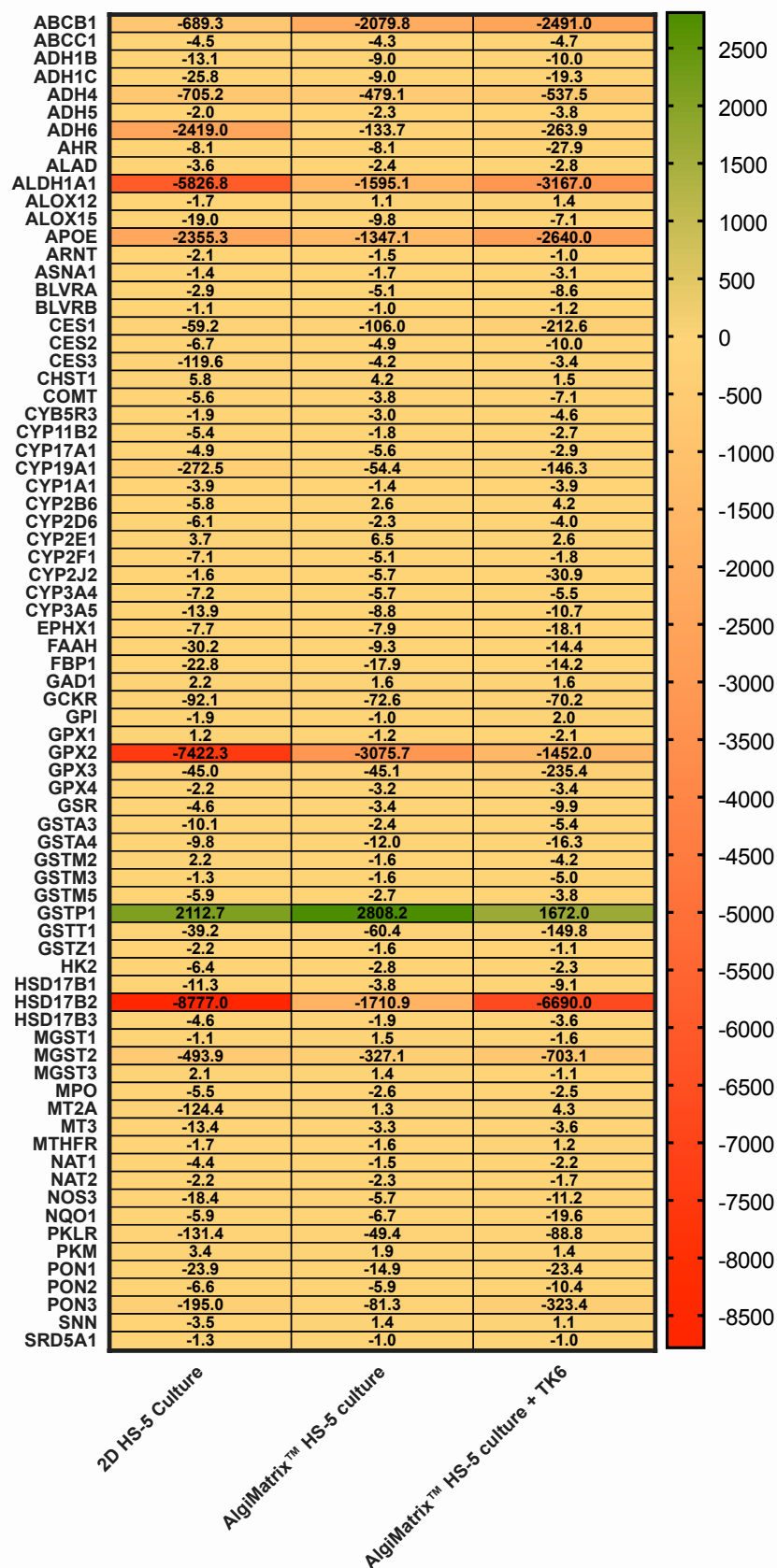


Figure 5-5. The change in gene expression of each HS-5 experimental condition compared to HepG2 spheroids indicated as FR. After normalisation the mean gene expression of HS-5 cells seeded within a flask, Algimatrix™ scaffold with and without TK6 were compared to that of the HepG2 spheroid. Cells in shades of red indicate a reduction in FR, green increase in FR and orange no change. Genes which gave a CT value >35 and therefore were negative in all conditions have been removed (n=3).

Table 5-3. Biologically relevant changes in gene expression compared to HepG2 spheroids. The FR and p values for gene expression between the HS-5 cells seeded within a flask, Algimatrix™ scaffold with and without TK6 were compared to that of the HepG2 spheroid. Those genes with a line inferes no cahnge in gene expression.

Gene	Compared to HepG2 spheroids					
	HS-5 grown within a flask		HS-5 grown in an Algimatrix™ scaffold		HS-5 grown in an Algimatrix™ scaffold + TK6	
	Fold regulation	P value	Fold regulation	P value	Fold regulation	P value
<i>ABCB1</i>	-689.3	<0.0001	-2080	<0.0001	-2491	<0.0001
<i>ABCC1</i>	-4.5	0.0003	-4.26	0.0003	-4.67	0.0005
<i>ACTB</i>	2.2	<0.0001	-	-	-	-
<i>ADH1B</i>	-13.1	0.0187	-8.95	0.0268	-10	0.0206
<i>ADH1C</i>	-25.8	0.0054	-9.04	0.0147	-19.32	0.0057
<i>ADH4</i>	-705.2	<0.0001	-479.1	<0.0001	-537.5	<0.0001
<i>ADH5</i>	-2.0	0.0009	-2.29	0.0045	-3.79	0.0002
<i>ADH6</i>	-2419.0	<0.0001	-133.7	<0.0001	-263.9	<0.0001
<i>AHR</i>	-8.1	<0.0001	-8.12	0.0005	-27.88	<0.0001
<i>ALAD</i>	-3.6	0.0001	-2.41	0.0032	-2.83	0.0007
<i>ALDH1A1</i>	-5826.8	0.0002	-1595	0.0002	-3167	0.0002
<i>ALOX15</i>	-19.0	0.0421	-9.78	0.0492	-	-
<i>APOE</i>	-2355.3	0.0001	-1347	0.0001	-2640	0.0001
<i>ARNT</i>	-2.1	0.0002	-	-	-	-
<i>ASNA1</i>	-	-	-	-	-3.06	0.0350
<i>B2M</i>	-	-	-	-	2.35	0.0001
<i>BLVRA</i>	-2.9	0.0185	-5.07	0.0115	-8.63	0.0064
<i>CES1</i>	-59.2	0.0001	-106	0.0001	-212.6	0.0001
<i>CES2</i>	-6.7	0.0012	-4.86	0.0018	-10.02	0.0010
<i>CES3</i>	-119.6	0.0026	-4.21	0.0070	-3.39	0.0092
<i>CHST1</i>	5.8	0.0256	-	-	-	-
<i>COMT</i>	-5.6	<0.0001	-3.82	0.0003	-7.08	<0.0001
<i>CYB5R3</i>	-	-	-2.99	0.0005	-4.56	0.0003
<i>CYP19A1</i>	-272.5	0.0004	-54.42	0.0004	-146.3	0.0004
<i>CYP2B6</i>	-	-	-	-	4.16	0.0150
<i>CYP2E1</i>	3.7	0.0112	-	-	-	-
<i>CYP2J2</i>	-	-	-5.65	0.0066	-30.9	0.0008
<i>CYP3A5</i>	-13.9	<0.0001	-8.8	0.0238	-10.74	<0.0001
<i>EPHX1</i>	-7.7	0.0016	-7.91	0.0095	-18.12	0.0012
<i>FAAH</i>	-30.2	0.0019	-9.26	0.0269	-14.41	0.0022
<i>FBP1</i>	-22.8	0.0001	-17.93	0.0001	-14.17	0.0001
<i>GCKR</i>	-92.1	0.0009	-72.55	0.0009	-70.22	0.0009
<i>GPX1</i>	-	-	-	-	-2.14	0.0016
<i>GPX2</i>	-7422.3	<0.0001	-3076	<0.0001	-1452	<0.0001
<i>GPX3</i>	-45.0	0.0005	-45.12	0.0006	-235.4	0.0005
<i>GPX4</i>	-2.2	0.0015	-3.19	0.0008	-3.37	0.0005
<i>GSTA4</i>	-9.8	0.0003	-11.97	0.0012	-16.27	0.0003
<i>GSTM2</i>	2.2	0.0008	-	-	-4.19	0.0045
<i>GSTM3</i>	-	-	-	-	-5.04	0.0030
<i>GSTP1</i>	2112.7	0.0011	2808	0.0151	1672	0.0010
<i>GSTT1</i>	-39.2	<0.0001	-60.41	<0.0001	-149.8	<0.0001
<i>GSTZ1</i>	-2.2	<0.0001	-	-	-	-
<i>HK2</i>	-6.4	0.0002	-2.77	0.0229	-2.33	0.0061
<i>HPRT1</i>	-2.0	0.0001	-	-	-2.01	0.0002
<i>HSD17B1</i>	-11.3	0.0018	-3.76	0.0112	-9.11	0.0021
<i>HSD17B2</i>	-8777.0	<0.0001	-1711	<0.0001	-6690	<0.0001
<i>MGST2</i>	-493.9	<0.0001	-327.1	<0.0001	-703.1	<0.0001
<i>MGST3</i>	2.1	0.0027	-	-	-	-
<i>MT2A</i>	-124.4	<0.0001	-	-	-	-
<i>NAT1</i>	-4.4	0.0012	-	-	-2.19	0.0062
<i>NAT2</i>	-2.2	0.0004	-	-	-	-
<i>NOS3</i>	-18.4	0.0204	-	-	-11.18	0.0239
<i>NQO1</i>	-5.9	<0.0001	-6.68	0.0002	-19.62	<0.0001
<i>PKLR</i>	-131.4	<0.0001	-49.35	<0.0001	-88.81	<0.0001
<i>PKM</i>	3.4	0.0001	-14.85	0.0043	-23.44	0.0016
<i>PON1</i>	39.7	0.0034	-5.85	<0.0001	-10.44	<0.0001
<i>PON2</i>	108.1	0.0035	-81.25	<0.0001	-323.4	<0.0001
<i>PON3</i>	176.5	0.0037	-	-	-	-
<i>RPLP0</i>	245.0	0.0039	-	-	-	-
<i>SNN</i>	313.4	0.0040	-	-	-	-

5.3.4. Addition of cyclophosphamide to TK6 seeded within a trans-well insert with or without HS-5 seeded scaffolds.

Now that the genetic expression of metabolic enzymes and selected drug transporters within HS-5 cells seeded in a flask and Algimatrix™ scaffold with/ without TK6 has been identified, it was relevant to explore if the same level of activation of the known pro-drug CPM, which is predominantly metabolised by CYP2B6 shown to be up-regulated from 2D to 3D (Figure 5-4) (Connarn *et al.*, 2015), when compared with the rat liver S9 fraction used within the regulatory *in vitro* MN assay, to identify if the expression in 2D was sufficient enough for activation of the compound.

Briefly, the results in Figure 5-6 show the addition of 500 µM of CPM added directly to either TK6 and or HS-5 with/ without the addition of S9. This concentration of CPM was also added to a co-culture of HS-5 seeded wells combined with TK6 in a trans-well insert, with all samples incubated for 24 hours before being washed and counted with TB. The addition of cyclophosphamide or its vehicle control (DMSO <0.005%) to TK6 without S9, induced a small but insignificant reduction (4 and 5 x 10⁵ cells respectively) in total cell number from the untreated control at 6 x 10⁵ cells. However, the addition of S9 significantly reduced the TK6 total cell number within all conditions when compared to the same without S9. No significant difference was seen between those conditions treated with S9, however a reduction of 7 x 10⁴ cells was seen between TK6 + S9 with or without DMSO and those treated with S9 + CPM. Conversely, HS-5 cells treated with DMSO or CPM with or without S9 did not see a change in total cell number from the untreated control.

When TK6 were added to a trans-well insert with 80% confluent HS-5 cells, there was no reduction in total TK6 cell number when treated with DMSO compared to those without. However, there was a significant decrease in cell number (5 to 1.5 x 10⁵ cells) with the addition of CPM compared to the untreated and DMSO co-culture controls. The result was also significantly decreased compared to the CPM treatment of TK6 without S9. Furthermore, the reduction in cell number was at a similar level to that seen with the TK6 + S9 + CPM treatment. Once again, CPM had no effect on HS-5 cells in co-culture; with a similar level of total cell number (3 x 10⁵ cells) seen with treatments without the addition of TK6.

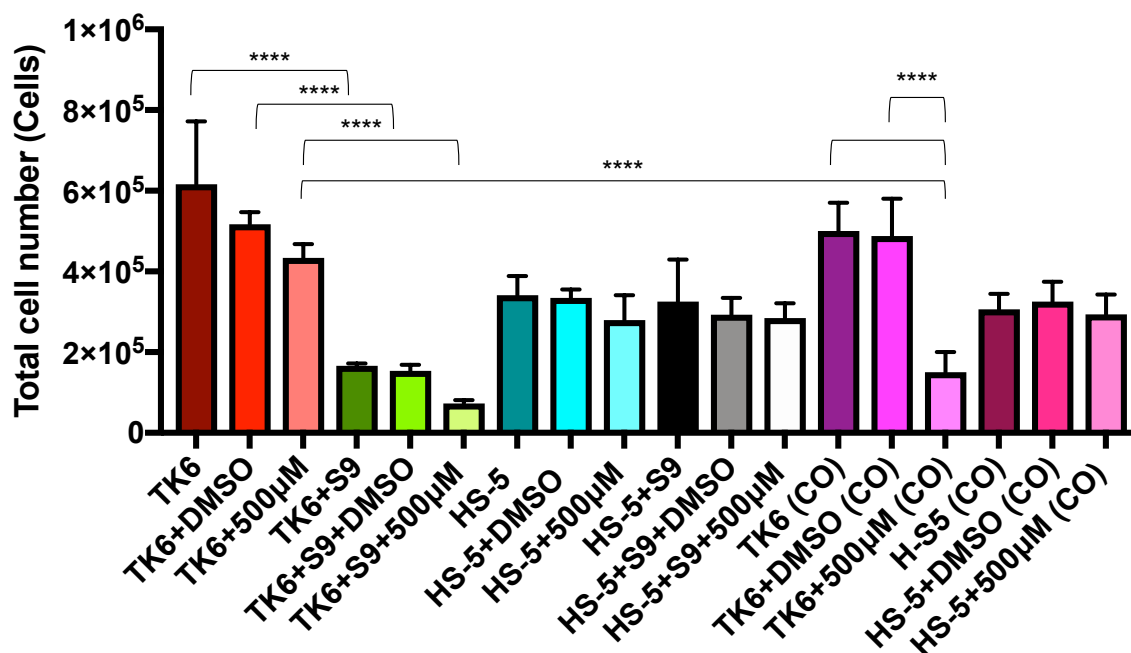


Figure 5-6. The cytotoxic effect of cyclophosphamide on TK6 with and without HS-5 cells and S9 fraction. HS-5 cells were seeded at 1×10^4 cells/cm² in a 12 well plate and left for 24 hours to adhere. TK6 cells were then added within a transwell insert and 500 µM of the pro-drug cyclophosphamide added, left for 24 hours, washed with PBS and cell number assessed via trypan blue. Each cell line was dosed with vehicle control (DMSO <0.005%), with/ without cyclophosphamide and the liver fraction S9. (n=3). Colour shading represents: Red = TK6 in isolation without S9; Green = TK6 in isolation with S9; Blue = HS5 in isolation without S9; Black/white = HS5 in isolation with S9; Purple = TK6 from co-culture with HS5; Pink = HS5 from co-culture with TK6. **Significant differences between samples were calculated using a Two-Way ANOVA followed by a Tukeys test. The P values are indicated by **** (p<0.0001).**

5.4. Discussion

The stroma of the *in vivo* BM has been seen to activate or detoxify compounds through metabolic enzymes and drug transporters similar to that seen within the liver, resulting in the reduction or induction of genotoxic alterations to haematopoietic cells by xenobiotic compounds (Ria *et al.*, 2020; Chen *et al.*, 2020; Alonso *et al.*, 2015; Boutin *et al.*, 2020). Within the 2D regulatory MN assay, the rat liver S9 fraction is used to induce a similar level of metabolic alteration seen within the liver, to assess the genotoxicity of pro-drugs. However, the BM is not made of hepatic tissue and therefore may not express the same metabolic components seen within the *in vivo* liver. Therefore, in order to create an *in vivo* relevant model of the BM *in vitro*, a metabolic profile similar to that seen within the *in vivo* BM stroma is necessary and may be the key to discovering the mechanism behind pharmacological positives.

In this chapter, HS-5 cells seeded within a flask and AlgiMatrix™ scaffold with/ without TK6 cells within a trans-well insert, were analysed by qPCR for the expression of phase 1 and 2 metabolic enzymes, drug transporters and associated genes, compared to their expression within the *in vivo* stroma reported in the literature, validating the use of 3D cultured HS-5 as a more *in vivo* relevant model for future genotoxicity study. The hepatocellular carcinoma cell line HepG2, was grown as spheroids and assessed as a positive control for the expression of each metabolic associated gene. Furthermore, this chapter also reports the comparison of cytotoxicity of CPM on TK6 cells within a trans-well insert, with/without S9 and /or HS-5 cells seeded within a well. However, the gene expression via qPCR, within each experimental sample mentioned above was conducted first.

The cut-off threshold for qPCR of 35 was conducted utilising the manufacturer's instructions and signifies that a CT value >35 indicates that gene expression is not present. It was found that many genes resulted in no change (of 1 or <1 cycle) near the 35 cut off (34 to 35), indicating that the gene was being expressed at equivalent, but extremely low amounts in both samples. However, if the expression of the gene was low and represented only 1 copy at 0 cycles, by the 34th cycle this would have notionally amplified to 1.7×10^{10} copies and again further doubled to 3.4×10^{10} by the 35th cycle showing an extremely large increase in copy number between the two cycles. This simple maths demonstrates that if a sample is not detected by cycle 34/35, it is reasonable to assume that gene expression is likely to be switched off. Literature has argued that a threshold >35 but <40 can still result in the

detection of gene expression, which can be altered with changes in starting cDNA concentrations and use of SYBR green or TaqMan probes (Caragual *et al.*, 2011; Lockey *et al.*, 1998). However, due to the nonspecific nature of SYBR green used within the RT² profiler, the quantity of starting cDNA from pure uncontaminated RNA analysed by nanodrop and agarose gel electrophoresis, optimised by the manufacturer for use with this plate, a threshold of 35 is justified. Furthermore, given the information above and that the positive (PPC and RTC) and negative (HGDC) controls within each plate giving the correct CT value, biological change in gene expression will be discussed in those genes present in both experimental samples. Additionally, if a gene is absent (CT >35) in one experimental sample but present in the next (CT <35) this will also be discussed.

5.4.1. The expression of Phase I metabolic enzymes

The phase I metabolic enzymes predominantly activate a compound through the addition or modification of a functional group through oxidation, reduction or hydrolysis (Bachmann, 2009; Winiwarter *et al.*, 2006). The CYP450 family of enzymes specifically those residing in the CYP1, CYP2, CYP3 and CYP4 families, induced *in vivo* by polycyclic aromatic hydrocarbons, barbiturates and glucocorticoids are fundamental to xenobiotic metabolism (Stanley, 2017). Out of the 15 phase I CYP450 metabolic enzymes tested for, within the three HS-5 experimental groups, 11 were seen to have expression in one or all of the experimental samples with *CYP2C19*, *CYP2C8*, *CYP2C9* and *CYP3A4* expression absent in all three conditions. The phase I metabolism enzymes expressed in all 3 HS-5 experimental groups included *CYP11B2*, *CYP17A1*, *CYP1A1*, *CYP2D6*, *CYP2E1*, *CYP2J2* and *CYP3A5* with *CYP19A1* and *CYP2B6* expression present in HS-5 seeded in AlgiMatrix™ with and without TK6 and *CYP2F1* only present in HS-5 seeded in AlgiMatrix™ with TK6. The only biologically significant increase in expression occurred in *CYP2B6* between HS-5 cells seeded in 3D compared to 2D, with the addition of TK6 causing no significant change in expression. Therefore, as AlgiMatrix™ seeded HS-5 cells with the addition of TK6 had the greatest number of expressing CYPs (Figure 5-3, Figure 5-4), compared to HS-5 seeded in a flask or AlgiMatrix™ without TK6, and more closely resembled the model seen in Figure 4-1, the results obtained from this experimental condition were compared to the literature for its ability to simulate expression of metabolic enzymes seen within the *in vivo* human BM.

The profile of phase I CYP450 enzymes, expressed by the *in vivo* BM stroma has limited literature. However, studies by Su (2019), Alonso (2015) and Chang (2019) found that within the primary human stroma, similar to the results obtained via qPCR analysis of HS-5 cells seeded in AlgiMatrix™ with the addition of TK6, the expression of *CYP17A1*, *CYP19A1*, *CYP11A1*, *CYP2D6*, *CYP2E1*, *CYP2F1* and *CYP3A5* were present. Conversely, the presence of *CYP11B2*, *CYP2B6* and *CYP2J2* were only found within the HS-5 samples not the *in vivo* stroma. Furthermore, HS-5 cells did not express *CYP2C19*, *CYP2C8* and *CYP3A4* which were present within the *in vivo* BM stroma. The lack of expression of *CYP3A4* within the HS-5 conditions was disconcerting as it is responsible for ~30-40% of phase I metabolism of drugs including antibiotics (erythromycin), antidepressants (diazepam) and steroids (testosterone) (Fang *et al.*, 2017). Therefore, the presence/ absence of these CYPs found in HS-5 will be explored for their role, if any, in the altered metabolism of compounds in the model during the final discussion. However, this lack of expression in either setting may be due to the constituents of the BM stroma itself versus the simple nature of the HS-5 culture. The human *in vivo* BM stroma is made up of fibroblasts, macrophages, adipocytes, osteoblasts and endothelial cells whereas only HS-5, (a fibroblastic but primarily BM stromal cell line) is present within the 3D HS-5 AlgiMatrix™ cell culture (Arrieta & Isringhausen, 2017).

The papers by Su (2019), Alonso (2015) and Chang (2019) were also the only to compare the expression of those CYPs seen within the *in vivo* BM stroma with a hepatic cell line (HepG2). The work found comparative levels of each CYP present within the BM stroma with that found in the HepG2 culture. However, the HepG2 culture within these papers was conducted as a monolayer not spheroid. It has been found that the expression of CYPs within HepG2 monolayers is dramatically reduced compared to spheroid culture, with the expression of many CYPs not present (Takahashi *et al.*, 2015). This could aid in the explanation of why in the current 3D HS-5 model (Figure 5-5, Table 5-3), the majority of CYPs tested when compared to the HepG2 spheroid had a down-regulation in expression compared to those seen within the studies above. Furthermore, as the liver is the primary organ for biotransformation of compounds, an increase in expression would be anticipated compared to the BM stroma (Trefts *et al.*, 2017). Therefore, the qPCR results acquired from the HepG2 spheroids, could only be used as a positive control for CYP expression. However, are HepG2 spheroids a more appropriate positive control for the expression of CYPs than a simple monolayer?

When investigating those CYPs predominantly expressed by the liver, responsible for the biotransformation of 70-80% of all drugs, *CYP3A4*, *CYP2C9*, *CYP2C8*, *CYP2E1*, *CYP1A2*, *CYP2A6*, *CYP2D6*, *CYP2B6*, *CYP2C19*, *CYP3A5*, *CYP2J2*, *CYP1A1* and *CYP1B1* were found to be expressed (Zanger & Schwab, 2013). When compared, HepG2 cells grown as spheroids in this study, showed expression of *CYP1A1*, *CYP2B6*, *CYP2D6*, *CYP2J2*, *CYP3A4* and *CYP3A5* unlike those grown in 2D within the papers mentioned previously, which expressed *CYP1A1*, *CYP2C8*, *CYP2C9*, *CYP2D6*, *CYP2E1*, *CYP3A4* and *CYP3A5*. Neither the 2D monolayer in the paper or spheroids within this study expressed all 13 CYPs predominantly found within the liver, with around half expressed in both conditions. As HepG2 cells are not primary hepatic tissue but an immortalised cell line and grown in two different conditions (2D and spheroid), it is understandable that all 13 would not be expressed. However, as around half of the key CYPs responsible for biotransformation of compound were expressed, its use as a positive control for the expression of phase I metabolic enzymes was justified.

5.4.2. The expression of Phase II metabolic enzymes

The phase II drug metabolism enzymes, unlike phase I, detoxify xenobiotic compounds through conjugation with charged species such as glutathione, sulphate, glycine or glucuronic acid occurring at carboxyl, hydroxyl, amino and sulphate groups (Jancova *et al.*, 2010). The expression of phase II enzymes residing within the carboxylesterases, decarboxylases, dehydrogenases, glutathione peroxidases, lipoxygenases, hydrolases, kinases, oxidoreductases, paraoxonases, glutathione S-transferases family of enzymes along with CHST1, COMT, NAT1 and NAT2 were assessed in all experimental conditions. It was found that the phase II genes *ADH6* (dehydrogenase), *CES3* (carboxylesterase), and *GSTM2* (glutathione S-transferase) were biologically up-regulated between the 2D and 3D HS-5 culture with the expression of *CES2* (carboxylesterase), *GSR* (oxidoreductase) and *GSTM2* (glutathione S-transferases) down-regulated between HS-5 grown in 3D with and without TK6. This indicated that there was a change in expression of phase II enzymes between 2D and 3D, with those seeded with an AlgiMatrix™ with/ without TK6 having greater expression than 2D, reinforcing the use of 3D models over 2D assays.

As this was the first study to identify the expression of phase II enzymes expressed by a cell line of the BM stroma, there was a lack of literature for *in vivo* comparison. However, many of these enzymes are present in the liver but can also be expressed in the small intestine,

kidneys, lungs, brain, haematopoietic/immune cells and the testis so may not be expressed in the *in vivo* BM (Laizure *et al.*, 2013; Rajendram *et al.*, 2016; Mashima & Okuyama, 2015; Draganov *et al.*, 2005; Nebert & Vasiliou, 2004). A collaborative database by Uhlén (2015) brought together 483 samples from 37 different human, normal, tissue types and 69 cell lines (none of which are HS-5 cells) for deep sequencing using RNA-seq which identified 15320 genes. Therefore, a comparison will be made between this collaborative data set and the results obtained from the qPCR analysis to assess if AlgiMatrix™ seeded HS-5 with/ without TK6, simulated the expression seen within the human *in vivo* BM more closely than HS-5 seeded in 2D, validating the use of 3D culture as a more *in vivo* relevant model for genotoxicity testing. The collaborative data set assessed the expression of genes within the BM tissue as a whole and within primary mesenchymal fibroblast cells. Therefore, a secondary comparison will be made to identify which cell lineage, if any particular one, HS-5 expression compares to in the *in vivo* BM environment.

The carboxylesterases assessed within HS-5 experimental samples included *CES1*, *CES2* and *CES3*. The collaborative data set found that within the *in vivo* human BM both *CES1* and *CES2* were present but *CES3* was not. When analysed within the database, the expression of both *CES1* and *CES2* were found within the primary fibroblast cell line but *CES3* was not, indicating that *CES1* and *CES2* could be expressed by fibroblasts of the BM unlike *CES3*. In line with the human tissue, the expression of *CES1* and *CES2* were seen within all HS-5 experimental conditions, however only HS-5 grown in a 2D flask were absent of *CES3*. This infers that *in vivo* *CES1* and *CES2* are expressed by fibroblasts of the BM, suggesting that those HS-5 cells seeded in 2D act more like fibroblasts of the *in vivo* BM than those cultured within an AlgiMatrix™ scaffold with/ without TK6. As previously noted, HS-5 are fibroblastic and can differentiate into fibroblasts but are primarily BM stromal cells, therefore the similar expression between 2D and *in vivo* indicates HS-5 could have differentiated into fibroblasts.

The decarboxylases *GAD1* and *GAD2*, were both detected within the BM tissue within the database but were negative within fibroblast cells, inferring that a differing cell lineage within the BM was responsible for their expression. The presence of *GAD1* corresponded that seen within all HS-5 experimental samples; however, the same HS-5 samples were negative for *GAD2*. This infers that the culture of HS-5 had no impact on the ability to replicate the *in vivo* positive and negative expression respectfully of *GAD1* and *GAD2*.

The dehydrogenase enzymes assessed in this study included *ADH1B*, *ADH4*, *ADH5*, *ADH6*, *HSD17B1*, *HSD17B2*, *HSD17B3*, *ADH1C*, *ALAD* and *ALDH1A1*. Those present within the *in vivo* BM tissue comprised of *ADH5*, *HSD17B1*, *ALAD* and *ALDH1A1* with all also present within the primary fibroblast cells tested. Therefore, it can be suggested that the fibroblasts of the *in vivo* BM are solely responsible for the expression of *ADH5*, *HSD17B1*, *ALAD* and *ALDH1A1*. However, when compared to the HS-5 experimental conditions, those HS-5 seeded within 2D expressed *ADH5*, *HSD17B1* and *ALAD*, AlgiMatrix™ without TK6 expressed 4 out of 4 and with TK6 expressing *ADH5*, *HSD17B1* and *ALAD*, inferring that HS-5 cells seeded in an AlgiMatrix™ without TK6 simulated the *in vivo* fibroblast population. Conversely, each HS-5 condition was seen to express further genes not denoted in the *in vivo* BM. When HS-5 cells were seeded within a flask, AlgiMatrix™ scaffold with and without TK6, a further 6, 4 and 2 genes were expressed. This suggests that HS-5 cells seeded in 2D are less comparable to the *in vivo* BM than those HS-5 cells seeded within an AlgiMatrix™ scaffold, with respect to the expression of dehydrogenase enzymes.

The glutathione peroxidase enzymes evaluated within this study included *GPX2*, *GPX3*, *GPX4*, *GPX5*, *GSTA3*, *GSTA4*, *GSTM2*, *GSTM3*, *GSTM5*, *GSTP1*, *GSTT1*, *GSTZ1*, *LPO* and *MPO*. Those genes found to be present in the *in vivo* BM tissue included *GPX3*, *GPX4*, *GSTM2*, *GSTM5*, *GSTP1*, *GSTZ1* and *MPO*. The genes present within the *in vivo* BM were also expressed by the fibroblast cell lines with the exception of *MPO*, inferring that cells other than fibroblasts of the BM are responsible for the expression of *MPO*. When compared to the HS-5 experimental conditions, those seeded within 2D and AlgiMatrix™ without TK6 expressed 6 out of the 7 genes expressed by the *in vivo* BM, with *GSTM5* absent. However, those HS-5 seeded in an AlgiMatrix™ with TK6 expressing 7 out of 7. This infers that those HS-5 cells seeded in an AlgiMatrix™ scaffold with TK6, simulated the *in vivo* BM more closely than 2D or 3D alone. However, as the condition did express *MPO*, HS-5 cells seeded on an AlgiMatrix™ scaffold with TK6 appears to simulate cells other than fibroblasts found in the *in vivo* BM. Conversely, each HS-5 condition was seen to express further genes not denoted in the *in vivo* BM but tested for in this study. When HS-5 cells were seeded within a flask, AlgiMatrix™ with and without TK6, a further 3, 2 and 2 genes were expressed. This once again, suggests that HS-5 cells seeded in 2D are less comparable to the *in vivo* BM than those HS-5 cells seeded within an AlgiMatrix™ scaffold.

The lipoxygenase enzymes evaluated within this study included *APOE*, *ALOX5*, *ALOX12* and *ALOX15*, with *APOE*, *ALOX5* and *ALOX12* present within the *in vivo* BM. The only

gene that was expressed in the fibroblast cell lines was *APO*, inferring that the expression of the lipooxygenase enzymes tested for, were expressed by cell lineages other than fibroblasts in the *in vivo* BM. When those genes expressed by the *in vivo* BM were compared to the HS-5 experimental conditions, all three conditions expressed *APO* and *ALOX12* but not *ALOX5*. This suggested that the expression of lipooxygenase enzymes was not altered by the culture condition of HS-5 cells. However, those HS-5 seeded within a flask expressed also *ALOX15* which was not seen to be expressed in the *in vivo* BM, reinforcing the use of 3D HS-5 as a more *in vivo* relevant model of the *in vivo* human BM when compared to 2D.

The hydrolase enzymes evaluated within the study included *ASNA2*, *EPHX1*, *FAAH* and *FBP1* with all present in the *in vivo* BM tissue and primary fibroblast cells, inferring that the primary source of expression of the hydrolase enzymes tested may be the primary fibroblast cell. When those genes expressed by the *in vivo* BM fibroblasts, were compared to all three HS-5 conditions, all three expressed *ASNA2*, *EPHX1* and *FAAH* but not *FBP1*, suggesting once again that the culture condition had no effect on the expression of the hydrolase enzymes tested.

The kinase enzymes evaluated within the HS-5 experimental conditions included *HK2*, *PKLR* and *PKM* with all present in the *in vivo* BM tissue. However only *HK2* and *PKM* were also expressed by the primary fibroblast cells, inferring that *PKLR* was expressed by a different population within the *in vivo* BM. Those HS-5 cells seeded in 2D and within an AlgiMatrix™ scaffold with TK6, simulated the expression seen within the *in vivo* fibroblast cells, with both *HK2* and *PKM* present, reinforcing the fibroblastic nature of HS-5. However, those HS-5 seeded within an AlgiMatrix™ scaffold without TK6 expressed all three genes, fully replicating the *in vivo* BM environment, unlike the other culture conditions used within this study.

The oxidoreductase enzymes evaluated in this study included *AOC1*, *BLVRA*, *BLVRB*, *CYB5R3*, *GSR*, *MTHFR*, *NOS3*, *NQO1*, *SRD5A1* and *SRD5A2*. Those genes expressed in both the *in vivo* BM and the primary fibroblast cells, comprised of *BLVRA*, *BLVRB*, *CYB5R3*, *GSR*, *MTHFR*, *NOS3* and *SRD5A1*. When compared to the HS-5 experimental conditions, HS-5 seeded onto an AlgiMatrix™ scaffold with/ without TK6 expressed all genes seen to be expressed by the fibroblast and *in vivo* BM, with those HS-5 cultured in 2D not expressing *NOS3*. This suggests that HS-5 cultured in 3D, simulated the expression of oxidoreductase

enzymes seen *in vivo*. However, all three conditions did also express *NQO1* not seen to be expressed in the *in vivo* BM.

The paraoxonase enzymes evaluated included *PON1*, *PON2* and *PON3* with only *PON2* present in the *in vivo* BM tissue and also expressed by the primary fibroblast cells. When the *in vivo* expression was compared to the HS-5 experimental conditions, those HS-5 cultured in 2D and AlgiMatrix™ scaffold without TK6 expressed all three genes. However, HS-5 cultured on AlgiMatrix™ scaffold with TK6 only expressed *PON2* and *PON3*. Even though HS-5 cultured on AlgiMatrix™ scaffold with TK6 did express *PON3*, it simulated the environment more closely than the 2D culture.

The glutathione S-transferase enzymes evaluated in this study included *GSTA3*, *GSTA4*, *GSTM2*, *GSTM3*, *GSTM5*, *GSTP1*, *GSTT1*, *MGST1*, *MGST2* and *MGST3*. Those present in both the *in vivo* BM and primary fibroblasts comprised of *GSTM2*, *GSTM5*, *GSTP1*, *GSTT1*, *MGST1*, *MGST2* and *MGST3*. HS-5 cells cultured on an AlgiMatrix™ scaffold with TK6, was more *in vivo* relevant as it expressed those genes seen within the *in vivo* BM above, with HS-5 cultured in 2D and AlgiMatrix™ without TK6 found to be absent of *GSTM5*. This reinforces the *in vivo* relevance of HS-5 cells cultured in 3D with TK6 present, as they appear to act like fibroblasts when expressing glutathione S-transferase enzymes. However, cells in 3D culture also expressed *GSTA3* and *GSTM3* not seen to be expressed by the *in vivo* BM. An additional four genes associated with phase II metabolism were also analysed namely *CHEST1*, *COMT*, *NAT1* and *NAT2*. Those present within the *in vivo* BM tissue, identified within the fibroblast population, comprised of *CHEST1*, *COMT* and *NAT1*. It was found that regardless of culture method all three HS-5 experimental conditions expressed all four genes.

In total 43 out of the 67 genes tested were expressed within the *in vivo* human BM, with 37 of these genes found within the primary mesenchymal fibroblasts, inferring that a multicellular environment is required within the *in vivo* BM for the complete expression of these metabolism enzymes. However, as described above, 38 out of the 43 genes found within the *in vivo* BM environment were expressed by HS-5 cells cultured within an AlgiMatrix™ scaffold with/ without TK6, compared to 35 expressed by those seeded in 2D, suggesting the expression seen within a multicellular *in vivo* BM can be achieved, in part, with HS-5 cells cultured in AlgiMatrix™ scaffolds. This comparison reinforces the use of HS-5 in 3D culture as more *in vivo* relevant model for genotoxicity study. However, HS-5 expressed a further 14, 6 and 10 genes in 2D, 3D without TK6 and 3D with TK6, not seen

within the *in vivo* BM, identifying a possible limitation of this cell line. Therefore, the present/ absence of these genes in HS-5 compared to the *in vivo* BM, will be explored for their role, if any, in altering compound metabolism in the final discussion.

As mentioned previously the main site of expression of these phase II metabolic enzymes is the liver therefore the downregulation compared to the HepG2 spheroids was expected. However, the highly biologically significant upregulation of *GSTP1* in all three HS-5 experimental samples was intriguing. The *GSTP1* gene codes for an enzyme which decreases oxidative damage in cells by catalysing the conjugation of toxic compounds to glutathione, and can have a downregulation, due to hypermethylation, in a cancerous state (Guiroli *et al.*, 2018). The HS-5 cell line has been transformed from a patient without disease however, HepG2 cells are taken from a hepatocellular carcinoma, inferring that the altered expression may actually be the result of possible hypermethylation of the gene in HepG2, not changes in the specific cell type.

5.4.3. The expression of drug transporter, receptor and protein genes associated with metabolism

The qPCR analysis of the 3 HS-5 experimental groups (2D flask, AlgiMatrix™ scaffold with/ without TK6) also looked at those key genes associated with metabolism but are not categorised into phase I or II. These genes, however, can be categorised into drug transporters (members of the metallothioneins and p-glycoprotein families), receptors (*AHR* and *ARNT*) and regulatory proteins (*GCKR* and *SNN*). Once again, as this is a novel piece of study, there is limited research in the literature pertaining to the expression of the above family of genes within *in vitro* BM models. As there is limited literature, a comparison will be made between the 3 experimental groups and those genes expressed by the *in vivo* human BM, for validation of its use as a more *in vivo* relevant model. This will identify if the HS-5 cell line simulates the expression seen within the *in vivo* BM therefore implicating its use as a surrogate for primary stromal cells.

The metallothionein family of proteins play a vital role in metal ion homeostasis and detoxification through binding to both physiological (zinc & copper) and xenobiotic (cadmium & mercury) heavy metals (Calvo *et al.*, 2017). The binding of these cysteine-rich cytosolic proteins to zinc and copper, vital for cellular health, aids in cell growth, proliferation and reduction of oxidative stress whilst also protecting against metal toxicity

caused by xenobiotic metals such as cadmium (Lang & Si. 2018). Those members of the metallothionein family analysed via qPCR included *MT2A* and *MT3* which were seen to be present in all 3 experimental HS-5 groups. When compared to those genes seen within the *in vivo* human BM, *MT2A* was present in the BM stromal cells of humans. However, the *in vivo* BM stroma did not express *MT3* unlike all HS-5 condition which expressed both *MT2A* and *MT3* (Ren *et al.*, 2011 & Uhlén *et al.*, 2015).

The p-glycoprotein family of ATP-driven transmembrane transporter proteins are involved in the efflux of compounds out of the cell and have been associated with multidrug resistance, with the co-administration of erythromycin increasing sensitivity to compounds (Li *et al.*, 2010). With a similar substrate spectrum to CYP3A4, they are involved in the transportation and therefore detoxification of antineoplastics (etoposide) compounds from the cell (Finch & Pillans. 2014). Those members of the p-glycoprotein family analysed included *ABCB1*, *ABCC1* and *GPI*. Gene expression of *ABCB1* was only present in those HS-5 cells seeded within a flask, whereas *ABCC1* and *GPI* were present in all 3 HS-5 experimental groups. Within the *in vivo* human BM stroma, fibroblasts have been seen to express all 3 genes inferring that the HS-5 seeded alone in 2D was more *in vivo* relevant than its 3D counterparts (Han *et al.*, 2016; Uhlén *et al.*, 2015)

The *AHR* gene encodes a ligand-dependent transcription factor which regulates the transcription of key metabolic enzymes such as the CYP450 family and interacts with hormone receptors and associated *ARNT*, in response to a wide range of compounds classed as polycyclic aromatic hydrocarbons, benzimidazole and flavonoids (Hýzďalová *et al.*, 2018). The presence of both genes was seen in all 3 HS-5 experimental groups. This falls in line with the literature regarding *in vivo* expression, as both *AHR* and *ARNT* are expressed by the fibroblasts of the BM (Heidel *et al.*, 1998; Uhlén *et al.*, 2015)

The *GCKR* gene encodes the protein of the same name responsible for inhibiting glucokinase in regulating glucose metabolism solely in the hepatic tissue not within the *in vivo* human BM (Rees *et al.*, 2014). This was found to be negative within all HS-5 experimental groups therefore, its expression within only the HepG2 spheroids corresponds with the *in vivo* human.

The *SNN* gene encodes the protein stannin which is associated with the toxic effects of organotines by acting and altering expression of cyclin D1, *TP53* and regulators of the G1

phase of cell cycle and was present in all 3 HS-5 experimental groups (Reese *et al.*, 2005). This expression corresponds with that seen in the *in vivo* human as the *in vivo* BM has been seen to express SNN (Uhlén *et al.*, 2015).

5.4.4. Assessment of the cytotoxicity of cyclophosphamide on TK6 cells with/without HS-5 or S9

The pro-drug CPM is metabolised predominantly by CYP2B6, which is present within the S9 fraction, to 4-hydroxy-cyclophosphamide which then enters the cells as aldophosphamide (Connarn *et al.*, 2015). This can then be converted into the genotoxic product, PM via β -elimination or inactivated by ALDH to *o*-carboxyethylphosphoramidate mustard (Kurauchi *et al.*, 2017). The addition of CPM within this study was conducted on TK6 cells seeded within a trans-well insert with/ without HS-5 cells seeded on the surface not 3D scaffold. However, when HS-5 cells were seeded in a flask and within an Algimatrix scaffold with/ without TK6, the *CYP2B6* gene was present and significantly up-regulated in the HS-5 3D scaffolds, with and without the addition of TK6 cells compared to those seeded within a well (Figure 5-4). As *CYP2B6* was not present in 2D, therefore CPM was not metabolised to its active compound in HS-5 cells seeded within a flask, this would elucidate the lack of cytotoxicity seen when CPM was added directly to HS-5 cells within the well. However, the total cell number of TK6 significantly reduced when CPM was added to the co-culture. As *CYP2B6* was present with HS-5 cells seeded onto an AlgiMatrix with TK6, this could infer that the addition of TK6 soluble factors was influential in the metabolism of CPM into PM as it appears to have induced CYP2B6 production.

The gene *ALDH1A1* part of the ALDH superfamily, also present within the S9 fraction, which catalyses the oxidation of toxic aldehydes to a non-toxic form, such as that seen above with aldophosphamide, was absent in HS-5 cells seeded within a flask and in 3D with the addition of TK6 (Cicccone *et al.*, 2018). As HS-5 cells were seeded within the well not a scaffold within this study, this would infer that *ALDH1A1* was absent, allowing the β -elimination of CPM to its genotoxic product PM. As *CYP2B6* was present and *ALDH1A1* absent within HS-5 cells seeded within an AlgiMatrix scaffold with the addition of TK6, combined with the results seen within the CPM study showing a significant reduction in TK6 when in co-culture, this infers that co-culture and addition of TK6 soluble factors is influential in the genotoxicity of the compound not necessarily the three-dimensionality.

However, as HS-5 cells seeded within a flask with the addition of TK6 were not analysed for gene expression this conclusion cannot be confirmed.

When the cytotoxicity of CPM was compared between those wells containing TK6 only with and without the addition of S9, a significant decrease in total cell number can be seen between all experimental groups (Figure 5-6). When in co-culture with HS-5 this significant reduction in TK6 total cell number can only be seen with those wells treated with CPM, inferring that a 24 hour treatment with S9 has a higher background cytotoxicity level than with the co-cultured HS-5 cells. However, S9 has been seen to be highly cytotoxic due to the compounds used to induce the production of metabolic enzymes, such as aroclor, therefore when used in the regulatory *in vitro* MN assay only a 3 hour direct treatment not 24 is used (Ooka *et al.*, 2020). However, when patients are given a clinically relevant dose of CPM, detoxification and excretion takes >24 hours, with around 5 µg/ml still present within the plasma at 24 hours (Adams *et al.*, 2014). As S9, due to its high level of cytotoxicity, is only present for 3 hours within the assay before being washed out, detoxification cannot be achieved, therefore it gives a false indication of the level of cytotoxicity produced. This infers that HS-5 cells in co-culture have the ability to simulate the exposure time identified *in vivo* without background cytotoxicity seen with S9 inferring a true level of cytotoxicity.

5.5. Conclusion

In recent years it has been determined that the *in vivo* BM stroma has the ability to activate and detoxify compounds causing drug resistance, reduced efficacy, protective role of HSC and increased genotoxicity in compounds which have been identified as non-genotoxic in regulatory *in vitro* MN assays (Ria *et al.*, 2020; Chen *et al.*, 2020). The use of a single cell culture with the addition of a liver S9 fraction, to simulate liver metabolism, does not take into account the variation in expression between the *in vivo* liver and BM providing a result which can over/ underestimate cytotoxicity.

The data presented here clearly demonstrates the difference in expression of metabolic enzymes, drug transporters, receptors and regulatory proteins between cell lines of the liver (HepG2) and BM (HS-5). The expression of phase I and II metabolic enzymes was greatly reduced in HS-5 (2D and 3D cultured) cells compared to that of the HepG2 spheroid liver cell line, which was hypothesised due to the liver being the primary source of metabolism *in vivo*. However, HepG2 spheroids acted as a positive control to identify metabolic enzyme's absence/ presence in HS-5 compared to the *in vivo* BM. The analysis of the expression of those genes tested within this study by the AlgiMatrix™ seeded HS-5 with/without TK6, more closely resembled that of the *in vivo* BM, reinforcing its use as a more *in vivo* relevant model compared with 2D culture. However, it was found that HS-5 cells in all three experimental conditions expressed further genes which were not denoted in the *in vivo* BM, therefore the possible role of these disparities in gene expression will be considered in altered genotoxicity in the final discussion.

When used as a substitute for metabolic activation inducing increased cytotoxicity of CPM, HS-5 cells seeded within a well induced the same level of cytotoxicity seen with the regulatory S9 fraction, with a reduction in background cytotoxicity. This would infer that a simple 2D culture of HS-5 cells in a flask, with the presence of TK6 in a trans-well insert would be a simpler model for cytotoxicity. However, as genotoxicity wasn't investigated with this simple model, it cannot be inferred that this is more *in vivo* relevant than the three-dimensional model trialled, only that the low levels of expression seen in 2D compared to 3D (Figure 5-4), is adequate for activation of the compound.

The data presented within this chapter is the first to assess the metabolic profile of a BM cell line in 2D and 3D to the best of our knowledge, with and without the addition of TK6. The

expression profile of HS-5 cells compared to that of a hepatic cell line and comparative *in vivo* data, highlights the need for the addition of a BM cell line for regulatory assessment of compounds, not liver, to give a true indication of their toxicity. Furthermore, the findings in this chapter suggest that soluble factors between TK6 and HS-5 cells are adequate for the expression of metabolic enzymes similar to the *in vivo* human BM. Overall, the HS-5 cell line appears to be an appropriate surrogate for the primary BM stromal cells in the assessment of compounds *in vitro*.

Chapter Six

6. Final Discussion

6.1. General discussion and conclusion

The human BM is a complex interplay between differing microenvironments containing a multitude of cell types upon a three-dimensional ECM (Baryawno *et al.*, 2019). This interaction between cell types of each niche has been seen to cause resistance or increased sensitivity to compounds within the *in vivo* human BM (Ria *et al.*, 2020). In an effort to try to predict the genotoxicity of new compounds seen within the *in vivo* BM, the single cell type and 2D *in vitro* regulatory MN assay is used before the compound, if negative, is moved into *in vivo* rodents. However, a single cell line within a flask does not simulate the complex environment seen *in vivo*, therefore may be responsible for the disparity between *in vitro* and *in vivo* MN results with compounds such as glucocorticoids (Hayes *et al.*, 2013).

The overall aim of this PhD was to develop an *in vitro* model of the human BM which would be more *in vivo* relevant for the assessment of genotoxic compounds, in an effort to predict discrepancies between regulatory *in vitro* and *in vivo* MN assays and potentially develop a model that may offer insight into mechanisms causing these discrepancies. This was achieved by first developing an *in vitro* co-culture of relevant BM and regulatory cell lines (HS-5 and TK6) upon an artificial ECM (chapter 3), which was then used to assess the genotoxicity of known positive, negative and pharmacological positive genotoxic compounds, and results compared to historical *in vivo* and *in vitro* MN data (chapter 4). Finally, the expression profile of phase 1 and 2 metabolic enzymes present within HS-5 cells was analysed, and compared with the *in vivo* BM stroma (chapter 5), as a possible mechanism of altered genotoxicity between the regulatory *in vitro* and *in vivo* MN assay. Here, it will be explained how these strands ‘knit together’ to show how the developed model simulates the genotoxicity and toxicity of compounds similar to that seen *in vivo*.

Over the past decade the use of 3D cell culture techniques to try to recreate the *in vivo* healthy or cancer states of the BM has gained popularity, with the majority of studies moving away from simple spheroids and instead opting to incorporate primary cell types found within the human BM (primary human MSC and HSCs), expanding and differentiating upon an

artificial matrix with little to no use of cell lines (Yeung *et al.*, 2019; Inglis *et al.*, 2019; Yu *et al.*, 2018; Elango *et al.*, 2019; Braham *et al.*, 2018; Fairfield *et al.*, 2019; Sieber *et al.*, 2018; Sun *et al.*, 2011). These cultures are then combined with medium supplementation by a fluidic system for a prolonged period of time in order to simulate the complexity seen within the *in vivo* BM (Raic *et al.*, 2019). Studies by Sieber (2018), Hauang (2016) and Raic (2014) highlighted that this type of system does create an environment which simulates that seen within the *in vivo* BM, containing relevant extracellular markers and signalling proteins whilst also withstanding long term culture (>28 days). However as stated previously, these systems are costly (peristaltic pumps, microfluidics and primary cells), require extensive optimisation (sheer force, flow rate, cells not adhering to scaffold, long term culture before and after seeding) and include polymorphic primary cells which expand into differing lineages making it difficult for assay-to-assay comparisons and identification of the influential factor in altered compound genotoxicity (Khurshid *et al.*, 2018; Campuzano & Peeling, 2019; Kovisto *et al.* 2019). These factors are not problematic for in-depth mechanistic studies where a full model of the BM is required. However, in order to replace a predictive routine assay, such as the regulatory *in vitro* MN assay, which utilises an economical single clonal cell culture within a static flask, allowing batch to batch comparisons, this system is too complex, variable and costly, and is still requires many years of development before becoming a routine regulatory assay with set guidelines. Furthermore, this complexity may not be necessary for the *in vitro* assessment of compounds.

In order to reduce cost, maintain batch to batch comparability and identify the cause of the altered genotoxicity of compounds, the two clonal cell lines, HS-5 and TK6, were used as a simple less complex foundation to elucidate if the fibroblastic nature of the stroma was influential in the altered genotoxicity of compounds, as denoted in the literature (Chen *et al.*, 2020), with scope to add further cell lines if necessary. This method allowed the simple evaluation of each addition rather than trying to analyse multiple layers at once seen with those models utilising primary MSC and HSC. The HS-5 cell line was chosen as it is the only non-cancerous BM stromal cell line currently on the market, reducing genotoxic influences which may occur as a result of a cancerous state (Adamo *et al.*, 2020). Furthermore, this is the first study to analyse the expression of metabolic enzymes and investigate the use of HS-5 cells within genotoxicity testing. The TK6 cell line was chosen because of its routine use within the *in vitro* MN assay therefore, results can be compared between the model and those obtained from the *in vitro* assay.

As can be seen in chapter 3, this research developed a 14 day culture procedure which incorporated both HS-5 and TK6 without the use of a fluidic system which maintained both viability and proliferation. The initial 7 day seeding protocol of HS-5, encapsulated within an AlgiMatrix™ with pore sizes that corresponded the BM ECM, reduced cells evacuating the scaffold which was a problem within recent fluidic and static studies, whilst also maintaining viability (Sieber *et al.*, 2018; Hauang *et al.*, 2016; Raic *et al.*, 2014). The seeding and culturing protocol for the direct addition of TK6 fulfilled the requirement of the MN assay by achieving actively proliferating TK6 for the addition of compound. When TK6 were added in a trans-well insert to HS-5 cells within an AlgiMatrix™ scaffold cultured for 7 days, an increase in HS-5 viability and live cell number was seen over the remaining 96-hour period, inferring a beneficial crosstalk between the two cell types. A trans-well insert was used to allow the separation of each cell type for analysis, this would also allow extraction of RNA from the HS-5 cells only, which had not been ‘diluted’ by RNA from the TK6. Due to this increase in HS-5 proliferation with the addition of TK6, RNA was extracted from HS-5 cells 48 hours after TK6 addition, as this was also the point at which TK6 began to enter the exponential phase of proliferation. As the addition of TK6 within a trans-well insert to HS-5 seeded on AlgiMatrix™ scaffolds was the closest resemblance to those experiments exposed to compound, the metabolic profiles of these HS-5 were used to potentially elucidate (part of) the mechanism(s) behind the change in genotoxicity and cytotoxicity seen within this model, compared to the results obtained from the regulatory *in vitro* MN assay and historical *in vivo* data identified in chapter 4.

The original analysis within chapter 4, inferred that the altered levels of genotoxicity and cytotoxicity seen with MMC, etoposide and paclitaxel within this model, was due to a reduction in bioavailability of each compound through adherence to the scaffold. However, it appears that the HS-5 cell line also played a detoxification role in reducing the genotoxic and cytotoxic damage not only to itself but to those cells around. As mention in chapter 5, the role of those genes found to be expressed in HS-5 cells were analysed for their role, if any, in altered compound toxicity. Out of the 63 genes found to be expressed by the AlgiMatrix™ seeded HS-5 with addition of TK6 in a trans-well insert, only 7 were inferred to have an influence on genotoxic and cytotoxic outcomes of the two clastogenic compounds MMC and etoposide specifically *MT2A*, *ABCC1*, *GSTP1*, *NQO1*, *MGST1*, *CYP3A5* and *CYB5R*, with the aneugen, paclitaxel, only correlating with *ABCC1*. The anti-cancer compounds MMC and etoposide exert their main effect by inducing potent DNA crosslinks

or inhibition of the topoisomerase II enzyme respectively. In both cases the primary mechanism generates reactive oxygen species (ROS) which in turn cause further genotoxic damage increasing the level of MN (Wang *et al.*, 2010; Shin *et al.*, 2016; Xu *et al.*, 2014). It was found that both compounds had a reduced level of MN and cytotoxicity, in line with historical *in vivo* data, at the concentrations used within the current 3D model compared to that seen within the regulatory *in vitro* MN assay.

The reduction in MN and cytotoxicity was in part due to the detected expression of antioxidant genes, which correlate with their associated protein reducing oxidative stress within the HS-5 cells. These genes included *MT2A*, *GSTP1*, *MGST1* and *NQO1*. The expression of *MT2A*, which in this 3D model was highly expressed, has been linked with MMC and etoposide resistance *in vivo* through the scavenging of free radicals through its cysteine residues (Rodrigo *et al.*, 2020; Mangelinck *et al.*, 2019). In a similar manner, both *GSTP1* and *MGST1* have also been shown to scavenge free radicals created by MMC and etoposide reducing the effects of either clastogen (Deng *et al.*, 2015; Gisbergen *et al.*, 2016). The expression of these genes correlates with that seen in the fibroblasts of the *in vivo* BM, highlighting the similarities between this 3D model and the *in vivo* setting (Uhlén *et al.*, 2015). Once again *NQO1* has been implicated in the reduction of ROS created by etoposide's interaction with the topoisomerase II enzyme however, *NQO1* bioactivates MMC through intercellular bioreduction leading to increased DNA interstrand crosslinks (Zhang *et al.*, 2015; Oh & Park, 2015). This bioactivation would explain the higher level of MN with MMC within the model than that of etoposide however, *NQO1* is not expressed in the *in vivo* BM.

The HS-5 cells also expressed the transporter *ABCC1* also found within fibroblasts of the *in vivo* BM and enzymes *CYP3A5* and *CYP5B* (Uhlén *et al.*, 2015). The *ABCC1* gene codes for the superfamily of ATP-binding cassette transporters, transporting molecules across extra- and intra-cellular membranes and is involved in multi-drug resistance (Zhou *et al.*, 2015). The overexpression of the gene has been implicated in resistance to MMC, etoposide, paclitaxel and cyclophosphamide as the transporter extracts the drug molecule as it is diffused across the membrane, flipping them to the outer leaflet or allowing them into the extracellular environment for detoxification (Sampson *et al.*, 2019). This would give further justification to the lack of cytotoxicity seen with MMC, etoposide, paclitaxel and cyclophosphamide within the 3D model. The presence of *CYP3A5* reinforces the increase in MN and cytotoxicity seen with etoposide compared to MMC, as the enzyme O-demethylates etoposide into catechol which is seen to increase geno- and cytotoxicity of the compound

(Kishi *et al.*, 2006). The enzyme CYPB5R, is key in mediating MMC redox cycling and generation of ROS with the addition of CYP2B4 which would increase geno- and cytotoxicity (Çelik & Arinç, 2013). However, due to the aforementioned antioxidant's presence within the model, these ROS would be scavenged reinforcing the reduction in MN and cytotoxicity seen between the *in vitro* 2D and 3D results.

This would infer that the addition of HS-5 to TK6 acted as an antioxidant, reducing the levels of ROS within the culture whilst also protecting itself through multidrug resistance transporters in a similar manner to that seen within the *in vivo* BM however, this is only the case if the TK6 cells do not express these genes in the regulatory *in vitro* MN assay. The metabolic profile of the TK6 cell was not conducted in this study as work by Revollo (2016) looked at the whole genome and normalised mRNA sequencing on the TK6 cell line in monoculture. Their work found that TK6 did in fact express the majority of the above genes, excluding *CYP3A5* and *CYP5R*, at a similar level seen within B cell lymphoblasts of the *in vivo* BM however, single nucleotide polymorphisms were detected within the *NQO1* and *ABCC1* genes decreasing their ability to function.

The addition of dexamethasone and prednisolone induced cytotoxicity and a higher induction of MN within our model, similar to that seen within the *in vivo* historical data, than induced at the same concentration within the regulatory *in vitro* MN assay. These results were interesting as even though the increase in MN correlated with the *in vivo* historical data, glucocorticoids of this nature have been seen to have a protective nature (Hassan *et al.*, 2018). The addition of dexamethasone or prednisolone has been seen to promote and overexpress CYP enzymes (*CYP3A5*, *CYP2E1*, *CYP2D6* and *CYP1A1*), antioxidant proteins (pon2, 3 MT2A) and multi-drug resistance transporters (*ABCC1*) found to be expressed by the *in vivo* BM and HS-5 cells, hence their routine use in combination with further compounds to reduce secondary toxicity (Lim & Kim, 2009; Vrzal *et al.*, 2015; Sato *et al.*, 2013; Aberuyi *et al.*, 2020). These data suggest that the ability of the glucocorticoids to promote the expression of these enzymes, infers that metabolic capability is not the mechanism of increased MN or cytotoxicity seen in the model, due to their protective role. A definitive mechanism behind the increase in MN within the *in vivo* setting has still not been identified however, the ability of glucocorticoid, specifically dexamethasone and prednisolone, to cause cytotoxicity has been well documented with one such mechanism having the ability to cause increased genotoxicity through the generation of ROS by glucocorticoid-induced apoptosis (Yin *et al.*, 2018). It has been seen that high levels of dexamethasone or prednisolone decreases the expression of glucose metabolism enzymes,

such as HK2, inducing apoptosis and the release of ROS within cells (Xu *et al.*, 2020). At the highest concentrations used within the model, a level of MN twice that of the vehicle control was observed, reinforcing the role of ROS in genotoxicity through glucocorticoid-induced apoptosis. However, as previously mentioned, glucocorticoids of this nature increase the expression of many antioxidant genes which would combat the genotoxic effects of ROS therefore, this would infer that ROS is not the main cause in the increase of MN seen within the model and *in vivo* BM.

Overall, the development of an *in vitro* model of the BM using appropriate cell lines has enabled the confirmation of the genotoxicity of known positive, negative and pharmacological positives seen within the *in vivo* historical data, but not identified within the regulatory *in vitro* MN assay. Furthermore, this study has identified the metabolic profile of HS-5 stromal cells and their ability to detoxify compounds, reducing MN induction, and the conversion of a pro-drug into its cytotoxic counterpart without the background toxicity observed with S9 fraction.

This study set out to achieve three key aims in order to achieve the final goal of creating a 3D model of the BM for toxicity and genotoxicity testing. In doing so, it has created a viable, proliferating co-culture of cell lines with the ability to identify a level of genotoxicity of known positive, negative and pharmacological positive compounds at a level seen within the *in vivo* BM. Identified the expression of phase I and II metabolic enzymes, for the first time in 2D and 3D HS-5 cultures with/ without TK6, whilst also showing that expression in 3D culture was more *in vivo* relevant than 2D. This research is the first within the literature to successfully simulate the genotoxicity of compounds without the use of fluidics, primary cells or complex scaffolds *in vitro*. The comparative nature of this simple, reproducible model to the *in vivo* BM, allows the true genotoxicity of compounds to be routinely assessed in any laboratory.

6.2. Limitations of the study

It is important to highlight that this study has not been without limitations which may have an impact on the findings. As the TK6 cell line was used to assess the genotoxicity of a compound, the model was cultured in complete RPMI 1640 medium as this is recommended for TK6 cell's growth in order to reduce influences on cell cycle. Conversely, the HS-5 cell line is recommended to be cultured in Dulbecco's Modified Eagle's Medium; as HS-5 were cultured in RPMI 1640 this could cause an altered gene expression and functionality from the HS-5 cells. However, HS-5 cells have been successfully cultured in RPMI-1640 previously but changes in gene expression were not noted (Beaulieu *et al.*, 2011).

The metabolic profile of the HS-5 cells, in co-culture with TK6, was conducted with a trans-well insert. Therefore, cellular communication only occurred through soluble signalling molecules not cell to cell contact, seen with those cells within the model treated with compound. As this separation was needed in order to reduce RNA contamination from the TK6 cells, only a correlational link can be established between the metabolic expression seen in the treated model and the trans-well insert studies.

As the reagents required for creating, maintaining and dissolving the Algimatrix™ scaffold altered the CD markers used for discrimination of TK6 from HS-5 cells, the increase in MN cannot be attributed to either HS-5 or TK6 as identification of MN within a single cell line could not be conducted. Further optimisation of different fluorophores and markers would negate this issue.

In order to maintain the cellular environment within the scaffold, medium within the scaffold during the compound wash day was left. Even though every effort was made to remove as much compound as possible the number of cells within the scaffold at this time was not identified. This lack of identification meant that the lack of cytotoxicity seen with some compounds could be due to inconsistency in medium removal at this stage. However, even without this cell number cytotoxicity did correlate with that seen within studies of the *in vivo* BM.

6.3. Future work

The model created in this study induced the same level of genotoxicity seen within the *in vivo* BM at the concentrations tested, inferring that the cellular communication and signalling molecules within corresponded with that of the human BM. Even though this is the first study to correctly predict the *in vivo* genotoxicity and cytotoxicity of known positive, negative, pharmacological positive and pro-drug compounds *in vitro*, the metabolic profile of the cells may only play a small part in the eventual genotoxic and cytotoxic outcome of a compound.

The *in vivo* BM contains a number of signalling pathways (JAK-STAT), chemokines/cytokines (interleukins, cyclin D1, c-Myc), receptors (C-X-C chemokine receptor) which replenish and differentiate the cellular components of the *in vivo* BM without genotoxic damage (Gomariz *et al.*, 2018; Yi *et al.*, 2019; Garcia *et al.*, 2012; Weng *et al.*, 2016). The alteration of any of these could lead to an induction of genotoxic damage, therefore could give an explanation to the results seen with the glucocorticoids. The mechanism by which glucocorticoids such as dexamethasone and prednisolone, induce their effect includes both genomic and non-genomic mechanisms, which alter the expression of interleukins, cellular proliferation and differentiation (Clarisse *et al.*, 2020; Shimba *et al.*, 2018; Gupta & Mayer, 2013). Now that the model is at a point that it simulates the genotoxicity seen within the *in vivo* BM, identifying the possible changes in cytokines, signalling pathways and receptor expression to compound could unpick the results seen with these compounds.

As the metabolic profile of the HS-5 was conducted with a trans-well insert, the addition of known genotoxic and pro-drug compounds to this experimental condition would allow the comparison between those MN induced within the contact model and those induced when cells are not in contact. If the level of MN was negatable between the two experimental conditions, this would reinforce the comparison of MN and the expression by HS-5 of metabolic enzymes seen in chapter 5. The metabolic profile of the HS-5 after treatment would also be beneficial to assess if the overexpression of those genes, discussed previously in this chapter, does occur in a manner seen within the *in vivo* BM. As the original aim of the study was to produce a simple model of the BM for genotoxicity testing of compounds, the addition of primary BM stromal cells would allow more mechanistic studies due to the expansion and differentiation of the cells. Utilising the Algimatrix™ scaffold and culturing technique, the addition of primary BM cells would require less optimisation, with the

eventual aim of producing a blood system within the flask for in-depth genotoxicity and mechanistic studies.

Within the 2D *in vitro* MN assay, an RPD is required in order to identify samples which MN can be counted in, this is not the case for the *in vivo* MN. However, 3D models, like the one constructed in this PhD, are not conducted *in vivo* therefore, require some form of RPD if they are to be used in regulatory genotoxicity testing in the future. Preliminary work was conducted to try and combine markers of apoptosis, proliferation and cell specificity in order to calculate an alternative to RPD, with extra time and resources this could be achieved changing cytotoxicity measurements in 3D cultures. It was also noted that in order to negate the issues with identification in co-culture, future work could be conducted on creating a stable transfected, GFP labelled TK6 cell line. This would allow ease identification of the TK6 cell line in a co-culture.

With more funding and time, the expansion of the 3D bio-printing in chapter 3 would be beneficial with the recent advances in printer technology. The use of printing will allow the production of bespoke scaffolds, with and without cells, connected to whole organ structures allowing the production of pharmacodynamic/ kinetic systems for drug development.

References

- Aanei, C. M., & Catafal, L. C. (2018). Evaluation of bone marrow microenvironment could change how myelodysplastic syndromes are diagnosed and treated. *Cytometry Part A*. 93 (9), p916–928.
- Abbuehl, J. P., Tatarova, Z., Held, W., & Huelsken, J. (2017). Long-Term Engraftment of Primary Bone Marrow Stromal Cells Repairs Niche Damage and Improves Hematopoietic Stem Cell Transplantation. *Cell Stem Cell*. 21 (2), p241-255.
- Abe-Suzuki, S., Kurata, M., Abe, S., Onishi, I., Kirimura, S., Nashimoto, M., Murayama, T., Hidaka, M., & Kitagawa, M. (2014). CXCL12+ stromal cells as bone marrow niche for CD34+ hematopoietic cells and their association with disease progression in myelodysplastic syndromes. *Laboratory Investigation*. 94 (11), p1212–1223.
- Aberuyi, N., Rahgozar, S., Pourabutaleb, E., & Ghaedi, K. (2020). Selective dysregulation of ABC transporters in methotrexate-resistant leukemia T-cells can confer cross-resistance to cytarabine, vincristine and dexamethasone, but not doxorubicin. *Current Research in Translational Medicine*. 1 (1), p103269.
- Acri, T. M., Laird, N. Z., Geary, S. M., Salem, A. K., & Shin, K. (2019). Effects of calcium concentration on nonviral gene delivery to bone marrow-derived stem cells. *Journal of Tissue Engineering and Regenerative Medicine*. 13 (12), p2256–2265.
- Adamo, A., Delfino, P., Gatti, A., Bonato, A., Takam Kamga, P., Bazzoni, R., Ugel, S., Mercuri, A., Caligola, S., & Krampera, M. (2020). HS-5 and HS-27A Stromal Cell Lines to Study Bone Marrow Mesenchymal Stromal Cell-Mediated Support to Cancer Development. *Frontiers in Cell and Developmental Biology*. 8 (1).
- Adams, L. M., Johnson, B., & Murray, S. (2014). A pharmacokinetic, pharmacodynamic, and safety study of intravenous cyclophosphamide with an oral casopitant antiemetic regimen in cancer patients. *Clinical Pharmacology in Drug Development*. 3 (2), p93–100.
- Addo, R. K., Heinrich, F., Heinz, G. A., Schulz, D., Sercan-Alp, Ö., Lehmann, K., Tran, C. L., Bardua, M., Matz, M., Löhning, M., Hauser, A. E., Kruglov, A., Chang, H. D., Durek, P., Radbruch, A., & Mashreghi, M. F. (2019). Single-cell transcriptomes of murine bone marrow stromal cells reveal niche-associated heterogeneity. *European Journal of Immunology*. 49 (9), p1372–1379.

- Agulhon, P., Robitzer, M., Habas, J. P., & Quignard, F. (2014). Influence of both cation and alginate nature on the rheological behavior of transition metal alginate gels. *Carbohydrate Polymers*. 112 (1), p525–531.
- Akihiro Shimba, A., Cui, G., Tani-ichi, S., Nagasawa, T., & Sch, unther. (2018). Glucocorticoids Drive Diurnal Oscillations in T Cell Distribution and Responses by Inducing Interleukin-7 Receptor and CXCR4. *Immunity*. 48 (1), p286–298.
- Al-Nbaheen, M., Vishnubalaji, R., Ali, D., Bouslimi, A., Al-Jassir, F., Megges, M., Prigione, A., Adjaye, J., Kassem, M., Aldahmash, A. (2013). Human Stromal (Mesenchymal) Stem Cells from Bone Marrow, Adipose Tissue and Skin Exhibit Differences in Molecular Phenotype and Differentiation Potential. *Stem Cell Reviews and Reports*. 9 (1), p32–43.
- Alexandrov, K., Rojas, M., & Rolando, C. (2006). DNA damage by benzo(a)pyrene in human cells is increased by cigarette smoke and decreased by a filter containing rosemary extract, which lowers free radicals. *Cancer Research*. 66 (24), p11938–11945.
- Alonso, S., Su, M., Jones, J. W., Ganguly, S., Kane, M. A., Jones, R. J., & Ghiaur, G. (2015). Human bone marrow niche chemoprotection mediated by cytochrome p450 enzymes. *Oncotarget*. 6 (17), p14905–14912.
- Alsabri, S. G., Mari, W. O., Younes, S., Alsadawi, M. A., & Oroszi, T. L. (2018). Kinetic and Dynamic Description of Caffeine. *Journal of Caffeine and Adenosine Research*. 8 (1), p3–9.
- Amer, K. M., Mohamed, S., Amer, R., Chaudhry, A., Winters, B., & Abraham, J. A. (2018). Effect of Mitomycin C on recurrence of plantar fibromas. *Journal of Orthopaedic Research*. 36 (9), p2554–2561.
- Andersen, T., Auk-Emblem, P., & Dornish, M. (2015). 3D Cell Culture in Alginate Hydrogels. *Microarrays*. 4 (2), p133–161.
- Andrews, S. W., Kabrah, S., May, J. E., Donaldson, C., Morse, R. H. (2013). Multiple myeloma: the bone marrow microenvironment and its relation to treatment. *BRITISH JOURNAL OF BIOMEDICAL SCIENCE*. 7 (3), p110-120.
- Anton, D., Burckel, H., Josset, E., & Noel, G. (2015). Three-dimensional cell culture: A breakthrough in vivo. In *International Journal of Molecular Sciences*. 16 (3), p5517–5527.
- Aqmasheh, S., Shamsasanjan, K., Akbarzadehlaleh, P., Sarvarm D. P., Timari, H.. (2017). Effects of Mesenchymal Stem Cell Derivatives on Hematopoiesis and Hematopoietic Stem Cells. *Advanced Pharmaceutical Bulletin*. 7 (2), p165-177.

- Armstrong, J. P. K., Burke, M., Carter, B. M., Davis, S. A., & Perriman, A. W. (2016). 3D Bioprinting Using a Templated Porous Bioink. *Advanced Healthcare Materials*. 5 (14), p1724–1730.
- Arranz-Marquez, E., Katsanos, A., Kozobolis, V. P., Konstas, A. G. P., & Teus, M. A. (2019). A Critical Overview of the Biological Effects of Mitomycin C Application on the Cornea Following Refractive Surgery. In *Advances in Therapy*. 36 (4), p786–797.
- Babaei, M. A., Kamalidehghan, B., Saleem, M., Huri, H. Z., & Ahmadipour, F. (2016). Receptor tyrosine kinase (c-Kit) inhibitors: A potential therapeutic target in cancer cells. In *Drug Design, Development and Therapy*. 10 (1), p2443–2459.
- Bachmann, K. (2009). Drug Metabolism. In *Pharmacology*. 1 (1), p131–173.
- Bakhuraysah, M. M., Siatskas, C., & Petratos, S. (2016). Hematopoietic stem cell transplantation for multiple sclerosis: Is it a clinical reality? In *Stem Cell Research and Therapy*. 7 (1).
- Baryawno, N., Przybylski, D., Kowalczyk, M. S., Kfoury, Y., Severe, N., Gustafsson, K., Kokkaliaris, K. D., Mercier, F., Tabaka, M., Hofree, M., Dionne, D., Papazian, A., Lee, D., Ashenberg, O., Subramanian, A., Vaishnav, E. D., Rozenblatt-Rosen, O., Regev, A., & Scadden, D. T. (2019). A Cellular Taxonomy of the Bone Marrow Stroma in Homeostasis and Leukemia. *Cell*. 177 (7), p1915–1932.
- Bateman, M. E., Strong, A. L., McLachlan, J. A., Burow, M. E., & Bunnell, B. A. (2017). The effects of endocrine disruptors on adipogenesis and osteogenesis in mesenchymal stem cells: A review. In *Frontiers in Endocrinology*. 7 (1), p171.
- Beaulieu, A., Poncin, G., Belaid-Choucair, Z., Humblet, C., Bogdanovic, G., Lognay, G., Boniver, J., & Defresne, M. P. (2011). Leptin reverts Pro-Apoptotic and antiproliferative effects of α -Linolenic acids in BCR-ABL positive leukemic cells: Involvement of PI3K pathway. *PLoS ONE*. 6 (10).
- Becher, B., Tugues, S., & Greter, M. (2016). GM-CSF: From Growth Factor to Central Mediator of Tissue Inflammation. In *Immunity*. 45 (5), p963–973.
- Bein, A., Shin, W., Jalili-Firoozinezhad, S., Park, M. H., Sontheimer-Phelps, A., Tovaglieri, A., Chalkiadaki, A., Kim, H. J., & Ingber, D. E. (2018). Microfluidic Organ-on-a-Chip Models of Human Intestine. In *CMGH*. 5 (4), p659–668.
- Belloni, D., Heltai, S., Ponzoni, M., Villa, A., Vergani, B., Pecciarini, L., Marcatti, M., Girlanda, S., Tonon, G., Ciceri, F., Caligaris-Cappio, F., Ferrarini, M., & Ferrero, E. (2018). Modeling multiple myeloma-bone marrow interactions and response to drugs in a 3d surrogate microenvironment. *Haematologica*. 103 (4), p707–716.

- Berg, J., Hiller, T., Kissner, M. S., Qazi, T. H., Duda, G. N., Hocke, A. C., Hippenstiel, S., Elomaa, L., Weinhart, M., Fahrenson, C., & Kurreck, J. (2018). Optimization of cell-laden bioinks for 3D bioprinting and efficient infection with influenza A virus. *Scientific Reports*. 8 (1).
- Bernacki, D. T., Bryce, S. M., Bemis, J. C., Dertinger, S. D., Witt, K. L., & Smith-Roe, S. L. (2019). Evidence for an Aneugenic Mechanism of Action for Micronucleus Induction by Black Cohosh Extract. *Environmental and Molecular Mutagenesis*. 60 (9), p845–856.
- Bindreither, D., Ecker, S., Gschirr, B., Kofler, A., Kofler, R., & Rainer, J. (2014). The synthetic glucocorticoids prednisolone and dexamethasone regulate the same genes in acute lymphoblastic leukemia cells. *BMC Genomics*. 15 (1), p662.
- Birbrair, A., Frenetic, P. S. (2016). Niche heterogeneity in the bone marrow. *Annals of The New York Academy Of Sciences*. 1370 (1), p82-96.
- Bodgi, L., Bahmad, H. F., Araji, T., Al Choboq, J., Bou-Gharios, J., Cheaito, K., Zeidan, Y. H., Eid, T., Geara, F., & Abou-Kheir, W. (2019). Assessing radiosensitivity of bladder cancer in vitro: A 2D vs. 3D approach. *Frontiers in Oncology*. 9 (3).
- Bologna-Molina, R., Bedoya-Borella, A. M., Soria-Moreira, L., & Soría-Suárez, S. (2013). Molecular biomarkers of cell proliferation in ameloblastomas. *World Journal of Stomatology*. 2 (4), p79.
- Borgå, O., Lilienberg, E., Bjeremo, H., Hansson, F., Heldring, N., & Dediu, R. (2019). Pharmacokinetics of Total and Unbound Paclitaxel After Administration of Paclitaxel Micellar or Nab-Paclitaxel: An Open, Randomized, Cross-Over, Explorative Study in Breast Cancer Patients. *Advances in Therapy*. 36 (10), p2825–2837.
- Borriello, F., Galdiero, M. R., Varricchi, G., Loffredo, S., Spadaro, G., & Marone, G. (2019). Innate immune modulation by GM-CSF and IL-3 in health and disease. In *International Journal of Molecular Sciences*. 20 (4).
- Bosch, D. E., Kilgore, M. R., Schmidt, R. A., Swanson, P. E., Rendi, M. H., & Chang, O. H. (2017). Comparison of Proliferation Markers Ki67 and Phosphohistone-H3 (pHH3) in Breast Ductal Carcinoma in Situ. *Applied Immunohistochemistry and Molecular Morphology*. 25 (8), p543–547.
- Boutin, L., Arnautou, P., Trignol, A., Ségot, A., Farge, T., Desterke, C., Soave, S., Clay, D., Raffoux, E., Sarry, J. E., Malfuson, J. V., Lataillade, J. J., Le Bousse-Kerdilès, M. C., & Anginot, A. (2020). Mesenchymal stromal cells confer chemoresistance

- to myeloid leukemia blasts through Side Population functionality and ABC transporter activation. *Haematologica*. 105 (4), p987–998.
- Bowen, D. E., Whitwell, J. H., Lillford, L., Henderson, D., Kidd, D., Mc Garry, S., Pearce, G., Beevers, C., & Kirkland, D. J. (2011). Evaluation of a multi-endpoint assay in rats, combining the bone-marrow micronucleus test, the Comet assay and the flow-cytometric peripheral blood micronucleus test. *Mutation Research - Genetic Toxicology and Environmental Mutagenesis*. 722 (1), p7–19.
- Braham, M. V. J., Deshantri, A. K., Minnema, M. C., Öner, F. C., Schiffelers, R. M., Fens, M. H. A. M., & Alblas, J. (2018). Liposomal drug delivery in an in vitro 3D bone marrow model for multiple myeloma. *International Journal of Nanomedicine*. 13 (1), p8105–8118.
- Brambilla, G., Mattioli, F., Robbiano, L., & Martelli, A. (2013). Genotoxicity and Carcinogenicity Studies of Bronchodilators and AntiAsthma Drugs. *Basic & Clinical Pharmacology & Toxicology*. 112 (5), p302–313.
- Brennan, C. M., Eichholz, K. F., & Hoey, D. A. (2019). The effect of pore size within fibrous scaffolds fabricated using melt electrowriting on human bone marrow stem cell osteogenesis. *Biomedical Materials (Bristol)*. 14 (6) p2.
- Bruce, A., Evans, R., Mezan, R., Shi, L., Moses, B. S., Martin, K. H., Gibson, L. F., & Yang, Y. (2015). Three-dimensional microfluidic tri-culture model of the bone marrow microenvironment for study of acute lymphoblastic leukemia. *PLoS ONE*. 10 (10).
- Brüsehafer, K., Manshian, B. B., Doherty, A. T., Zaïr, Z. M., Johnson, G. E., Doak, S. H., & Jenkins, G. J. S. (2016). The clastogenicity of 4NQO is cell-type dependent and linked to cytotoxicity, length of exposure and p53 proficiency. *Mutagenesis*. 31 (2), p171–180.
- Brüsehafer, K., Rees, B. J., Manshian, B. B., Doherty, A. T., Richard O'donovan, M., Doak, S. H., James, G., & Jenkins, S. (2014). Chromosome Breakage Induced by the Genotoxic Agents Mitomycin C and Cytosine arabinoside is Concentration and p53 Dependent. *TOXICOLOGICAL SCIENCES*. 140 (1), p94–102.
- Bryce, S. M., Avlasevich, S. L., Bemis, J. C., Lukamowicz, M., Elhajouji, A., Van Goethem, F., De Boeck, M., Beerens, D., Aerts, H., Van Gompel, J., Collins, J. E., Ellis, P. C., White, A. T., Lynch, A. M., & Dertinger, S. D. (2008). Interlaboratory evaluation of a flow cytometric, high content in vitro micronucleus assay. *Mutation Research - Genetic Toxicology and Environmental Mutagenesis*. 650 (2), p181–195.

- Bryce, S. M., Avlasevich, S. L., Bemis, J. C., Tate, M., Walmsley, R. M., Saad, F., Van Dijck, K., De Boeck, M., Van Goethem, F., Lukamowicz-Rajska, M., Elhajouji, A., & Dertinger, S. D. (2013). Flow cytometric 96-well microplate-based in vitro micronucleus assay with human TK6 cells: Protocol optimization and transferability assessment. *Environmental and Molecular Mutagenesis*, 54 (3), p180–194.
- Bryce, S. M., Shi, J., Nicolette, J., Diehl, M., Sonders, P., Avlasevich, S., Raja, S., Bemis, J. C., & Dertinger, S. D. (2010). High content flow cytometric micronucleus scoring method is applicable to attachment cell lines. *Environmental and Molecular Mutagenesis*, 51 (3), p260–266.
- Buick, J. K., Moffat, I., Williams, A., Swartz, C. D., Recio, L., Hyduke, D. R., Li, H. H., Fornace, A. J., Aubrecht, J., & Yauk, C. L. (2015). Integration of metabolic activation with a predictive toxicogenomics signature to classify genotoxic versus nongenotoxic chemicals in human TK6 cells. *Environmental and Molecular Mutagenesis*, 56 (6), p520–534.
- Caldecott, K. W. (2008). Single-strand break repair and genetic disease. In *Nature Reviews Genetics*, 9 (8), p619–631.
- Calvo, J., Jung, H., & Meloni, G. (2017). Copper metallothioneins. In *IUBMB Life*, 69 (4), p236–245.
- Campuzano, S., & Pelling, A. E. (2019). Scaffolds for 3D Cell Culture and Cellular Agriculture Applications Derived From Non-animal Sources. In *Frontiers in Sustainable Food Systems*, 3 (1), p 38.
- Cao, N., Chen, X. B., Schreyer, D. J. (2012). Influence of Calcium Ions on Cell Survival and Proliferation in the Context of an Alginate Hydrogel. *ISRN Chemical Engineering*, 2012 (1), p1-9.
- Caraguel, C. G. B., Stryhn, H., Gagné, N., Dohoo, I. R., & Hammell, K. L. (2011). Selection of a cutoff value for real-time polymerase chain reaction results to fit a diagnostic purpose: Analytical and epidemiologic approaches. In *Journal of Veterinary Diagnostic Investigation*, 23 (1), p2–15.
- Cardoso, B. A., Belo, H., Barata, J. T., & Almeida, A. M. (2015). The Bone Marrow-Mediated Protection of Myeloproliferative Neoplastic Cells to Vorinostat and Ruxolitinib Relies on the Activation of JNK and PI3K Signalling Pathways. *PLOS ONE*, 10 (12).

- Casey, L. S., Herring, V., Hu, Z., Witbrodt, K., & Parker, R. B. (2013). The role of human carboxylesterases in drug metabolism: Have we overlooked their importance? In *Pharmacotherapy*. 33 (2), p210–222.
- Casey, A., Gargotti, M., Bonnier, F., & Byrne, H. J. (2016). Chemotherapeutic efficiency of drugs in vitro: Comparison of doxorubicin exposure in 3D and 2D culture matrices. *Toxicology in Vitro*. 33 (1), p99–104.
- Castiaux, A. D., Spence, D. M., & Martin, R. S. (2019). Review of 3D cell culture with analysis in microfluidic systems. In *Analytical Methods*. 11 (33), p4220–4232.
- Çelik, E., Bayram, C., Akçapınar, R., Türk, M., & Denkbaş, E. B. (2016). The effect of calcium chloride concentration on alginate/Fmoc-diphenylalanine hydrogel networks. *Materials Science and Engineering C*. 66 (1), p221–229.
- Çelik, H., & Arınç, E. (2013). Evaluation of bioreductive activation of anticancer drugs idarubicin and mitomycin C by NADH-cytochrome b5 reductase and cytochrome P450 2B4. *Xenobiotica*. 43 (3), p263–275.
- Cevc, G., & Blume, G. (2004). Hydrocortisone and dexamethasone in very deformable drug carriers have increased biological potency, prolonged effect, and reduced therapeutic dosage. *Biochimica et Biophysica Acta – Biomembranes*. 1663 (1–2), p61–73.
- Chaicharoenaudomrung, N., Kunhorm, P., & Noisa, P. (2019). Three-dimensional cell culture systems as an in vitro platform for cancer and stem cell modeling. In *World Journal of Stem Cells*. 11 (12), p1065–1083.
- Chang, Y. T., Hernandez, D., Alonso, S., Gao, M., Su, M., Ghiaur, G., Levis, M. J., & Jones, R. J. (2019). Role of CYP3A4 in bone marrow microenvironment-mediated protection of FLT3/ITD AML from tyrosine kinase inhibitors. *Blood Advances*. 3 (6), p908–916.
- Chapman, K. E., Wilde, E. C., Chapman, F. M., Verma, J. R., Shah, U. K., Stannard, L. M., Seager, A. L., Tonkin, J. A., Brown, M. R., Doherty, A. T., Johnson, G. E., Doak, S. H., & Jenkins, G. J. S. (2020). Multiple-endpoint in vitro carcinogenicity test in human cell line TK6 distinguishes carcinogens from non-carcinogens and highlights mechanisms of action. *Archives of Toxicology*. 1 (3).
- Charles, E. M., & Rehm, M. (2014). Key regulators of apoptosis execution as biomarker candidates in melanoma. *Molecular & Cellular Oncology*. 1 (3), p964037.
- Chen, C., Townsend, A. D., Hayter, E. A., Birk, H. M., Sell, S. A., & Martin, R. S. (2018). Insert-based microfluidics for 3D cell culture with analysis. *Analytical and Bioanalytical Chemistry*. 410 (12), p3025–3035.

- Chen, M., Vial, M. L., & St John, J. A. (2019). 3D-tips: User-friendly mesh barrier pipette tips for 3D-spheroid culture. *Journal of Biological Engineering*. 13 (1).
- Chen, T., Zhang, G., Kong, L., Xu, S., Wang, Y., & Dong, M. (2019). Leukemia-derived exosomes induced IL-8 production in bone marrow stromal cells to protect the leukemia cells against chemotherapy. *Life Sciences*. 221 (1), p187–195.
- Chen, W. C., Hu, G., & Hazlehurst, L. A. (2020). Contribution of the bone marrow stromal cells in mediating drug resistance in hematopoietic tumors. In *Current Opinion in Pharmacology*. 54 (1), p36–43.
- Chen, Z., Yan, X., Yin, S., Liu, L., Liu, X., Zhao, G., Ma, W., Qi, W., Ren, Z., Liao, H., Liu, M., Cai, D., & Fang, H. (2020). Influence of the pore size and porosity of selective laser melted Ti6Al4V ELI porous scaffold on cell proliferation, osteogenesis and bone ingrowth. *Materials Science and Engineering C*. 106 (1).
- Cherry, H. M., Roelofs, A. J., Kurth, T. B., & De Bari, C. (2014). In vivo phenotypic characterisation of nucleoside label-retaining cells in mouse periosteum. *European Cells and Materials*. 27 (1), p185–195.
- Chirani, N., Yahia, L., Gritsch, L., Motta, F. L., Chirani, S., Fare, S. (2015). History and Applications of Hydrogels. *Journal of Biomedical Sciences*. 4 (2), p1-5.
- Chondrou, V., Trochoutsou, K., Panayides, A., Efthimiou, M., Stephanou, G., & Demopoulos, N. A. (2018). Combined study on clastogenic, aneugenic and apoptotic properties of doxorubicin in human cells in vitro. *Journal of Biological Research (Greece)*. 25 (1).
- Choudhury, R. C., Palo, A. K., & Sahu, P. (2004). Cytogenetic risk assessment of etoposide from mouse bone marrow. *Journal of Applied Toxicology*. 24 (2), p115–122.
- Ciccone, V., Terzuoli, E., Donnini, S., Giachetti, A., Morbidelli, L., & Ziche, M. (2018). Stemness marker ALDH1A1 promotes tumor angiogenesis via retinoic acid/HIF-1 α /VEGF signalling in MCF-7 breast cancer cells. *Journal of Experimental & Clinical Cancer Research*. 37 (1), p311.
- Ciciarello, M., Corradi, G., Loscocco, F., Visani, G., Monaco, F., Cavo, M., Curti, A., & Isidori, A. (2019). The yin and yang of the bone marrow microenvironment: Pros and cons of mesenchymal stromal cells in acute myeloid leukemia. *Frontiers in Oncology*. 9 (10).
- Cidonio, G., Cooke, M., Glinka, M., Dawson, J. I., Grover, L., & Oreffo, R. O. C. (2019). Printing bone in a gel: using nanocomposite bioink to print functionalised bone scaffolds. *Materials Today Bio*. 4 (1).

- Clarisse, D., Offner, F., & De Bosscher, K. (2020). Latest perspectives on glucocorticoid-induced apoptosis and resistance in lymphoid malignancies. In *Biochimica et Biophysica Acta - Reviews on Cancer*. 1874 (2), p188430.
- Connarn, J. N., Zhang, X., Babiskin, A., & Sun, D. (2015). Metabolism of Bupropion by carbonyl reductases in liver and intestine. *Drug Metabolism and Disposition*. 43 (7), p1019–1027.
- Cordeiro-Spinetti, E., Taichman, R. S., Balduino, A. (2015). The bone marrow endosteal niche: how far from the surface?. *Journal of Cell Biochemistry*. 116 (1), p6-11.
- Corvi, R., Madia, F. (2017). In vitro genotoxicity testing. Can the performance be enhanced? *Food and Chemical Toxicology*. 106 (1), p600-608.
- Czarna, A., Sanada, F., Matsuda, A., Kim, J., Signore, S., Pereira, J. D., Sorrentino, A., Kannappan, R., Cannatà, A., Hosoda, T., Rota, M., Crea, F., Anversa, P., & Leri, A. (2017). Single-cell analysis of the fate of c-kit-positive bone marrow cells. *Npj Regenerative Medicine*. 2 (1), p1–15.
- Davis, A. J., & Chen, D. J. (2013). DNA double strand break repair via non-homologous end-joining. In *Translational Cancer Research*. 2 (3), p130–143.
- Deans, A. J., & West, S. C. (2011). DNA interstrand crosslink repair and cancer. In *Nature Reviews Cancer*. 11 (7), p467–480.
- Deng, X., Yang, X., Cheng, Y., Liu, X., Li, X., Zhao, R., Qin, C., Lu, Q., & Yin, C. (2015). GSTP1 and GSTO1 single nucleotide polymorphisms and the response of bladder cancer patients to intravesical chemotherapy. *Scientific Reports*. 5 (1), p14000.
- Desjardins, P., & Conklin, D. (2010). NanoDrop microvolume quantitation of nucleic acids. *Journal of Visualized Experiments*. 45 (1).
- DesRochers, T. M., Kimmerling, E. P., Jandhyala, D. M., El-Jouni, W., Zhou, J., Thorpe, C. M., Leong, J. M., & Kaplan, D. L. (2015). Effects of Shiga toxin type 2 on a bioengineered three-dimensional model of human renal tissue. *Infection and Immunity*. 83 (1), p28–38.
- Deynoux, M., Sunter, N., Ducrocq, E., Dakik, H., Guibon, R., Burlaud-Gaillard, J., Brisson, L., Rouleux-Bonnin, F., le Nail, L. R., Hérault, O., Domenech, J., Roingeard, P., Fromont, G., & Mazurier, F. (2020). A comparative study of the capacity of mesenchymal stromal cell lines to form spheroids. *PLoS ONE*. 15 (6).
- Ding, L., Saunders, T. L., Enikolopov, G., Morrison, S. J. (2012). Endothelial and perivascular cells maintain haematopoietic stem cells. *Nature*. 481 (7382), p457-462.

- Doherty, A. T. (2012). The in vitro micronucleus assay. *Methods in Molecular Biology*. 817 (1), p121–141.
- Downes, D. J., Chonofsky, M., Tan, K., Pfannenstiel, B. T., Reck-Peterson, S. L., & Todd, R. B. (2014). Characterization of the mutagenic spectrum of 4-nitroquinoline 1-oxide (4NQO) in *Aspergillus nidulans* by whole genome sequencing. *G3: Genes, Genomes, Genetics*. 4 (12), p2483–2492.
- Draganov, D. I., Teiber, J. F., Speelman, A., Osawa, Y., Sunahara, R., & La Du, B. N. (2005). Human paraoxonases (PON1, PON2, and PON3) are lactonases with overlapping and distinct substrate specificities. *Journal of Lipid Research*. 46 (6), p1239–1247.
- Duarte, D., Hawkins, E. D., & Lo Celso, C. (2018). The interplay of leukemia cells and the bone marrow microenvironment. In *Blood*. 131 (14), p1507–1511.
- Duong, J. K., Veal, G. J., Nath, C. E., Shaw, P. J., Errington, J., Ladenstein, R., & Boddy, A. V. (2019). Population pharmacokinetics of carboplatin, etoposide and melphalan in children: a re-evaluation of paediatric dosing formulas for carboplatin in patients with normal or mild impairment of renal function. *British Journal of Clinical Pharmacology*. 85 (1), p136–146.
- Duque-Fernandez, A., Gauthier, L., Simard, M., Jean, J., Gendreau, I., Morin, A., Soucy, J., Auger, M., & Pouliot, R. (2016). A 3D-psoriatic skin model for dermatological testing: The impact of culture conditions. *Biochemistry and Biophysics Reports*. 8 (1), p268–276.
- Duval, K., Grover, H., Han, L. H., Mou, Y., Pegoraro, A. F., Fredberg, J., & Chen, Z. (2017). Modeling physiological events in 2D vs. 3D cell culture. In *Physiology*. 32 (4), p266–277.
- Edmondson, R., Broglie, J. J., Adcock, A. F., Yang, L. (2014). Three-Dimensional Cell Culture Systems and Their Applications in Drug Discovery and Cell-Based Biosensors. *ASSAY AND DRUG DEVELOPMENT TECHNOLOGIES*. 12 (4), p207-218.
- Elango, J., Saravanakumar, K., Rahman, S. U., Henrotin, Y., Regenstein, J. M., Wu, W., & Bao, B. (2019). Chitosan-collagen 3d matrix mimics trabecular bone and regulates rankl-mediated paracrine cues of differentiated osteoblast and mesenchymal stem cells for bone marrow macrophage-derived osteoclastogenesis. *Biomolecules*. 9 (5).
- Emmons, R., Niemiro, G. M., Owolabi, O., & De Lisio, M. (2016). Acute exercise mobilizes hematopoietic stem and progenitor cells and alters the mesenchymal stromal cell secretome. *Journal of Applied Physiology*. 120 (6), p624–632.

- Encalada-Diaz, I., Cole, B. J., MacGillivray, J. D., Ruiz-Suarez, M., Kercher, J. S., Friel, N. A., & Valero-Gonzalez, F. (2011). Rotator cuff repair augmentation using a novel polycarbonate polyurethane patch: Preliminary results at 12 months' follow-up. *Journal of Shoulder and Elbow Surgery*. 20 (5), p788–794.
- Eustermann, S., Wu, W. F., Langelier, M. F., Yang, J. C., Easton, L. E., Riccio, A. A., Pascal, J. M., & Neuhaus, D. (2015). Structural Basis of Detection and Signaling of DNA Single-Strand Breaks by Human PARP-1. *Molecular Cell*. 60 (5), p742–754.
- Ewa, B., & Danuta, M. Š. (2017). Polycyclic aromatic hydrocarbons and PAH-related DNA adducts. In *Journal of Applied Genetics*. 58 (3), p321–330.
- Fairfield, H., Falank, C., Farrell, M., Vary, C., Boucher, J. M., Driscoll, H., Liaw, L., Rosen, C. J., & Reagan, M. R. (2019). Development of a 3D bone marrow adipose tissue model. *Bone*. 118 (1), p77–88.
- Fang, P., Tang, P. F., Xu, R. A., Zheng, X., Wen, J., Bao, S. S., Cai, J. P., & Hu, G. X. (2017). Functional assessment of CYP3A4 allelic variants on lidocaine metabolism in vitro. *Drug Design, Development and Therapy*. 11 (1), p3503–3510.
- Fang, Y. P., Hu, P. Y., & Huang, Y. Bin. (2018). Diminishing the side effect of mitomycin c by using ph-sensitive liposomes: In vitro characterization and in vivo pharmacokinetics. *Drug Design, Development and Therapy*. 12 (1), p159–169.
- Fellows, M. D., O'Donovan, M. R., Lorge, E., & Kirkland, D. (2008). Comparison of different methods for an accurate assessment of cytotoxicity in the in vitro micronucleus test. II: Practical aspects with toxic agents. *Mutation Research - Genetic Toxicology and Environmental Mutagenesis*. 655 (1–2), p4–21.
- Fenech, M., Chang, W. P., Kirsch-Volders, M., Holland, N., Bonassi, S., & Zeiger, E. (2003). HUMN project: Detailed description of the scoring criteria for the cytokinesis-block micronucleus assay using isolated human lymphocyte cultures. *Mutation Research - Genetic Toxicology and Environmental Mutagenesis*. 534 (1–2), p65–75.
- Fennema, E., Rivron, N., Rouwkema, J., Blitterswijk, C. V., Boer, J. D. (2013). Spheroid culture as a tool for creating 3D complex tissues. *Cell Press*. 31 (2), p108–115.
- Finch, A., & Pillans, P. (2014). P-glycoprotein and its role in drug-drug interactions. *Australian Prescriber*. 37 (4), p137–139.
- Firth, A. L., & Yuan, J. X. J. (2012). Identification of functional progenitor cells in the pulmonary vasculature. *Pulmonary Circulation*. 2 (1), p84–100.
- Fizeşan, I., Cambier, S., Moschini, E., Chary, A., Nelissen, I., Ziebel, J., Audinot, J. N., Wirtz, T., Kruszewski, M., Pop, A., Kiss, B., Serchi, T., Loghin, F., & Gutleb, A.

- C. (2019). In vitro exposure of a 3D-tetraculture representative for the alveolar barrier at the air-liquid interface to silver particles and nanowires. *Particle and Fibre Toxicology*. 16 (1).
- Fontoura, J. C., Viezzer, C., dos Santos, F. G., Ligabue, R. A., Weinlich, R., Puga, R. D., Antonow, D., Severino, P., & Bonorino, C. (2020). Comparison of 2D and 3D cell culture models for cell growth, gene expression and drug resistance. *Materials Science and Engineering C*. 107 (1), p110264.
- Foster, B. M., Zaidi, D., Young, T. R., Mobley, M. E., & Kerr, B. A. (2018). CD117/c-kit in cancer stem cell-mediated progression and therapeutic resistance. In *Biomedicines*. 6 (1).
- Ganesan, S., & Keating, A. F. (2015). Phosphoramidate mustard exposure induces DNA adduct formation and the DNA damage repair response in rat ovarian granulosa cells. *Toxicology and Applied Pharmacology*. 282 (3), p252–258.
- García-Cuesta, E. M., Santiago, C. A., Vallejo-Díaz, J., Juarranz, Y., Rodríguez-Frade, J. M., & Mellado, M. (2019). The Role of the CXCL12/CXCR4/ACKR3 Axis in Autoimmune Diseases. In *Frontiers in Endocrinology*. 10 (1), p585.
- Gerson, S. L., Caimi, P. F., William, B. M., & Creger, R. J. (2018). Pharmacology and Molecular Mechanisms of Antineoplastic Agents for Hematologic Malignancies. In *Hematology: Basic Principles and Practice*. 1 (1), p849–912.
- Gniesmer, S., Brehm, R., Hoffmann, A., de Cassan, D., Menzel, H., Hoheisel, A. L., Glasmacher, B., Willbold, E., Reifenrath, J., Wellmann, M., Ludwig, N., Tavassol, F., Zimmerer, R., Gellrich, N. C., & Kampmann, A. (2019). In vivo analysis of vascularization and biocompatibility of electrospun polycaprolactone fibre mats in the rat femur chamber. *Journal of Tissue Engineering and Regenerative Medicine*. 13 (7), p1190–1202.
- Godugu, C., & Singh, M. (2016). Algimatrix™-based 3d cell culture system as an in vitro tumor model: An important tool in cancer research. In *Methods in Molecular Biology*. 1379 (1), p117–128.
- Gollapudi, P., Bhat, V. S., & Eastmond, D. A. (2019). Concentration-response studies of the chromosome-damaging effects of topoisomerase II inhibitors determined in vitro using human TK6 cells. *Mutation Research - Genetic Toxicology and Environmental Mutagenesis*, 841 (1), p49–56.
- Gomariz, A., Helbling, P. M., Isringhausen, S., Suessbier, U., Becker, A., Boss, A., Nagasawa, T., Paul, G., Goksel, O., Székely, G., Stoma, S., Nørrelykke, S. F., Manz, M. G., & Nombela-Arrieta, C. (2018). Quantitative spatial analysis of

- haematopoiesis-regulating stromal cells in the bone marrow microenvironment by 3D microscopy. *Nature Communications*. 9 (1), p1–15.
- González-García, S., García-Peydró, M., Alcain, J., & Toribio, M. L. (2012). *Notch1 and IL-7 Receptor Signalling in Early T-cell Development and Leukaemia*. 1 (1), p47–73.
- Grijalvo, S., Nieto-Díaz, M., Maza, R. M., Eritja, R., & Díaz, D. D. (2019). Alginate Hydrogels as Scaffolds and Delivery Systems to Repair the Damaged Spinal Cord. In *Biotechnology Journal*. 14 (12).
- Gruppetta, M., Formosa, R., Falzon, S., Ariff Scicluna, S., Falzon, E., Degeatano, J., & Vassallo, J. (2017). Expression of cell cycle regulators and biomarkers of proliferation and regrowth in human pituitary adenomas. *Pituitary*. 20 (3), p358–371.
- Guadagni, S., Fiorentini, G., Clementi, M., Palumbo, P., Mambrini, A., & Masedu, F. (2017). Mitomycin C hypoxic pelvic perfusion for unresectable recurrent rectal cancer: Pharmacokinetic comparison of surgical and percutaneous techniques. *Updates in Surgery*. 69 (3), p403–410.
- Gupta, N., & Mayer, D. (2013). Interaction of JAK with steroid receptor function. *JAK-STAT*. 2 (4), p24911.
- Gupte, M. J., Swanson, W. B., Hu, J., Jin, X., Ma, H., Zhang, Z., Liu, Z., Feng, K., Feng, G., Xiao, G., Hatch, N., Mishina, Y., & Ma, P. X. (2018). Pore size directs bone marrow stromal cell fate and tissue regeneration in nanofibrous macroporous scaffolds by mediating vascularization. *Acta Biomaterialia*. 82 (1), p1–11.
- Gurioli, G., Martignano, F., Salvi, S., Costantini, M., Gunelli, R., & Casadio, V. (2018). GSTP1 methylation in cancer: A liquid biopsy biomarker? In *Clinical Chemistry and Laboratory Medicine*. 56 (5), p705–717.
- Ham, J., Lever, L., Fox, M., & Reagan, M. R. (2019). In Vitro 3D Cultures to Reproduce the Bone Marrow Niche. *JBMR Plus*. 3 (10).
- Han, N., Li, Z., Cai, Z., Yan, Z., Hua, Y., & Xu, C. (2016). P-glycoprotein overexpression in bone marrow-derived multipotent stromal cells decreases the risk of steroid-induced osteonecrosis in the femoral head. *Journal of Cellular and Molecular Medicine*. 20 (11), p2173–2182.
- Hardonnière, K., Saunier, E., Lemarié, A., Fernier, M., Gallais, I., Héliers-Toussaint, C., Mograbi, B., Antonio, S., Bénit, P., Rustin, P., Janin, M., Habarou, F., Ottolenghi, C., Lavault, M. T., Benelli, C., Sergent, O., Huc, L., Bortoli, S., & Lagadic-Gossmann, D. (2016). The environmental carcinogen benzo[a]pyrene induces a

- Warburg-like metabolic reprogramming dependent on NHE1 and associated with cell survival. *Scientific Reports*. 6 (1), p1–13.
- Hardouin, P., Pansini, V., Cortet, B. (2014). Bone Marrow Fat. *Joint Bone Spine*. 81 (4), p313-319.
- Hashimoto, K., Nakajima, Y., Uematsu, R., & Chatani, F. (2012). Difference in susceptibility to morphological changes in the nucleus to aneuploids between p53-competent and p53-abrogated lymphoblastoid cell lines (TK6 and NH32 cells) in the in vitro micronucleus assay. *Mutagenesis*. 27 (3), p287–293.
- Hassan, H. M., Yousef, B. A., Guo, H., Xiaoxin, L., Zhang, L., & Jiang, Z. (2018). Investigating the CYP2E1 potential role in the mechanisms behind INH/LPS-induced hepatotoxicity. *Frontiers in Pharmacology*. 9 (1).
- Hasselgren, C., Ahlberg, E., Akahori, Y., Amberg, A., Anger, L. T., Atienzar, F., Auerbach, S., Beilke, L., Bellion, P., Benigni, R., Bercu, J., Booth, E. D., Bower, D., Brigo, A., Cammerer, Z., Cronin, M. T. D., Crooks, I., Cross, K. P., Custer, L., ... Myatt, G. J. (2019). Genetic toxicology in silico protocol. *Regulatory Toxicology and Pharmacology*. 107 (1), p104403.
- Hayashi, M. (2016). The micronucleus test-most widely used in vivo genotoxicity test. In *Genes and Environment*. 38 (1).
- Hayes, J. E., Doherty, A. T., Coulson, M., Foster, J. R., Cotton, P. T., O'Donovan, M. R. (2013). Micronucleus induction in the bone marrow of rats by pharmacological mechanisms. I: glucocorticoid receptor agonism. *Mutagenesis*. 28 (2), p227-232.
- Heard, P., Ackerman, J., Coffing, S., Dobo, K., & Schuler, M. (2017). Fluorescent tubulin polymerization assay to characterize moa of genotoxic compounds — A validation study. *Journal of Pharmacological and Toxicological Methods*. 85 (1), p89.
- Heidel, S. M., Czuprynski, C. J., & Jefcoate, C. R. (1998). Bone marrow stromal cells constitutively express high levels of cytochrome P4501b1 that metabolize 7,12-dimethylbenz[a]anthracene. *Molecular Pharmacology*. 54 (6), p1000–1006.
- Hernández-González, A. C., Téllez-Jurado, L., & Rodríguez-Lorenzo, L. M. (2020). Alginate hydrogels for bone tissue engineering, from injectables to bioprinting: A review. In *Carbohydrate Polymers*. 229 (1), p115514.
- Highley, M. S., Harper, B., Harper, P. G., Dumez, H., Guetens, G., De Boeck, G., Prenen, H., Schrijvers, D., Maes, R. A. A., & De Bruijn, E. A. (2006). The pharmacokinetics of mitomycin C in the mitomycin C, ifosfamide and cisplatin (MIC) regimen. *International Journal of Pharmacology*. 2 (3), p293–297.

- Hintzsche, H., Montag, G., & Stopper, H. (2018). Induction of micronuclei by four cytostatic compounds in human hematopoietic stem cells and human lymphoblastoid TK6 cells. *Scientific Reports*. 8 (1).
- Ho, C. C. M., Chhabra, A., Starkl, P., Schnorr, P. J., Wilmes, S., Moraga, I., Kwon, H. S., Gaudenzio, N., Sibilano, R., Wehrman, T. S., Gakovic, M., Sockolosky, J. T., Tiffany, M. R., Ring, A. M., Piehler, J., Weissman, I. L., Galli, S. J., Shizuru, J. A., & Garcia, K. C. (2017). Decoupling the Functional Pleiotropy of Stem Cell Factor by Tuning c-Kit Signaling. *Cell*. 168 (6), p1041-1052.
- Hoch, A. I., Duhr, R., Di Maggio, N., Mehrkens, A., Jakob, M., & Wendt, D. (2017). Expansion of Bone Marrow Mesenchymal Stromal Cells in Perfused 3D Ceramic Scaffolds Enhances In Vivo Bone Formation. *Biotechnology Journal*. 12 (12).
- Hornberg, J. J., Laursen, M., Brendoen, N., Persson, M., Thougarrd, A. V., Toft, D. B., Mow, T. (2014). Exploratory toxicology as an intergrated part of drug discovery. Part I: Why and how. *Drug Discovery Today*. 19 (8), p1131-1136.
- Huang, Q. M., Zeng, Y. M., Zhang, H. P., Lv, L. C., Yang, D. Y., & Lin, H. H. (2016). 4-Nitroquinoline-1-oxide effects human lung adenocarcinoma A549 cells by regulating the expression of POLD4. *Biomedical Reports*. 4 (3), p345–348.
- Huang, X., Zhu, B., Wang, X., Xiao, R., & Wang, C. (2016). Three-dimensional co-culture of mesenchymal stromal cells and differentiated osteoblasts on human bio-derived bone scaffolds supports active multi-lineage hematopoiesis in vitro: Functional implication of the biomimetic HSC niche. *International Journal of Molecular Medicine*. 38 (4), p1141–1151.
- Huh, D., Hamilton, G. A., & Ingber, D. E. (2011). From 3D cell culture to organs-on-chips. In *Trends in Cell Biology*. 21 (12), p745–754.
- Hýzďalová, M., Pivnicka, J., Zapletal, O., Vázquez-Gómez, G., Matthews, J., Neca, J., Pencíková, K., MacHala, M., & Vondráček, J. (2018). Aryl Hydrocarbon Receptor-Dependent Metabolism Plays a Significant Role in Estrogen-Like Effects of Polycyclic Aromatic Hydrocarbons on Cell Proliferation. *Toxicological Sciences*. 165 (2), p447–461.
- ICH S9 Guidance on genotoxicity testing and data interpretation for pharmaceuticals intended for human use. Step 4. International Conference on Harmonisation. 29 October 2009. Available from:
http://www.ich.org/fileadmin/Public_Web_Site/ICH_Products/Guidelines/Safety/S9/Step4/S9_Step4_Guideline.pdf [Accessed 1 May 2020]

- Inglis, S., Kanczler, J. M., & Oreffo, R. O. C. (2019). 3D human bone marrow stromal and endothelial cell spheres promote bone healing in an osteogenic niche. *FASEB Journal*. 33 (3), p3279–3290.
- Izzo, L., Tunesi, M., Boeri, L., Laganà, M., Giordano, C., & Raimondi, M. T. (2019). Influence of the static magnetic field on cell response in a miniaturized optically accessible bioreactor for 3D cell culture. *Biomedical Microdevices*. 21 (1), p29.
- Jagannathan-Bogdan, M., & Zon, L. I. (2013). Hematopoiesis. *Development (Cambridge)*. 140 (12), p2463–2467.
- Jancova, P., Anzenbacher, P., & Anzenbacherova, E. (2010). Phase II drug metabolizing enzymes. *Biomedical Papers*. 154 (2), p103–116.
- Janssens, R., Struyf, S., & Proost, P. (2018). The unique structural and functional features of CXCL12. In *Cellular and Molecular Immunology*. 15 (4), p299–311.
- Jaroch, K., Jaroch, A., & Bojko, B. (2018). Cell cultures in drug discovery and development: The need of reliable in vitro-in vivo extrapolation for pharmacodynamics and pharmacokinetics assessment. In *Journal of Pharmaceutical and Biomedical Analysis*. 147 (1), p297–312.
- Jensen, C., & Teng, Y. (2020). Is It Time to Start Transitioning From 2D to 3D Cell Culture? In *Frontiers in Molecular Biosciences*. 7 (1), p33.
- Jeong, J. A., Ko, K.-M., Bae, S., Jeon, C.-J., Koh, G. Y., & Kim, H. (2009). Genome-Wide Differential Gene Expression Profiling of Human Bone Marrow Stromal Cells. *Stem Cells*. 25 (4), p994–1002.
- Jia, W., Gungor-Ozkerim, P. S., Zhang, Y. S., Yue, K., Zhu, K., Liu, W., Pi, Q., Byambaa, B., Dokmeci, M. R., Shin, S. R., & Khademhosseini, A. (2016). Direct 3D bioprinting of perfusable vascular constructs using a blend bioink. *Biomaterials*. 106 (1), p58–68.
- Jia, W., Jiang, X., Liu, W., Wang, L., Zhu, B., Zhu, H., Liu, X., Zhong, M., Xie, D., Huang, W., Jia, W., Li, S., Liu, X., Zuo, X., Cheng, D., Dai, J., & Ren, C. (2018). Effects of three-dimensional collagen scaffolds on the expression profiles and biological functions of glioma cells. *International Journal of Oncology*. 52 (6), p1787–1800.
- Jobe, A. H., Milad, M. A., Peppard, T., & Jusko, W. J. (2020). Pharmacokinetics and Pharmacodynamics of Intramuscular and Oral Betamethasone and Dexamethasone in Reproductive Age Women in India. *Clinical and Translational Science*. 13 (2), p391–399.

- Johnson, L. A., Malayappan, B., Tretyakova, N., Campbell, C., Macmillan, M. L., Wagner, J. E., & Jacobson, P. A. (2012). Formation of cyclophosphamide specific DNA adducts in hematological diseases. *Pediatric Blood and Cancer*. 58 (5), p708–714.
- Juríková, M., Danihel, L., Polák, Š., & Varga, I. (2016). Ki67, PCNA, and MCM proteins: Markers of proliferation in the diagnosis of breast cancer. In *Acta Histochemica*. 118 (5), p544–552.
- kabrah, S. M., May, J., Morse, R., & Donaldson, C. (2016). 3D culture of human bone marrow mesenchymal stem cells protects from genotoxic effects of melphalan exposure. *Mutagenesis*. 31 (6).
- Kalinina, N. I., Sysoeva, V. Y., Rubina, K. A., Parfenova, Y. V., & Tkachuk, V. A. (2011). Mesenchymal Stem Cells in Tissue Growth and Repair. *Acta Naturae*. 3 (4), p30–37.
- Kameyama, T., Ohuchi, K., Funato, M., Ando, S., Inagaki, S., Sato, A., Seki, J., Kawase, C., Tsuruma, K., Nishino, I., Nakamura, S., Shimazawa, M., Saito, T., Takeda, S., Kaneko, H., & Hara, H. (2018). Efficacy of prednisolone in generated myotubes derived from fibroblasts of duchenne muscular dystrophy patients. *Frontiers in Pharmacology*. 9 (1).
- Kapałczyńska, M., Kolenda, T., Przybyła, W., Zajączkowska, M., Teresiak, A., Filas, V., Ibbs, M., Bliźniak, R., Łuczewski, Ł., & Lamperska, K. (2018). 2D and 3D cell cultures – a comparison of different types of cancer cell cultures. *Archives of Medical Science*. 14 (4), p910–919.
- Karampinos, D. C., Ruschke, S., Dieckmeyer, M., Diefenbach, M., Franz, D., Gersing, A. S., Krug, R., & Baum, T. (2018). Quantitative MRI and spectroscopy of bone marrow. In *Journal of Magnetic Resonance Imaging*. 47 (2), p332–353.
- Karimpoor, M., Yebra-Fernandez, E., Parhizkar, M., Craig, D., Khorashad, J. S., & Edirisinghe, M. (2018). Alginate foam-based three-dimensional culture to investigate drug sensitivity in primary leukaemia cells. *Interface*. 15 (1).
- Kaur, G., & Dufour, J. M. (2012). Cell lines. *Spermatogenesis*. 2 (1), p1–5.
- Khurshid, M., Mulet-Sierra, A., Adesida, A., & Sen, A. (2018). Osteoarthritic human chondrocytes proliferate in 3D co-culture with mesenchymal stem cells in suspension bioreactors. *Journal of Tissue Engineering and Regenerative Medicine*. 12 (3), p1418–1432.
- Kim, M. J., Chi, B. H., Yoo, J. J., Ju, Y. M., Whang, Y. M., & Chang, I. H. (2019). Structure establishment of three-dimensional (3D) cell culture printing model for bladder cancer. *PLOS ONE*. 14 (10), p223689.

- Kimura, H., Sakai, Y., & Fujii, T. (2018). Organ/body-on-a-chip based on microfluidic technology for drug discovery. In *Drug Metabolism and Pharmacokinetics*. 33 (1), p43–48.
- King, K. Y., & Goodell, M. A. (2011). Inflammatory modulation of HSCs: Viewing the HSC as a foundation for the immune response. In *Nature Reviews Immunology*. 11 (10), p685–692.
- Kishi, S., Yang, W., Boureau, B., Morand, S., Das, S., Chen, P., Cook, E. H., Rosner, G. L., Schuetz, E., Pui, C. H., & Relling, M. V. (2004). Effects of prednisone and genetic polymorphisms on etoposide disposition in children with acute lymphoblastic leukemia. *Blood*, 103 (1), p67–72.
- Kishino, Y., Hasegawa, T., Arakawa, S., Shibaya, Y., Yamoto, T., & Mori, K. (2019). Effect of the metabolic capacity in rat liver s9 on the positive results of in vitro micronucleus tests. *Journal of Toxicological Sciences*. 44 (3), p145–153.
- Kishino, Y., Hasegawa, T., Yamoto, T., & Mori, K. (2019). Species differences in micronucleus induction of the clastogenic compounds associated with drug metabolic profile. *Journal of Toxicological Sciences*. 44 (10), p701–709.
- Knight, E., & Przyborski, S. (2015). Advances in 3D cell culture technologies enabling tissue-like structures to be created in vitro. In *Journal of Anatomy*. 227 (6), p746–756.
- Koivisto, J. T., Gering, C., Karvinen, J., Maria Cherian, R., Belay, B., Hyttinen, J., Aalto-Setälä, K., Kellomäki, M., & Parraga, J. (2019). Mechanically Biomimetic Gelatin-Gellan Gum Hydrogels for 3D Culture of Beating Human Cardiomyocytes. *ACS Applied Materials and Interfaces*. 11 (23).
- Koski, C., Onuiké, B., Bandyopadhyay, A., & Bose, S. (2018). Starch-hydroxyapatite composite bone scaffold fabrication utilizing a slurry extrusion-based solid freeform fabricator. *Additive Manufacturing*. 24 (1), p47–59.
- Kosol, W., Kumar, S., Marrero-Berríos, I., & Berthiaume, F. (2020). Medium conditioned by human mesenchymal stromal cells reverses low serum and hypoxia-induced inhibition of wound closure. *Biochemical and Biophysical Research Communications*. 522 (2), p335–341.
- Koutsilieris, S., Tzioufa, F., Sismanoglou, D. C., & Patrinos, G. P. (2020). Unveiling the guidance heterogeneity for genome-informed drug treatment interventions among regulatory bodies and research consortia. *Pharmacological Research*. 153 (1).

- Kowalski, K., Dos Santos, M., Maire, P., Ciemerych, M. A., & Brzoska, E. (2018). Induction of bone marrow-derived cells myogenic identity by their interactions with the satellite cell niche. *Stem Cell Research and Therapy*. 9 (1).
- Kozyra, M., Johansson, I., Nordling, Å., Ullah, S., Lauschke, V. M., & Ingelman-Sundberg, M. (2018). Human hepatic 3D spheroids as a model for steatosis and insulin resistance. *Scientific Reports*. 8 (1).
- Krüger, C. T., Hofmann, M., & Hartwig, A. (2015). The in vitro PIG-A gene mutation assay: mutagenicity testing via flow cytometry based on the glycosylphosphatidylinositol (GPI) status of TK6 cells. *Archives of Toxicology*. 89 (12), p2429–2443.
- Kumar, B., Garcia, M., Weng, L., Jung, X., Murakami, J. L., Hu, X., McDonald, T., Lin, A., Kumar, A. R., Digiusto, D. L., Stein, A. S., Pullarkat, V. A., Hui, S. K., Carlesso, N., Kuo, Y. H., Bhatia, R., Marcucci, G., & Chen, C. C. (2018). Acute myeloid leukemia transforms the bone marrow niche into a leukemia-permissive microenvironment through exosome secretion. *Leukemia*. 32 (3), p575–587.
- Kurauchi, K., Nishikawa, T., Miyahara, E., Okamoto, Y., & Kawano, Y. (2017). Role of metabolites of cyclophosphamide in cardiotoxicity. *BMC Research Notes*. 10 (1), p406.
- Kutscher, H. L., Morse, G. D., Prasad, P. N., & Reynolds, J. L. (2019). In vitro Pharmacokinetic Cell Culture System that Simulates Physiologic Drug and Nanoparticle Exposure to Macrophages. *Pharmaceutical Research*. 36 (3), p44.
- LaBonia, G. J., Lockwood, S. Y., Heller, A. A., Spence, D. M., & Hummon, A. B. (2016). Drug penetration and metabolism in 3D cell cultures treated in a 3D printed fluidic device: assessment of irinotecan via MALDI imaging mass spectrometry. *Proteomics*. 16 (11–12), p1814–1821.
- Langhans, S. A. (2018). Three-dimensional in vitro cell culture models in drug discovery and drug repositioning. In *Frontiers in Pharmacology*. 9 (1), p.6.
- Lee, G. E., & Shin, C. G. (2018). Influence of pretreatment with immunosuppressive drugs on viral proliferation. *Journal of Microbiology and Biotechnology*. 28 (10), p1716–1722.
- Lee, J. E., Lee, J., Kim, J. H., Cho, N., Lee, S. H., Park, S. B., Koh, B., Kang, D., Kim, S., & Yoo, H. M. (2019). Characterization of the anti-cancer activity of the probiotic bacterium *Lactobacillus fermentum* using 2D vs. 3D culture in colorectal cancer cells. *Biomolecules*. 9 (10).

- Lee, J. Y., & Hong, S.-H. (2019). Hematopoietic Stem Cells and Their Roles in Tissue Regeneration. *International Journal of Stem Cells*. 13 (1), p1–12.
- Lee, J.-H., Kim, S.-K., Khawar, I. A., Jeong, S.-Y., Chung, S., & Kuh, H.-J. (2018). Microfluidic co-culture of pancreatic tumor spheroids with stellate cells as a novel 3D model for investigation of stroma-mediated cell motility and drug resistance. *Journal of Experimental & Clinical Cancer Research*. 37 (1), p4.
- Lee, Y., Arai, Y., Ahn, J., Kim, D., Oh, S., Kang, D., Lee, H., Moon, J. J., Choi, B., & Lee, S. H. (2019). Three-dimensional microenvironmental priming of human mesenchymal stem cells in hydrogels facilitates efficient and rapid retroviral gene transduction via accelerated cell cycle synchronization. *NPG Asia Materials*. 11 (1), p1–11.
- Lemaire, M., Deleu, S., De Bruyne, E., Van Valckenborgh, E., Menu, E., & Vanderkerken, K. (2011). The Microenvironment and Molecular Biology of the Multiple Myeloma Tumor. In *Advances in Cancer Research*. 110 (1), p19–42.
- Leonard, A., Yapundich, M., Nassehi, T., Gamer, J., Drysdale, C. M., Haro-Mora, J. J., Demirci, S., Hsieh, M. M., Uchida, N., & Tisdale, J. F. (2019). Low-Dose Busulfan Reduces Human CD34+ Cell Doses Required for Engraftment in c-kit Mutant Immunodeficient Mice. *Molecular Therapy - Methods & Clinical Development*. 15 (1), p430–437.
- Lev, A., Deihimi, S., Shagisultanova, E., Xiu, J., Lulla, A. R., Dicker, D. T., & El-Deiry, W. S. (2017). Preclinical rationale for combination of crizotinib with mitomycin C for the treatment of advanced colorectal cancer. *Cancer Biology and Therapy*. 18 (9), p694–704.
- Li, D. W., He, F. L., He, J., Deng, X., Liu, Y. L., Liu, Y. Y., Ye, Y. J., & Yin, D. C. (2017). From 2D to 3D: The morphology, proliferation and differentiation of MC3T3-E1 on silk fibroin/chitosan matrices. *Carbohydrate Polymers*. 178 (1), p69–77.
- Li, J., Chen, R., Yao, Q. Y., Liu, S. J., Tian, X. Y., Hao, C. Y., Lu, W., & Zhou, T. Y. (2018). Time-dependent pharmacokinetics of dexamethasone and its efficacy in human breast cancer xenograft mice: A semi-mechanism-based pharmacokinetic/pharmacodynamic model. *Acta Pharmacologica Sinica*. 39 (3), p472–481.
- Li, K., Wu, D., Chen, X., Zhang, T., Zhang, L., Yi, Y., Miao, Z., Jin, N., Bi, X., Wang, H., Xu, J., & Wang, D. (2014). Current and Emerging Biomarkers of Cell Death in Human Disease. *BioMed Research International*. 2014 (1).

- Li, X., Wan, T., Zhang, S., Li, D., & Han, X. (2016). Quantitative proteomic analysis and comparison of two bone marrow stromal cell lines using the SILAC method. *Experimental Hematology*. 44 (11), p1059–1071.
- Li, Y. F., Zhang, C., Zhou, S., He, M., Zhang, H., Chen, N., Li, F., Luan, X., Pai, M., Yuan, H., Sun, D., & Li, Y. (2018). Species difference in paclitaxel disposition correlated with poor pharmacological efficacy translation from mice to humans. *Clinical Pharmacology: Advances and Applications*. 10 (1), p165–174.
- Li, Y., Yuan, H., Yang, K., Xu, W., Tang, W., & Li, X. (2010). The Structure and Functions of P-Glycoprotein. *Current Medicinal Chemistry*. 17 (8), p786–800.
- Li, Z., & MacDougald, O. A. (2019). Stem cell factor: The bridge between bone marrow adipocytes and hematopoietic cells. In *Haematologica*. 104 (9), p1689–1691.
- Liamin, M., Boutet-Robinet, E., Jamin, E. L., Fernier, M., Khoury, L., Kopp, B., Le Ferrec, E., Vignard, J., Audebert, M., & Sparfel, L. (2017). Benzo[a]pyrene-induced DNA damage associated with mutagenesis in primary human activated T lymphocytes. *Biochemical Pharmacology*. 137 (1), p113–124.
- Lim, J. A., & Kim, S. H. (2009). Transcriptional activation of an anti-oxidant mouse Pon2 gene by dexamethasone. *BMB Reports*. 42 (7), p421–426.
- Limongi, T., Dattola, E., Botta, C., Coluccio, M. L., Candeloro, P., Cucè, M., Scopacasa, B., Cantafio, M. E. G., Critello, C. D., Pullano, S. A., Fiorillo, A. S., Tagliaferri, P., Tassone, P., Lamanna, E., Di Fabrizio, E., & Perozziello, G. (2020). Influence of the fabrication accuracy of hot-embossed PCL scaffolds on cell growths. *Frontiers in Bioengineering and Biotechnology*. 8 (1).
- Lin, C. S., Xin, Z. C., Dai, J., & Lue, T. F. (2013). Commonly used mesenchymal stem cell markers and tracking labels: Limitations and challenges. In *Histology and Histopathology*. 28 (9), p1109–1116.
- Lin, R., Chang, H. (2008). Recent advances in three-dimensional multicellular spheroid culture for biomedical research. *Biotechnology Journal*. 3 (9-10), p1172-1184.
- Lockey, C., Otto, E., & Long, Z. (1998). Real-time fluorescence detection of a single DNA molecule. *BioTechniques*. 24 (5), p744–746.
- Long, H. yong, Huang, Q. X., Yu, Y. yang, Zhang, Z. bin, Yao, Z. wu, Chen, H. bing, & Feng, J. wei. (2019). Dehydrocostus lactone inhibits in vitro gastrinoma cancer cell growth through apoptosis induction, sub-G1 cell cycle arrest, DNA damage and loss of mitochondrial membrane potential. *Archives of Medical Science*. 15 (3), p765–773.

- Lundström, W., Fewkes, N. M., & Mackall, C. L. (2012). IL-7 in human health and disease. In *Seminars in Immunology*. 24 (3), p218–224.
- Lv, D., Hu, Z., Lu, L., Lu, H., & Xu, X. (2017). Three-dimensional cell culture: A powerful tool in tumor research and drug discovery. In *Oncology Letters*. 14 (6), p6999–7010.
- Ma, H., Zhang, Y., Wang, H., Han, C., Lei, R., Zhang, L., Yang, Z., Rao, L., Qing, H., Xiang, J., & Deng, Y. (2013). Effect and mechanism of mitomycin C combined with recombinant adeno-associated virus type II against glioma. *International Journal of Molecular Sciences* 15 (1), p1–14.
- Macallan, D. C., Busch, R., & Asquith, B. (2019). Current estimates of T cell kinetics in humans. In *Current Opinion in Systems Biology*. 18 (1), p77–86.
- Mader, R. M., Steger, G. G., Moser, K., Rainer, H., Krenmayer, P., & Dittrich, C. (1991). Instability of the anticancer agent etoposide under in vitro culture conditions. *Cancer Chemotherapy and Pharmacology*. 27 (5), p354–360.
- Magee, M. H., Blum, R. A., Lates, C. D., & Jusko, W. J. (2001). Prednisolone pharmacokinetics and pharmacodynamics in relation to sex and race. *Journal of Clinical Pharmacology*. 41 (11), p1180–1194.
- Maleki, M., Ghanbarvand, F., Behvarz, M. R., Ejtemaei, M., & Ghadirkhomi, E. (2014). Comparison of mesenchymal stem cell markers in multiple human adult stem cells. *International Journal of Stem Cells*. 7 (2), p118–126.
- Malkiewicz, A., Dziedzic, M. (2012). Bone marrow reconversion – imaging of physiological changes in bone marrow. *Polish Journal of Radiology*. 77 (4), p45–50.
- Manzella, C., Singhal, M., Alrefai, W. A., Saksena, S., Dudeja, P. K., & Gill, R. K. (2018). Serotonin is an endogenous regulator of intestinal CYP1A1 via AhR. *Scientific Reports* 8 (1).
- Marinus, M. G. (2012). DNA Mismatch Repair. *EcoSal Plus*. 5 (1).
- Marti, L. C., Bacal, N. S., Bento, L. C., & Rocha, F. A. (2017). Phenotypic Markers and Functional Regulators of Myelomonocytic Cells. In *Biology of Myelomonocytic Cells*. 1 (1)
- Mashima, R., & Okuyama, T. (2015). The role of lipoxygenases in pathophysiology; new insights and future perspectives. In *Redox Biology*. 6 (1), p297–310.
- Mathews Griner, L. A., Zhang, X., Guha, R., McKnight, C., Goldlust, I. S., Lal-Nag, M., Wilson, K., Michael, S., Titus, S., Shinn, P., Thomas, C. J., & Ferrer, M. (2016).

- Large-scale pharmacological profiling of 3D tumor models of cancer cells. *Cell Death and Disease*. 7 (12).
- May, J. E., Morse, H. R., Xu, J., & Donaldson, C. (2012). Development of a novel, physiologically relevant cytotoxicity model: Application to the study of chemotherapeutic damage to mesenchymal stromal cells. *Toxicology and Applied Pharmacology*. 263 (3), p374–389.
- McDonnell, PharmD, BCOP, A. M., & Dang, PharmD, BCPS, C. H. (2013). Basic Review of the Cytochrome P450 System. *Journal of the Advanced Practitioner in Oncology*. 4 (4), p263.
- McKee, C., & Chaudhry, G. R. (2017). Advances and challenges in stem cell culture. In *Colloids and Surfaces B: Biointerfaces*. 159 (1), p62–77.
- McKenna, E., Traganos, F., Zhao, H., & Darzynkiewicz, Z. (2012). Persistent DNA damage caused by low levels of mitomycin C induces irreversible cell senescence. *Cell Cycle*. 11 (16).
- Mehta, A., Awah, C. U., & Sonabend, A. M. (2018). Topoisomerase II poisons for glioblastoma; Existing challenges and opportunities to personalize therapy. In *Frontiers in Neurology*. 9 (6), p.459.
- Menon, S. S., Guruvayoorappan, C., Sakthivel, K. M., & Rasmi, R. R. (2019). Ki-67 protein as a tumour proliferation marker. In *Clinica Chimica Acta*. 491(1), p39–45.
- Merlos Rodrigo, M. A., Jimenez Jimenez, A. M., Haddad, Y., Bodoor, K., Adam, P., Krizkova, S., Heger, Z., & Adam, V. (2020). Metallothionein isoforms as double agents – Their roles in carcinogenesis, cancer progression and chemoresistance. In *Drug Resistance Updates*. 52 (1), p100691.
- Miller, I., Min, M., Yang, C., Tian, C., Gookin, S., Carter, D., & Spencer, S. L. (2018). Ki67 is a Graded Rather than a Binary Marker of Proliferation versus Quiescence. *Cell Reports*. 24 (5), p1105-1112.
- Montecucco, A., Zanetta, F., & Biamonti, G. (2015). Molecular mechanisms of etoposide. *EXCLI Journal*. 14 (1), p95.
- Morikawa, S., Mabuchi, Y., Kubota, Y., Nagai, Y., Niibe, K., Hiratsu, E., Suzuki, S., Miyauchi-Hara, C., Nagoshi, N., Sunabori, T., Shimmura, S., Miyawaki, A., Nakagawa, T., Suda, T., Okano, H., & Matsuzaki, Y. (2009). Prospective identification, isolation, and systemic transplantation of multipotent mesenchymal stem cells in murine bone marrow. *Journal of Experimental Medicine*. 206 (11), p2483–2496.

- Mraz, M., Zent, C. S., Church, A. K., Jelinek, D. F., Wu, X., Pospisilova, S., Ansell, S. M., Novak, A. J., Kay, N. E., Witzig, T. E., Nowakowski, G. S. (2011). Bone Marrow Stromal Cells Protect Lymphoma B-cells from Rituximab-Induced Apoptosis and Targeting Integrin α 4- β 1 (VLA-4) with Natalizumab can Overcome this Resistance. *British Journal of Haematology*. 155 (1), p53-64.
- Nath, S., & Devi, G. R. (2016). Three-dimensional culture systems in cancer research: Focus on tumor spheroid model. In *Pharmacology and Therapeutics*. 163 (1), p94–108.
- Nath, S., & Devi, G. R. (2016). Three-dimensional culture systems in cancer research: Focus on tumor spheroid model. In *Pharmacology and Therapeutics*. 163 (1), p94–108.
- Nava-Salazar, S., Gómez-Manzo, S., Marcial-Quino, J., Marhx-Bracho, A., Phillips-Farfán, B. V., Diaz-Avalos, C., & Vanoye-Carlo, A. (2018). Effect of nicotine on CYP2B1 expression in a glioma animal model and analysis of CYP2B6 expression in pediatric gliomas. *International Journal of Molecular Sciences*. 19 (6).
- Nebert, D. W., & Vasiliou, V. (2004). Analysis of the glutathione S-transferase (GST) gene family. *Human Genomics*. 1 (6), p460–464.
- Nesslany, F. (2017). The current limitations of in vitro genotoxicity testing and their relevance to the in vivo situation. *Food and Chemical Toxicology*. 106 (B), p609–615.
- Ngo, L. P., Chan, T. K., Ge, J., Samson, L. D., & Engelward, B. P. (2019). Microcolony Size Distribution Assay Enables High-Throughput Cell Survival Quantitation. *Cell Reports*. 26 (6), p1668-1678.
- Nguyen-Ngoc, K. V., Shamir, E. R., Huebner, R. J., Beck, J. N., Cheung, K. J., & Ewald, A. J. (2014). 3D culture assays of murine mammary branching morphogenesis and epithelial invasion. In *Tissue Morphogenesis: Methods and Protocols*. 1189 (1), p135–162.
- Niikawa, M., Nakamura, T., & Nagase, H. (2001). Suppressive effect of aspirin on chromosome aberration induced by mitomycin C in mice. *Biological and Pharmaceutical Bulletin*. 24 (8), p964–966.
- Noh, K., Nepal, M. R., Jeong, K. S., Kim, S. A., Um, Y. J., Seo, C. S., Kang, M. J., Park, P. H., Kang, W., Hye Gwang, H. G., & Jeong, T. C. (2015). Effects of baicalin on oral pharmacokinetics of caffeine in rats. *Biomolecules and Therapeutics*. 23 (2), p201–206.

- Nombela-Arrieta, C., & Isringhausen, S. (2017). The role of the bone marrow stromal compartment in the hematopoietic response to microbial infections. In *Frontiers in Immunology*. 7 (1), p1.
- Nudischer, R., Renggli, K., Hierlemann, A., Roth, A. B., & Bertinetti-Lapatki, C. (2020). Characterization of a long-term mouse primary liver 3D tissue model recapitulating innate-immune responses and drug-induced liver toxicity. *PLOS ONE*. 15 (7).
- O'Connor, M. J. (2015). Targeting the DNA Damage Response in Cancer. In *Molecular Cell*. 60 (4), p547–560.
- OECD. (2017). Test No. 460: Fluorescein Leakage Test Method for Identifying Ocular Corrosives and Severe Irritants. *OECD Guidelines for the Testing of Chemicals*, October, 16.
- Oh, E. T., & Park, H. J. (2015). Implications of NQO1 in cancer therapy. In *BMB Reports*, 48 (11), p609–617.
- Ooka, M., Lynch, C., & Xia, M. (2020). Application of in vitro metabolism activation in high-throughput screening. In *International Journal of Molecular Sciences*. 21 (21), p1–16.
- Ostrem Loss, E. M., & Yu, J.-H. (2018). Bioremediation and microbial metabolism of benzo(a)pyrene. *Molecular Microbiology*. 109 (4), p433–444.
- Pan, X., Ning, M., & Jeong, H. (2017). Transcriptional regulation of CYP2D6 expression. In *Drug Metabolism and Disposition*. 45 (1), p42–48.
- Paragliola, R. M., Papi, G., Pontecorvi, A., & Corsello, S. M. (2017). Treatment with synthetic glucocorticoids and the hypothalamus-pituitary-adrenal axis. In *International Journal of Molecular Sciences*. 18 (10).
- Passos Cor, V., Rodrigues, G., Petit Teof, M., Carla Carn, L., Medeiros L, D., Karine Pae, H., de Oliveir, M., & Vieira de, A. (2017). Evaluation of the Mutagenic Potential of Glucocorticoids by *Allium cepa*. *Research Journal of Mutagenesis*. 7 (1), p1–7.
- Pastor, D. M., Poritz, L. S., Olson, T. L., Kline, C. L., Harris, L. R., Koltun, W. A., Chinchilli, V. M., & Irby, R. B. (2010). Primary cell lines: False representation or model system? A comparison of four human colorectal tumors and their coordinately established cell lines. *International Journal of Clinical and Experimental Medicine*. 3 (1), p69–83.
- Pepelanova, I., Kruppa, K., Scheper, T., & Lavrentieva, A. (2018). Gelatin-methacryloyl (GelMA) hydrogels with defined degree of functionalization as a versatile toolkit for 3D cell culture and extrusion bioprinting. *Bioengineering*. 5 (3).

- Pickup, K. E., Pardow, F., Carbonell-Caballero, J., Lioutas, A., Villanueva-Cañas, J. L., Wright, R. H. G., & Beato, M. (2019). Expression of oncogenic drivers in 3D cell culture depends on nuclear ATP synthesis by NUDT5. *Cancers*. 11 (9), p1337.
- Pires, E., Sung, P., & Wiese, C. (2017). Role of RAD51AP1 in homologous recombination DNA repair and carcinogenesis. In *DNA Repair*. 59 (1), p76–81.
- Podszywalow-Bartnicka, P., Kominek, A., Wolczyk, M., Kolba, M. D., Swatler, J., & Piwocka, K. (2018). Characteristics of live parameters of the HS-5 human bone marrow stromal cell line cocultured with the leukemia cells in hypoxia, for the studies of leukemia-stroma cross-talk. *Cytometry Part A*. 93 (9), p929–940.
- Pontén, I., Mutch, P., Nicholls, D. J., Saad, A., Pohl, C. D., Young, A., Fred, C., O'Donovan, M. R., & Åberg, P. (2013). Micronucleus induction in the bone marrow of rats by pharmacological mechanisms. II: long-acting beta-2 agonism. *Mutagenesis*. 28 (2), p233–239.
- Ponticelli, C., Locatelli, F. (2018). Glucocorticoids in the treatment of glomerular diseases: Pitfalls and pearls. In *Clinical Journal of the American Society of Nephrology*. 13 (5), p815–822).
- Prabhakarandian, B., Shen, M. C., Pant, K., & Kiani, M. F. (2011). Microfluidic devices for modeling cell-cell and particle-cell interactions in the microvasculature. In *Microvascular Research*. 82 (3), p210–220.
- Qiu, Z., Lin, A., Li, K., Lin, W., Wang, Q., Wei, T., Zhu, W., Luo, P., & Zhang, J. (2019). A novel mutation panel for predicting etoposide resistance in small-cell lung cancer. *Drug Design, Development and Therapy*. 13 (1), p2021–2041.
- Ra'em, T., & Cohen, S. (2012). Microenvironment design for stem cell fate determination. *Advances in Biochemical Engineering/Biotechnology*. 126 (1), p227–262.
- Rabah, S. O., Ali, S. S., Alsaggaf, S. M., Ayuob, N. N., Rabaht, S. O., & Alsaggaf, S. M. (2010). Acute Taxol Toxicity: the Effects on Bone Marrow Mitotic Index and the Histology of Mice Hepatocytes. *Journal of Applied Animal Research*. 38 (2), p201–207.
- Raic, A., Naolou, T., Mohra, A., Chatterjee, C., & Lee-Thedieck, C. (2019). 3D models of the bone marrow in health and disease: Yesterday, today, and tomorrow. In *MRS Communications*, 9 (1), p. 37–52.
- Raic, A., Rödling, L., Kalbacher, H., & Lee-Thedieck, C. (2014). Biomimetic macroporous PEG hydrogels as 3D scaffolds for the multiplication of human hematopoietic stem and progenitor cells. *Biomaterials*. 35 (3), p929–940.

- Rajendram, R., Rajendram, R., & Preedy, V. R. (2016). Ethanol Metabolism and Implications for Disease. In *Neuropathology of Drug Addictions and Substance Misuse*. 1 (1), p378–388.
- Ramakrishnan, A., Took-Storb, B., Pillai, M. M. (2013). Primary Marrow Derived Stromal Cells: Isolation and Manipulation. *Methods in Molecular Biology*. 1035 (1), p75–101.
- Ramamoorthy, S., & Cidlowski, J. A. (2016). Corticosteroids. Mechanisms of Action in Health and Disease. In *Rheumatic Disease Clinics of North America*. 42 (1), p15–31.
- Ravi, M., Paramesh, V., Kaviya, S. R., Anuradha, E., & Paul Solomon, F. D. (2015). 3D cell culture systems: Advantages and applications. *Journal of Cellular Physiology*. 230 (1), p16–26.
- Rees, M. G., Raimondo, A., Wang, J., Ban, M. R., Davis, M. I., Barrett, A., Ranft, J., Jagdhuhn, D., Waterstradt, R., Baltrusch, S., Simeonov, A., Collins, F. S., Hegele, R. A., & Gloyn, A. L. (2014). Inheritance of rare functional GCKR variants and their contribution to triglyceride levels in families. *Human Molecular Genetics*. 23 (20), p5570–5578.
- Reese, B. E., Krissinger, D., Yun, J. K., & Billingsley, M. L. (2005). Elucidation of stannin function using microarray analysis: Implications for cell cycle control. *Gene Expression*. 13 (1), p41–52.
- Reisinger, K., Blatz, V., Brinkmann, J., Downs, T. R., Fischer, A., Henkler, F., Hoffmann, S., Krul, C., Liebsch, M., Luch, A., Pirow, R., Reus, A. A., Schulz, M., & Pfuhrer, S. (2018). Validation of the 3D Skin Comet assay using full thickness skin models: Transferability and reproducibility. *Mutation Research - Genetic Toxicology and Environmental Mutagenesis*. 827 (1), p27–41.
- Reizer, E., Csizmadia, I. G., Palotás, Á. B., Viskolcz, B., & Fiser, B. (2019). Formation mechanism of benzo(a)pyrene: One of the most carcinogenic polycyclic aromatic hydrocarbons (PAH). *Molecules*. 24 (6).
- Ren, J., Jin, P., Sabatino, M., Balakumaran, A., Feng, J., Kuznetsov, S. A., Klein, H. G., Robey, P. G., & Stroncek, D. F. (2011). Global transcriptome analysis of human bone marrow stromal cells (BMSC) reveals proliferative, mobile and interactive cells that produce abundant extracellular matrix proteins, some of which may affect BMSC potency. *Cytotherapy*. 13 (6), p661–674.
- Ren, J., Ward, D., Chen, S., Tran, K., Jin, P., Sabatino, M., Robey, P. G., & Stroncek, D. F. (2018). Comparison of human bone marrow stromal cells cultured in human

- platelet growth factors and fetal bovine serum. *Journal of Translational Medicine*. 16 (1), p65.
- Revollo, J., Petibone, D. M., McKinzie, P., Knox, B., Morris, S. M., Ning, B., & Dobrovolsky, V. N. (2016). Whole genome and normalized mRNA sequencing reveal genetic status of TK6, WTK1, and NH32 human B-lymphoblastoid cell lines. *Mutation Research - Genetic Toxicology and Environmental Mutagenesis*. 795 (1), p60–69.
- Rhen, T., & Cidlowski, J. A. (2005). Antiinflammatory action of glucocorticoids - New mechanisms for old drugs. In *New England Journal of Medicine*. 353, (16).
- Rhizobium, G. E. (2013). Complete Genome Sequence of the Sesbania Symbiont and Rice. *Nucleic Acids Research*. 1 (1256879), p13–14.
- Ria, R., & Vacca, A. (2020). Bone marrow stromal cells-induced drug resistance in multiple myeloma. In *International Journal of Molecular Sciences*. 21 (2).
- Riedl, A., Schleder, M., Pudielko, K., Stadler, M., Walter, S., Unterleuthner, D., Unger, C., Kramer, N., Hengstschläger, M., Kenner, L., Pfeiffer, D., Krupitza, G., & Dolznig, H. (2017). Comparison of cancer cells in 2D vs 3D culture reveals differences in AKT-mTOR-S6K signaling and drug responses. *Journal of Cell Science*. 130 (1), p203–218.
- Rimessi, A., Giorgi, C., Pinton, P., Rizzuto, R. (2008). The versatility of mitochondrial calcium signals: From stimulation of cell metabolism to induction of cell death. *Biochimica et Biophysica Acta (BBA) - Bioenergetics*. 1777 (7-8), p808-816.
- Risitano, A., Maciejewski, J., Selleri, C., Rotoli, B., M. Risitano, A., & P. Maciejewski, J. (2007). Function and Malfunction of Hematopoietic Stem Cells in Primary Bone Marrow Failure Syndromes. *Current Stem Cell Research & Therapy*. 2 (1), p39–52.
- Robin, C., & Durand, C. (2010). The roles of BMP and IL-3 signaling pathways in the control of hematopoietic stem cells in the mouse embryo. In *International Journal of Developmental Biology*. 54 (6–7), p1189–1200.
- Rocha, S., Carvalho, J., Oliveira, P., Voglstaetter, M., Schwartz, D., Thomsen, A. R., Walter, N., Khanduri, R., Sanchez, J. C., Keller, A., Oliveira, C., & Nazarenko, I. (2019). 3D Cellular Architecture Affects MicroRNA and Protein Cargo of Extracellular Vesicles. *Advanced Science*. 6 (4).
- Rodrigues, M. A., Beaton-Green, L. A., Wilkins, R. C., & Fenech, M. F. (2018). The potential for complete automated scoring of the cytokinesis block micronucleus cytome assay using imaging flow cytometry. In *Mutation Research - Genetic Toxicology and Environmental Mutagenesis*. 836 (1), p53–64.

- Rodrigues, P. M., Ribeiro, A. R., Serafini, N., Meireles, C., Di Santo, J. P., & Alves, N. L. (2018). Intrathymic Deletion of IL-7 Reveals a Contribution of the Bone Marrow to Thymic Rebound Induced by Androgen Blockade. *The Journal of Immunology*. 200 (4), p1389–1398.
- Rumman, M., Majumder, A., Harkness, L., Venugopal, B., Vinay, M. B., Pillai, M. S., Kassem, M., & Dhawan, J. (2018). Induction of quiescence (G0) in bone marrow stromal stem cells enhances their stem cell characteristics. *Stem Cell Research*. 30 (1), p69–80.
- Salama, M. M., El-Naggar, D. A., Abdel-Rahman, R. H., & Elhak, S. A. G. (2018). Toxic effects of trichloroethylene on rat neuroprogenitor cells. *Frontiers in Pharmacology*. 9 (1).
- Salerno, A., Cesarelli, G., Pedram, P., & Netti, P. A. (2019). Modular Strategies to Build Cell-Free and Cell-Laden Scaffolds towards Bioengineered Tissues and Organs. *Journal of Clinical Medicine*. 8 (11), p1816.
- Salzig, D., Leber, J., Merkewitz, K., Lange, M. C., Koster, N., Czermak, P. (2016). Attachment, Growth, and Detachment of Human Mesenchymal Stem Cells in a Chemically Defined Medium. *Stem Cells International*. 2016 (1), p1-10.
- Sampson, A., Peterson, B. G., Tan, K. W., & Iram, S. H. (2019). Doxorubicin as a fluorescent reporter identifies novel MRP1 (ABCC1) inhibitors missed by calcein-based high content screening of anticancer agents. *Biomedicine and Pharmacotherapy*. 118 (1), p109289.
- Sant, S., & Johnston, P. A. (2017). The production of 3D tumor spheroids for cancer drug discovery. In *Drug Discovery Today: Technologies*. 23 (1) , p27–36.
- Santegoets, S. J. A. M., Dijkgraaf, E. M., Battaglia, A., Beckhove, P., Britten, C. M., Gallimore, A., Godkin, A., Gouttefangeas, C., de Gruijl, T. D., Koenen, H. J. P. M., Scheffold, A., Shevach, E. M., Staats, J., Taskén, K., Whiteside, T. L., Kroep, J. R., Welters, M. J. P., & van der Burg, S. H. (2015). Monitoring regulatory T cells in clinical samples: consensus on an essential marker set and gating strategy for regulatory T cell analysis by flow cytometry. *Cancer Immunology, Immunotherapy*. 64 (10), p1271–1286.
- Santovito, A., Cannarsa, E., Schleicherova, D., & Cervella, P. (2018). Clastogenic effects of bisphenol A on human cultured lymphocytes. *Human & Experimental Toxicology*. 37 (1), p69–77.

- Sasine, J. P., yeo, K. T., Chute, J. P. (2016). Concise Review: Paracrine Functions of Vascular Niche Cells in Regulating Hematopoietic Stem Cell Fate. *Stem Cells Translational Medicine*. 5, p1-8.
- Sato, S., Shirakawa, H., Tomita, S., Tohkin, M., Gonzalez, F. J., & Komai, M. (2013). The aryl hydrocarbon receptor and glucocorticoid receptor interact to activate human metallothionein 2A. *Toxicology and Applied Pharmacology*. 273 (1), p90–99.
- Scherzad, A., Hackenberg, S., Froelich, K., Rak, K., Hagen, R., Taeger, J., Bregenzer, M., & Kleinsasser, N. (2016). Chronic exposure of low dose salinomycin inhibits MSC migration capability in vitro. *Biomedical Reports*. 4 (3), p325–330.
- Schmid, J., Schwarz, S., Meier-Staude, R., Sudhop, S., Clausen-Schaumann, H., Schieker, M., & Huber, R. (2018). A perfusion bioreactor system for cell seeding and oxygen-controlled cultivation of three-dimensional cell cultures. *Tissue Engineering - Part C: Methods*. 24 (10), p585–595.
- Schmidt, M., Scholz, C. J., Polednik, C., & Roller, J. (2016). Spheroid-based 3-dimensional culture models: Gene expression and functionality in head and neck cancer. *Oncology Reports*. 35 (4), p2431–2440.
- Schreiber, M., Weigelt, M., Karasinsky, A., Anastassiadis, K., Schallenberg, S., Petzold, C., Bonifacio, E., Kretschmer, K., & Hommel, A. (2019). Inducible IL-7 hyperexpression influences lymphocyte homeostasis and function and increases allograft rejection. *Frontiers in Immunology*. 10 (4).
- Seita, J., Weissman, I. L. (2010). Hematopoietic Stem Cell: Self-renewal versus Differentiation. *Wiley Interdisciplinary Reviews: Systems Biology and Medicine*. 6 (2), p640-653.
- Shan, F., Close, D. A., Camarco, D. P., & Johnston, P. A. (2018). High-Content Screening Comparison of Cancer Drug Accumulation and Distribution in Two-Dimensional and Three-Dimensional Culture Models of Head and Neck Cancer. *Assay and Drug Development Technologies*. 16 (1), p27–50.
- Sharma, S., & Bhonde, R. (2015). Influence of Nuclear Blebs and Micronuclei Status on the Growth Kinetics of Human Mesenchymal Stem Cells. *Journal of Cellular Physiology*. 230 (3), p657–666.
- Sharma, S., & Bhonde, R. (2015). Mesenchymal stromal cells are genetically stable under a hostile in vivo-like scenario as revealed by in vitro micronucleus test. *Cytotherapy*. 17 (10), p1384–1395.

- Shin, H. J., Kwon, H. K., Lee, J. H., Anwar, M. A., & Choi, S. (2016). Etoposide induced cytotoxicity mediated by ROS and ERK in human kidney proximal tubule cells. *Scientific Reports*. 6 (1), p1–13.
- Shin, T. H., Lee, S., Choi, K. R., Lee, D. Y., Kim, Y., Paik, M. J., Seo, C., Kang, S., Jin, M. S., Yoo, T. H., Kang, S. H., & Lee, G. (2017). Quality and freshness of human bone marrow-derived mesenchymal stem cells decrease over time after trypsinization and storage in phosphate-buffered saline. *Scientific Reports*. 7 (1).
- Si, M., & Lang, J. (2018). The roles of metallothioneins in carcinogenesis. In *Journal of Hematology and Oncology*. 11 (1), p1–20.
- Siddens, L. K., Larkin, A., Krueger, S. K., Bradfield, C. A., Waters, K. M., Tilton, S. C., Pereira, C. B., Löhr, C. V., Arlt, V. M., Phillips, D. H., Williams, D. E., & Baird, W. M. (2012). Polycyclic aromatic hydrocarbons as skin carcinogens: Comparison of benzo[a]pyrene, dibenzo[def,p]chrysene and three environmental mixtures in the FVB/N mouse. *Toxicology and Applied Pharmacology*. 264 (3), p377–386.
- Sieber, S., Wirth, L., Cavak, N., Koenigsmark, M., Marx, U., Lauster, R., & Rosowski, M. (2018). Bone marrow-on-a-chip: Long-term culture of human haematopoietic stem cells in a three-dimensional microfluidic environment. *Journal of Tissue Engineering and Regenerative Medicine*. 12 (2), p479–489.
- Singh, H., Singh, J. R., Dhillon, V. S., Bali, D., & Paul, H. (1994). In vitro and in vivo genotoxicity evaluation of hormonal drugs. II. Dexamethasone. *Mutation Research Regular Papers*. 308 (1), p89–97.
- Smart, D. J., Helbling, F. R., Verardo, M., Huber, A., McHugh, D., & Vanscheeuwijck, P. (2020). Development of an integrated assay in human TK6 cells to permit comprehensive genotoxicity analysis in vitro. *Mutation Research - Genetic Toxicology and Environmental Mutagenesis*. 849 (1), p503129.
- Smart, D. J., Helbling, F. R., Verardo, M., McHugh, D., & Vanscheeuwijck, P. (2019). Mode-of-action analysis of the effects induced by nicotine in the in vitro micronucleus assay. *Environmental and Molecular Mutagenesis*. 60 (9), p778–791.
- Soares, C. P., Midlej, V., Oliveira, M. E. W., Benchimol, M., Costa, M. L., Mermelstein, C. (2012). 2D and 3D-Organized Cardiac Cells Shows Differences in Cellular Morphology, Adhesion Junctions, Presence of Myofibrils and Protein Expression. *PLOS one*. 7 (5), p38147.
- Souza, A. G., Silva, I. B. B., Campos-Fernandez, E., Barcelos, L. S., Souza, J. B., Marangoni, K., Goulart, L. R., & Alonso-Goulart, V. (2018). Comparative Assay of

- 2D and 3D Cell Culture Models: Proliferation, Gene Expression and Anticancer Drug Response. *Current Pharmaceutical Design*. 24 (15), p1689–1694.
- Spivak, G. (2015). Nucleotide excision repair in humans. In *DNA Repair*. 36 (1), p13–18.
- Stacey, G. (2006). Primary Cell Cultures and Immortal Cell Lines. In *Encyclopedia of Life Sciences*. John Wiley & Sons, Ltd.
- Stage, T. B., Bergmann, T. K., & Kroetz, D. L. (2018). Clinical Pharmacokinetics of Paclitaxel Monotherapy: An Updated Literature Review. In *Clinical Pharmacokinetics*. 57 (1), p7–19.
- Stagnaro, P., Schizzi, I., Utzeri, R., Marsano, E., & Castellano, M. (2018). Alginate-polymethacrylate hybrid hydrogels for potential osteochondral tissue regeneration. *Carbohydrate Polymers*. 185 (1), p56–62.
- Stanley, L. A. (2017). Drug Metabolism. In *Pharmacognosy: Fundamentals, Applications and Strategy*. 1 (1), p527–545.
- Stern, S. T., Martinez, M. N., & Stevens, D. M. (2016). When is it important to measure unbound drug in evaluating nanomedicine pharmacokinetics? *Drug Metabolism and Disposition*. 44 (12), p1934–1939.
- Stiborová, M., Arlt, V. M., Henderson, C. J., Wolf, C. R., Kotrbová, V., Moserová, M., Hudeček, J., Phillips, D. H., & Frei, E. (2008). Role of hepatic cytochromes P450 in bioactivation of the anticancer drug ellipticine: Studies with the hepatic NADPH:Cytochrome P450 reductase null mouse. *Toxicology and Applied Pharmacology*. 226 (3), p318–327.
- Su, M., Chang, Y. T., Hernandez, D., Jones, R. J., & Ghiaur, G. (2019). Regulation of drug metabolizing enzymes in the leukaemic bone marrow microenvironment. *Journal of Cellular and Molecular Medicine*. 23 (6), p4111–4117.
- Sun, H., Tsai, Y., Nowak, I., Dertinger, S. D., Wu, J. H. D., & Chen, Y. (2011). Response kinetics of radiation-induced micronucleated reticulocytes in human bone marrow culture. *Mutation Research - Genetic Toxicology and Environmental Mutagenesis*. 718 (1–2), p38–43.
- Sun, X., & Kaufman, P. D. (2018). Ki-67: more than a proliferation marker. In *Chromosoma*. 127 (2), p175–186.
- Takahashi, Y., Hori, Y., Yamamoto, T., Urashima, T., Ohara, Y., & Tanaka, H. (2015). 3D spheroid cultures improve the metabolic gene expression profiles of HepaRG cells. *Bioscience Reports*. 35 (3), p1–7.
- Teles, K. A., Medeiros-Souza, P., Lima, F. A. C., Araújo, B. G. de, & Lima, R. A. C. (2017). Cyclophosphamide administration routine in autoimmune rheumatic

- diseases: a review. *Revista Brasileira de Reumatologia (English Edition)*. 57 (6), p596–604.
- The Organisation for Economic Co-operation and Development. (1997). Test No. 471: Bacterial Reverse Mutation Test. In: OECD *OECD Guidelines for the Testing of Chemicals, Section 4*. OECD publishing. P11.
- The Organisation for Economic Co-operation and Development. (2016). Test No. 489: *In Vivo* Mammalian Alkaline Comet Assay. In: OECD *OECD Guidelines for the Testing of Chemicals, Section 4*. OECD publishing. p27.
- The Organisation for Economic Co-operation and Development. (2016). Test No. 475: Mammalian Bone Marrow Chromosomal Aberration test. In: OECD *OECD Guidelines for the Testing of Chemicals, Section 4*. OECD publishing. P18.
- The Organisation for Economic Co-operation and Development. (2016). Test No. 487: *In Vitro* Mammalian Cell Micronucleus Test. In: OECD *OECD Guidelines for the Testing of Chemicals, Section 4*. OECD publishing. p29.
- The Organisation for Economic Co-operation and Development. (2016). Test No. 473: *In Vitro* Mammalian Chromosomal Aberration Test. In: OECD *OECD Guidelines for the Testing of Chemicals, Section 4*. OECD publishing. P22.
- The Organisation for Economic Co-operation and Development. (2016). Test No. 474: Mammalian Erythrocyte Micronucleus Test. In: OECD *OECD Guidelines for the Testing of Chemicals, Section 4*. OECD publishing. p21.
- The Organisation for Economic Co-operation and Development. (2016). Test No. 490: *In Vitro* Mammalian Cell Gene Mutation Tests Using the Thymidine Kinase Gene. In: OECD *OECD Guidelines for the Testing of Chemicals, Section 4*. OECD publishing. P24.
- Thougaard, A. V., Christiansen, J., Mow, T., & Hornberg, J. J. (2014). Validation of a high throughput flow cytometric *in vitro* micronucleus assay including assessment of metabolic activation in TK6 cells. *Environmental and Molecular Mutagenesis*. 55 (9), p704–718.
- Tikhonova, A. N., Dolgalev, I., Hu, H., Sivaraj, K. K., Hoxha, E., Cuesta-Domínguez, Á., Pinho, S., Akhmetzyanova, I., Gao, J., Witkowski, M., Guillamot, M., Gutkin, M. C., Zhang, Y., Marier, C., Diefenbach, C., Kousteni, S., Heguy, A., Zhong, H., Fooksman, D. R., ... Aifantis, I. (2019). The bone marrow microenvironment at single-cell resolution. *Nature*. 569 (7755), p222–228.
- Torisawa, Y. (2019). Engineering bone marrow-on-a-chip. *Microphysiological Systems*. 3 (1), p2–12.

- Torisawa, Y. S., Mammoto, T., Jiang, E., Jiang, A., Mammoto, A., Watters, A. L., Bahinski, A., & Ingber, D. E. (2016). Modeling Hematopoiesis and Responses to Radiation Countermeasures in a Bone Marrow-on-a-Chip. *Tissue Engineering - Part C: Methods*. 22 (5), p509–515.
- Torisawa, Y. S., Spina, C. S., Mammoto, T., Mammoto, A., Weaver, J. C., Tat, T., Collins, J. J., & Ingber, D. E. (2014). Bone marrow-on-a-chip replicates hematopoietic niche physiology in vitro. *Nature Methods*. 11 (6), p663–669.
- Trefts, E., Gannon, M., & Wasserman, D. H. (2017). The liver. In *Current Biology*. 27 (21), p1147–1151.
- Tsai, H. H., Yang, K. C., Wu, M. H., Chen, J. C., & Tseng, C. L. (2019). The effects of different dynamic culture systems on cell proliferation and osteogenic differentiation in human mesenchymal stem cells. *International Journal of Molecular Sciences*. 20 (16).
- Tung, E. W. Y., Philbrook, N. A., Belanger, C. L., Ansari, S., & Winn, L. M. (2014). Benzo[a]pyrene increases DNA double strand break repair in vitro and in vivo: A possible mechanism for benzo[a]pyrene-induced toxicity. *Mutation Research - Genetic Toxicology and Environmental Mutagenesis*. 760 (1), p64–69.
- Turner, R. T., Martin, S. A., & Iwaniec, U. T. (2018). Metabolic Coupling Between Bone Marrow Adipose Tissue and Hematopoiesis. In *Current Osteoporosis Reports*. 16 (2), p95–104.
- Turner, S. D., Wijnhoven, S. W. P., Tinwell, H., Lashford, L. S., Rafferty, J. A., Ashby, J., Vrieling, H., & Fairbairn, L. J. (2001). Assays to predict the genotoxicity of the chromosomal mutagen etoposide - Focussing on the best assay. *Mutation Research - Genetic Toxicology and Environmental Mutagenesis*. 493 (1–2), p139–147.
- Tweats, D. J., Blakey, D., Heflich, R. H., Jacobs, A., Jacobsen, S. D., Morita, T. Nohmi, T., O'Donovan, M. R., Sasaki, Y. F., Sofuni, T., Tice, R. (2007). Report of the IWGT working group on strategies and interpretation of regulatory in vivo tests: I. Increases in micronucleated bone marrow cells in rodents that do not indicate genotoxic hazards. *Mutation Research/Genetic Toxicology and Environmental Mutagenesis*. 627 (1), p78-91.
- Uhlen, M., Fagerberg, L., Hallstrom, B. M., Lindskog, C., Oksvold, P., Mardinoglu, A., Sivertsson, A., Kampf, C., Sjostedt, E., Asplund, A., Olsson, I., Edlund, K., Lundberg, E., Navani, S., Szigartyo, C. A.-K., Odeberg, J., Djureinovic, D., Takanen, J. O., Hober, S., ... Ponten, F. (2015). Tissue-based map of the human proteome. *Science*. 347 (6220), p1260419–1260419.

- Ullah, I., Subbarao, R. B., & Rho, G. J. (2015). Human mesenchymal stem cells - Current trends and future prospective. In *Bioscience Reports*. 35 (2).
- Ushach, I., & Zlotnik, A. (2016). Biological role of granulocyte macrophage colony-stimulating factor (GM-CSF) and macrophage colony-stimulating factor (M-CSF) on cells of the myeloid lineage. *Journal of Leukocyte Biology*. 100 (3), p481–489.
- Vaiselbuh, S. R., Edelman, M., Lipton, J. M., Liu, J. M. (2010). Ectopic Human Mesenchymal Stem Cell-Coated Scaffolds in NOD/SCID Mice: An In Vivo Model of the Leukemia Niche. *Tissue Engineering: Part C*. 16 (6), p1523-1531.
- Van Gisbergen, M. W., Cebula, M., Zhang, J., Ottosson-Wadlund, A., Dubois, L., Lambin, P., Tew, K. D., Townsend, D. M., Haenen, G. R. M. M., Driittij-Reijnders, M. J., Saneyoshi, H., Araki, M., Shishido, Y., Ito, Y., Arnér, E. S. J., Abe, H., Morgenstern, R., & Johansson, K. (2016). Chemical Reactivity Window Determines Pro-drug Efficiency toward Glutathione Transferase Overexpressing Cancer Cells. *Molecular Pharmaceutics*, 13 (6), p2010–2025.
- Verjans, E., Doijen, j., Luyten, W., Landuyt, B., Schoofs, L. (2017). Three-dimensional cell culture models for anticancer drug screening: Worth the effort. *Cellular Physiology*. 9999 (1), p1-11.
- Vrzal, R., Zenata, O., Bachleda, P., & Dvorak, Z. (2015). The effects of drugs with immunosuppressive or immunomodulatory activities on xenobiotics-metabolizing enzymes expression in primary human hepatocytes. *Toxicology in Vitro*. 29 (5), p1088–1099.
- Wallace, S. S. (2014). Base excision repair: A critical player in many games. *DNA Repair*. 19 (1), p14–26.
- Wang, H., Boussouar, A., Mazelin, L., Tauszig-Delamasure, S., Sun, Y., Goldschneider, D., Paradisi, A., & Mehlen, P. (2018). The Proto-oncogene c-Kit Inhibits Tumor Growth by Behaving as a Dependence Receptor. *Molecular Cell*. 72 (3), p413-425.
- Wang, L. E., Li, C., Xiong, P., Gershenwald, J. E., Prieto, V. G., Duvic, M., Lee, J. E., Grimm, E. A., Hsu, T. C., & Wei, Q. (2016). 4-Nitroquinoline-1-oxide-induced mutagen sensitivity and risk of cutaneous melanoma: A case-control analysis. *Melanoma Research*. 26 (2), p181–187.
- Wang, L. H., Yang, X. y., Zhang, X., Farrar, W. L. (2007). Inhibition of adhesive interaction between multiple myeloma and bone marrow stromal cells by PPAR γ cross talk with NF- κ B and C/EBP β . *Blood*. 110 (13), p4373-4384.

- Wang, Y., Gray, J. P., Mishin, V., Heck, D. E., Laskin, D. L., & Laskin, J. D. (2010). Distinct roles of cytochrome P450 reductase in mitomycin c redox cycling and cytotoxicity. *Molecular Cancer Therapeutics*. 9 (6), p1852–1863.
- Wang, Y., Li, X., Wang, L., Xu, Y., Cheng, X., & Wei, P. (2011). Formulation and pharmacokinetic evaluation of a paclitaxel nanosuspension for intravenous delivery. *International Journal of Nanomedicine*. 6 (1), p1497–1507.
- Wang, Z., Shen, H., Song, S., Zhang, L., Chen, W., Dai, J., & Zhang, Z. (2017). Graphene Oxide Incorporated PLGA Nanofibrous Scaffold for Solid Phase Gene Delivery into Mesenchymal Stem Cells. *Journal of Nanoscience and Nanotechnology*. 18 (4), p2286–2293.
- Ward, T. H., Cummings, J., Dean, E., Greystoke, A., Hou, J. M., Backen, A., Ranson, M., & Dive, C. (2008). Biomarkers of apoptosis. In *British Journal of Cancer*. 99 (6), p841–846.
- Watanabe, S., Tominaga, T., & Matsumoto, M. (2019). Alternate soaking technique for micropatterning alginate hydrogels on wettability-patterned substrates. *Journal of Oleo Science*. 68 (1), p53–60.
- Weaver, B. A. (2014). How Taxol/paclitaxel kills cancer cells. In *Molecular Biology of the Cell*. 25 (18), p2677–2681.
- Weber, L. M., He, J., Bradley, B., Haskins, K., Anseth, K. S. (2006). PEG-based hydrogels as an in vitro encapsulation platform for testing controlled β -cell microenvironments. *Acta Biomaterialia*. 2 (1), p1-8.
- Wei, Q., & Frenette, P. S. (2018). Niches for Hematopoietic Stem Cells and Their Progeny. In *Immunity*. 48 (4), p632–648.
- Weng, S., Stoner, S. A., & Zhang, D. E. (2016). Sex chromosome loss and the pseudoautosomal region genes in hematological malignancies. *Oncotarget*. 7 (44), p72356–72372.
- Wexler, S. A., Donaldson, C., Denning-Kendall, P., Rice, C., Bradley, B., & Hows, J. M. (2003). Adult bone marrow is a rich source of human mesenchymal “stem” cells but umbilical cord and mobilized adult blood are not. *British Journal of Haematology*. 121 (2), p368–374.
- Wexler, S. A., Donaldson, C., Denning-Kendall, P., Rice, C., Bradley, B., & Hows, J. M. (2003). Adult bone marrow is a rich source of human mesenchymal ‘stem’ cells but umbilical cord and mobilized adult blood are not. *British Journal of Haematology*. 121 (2), p368–374.

- White, J. R., Padowski, J. M., Zhong, Y., Chen, G., Luo, S., Lazarus, P., Layton, M. E., & McPherson, S. (2016). Pharmacokinetic analysis and comparison of caffeine administered rapidly or slowly in coffee chilled or hot versus chilled energy drink in healthy young adults. *Clinical Toxicology*. 54 (4), p308–312.
- Wigren, M., Svenugnsson, E., Mattisson, I. Y., Gustafsson, J. T., Gunnarsson, I., Zickert, A., Elvin, K., Jensen-Urstad, K., Bengtsson, A., Gullstrand, B., Fredrikson, G. N., & Nilsson, J. (2018). Cardiovascular disease in systemic lupus erythematosus is associated with increased levels of biomarkers reflecting receptor-activated apoptosis. *Atherosclerosis*. 270 (1), p1–7.
- Wilde, S., Dambowsky, M., Hempt, C., Sutter, A., & Queisser, N. (2017). Classification of in vitro genotoxicants using a novel multiplexed biomarker assay compared to the flow cytometric micronucleus test. *Environmental and Molecular Mutagenesis*. 58 (9), p662–677.
- Windus, L. C. E., Glover, T. T., & Avery, V. M. (2013). Bone-stromal cells up-regulate tumourigenic markers in a tumour-stromal 3D model of prostate cancer. *Molecular Cancer*. 12 (1), p112.
- Winiwarter, S., Ridderström, M., Ungell, A. L., Andersson, T. B., & Zamora, I. (2006). Use of molecular descriptors for absorption, distribution, metabolism, and excretion predictions. In *Comprehensive Medicinal Chemistry II*. 5 (1), p531–554.
- Wittwer, N. L., Brumatti, G., Marchant, C., Sandow, J. J., Pudney, M. K., Dottore, M., D'Andrea, R. J., Lopez, A. F., Ekert, P. G., & Ramshaw, H. S. (2017). High CD123 levels enhance proliferation in response to IL-3, but reduce chemotaxis by downregulating CXCR4 expression. *Blood Advances*. 1 (15), p1067–1079.
- World Health Organisation. (2019). *WHO | JECFA*. <https://apps.who.int/food-additives-contaminants-jecfa-database/chemical.aspx?chemID=1882>
- Worthington, P., Pochan, D. J., Langhans, S. A. (2015). Peptide Hydrogels – Versatile Matrices for 3D Cell Culture in Cancer Medicine. *Frontiers in Oncology*. 5 (92), p1-10.
- Wright, W. D., Shah, S. S., & Heyer, W. D. (2018). Homologous recombination and the repair of DNA double-strand breaks. In *Journal of Biological Chemistry*. 2930 (27), p10524–10535.
- Wu, Y., Xie, L., Wang, M., Xiong, Q., Guo, Y., Liang, Y., Li, J., Sheng, R., Deng, P., Wang, Y., Zheng, R., Jiang, Y., Ye, L., Chen, Q., Zhou, X., Lin, S., & Yuan, Q. (2018). Mettl3-mediated m⁶A RNA methylation regulates the fate of bone marrow mesenchymal stem cells and osteoporosis. *Nature Communications*. 9 (1).

- Xu, B., Wang, W., Guo, H., Sun, Z., Wei, Z., Zhang, X., Liu, Z., Tischfield, J. A., Gong, Y., & Shao, C. (2014). Oxidative stress preferentially induces a subtype of micronuclei and mediates the genomic instability caused by p53 dysfunction. *Mutation Research - Fundamental and Molecular Mechanisms of Mutagenesis*. 770 (1), p1–8.
- Xu, L., Xia, H., Ni, D., Hu, Y., Liu, J., Qin, Y., Zhou, Q., Yi, Q., & Xie, Y. (2020). High-dose dexamethasone manipulates the tumor microenvironment and internal metabolic pathways in anti-tumor progression. *International Journal of Molecular Sciences*. 21 (5).
- Xu, R., Shen, X., Si, Y., Fu, Y., Zhu, W., Xiao, T., Fu, Z., Zhang, P., Cheng, J., & Jiang, H. (2018). MicroRNA-31a-5p from aging BMSCs links bone formation and resorption in the aged bone marrow microenvironment. *Aging Cell*. 17 (4).
- Yang, C., Zhang, J., Ding, M., Xu, K., Li, L., Mao, L., & Zheng, J. (2018). Ki67 targeted strategies for cancer therapy. In *Clinical and Translational Oncology*. 20 (5), p570–575.
- Yang, H., Wang, M., Huang, Y., Qiao, Q., Zhao, C., & Zhao, M. (2019). In vitro and in vivo evaluation of a novel mitomycin nanomicelle delivery system. *RSC Advances*. 9 (26), p14708–14717.
- Yang, J., Bogni, A., Schuetz, E. G., Ratain, M., Eileen Dolan, M., McLeod, H., Gong, L., Thorn, C., Relling, M. V., Klein, T. E., & Altman, R. B. (2009). Etoposide pathway. In *Pharmacogenetics and Genomics*. 19 (7), p552–553.
- Yang, J., Cornelissen, F., Papazian, N., Reijmers, R. M., Llorian, M., Cupedo, T., Coles, M., & Seddon, B. (2018). IL-7-dependent maintenance of ILC3s is required for normal entry of lymphocytes into lymph nodes. *Journal of Experimental Medicine*. 215 (4), p1069–1077.
- Yener, Y. (2013). Effects of long term low dose acrylamide exposure on rat bone marrow polychromatic erythrocytes. *Biotechnic and Histochemistry*. 88 (6), p356–360.
- Yeung, P., Cheng, K. H., Yan, C. H., & Chan, B. P. (2019). Collagen microsphere based 3D culture system for human osteoarthritis chondrocytes (hOACs). *Scientific Reports*. 9 (1).
- Yi, K. W., Mamillapalli, R., Sahin, C., Song, J., Tal, R., & Taylor, H. S. (2019). Bone marrow-derived cells or C-X-C motif chemokine 12 (CXCL12) treatment improve thin endometrium in a mouse model. *Biology of Reproduction*. 100 (1), p61.

- Yin, J., Han, L., & Cong, W. (2018). Alpinumisoflavone rescues glucocorticoid-induced apoptosis of osteocytes via suppressing Nox2-dependent ROS generation. *Pharmacological Reports*. 70 (2), p270–276.
- Yu, L., Wu, Y., Liu, J., Li, B., Ma, B., Li, Y., Huang, Z., He, Y., Wang, H., Wu, Z., & Qiu, G. (2018). 3D Culture of Bone Marrow-Derived Mesenchymal Stem Cells (BMSCs) Could Improve Bone Regeneration in 3D-Printed Porous Ti6Al4V Scaffolds. *Stem Cells International*. 2018 (1).
- Zabirowicz, E. S., & Gan, T. J. (2018). Pharmacology of postoperative nausea and vomiting. In *Pharmacology and Physiology for Anesthesia: Foundations and Clinical Application*. 1 (1), p671–692.
- Zaid, M. M., Mohammed, M., & Al-Sharif, Z. (2012). Studies on the Genotoxic Effects of Anticancer Drug Paclitaxel (Taxol) in Mice. *World Applied Sciences Journal*. 16 (7), p989–997.
- Zanger, U. M., & Schwab, M. (2013). Cytochrome P450 enzymes in drug metabolism: Regulation of gene expression, enzyme activities, and impact of genetic variation. In *Pharmacology and Therapeutics*. 138 (1), p103–141.
- Zhang, B., Zhao, J., Li, S., Zeng, L., Chen, Y., & Fang, J. (2015). Mangiferin activates the Nrf2-ARE pathway and reduces etoposide-induced DNA damage in human umbilical cord mononuclear blood cells. *Pharmaceutical Biology*. 53 (4), p503–511.
- Zhang, J., Ke, J., Zhu, Y., Song, J., Yang, J., Wen, C., & Zhang, L. (2020). Influence of divalent cations on the biofouling behaviors of alginate hydrogels. *Biomedical Materials (Bristol)*. 15 (1).
- Zhang, X., Battiston, K. G., McBane, J. E., Matheson, L. A., Labow, R. S., & Paul Santerre, J. (2016). Design of Biodegradable Polyurethanes and the Interactions of the Polymers and Their Degradation By-Products Within in Vitro and in Vivo Environments. In *Advances in Polyurethane Biomaterials*. 1 (1), p75–114.
- Zhang, Y., Dépond, M., He, L., Foudi, A., Kwarteng, E. O., Lauret, E., Plo, I., Desterke, C., Dessen, P., Fujii, N., Opolon, P., Herault, O., Solary, E., Vainchenker, W., Joulin, V., Louache, F., & Wittner, M. (2016). CXCR4/CXCL12 axis counteracts hematopoietic stem cell exhaustion through selective protection against oxidative stress. *Scientific Reports*. 6 (1).
- Zhao, E., Xu, H., Wang, L., Kryczek, I., Wu, K., Hu, Y., Wang, G., & Zou, W. (2012). Bone marrow and the control of immunity. In *Cellular and Molecular Immunology*. 9 (1), p11–19.

- Zhou, B. O., Yue, R., Murphy, M. M., Peyer, J. G., & Morrison, S. J. (2014). Leptin-receptor-expressing mesenchymal stromal cells represent the main source of bone formed by adult bone marrow. *Cell Stem Cell*. 15 (2), p154–168.
- Zhou, Q., Ye, M., Lu, Y., Zhang, H., Chen, Q., Huang, S., & Su, S. (2015). Curcumin improves the tumoricidal effect of mitomycin C by suppressing ABCG2 expression in stem cell-like breast cancer cells. *PLoS ONE*. 10 (8).
- Zhou, Y., Chen, H., Li, H., & Wu, Y. (2017). 3D culture increases pluripotent gene expression in mesenchymal stem cells through relaxation of cytoskeleton tension. *Journal of Cellular and Molecular Medicine*. 21 (6), p1073–1084.
- Zhou, Y., Shen, J. X., & Lauschke, V. M. (2019). Comprehensive evaluation of organotypic and microphysiological liver models for prediction of drug-induced liver injury. In *Frontiers in Pharmacology*. 10 (9).
- Zhu, L., & Chen, L. (2019). Progress in research on paclitaxel and tumor immunotherapy. *Cellular and Molecular Biology Letters*. 24 (1).
- Zuppinger, C. (2019). 3D Cardiac Cell Culture: A Critical Review of Current Technologies and Applications. In *Frontiers in Cardiovascular Medicine*. 6 (1).

Appendices

Appendix 1 1: The P values calculated within this thesis

Figure 3-1 ** p=0.0074

Figure 3-2 A. ** p=0.0049, * p=0.0373

B. *** p=0.0004, **** p<0.0001 C. *** p=0.0002.

Figure 3-3 A. * p=0.0135, ** p=0.0089

B. **** p <0.0001, *** p <0.0010

C. * p=0.0127, * p=0.0401.

Figure 3-4 A. * p=0.0131, **** p <0.0001

B. **** p<0.0001.

Figure 3-9 A. **** p <0.0001, * p=0.0420, ** p=0.0021

B. **** p <0.0001, * p=0.0284

C. *** p=0.0002, ** p=0.0017, * p=0.0186, * p=0.0102

D. **** p <0.0001

E. ** p=0.0013, *** p=0.0004, **p=0.0026, *** p=0.0006, * p=0.0107

F. *** p=0.0004, **** p <0.0001

G. **** p <0.0001, ** p=0.0075, *** p=0.0004, *** p=0.0006

H. * p=0.0309, **** p <0.0001.

Figure 3-10 A. 25 vs 24 **** p <0.001, 25 vs 12 *** p=0.0010 & 12 vs 24 ****p <0.0001

B. 25 vs 24 ** p=0.0014 & 12 vs 24 * p=0.0286

C. 25 vs 24 **** <0.0001, 25 vs 12 *** p=0.002 & 12 vs 24 * p=0.0148

Figure 3-11 B. 24 hour 2.5 vs 168 hour 2.5 **** p <0.0001, 168 hour 2.5 vs 5 **** p <0.0001

C. 24 hour 2.5 vs 168 hour 2.5 ****p <0.0001

Figure 3-12 ** p=0.0015, **** p<0.0001

Figure 3-15 A. ** p=0.0015, *** p=0.0003

B. ** p=0.0121, **** p <0.0001

Figure 4-6 A. ** p=0.0015

B. **** p<0.0001

C. * p=0.0409, **** p<0.0001

D. **** p<0.0001

Figure 4.7 A & B. **** p<0.0001

Figure 4.8 **** p<0.0001

Figure 4-11 A. * $p=0.034$, *** $p=0.001$, **** $p<0.0001$

B. ** $p=0.0032$, *** $p=0.001$, **** $p<0.0001$

C. * $p=0.023$, *** $p=0.001$, **** $p<0.0001$

D. * $p=0.0325$, * $p=0.0421$, * $p=0.0318$, ** $p=0.0022$, ** $p=0.0044$

E. ** $p=0.023$, **** $p<0.0001$

F. *** $p=0.0002$

Research output

Publications

Vernon, A., Morse, R., David, R., Doherty, A. (2018). Evaluating different 3D scaffolds for the development of an *in vitro* bone marrow model for genotoxicity testing. *Mutagenesis*. 33 (5-6) (abstract).

Oral/ poster presentation

Vernon, A., Morse, R., David, R., Doherty, A. (2019). Bridging *in vitro* and *in vivo* testing: the utilisation of a novel *in vitro* three-dimensional model of the human bone marrow for genotoxicity testing. Industry Toxicology Training Program annual meeting, Leicester.

Vernon, A., Morse, R., David, R., Doherty, A. (2019). Cell specific genotoxicity assessment in a 3D metabolically competent bone marrow model. The 43rd United Kingdom Environmental Mutagen Society conference, Cambridge.

Vernon, A., Morse, R., David, R., Doherty, A. (2019). Cell specific genotoxicity assessment in a 3D metabolically competent bone marrow model. The British Toxicology Society congress, Cambridge.

Vernon, A., Morse, R., David, R., Doherty, A. (2018). Bridging *in vitro* and *in vivo* testing: the utilisation of a novel *in vitro* three-dimensional model of the human bone marrow for genotoxicity testing. Industry Toxicology Training Program annual meeting, Leicester

Vernon, A., Morse, R., David, R., Doherty, A. (2018). Evaluating different 3D scaffolds for the development of an *in vitro* bone marrow model for genotoxicity testing. The 42nd United Kingdom Environmental Mutagen Society conference, Oxford.

Vernon, A., Morse, R. (2018). A new 3D hydrogel for genotoxicity testing. the Centre for Research in Bioscience annual conference, Bristol.

Vernon, A., Morse, R. (2018). Bridging *in vitro* and *in vivo* testing: the utilisation of a novel *in vitro* three-dimensional model of the human bone marrow for genotoxicity testing. The 1st UWE 3D symposium, Bristol.

Vernon, A., Morse, R., Kabrah., David, R., Dohert, A. (2017). Bridging the gap between *in vitro* and *in vivo* genotoxicity assays: the development of a novel 3D *in vitro* model of the human bone marrow. The Centre for Research in Bioscience annual conference, Bristol.

Vernon, A., Morse, R., Kabrah., David, R., Dohert, A. (2017). Bridging the gap between *in vitro* and *in vivo* genotoxicity assays: the development of a novel 3D *in vitro* model of the human bone marrow. Industry Toxicology Training Program annual meeting, Leicester.